NACA RM A56C01

3 1176 00105 6382

C.1

NACA

RESEARCH MEMORANDUM

THE EFFECTS OF BLOWING OVER VARIOUS TRAILING-EDGE FLAPS ON AN NACA 0006 AIRFOIL SECTION, COMPARISONS WITH VARIOUS TYPES OF FLAPS ON OTHER AIRFOIL SECTIONS, AND AN ANALYSIS OF FLOW AND POWER RELATIONSHIPS FOR BLOWING SYSTEMS

By Jules B. Dods, Jr., and Earl C. Watson

Ames Aeronautical Laboratory
Moffett Field, Calif.

CLASSIFICATION CHANGED

To UNCLASSIFIED

By authority of NACA Res Abs RN-126 effective Date Apr. 15, 1958
Amt 5-8-58

LIBRARY COPY
JUN 1 1956
LANGLEY AERONAUTICAL LABORATORY
LIBRARY, NACA
LANGLEY FIELD, VIRGINIA

CLASSIFIED DOCUMENT

This material contains information affecting the National Defense of the United States within the meaning of the espionage laws, Title 18, U.S.C., Secs. 793 and 794, the transmission or revelation of which in any manner to an unauthorized person is prohibited by law.

NATIONAL ADVISORY COMMITTEE FOR AERONAUTICS

WASHINGTON

June 12, 1956

NATIONAL ADVISORY COMMITTEE FOR AERONAUTICS

RESEARCH MEMORANDUM

THE EFFECTS OF BLOWING OVER VARIOUS TRAILING-EDGE FLAPS ON AN NACA 0006 AIRFOIL SECTION, COMPARISONS WITH VARIOUS TYPES OF FLAPS ON OTHER AIRFOIL SECTIONS, AND AN ANALYSIS OF FLOW AND POWER RELATIONSHIPS FOR BLOWING SYSTEMS

By Jules B. Dods, Jr., and Earl C. Watson

SUMMARY

The investigation reported herein consists of three phases: (1) an experimental investigation of a thin airfoil with blowing over a trailing-edge flap; (2) a comparison of the results of the experimental investigation with the results of other similar investigations; and (3) a theoretical study of the relationships among the air-flow and power parameters for the general blowing case.

The experimental investigation employed a two-dimensional model of the NACA 0006 airfoil equipped with a nose flap and six alternate trailing-edge flaps. The blowing slot was in the body of the airfoil ahead of the trailing-edge flap. Only subcritical blowing pressure ratios could be investigated. Lift, pitching moment, and chordwise distribution of pressure were measured over a range of angles of attack for Reynolds numbers from 2.3 million to 4 million. The variables investigated include flap position and contour, nozzle height, and blowing quantity.

The comparison and evaluation phase of the investigation used data from this experimental investigation together with those obtained from other investigations which employed thicker airfoil sections. Several relationships for evaluating the effects of blowing are presented. The increments of lift coefficient which were obtained with the 6-percent-thick airfoil of the present investigation compared favorably with those obtained with the thicker airfoils of the other investigations. It was found that for flap deflection up to 60° or 70°, the theoretical increment of lift coefficient due to flap deflection alone (i.e., without blowing) could be attained or exceeded, depending on the blowing quantity.

The power and flow quantities that may be required of a blowing system were shown to vary greatly, depending on the arrangement of the flap and blowing system.

The results of the theoretical study of the air flow and power relationships are presented in chart form and are applicable to blowing systems employing either subcritical or supercritical pressure ratios.

INTRODUCTION

Approximately 30 years ago, Seewald (ref. 1), Reid and Bamber (ref. 2), and Wieland (ref. 3) demonstrated that the lift of an airfoil could be increased a substantial amount by ejecting compressed air over the upper surface. The power and equipment necessary to supply the large quantity of compressed air that was required for lift augmentation deterred further investigation. However, the development of the turbojet engine, a convenient source of compressed air, renewed interest in this phenomenon. Later investigators (refs. 4 to 12) were concerned with jets used in conjunction with a trailing-edge flap. Several types of airfoil sections were used in these investigations, but one common feature among them was that all the applications were to moderately thick airfoils. From these previous studies of blowing over airfoils it became apparent that additional experimental data and analytical studies of the effects of blowing were needed to provide the information necessary for practical applications of blowing to airplanes. In particular, experimental data were required to show the effects of blowing over a thin airfoil. A summary and analysis of the existing two-dimensional data were needed to provide a basis for future evaluations of the effects of blowing. Comparatively little information has been published on the many theoretical aspects of blowing over airfoils, and one important aspect in need of study pertains to the manner in which the flow and power parameters vary with changes in the blowing-system pressure, the nozzle exit opening, and the free-stream Mach number.

The present investigation was undertaken to provide some of this needed information. It consists of three phases: (1) an investigation to obtain experimental data for a thin airfoil with blowing over the trailing-edge flap; (2) comparisons of the results of the experimental investigation with the results of previous investigations; and (3) an analytical study to obtain the theoretical relationships among the flow and power parameters for the general blowing case.

The experimental phase of the investigation included a study of the effects of changes in the flap profile, flap position, flap deflection, nozzle height, the air-flow quantities, and, to a limited extent, the ratio of flap chord to wing chord. The constant-chord model had the NACA 0006 profile. It completely spanned the 4-foot dimension of the 4- by 10-foot test section of a modified 7- by 10-foot wind tunnel at Ames Aeronautical Laboratory. The pressure ratios available with the equipment supplying the air for the blowing system were subcritical, resulting, of course, in subsonic jet velocities. However, it was

possible to investigate a range of nozzle heights and nozzle flows of interest for blowing systems which may operate with supercritical pressure ratios and supersonic jet velocities. In reference 13 it was shown that for pressure ratios from subcritical to 2.9, the lift obtained with a given momentum coefficient was independent of the jet Mach number, and the wing Reynolds number in the range from 5.8 to 10.1 million.

In the phase of this investigation concerned with the comparisons and the evaluation of the effects of blowing on lift, only data from pertinent two-dimensional investigations were considered: those obtained with the thin airfoil of the present investigation, and those obtained with the thicker airfoils of references 4, 5, 9, and 12.

The analytical study of the relationships among the air-flow and power parameters is summarized in the form of charts.

NOTATION

A	cross-sectional area, sq ft
a	speed of sound, ft/sec
b	wing span, ft
c	wing chord, ft
c_f	chord of trailing-edge flap, ft
c_l	section lift coefficient, $\frac{l}{q_o c}$
c_m	section pitching-moment coefficient referred to the quarter chord, $\frac{m}{q_o c^2}$
Δc_l	lift-coefficient increment at 0° angle of attack due to blowing and flap deflection
$(\Delta c_l)_i$	lift-coefficient increment at the "ideal" angle of attack due to blowing and flap deflection (see sketch (a), page 12)
$(\Delta c_l)_{th}$	theoretical lift-coefficient increment due to flap deflection
Δc_m	pitching-moment-coefficient increment due to blowing and flap deflection

c_Q section mass-flow coefficient, $\frac{\text{mass-flow rate of blowing air per foot of span}}{\rho_o c V_o}$

c_μ section jet-momentum coefficient, $\frac{\rho_j s V_j^2 + s(p_j - p_o)}{q_o c}$ (p_j assumed equal to p_o except as noted)

C_Q mass-flow coefficient, $\frac{\text{mass-flow rate of blowing air}}{\rho_o S_w V_o}$

C_μ jet-momentum coefficient, $\frac{\rho_j A_j V_j^2 + A_j(p_j - p_o)}{q_o S_w}$ (p_j assumed equal to p_o except as noted), see Appendix A

$C_{1...5}$ coefficients in the equations for wind-tunnel wall corrections

h height of test section, ft

l section lift, lift per unit span, lb/ft

m section pitching moment, pitching moment per unit span, ft-lb/ft

M Mach number, $\frac{V}{a}$

p pressure,[1] lb/sq ft

q dynamic pressure, lb/sq ft

P pressure coefficient, $\frac{p - p_o}{q_o}$

r radius, in., or fraction of wing chord

R Reynolds number based on the wing chord

s height of the nozzle opening measured normal to the wing chord line at the minimum cross-sectional area of the nozzle, ft

s_e height of the nozzle opening at the exit of a convergent-divergent nozzle, ft

S_w the reference wing area affected by the nozzle span, sq ft

t airfoil thickness, ft

[1]When used without subscript t, the symbols p, ρ, and T denote static pressure, static density, and static temperature, respectively.

T	absolute temperature,[2] °R
V	velocity, ft/sec
x	chordwise distance, in. or ft
y	distance normal to the airfoil chord line, in. or ft
x_f, y_f	coordinates for identifying the position of the nose of the trailing-edge flap, percent of wing chord (see fig. 7)
α	section angle of attack, deg
$(\alpha_\delta)_{c_l}$	flap effectiveness parameter, $-\frac{c_{l_\delta}}{c_{l_\alpha}}$
γ	ratio of specific heats, 1.4 for air
δ	angle of deflection of the trailing-edge flap, deg
δ_n	angle of deflection of the nose flap, deg
λ	correction factor for atmospheric conditions different from standard conditions, $\left(\frac{T_a}{T_{std}}\right)^{1/2}\left(\frac{p_a}{p_{std}}\right)$
ρ	mass density of air,[2] slugs/cu ft

Subscripts

a	ambient conditions
i	ideal angle of attack
j	conditions in the jet at the exit of the nozzle
max	maximum
o	free-stream conditions
std	sea-level standard conditions
t	total conditions (i.e., isentropic stagnation conditions)
u	uncorrected

[2]See footnote 1, page 4.

Superscripts

* conditions where $M = 1.0$

EXPERIMENTAL INVESTIGATION WITH A THIN AIRFOIL

Tunnel, Model, and Apparatus

Tunnel.- Because of the limitations of the auxiliary air supply for the Ames 7- by 10-foot wind tunnel, it was necessary to modify the test section of the tunnel to accommodate a model with a reduced span. Figure 1 shows the symmetrically spaced flow dividers which were installed in the tunnel to provide a 4- by 10-foot test section. Each divider extended upstream about 13 feet and downstream 12 feet from the center line of rotation of the model. The 6-foot-diameter aluminum turntables were supported flush with the surfaces of the dividers, as shown in figure 2, and were alined with, and connected to the existing tunnel turntables. Airfoil-shaped fairings were used to shield the model support structure from the air flow between the flow dividers and the original floor and ceiling of the tunnel test section. These fairings had the NACA 65_2-415 airfoil section and a 58.75-inch chord. They were supported from the turntables in the floor and ceiling of the original tunnel and were arranged to change angle of attack with the model. Pressure surveys in the modified test section indicated that the flow between the dividers in the 4- by 10-foot test section was essentially uniform. Calibrated static orifices on the walls of the test section approximately 6 feet upstream from the center line of rotation of the model were used to indicate free-stream static pressure.

Model.- In figure 2, the 4-foot-chord model is shown installed in the modified test section. The basic airfoil section of the model was the NACA 0006, modified to accommodate the nozzle used with the air blowing system and the various trailing-edge flaps. A detailed view of the exit of the nozzle, which extended along the entire span of the model on the upper surface, is shown in figure 3. Some details of the plenum chamber and nozzle shape are shown in figure 4 together with the 15-percent-chord nose flap. The steel plates forming the nozzle could be positioned by means of 19 spacers and tightening screws located at 2-1/2-inch intervals along the span. The ratio of the cross-sectional area of the plenum chamber to the nozzle exit area was large enough to ensure that the velocity of flow in the plenum chamber was negligible with respect to the exiting velocity. (With a nozzle exit height of 0.053 inch, $s/c = 0.00110$, this area ratio was about 20 to 1.)

Details of the trailing-edge flaps are shown in figure 5. Each of the flaps could be deflected and positioned independently of the wing.

A removable fairing which could be inserted in the nozzle exit was used in conjunction with flap A to form the typical single-slotted flap arrangement. (The coordinates for flap A are presented in fig. 4.) The plain flaps were designed to deflect about the hinge points shown in figure 5. Each of these plain flaps was designed so that it faired into the unmodified airfoil contour at about the $x/c = 0.75$ station. Flap B provided the basic shape to which various nose sections were fitted to form flaps C, D, and E. Flap B was symmetrical and was formed by straight lines from the trailing edge tangent to the nose radius of the flap. A comparison of the profiles of flaps A, B, and C for the same flap deflection is shown in figure 6 to emphasize the different flap contours presented to the air exiting from the nozzle. The chord of flap A was 30 percent; flaps B and C were 25-percent chord, and flaps D and E differed slightly from 25 percent, depending on the location of their hinge points. Flap F provided a 15-percent-chord flap based on a total wing chord of 42.35 inches. This reduction in wing chord was a result of shortening the chord of the flap. Thus with flap F, the airfoil section profile deviated from the NACA 0006 profile, the thickness based on the shortened chord was 6.8 percent, and the nose flap was 17 percent of the chord. A filler block and an adjustable plate were attached to the main wing to provide similar wing-flap junctures for all the plain flaps (fig. 5). For all tests with the plain flaps deflected or undeflected, the gap between the end of the adjustable plate and the flap was 0.1 percent of the wing chord.

Chordwise pressure distributions were obtained from three rows of orifices, one row at the midspan, and a row 6 inches from each end of the span. Both static- and total-pressure tubes were installed in the plenum chamber along the span to measure pressures of the internal flow. Temperatures in the plenum chamber were measured by shielded thermocouples at three spanwise stations.

Apparatus.- A variable-speed air compressor located outside of the wind tunnel was used as the source for the compressed air. The maximum pressure ratios (ratio of plenum-chamber pressure to free-stream static pressure) available with this equipment were of the order of 1.7 to 1.8. A section of flexible piping was included in the ducting between the air compressor and the structure supporting the model to prevent any of the forces in the ducting from acting on the scale system. An "O" ring seal was used in the ducting approaching the model so that the angle of attack of the model could be varied without appreciable loss of air from the blowing system. The mass rate of air flow through the ducting was measured by a calibrated orifice meter installed in the line between the seal and the compressor.

Test Methods

Procedure.- Data were obtained for free-stream Reynolds numbers of 2.3, 3.3, and 4.0 million; the corresponding free-stream Mach numbers were 0.082, 0.117, and 0.143. Air flow through the nozzle was varied from zero to the maximum values obtainable with the air compressor, and was expressed in terms of the mass-flow coefficient, c_Q, and the jet-momentum coefficient, c_μ. The rate of air flow measured with the orifice meter was used to calculate the mass-flow coefficient, c_Q. In addition, measurements of the pressure and temperature in the plenum chamber were used to establish the reservoir conditions of the jet flow exiting from the nozzle to calculate the momentum coefficient, c_μ. Isentropic flow from the reservoir conditions in the plenum chamber to the nozzle exit and a static pressure in the jet at the exit equal to free-stream static pressure were assumed in order to calculate the momentum of the measured mass flow leaving the nozzle. Pressure measurements taken along the span in the plenum chamber were nearly equal for all except the lowest operating pressure ratios, and, consequently, it was assumed that the flow ejected from the nozzle was uniform along the span. Because of the limited pressure ratio available, and because of the range of nozzle heights tested, it was necessary to reduce the free-stream velocity from 160 feet per second ($R = 4.0$ million) to 92 feet per second ($R = 2.3$ million) for some tests to cover the range of momentum coefficients of interest. The nozzle-height to wing-chord ratios quoted herein are "effective" values; that is, they were calculated from the isentropic flow relationships by the use of measured values of the pressure ratio, the flow coefficients, (c_Q and c_μ) and the wind-tunnel dynamic pressure for a wide range of flow conditions. These values, in most cases, agreed very well with physical measurements of the nozzle height made with pressure in the nozzle. The effect of the maximum internal pressure forces on the nozzle was to increase the nozzle height by about 0.002 inch ($s/c = 0.00004$). This increase due to the internal pressure forces did not vary with changes in the nozzle-height to wing-chord ratio.

Lift measurements were made with the wind-tunnel balance system for each flap at the various free-stream Reynolds numbers. Data were obtained for each flap deflection with the nose of the flap in various positions relative to the nozzle exit (or, relative to the fairing in the case of the single-slotted flap). These tests, or surveys, as they will be called herein, were made to establish the best position of a flap for purposes of further testing. The nozzle exit was sealed by the fairing for the tests with the single-slotted flap. The selected locations of the nose of the single-slotted flap are shown in figure 7(a) for each of the flap deflections tested. With the other flaps the surveys were made for various blowing conditions. Extensive surveys were made with flap A, and the various selected locations for the nose of the flap are shown in figure 7(b). Three categories of flap position for flap A were arbitrarily established for purposes of discussion: these are the extended,

intermediate, and against-the-nozzle positions indicated in figure 7(b). The reasons for testing the flap in these positions are discussed in a following section (Effect of flap position). Surveys were made with the plain flaps in order to determine the effect of vertical location of the flaps with respect to the jet. In these surveys, the flap was moved longitudinally the small amount required to close the gap between the flap and the nozzle.

Two operating procedures for obtaining the data were employed: First the quantity of air exiting from the nozzle (i.e., c_Q or c_μ) was maintained constant and the angle of attack was varied. Secondly, the angle of attack was maintained constant while the nozzle flow was varied from high values of c_Q or c_μ to zero. The hysterisis effect on the lift coefficient between increasing or decreasing nozzle flows was found to be negligible in the limited, but representative, number of tests conducted to evaluate this effect.

Corrections.- Corrections to the angle of attack, lift, and pitching moment were applied as follows using the method of reference 14:

$$\alpha = \alpha_u + C_1 c_{l_u} + C_2 c_{m_u}$$

$$c_l = C_3 c_{l_u}$$

$$c_m = C_4 c_{m_u} + C_5 c_{l_u}$$

c/h	$R \times 10^{-6}$	C_1	C_2	C_3	C_4	C_5
0.400	2.3	0.301	1.204	0.960	0.993	0.008
	3.3	.302	1.208	.959	.993	.008
	4.0	.303	1.213	.959	.993	.008
0.353	2.3	.234	.938	.968	.993	.006
	3.3	.235	.941	.967	.993	.007
	4.0	.236	.944	.967	.993	.007

With the modified tunnel, the ratio of the wing chord to test-section height was 0.400 for the model with each of the flaps except flap F. In the latter case, the ratio was 0.353. Blockage corrections for the condition with a blowing jet of air are unknown. However, on the basis of the blockage studies presented in reference 12 for a chord to height ratio of 0.32, it was assumed that the blockage was small for the chord to height ratios of the present tests. No further analysis of the change in the wind-tunnel wall corrections due to the effects of a blowing jet was made.

Test Results

The lift data are assembled according to an arbitrary grouping of the flaps, and include data with and without blowing. The data with blowing over the flap are presented in two forms: (1) section lift coefficient as a function of the angle of attack (for a given nose and trailing-edge flap deflection, and for various constant values of the section jet-momentum and the mass-flow coefficients), and (2) the section lift coefficient as a function of the jet-momentum and the mass-flow coefficients (for a given nose and trailing-edge flap deflection and for various angles of attack). Representative moment and midspan pressure-distribution data are presented only for flap A. These typical pressure-distribution data should be of value for flap loading analyses as well as for their general aerodynamic interest. The test data from the investigation are presented in figures 8 through 60. For convenience, an index to these data is presented in table I.

Single-slotted flap.- Data were obtained with the single-slotted flap for comparison with the data obtained with the blowing flaps. Figure 8 presents the test data for various nose flap deflections (for a trailing-edge flap deflection of 50°), from which a nose flap deflection of 30° was selected as optimum for use in further tests of the single-slotted flap without blowing. The basic data for various trailing-edge flap deflections with this nose flap deflection, and also with the nose flap undeflected, are presented in figure 9.

Flap A.- Data showing effects of blowing with both the nose flap and the trailing-edge flap A undeflected are shown in figure 10. A limited amount of data with the nose flap undeflected is presented in figures 11 and 12. Figure 11 shows the effect of deflecting the trailing-edge flap 50° and 60° (in the extended position) without blowing and with a large amount of blowing. Figure 12 shows the effect of various amounts of blowing for one trailing-edge flap deflection ($\delta = 50°$). The effects of deflecting the nose flap are shown in figure 13 for specified blowing quantities and trailing-edge flap deflections. These data were used to select a value for the nose flap deflection for use in the tests with blowing. A value of 35° was considered to be the optimum value and it was used, except as noted, in the tests with blowing. The effects of blowing on the lift coefficients for various trailing-edge flap deflections are shown in figures 14 to 19 with the trailing-edge flap in extended positions (and with the nose flap deflected 35°). Data obtained with the flap against the nozzle and for trailing-edge flap deflections of 50°, 60°, and 70° are presented in figures 20 to 22.

The effects of sealing the wing-flap gap, when the flap was against the nozzle, are presented in figure 23.

An investigation of the effects of changes in the nozzle heights was made with flap A against the nozzle and the data are presented in figures 24 to 29.

In order to obtain some indication of the effect of blowing over various portions of the span of the flap, a brief investigation was made with various spanwise portions of the nozzle blocked off. The data are presented in figure 30.

Plain flaps B, C, D, E, F.- Except for a limited number of tests conducted with flap C with the nose flap undeflected, the tests with the plain flaps were conducted with the nose flap deflected 35°. The effect of deflecting flap B is presented in figure 31 and the effects of blowing are given in figures 32 to 34. Similar data are presented for flaps C and D in figures 35 to 42. Data of this type were not presented for flap E because the flow over the flap at the larger flap deflections was separated even for the highest blowing quantities. The effect of deflecting flap F is presented in figure 43 and the effects of blowing are given in figures 44 to 46.

Pitching moments and pressure distributions with flap A.- Typical changes of the pitching-moment coefficient associated with changes of flap deflection, nozzle height, and blowing quantity are presented in figures 47 to 51. Representative wing-flap pressure distributions at the midspan of the model are given in figures 52 through 59 for flap A in both the extended position and against the nozzle.

Discussion of Test Results

Definitions.- The test results to be discussed are summarized in figures 60 to 63. In the discussion herein of the various effects of blowing over the trailing-edge flap of a thin airfoil, three frequently used quantities are the critical momentum coefficient, the ideal angle of attack, and the increment of lift coefficient at the ideal angle of attack. The critical momentum coefficient is defined as the value of the momentum coefficient at which a large change occurs in the slope $(dc_l/dc_\mu)_{\alpha,\delta}$ and above which only small increases in c_l are obtained with additional increases in c_μ for a constant angle of attack and flap deflection. The critical momentum coefficients presented herein were determined from the data for an angle of attack of 0°. Observations of the pressure distribution over the various flaps indicated, in general, that the flow over the flaps was attached at values of the momentum coefficient that were slightly lower than the critical momentum coefficient as defined herein.

Because of the combined effects of the nose flap, trailing-edge flap, and the blowing quantity on the lift characteristics of a thin airfoil,

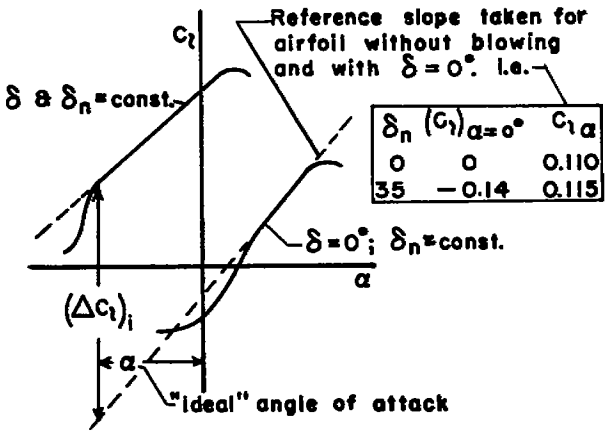

Sketch (a)

difficulty was encountered in selecting an angle of attack suitable for comparing lift increments. In order to resolve this difficulty satisfactorily, the increment of lift coefficient (labeled $(\Delta c_l)_i$ in sketch (a)) was measured at the largest negative angle of attack for which the lift curve was essentially linear. Pressure distributions indicated that at this angle no separation of the flow occurred on the lower surface of the airfoil with the trailing-edge flap deflected. This angle of attack is defined as the "ideal" angle of attack, and the lift increments measured at this angle reveal the effects of changes in the blowing parameters and flap characteristics in a manner that is reasonably independent of interference from other factors. One reason for this is that at the ideal angle of attack the pressure gradient on the upper surface of the forward portion of the airfoil is the most favorable that exists on the airfoil for any angle of attack for which there is no separation from the lower surface. The increment of lift coefficient was measured from the linearly extended lift curve for the model with the trailing-edge flap undeflected and with no blowing. It was necessary to extend this curve because the flow separation from the lower surface of the airfoil near the ideal angle of attack without blowing produced a change in the slope of the lift curve which was otherwise constant for a wide range of angles of attack.

The experimental results are also compared with theoretical lift increments computed by the use of Glauert's relationship for a thin airfoil with a hinged flap (ref. 15), without consideration of the effects of blowing, but corrected for the effects of airfoil thickness ratio

$$(\Delta c_l)_{th} = \frac{-2\pi}{57.3}\left(1 + 0.77\,\frac{t}{c}\right)\left(\alpha_\delta\right)_{c_l}\delta$$

Effect of flap position.- Surveys were made to select the location of each flap for each flap deflection. With the single-slotted flap, the locations of the flap were selected to provide the optimum lift characteristics. Shown in figure 7(a) are the selected locations of the nose of the flap for flap deflections of 40°, 50°, and 60°. It is apparent that the optimum position of the nose of the flap was always below, and near the exit of the slot lip.

The selected locations for the nose of flap A are indicated in figure 7(b) for each of the specified flap deflections. With the flap in the extended positions, the selected locations of the nose were determined from surveys conducted to determine the optimum lift characteristics for a high value of the momentum coefficient. Thus, in figure 7(b), the line connecting the points locating the nose of the flap represents the flap path required to obtain the optimum lift characteristics for a high value of the momentum coefficient. It is worthy of note that for flap deflections of 50° and above, and for the flap in either the extended or against-the-nozzle positions, the nose of the flap always protruded into the jet (see fig. 7(b)). The surveys indicated that at these flap deflections the flow would not remain attached when the flap was removed from the jet. The effect of flap position is evident in the basic lift data (figs. 17 through 22) for the flap in the extended and against-the-nozzle positions. Figure 60 (which includes the small amount of data for the flap in the intermediate positions) presents lift data for 0° angle of attack to provide a more direct comparison of the effect of longitudinal position of the flap. It appears from figure 60 that the rate of change of critical momentum coefficient with increasing distance of the flap from the nozzle exit continually increased. For example, with the flap deflected 60°, moving the flap longitudinally 0.5-percent chord away from the nozzle doubled the critical momentum coefficient, and with the flap in the extended position, the critical momentum coefficient was increased approximately eight times. It can also be seen in figure 60 that the rate of change of the lift coefficient at the critical momentum coefficient with increasing distance of the flap from the nozzle exit was approximately constant.

The surveys with the plain flaps were made to determine the effect of vertical location of the flap with respect to the jet. The data presented in figures 31 through 46 are for the optimum flap positions which showed that the upper surface of the flap should be near the center of the jet. However, the effects of vertical position were found to be small so long as the upper surface of the nose of the flap was in the jet but below the upper surface of the airfoil contour. It should be noted that the hinge points for which the data are presented were shifted slightly from the design hinge points indicated in figure 5; the longitudinal location was closer to the exit of the nozzle and the vertical location was shifted the small amount required to place the nose of the flap near the center line of the jet.

In considering the effects of flap position (and also the effects of flap profile presented in the following section), it should be remembered that in this investigation the velocity at the exit of the nozzle was subsonic and calculated with the assumption of isentropic expansion of the jet flow to free-stream static pressure. With supersonic jet velocities, the question arises as to whether or not it would be desirable for a flap to protrude into the jet. However, consideration of the results of the present investigation which were obtained with subcritical pressure

ratios, and those of reference 13 which were obtained with both subcritical and supercritical pressure ratios, suggests that at least with plain flaps and convergent nozzles, the effects of flap position determined by the present investigation would be the same for pressure ratios up to moderate supercritical values.

Effect of flap profile.- The effects of flap profile are shown in figure 61 in which the lift coefficients at 0° angle of attack are given as a function of both the momentum coefficient and the mass-flow coefficient. A study of the flap profiles (figs. 5 and 6) in conjunction with these data indicates that the profile of the flap was of importance in securing a low critical momentum coefficient, but that the profile was of lesser importance for values of the momentum coefficient larger than the critical value. For a given flap deflection (see fig. 6), the flaps whose profile enabled the exiting nozzle flow to be turned in a gradual manner had a lower critical momentum coefficient than the flap whose profile turned the exiting nozzle flow in an abrupt manner. Although both flaps A and C turned the air in a gradual manner, flap A had a lower critical momentum coefficient than flap C, particularly at the larger flap deflections. This may be due to the more gentle curvature of the profile of flap A compared to flap C (in the region away from the nose of the flaps), and it may also be due to the sharp nose shape of flap A, which projected into the jet close to the exit of the nozzle.

In addition to illustrating the effects of flap profile, the data of figure 61 permit the effect of the ratio of flap chord to wing chord to be estimated. This can be done by a comparison of the data for flap F ($c_f/c = 0.15$) with the data for the other flaps ($c_f/c = 0.25$ to 0.30). As a result of the design criteria for flap F (see the discussion in the section "Model") the profile of the flap was poor, resulting in a high critical momentum coefficient. From the previous discussion of the effects of flap profile it would appear that with a better flap shape, the high critical momentum coefficient could be reduced. However, the important point to note in figure 61 is that at high values of the momentum coefficient, where the effect of the profile has been shown to be of lesser importance, the lift obtained with flap F compares favorably with that obtained with the flaps having larger ratios of flap chord to wing chord. This is evident particularly at the largest flap deflection, $\delta = 70^{\circ}$. Thus, it may be true that, with blowing, the lift is relatively insensitive to the flap-chord ratio.

Effect of changes in nozzle height.- The effect of changes in the ratio of nozzle height to wing chord on the lift increment at the ideal angle of attack as a function of the momentum and the mass-flow coefficients was investigated using flap A in its position against the nozzle. The results are presented for trailing-edge flap deflections of 50° and 60° in figure 62. The large reduction in the mass-flow coefficient, c_Q, with reduction in the nozzle height for a given lift increment is apparent. In the range of nozzle height to wing-chord ratios from 0.00017

to 0.00065, the effects of height-chord ratio on the lift increment for a given momentum coefficient were very small. In the investigation of reference 9 height-chord ratios in a low range (s/c = 0.00036 to 0.00072) were also tested, and the results showed no effect of changes in the nozzle height on the lift increment. Reference 13, which presents the results of a three-dimensional, full-scale investigation of the effects of the blowing air from a duct located in the flap of a swept-wing airplane, also showed that the lift obtained at a given momentum coefficient was independent of the nozzle height for the range of values investigated (ratios of nozzle height to mean aerodynamic chord between 0.00017 and 0.00067).

In the tests of the present investigation, however, an increase in the nozzle-height to wing-chord ratio from 0.00065 to 0.00110 resulted in a considerable loss in the lift increment obtained at momentum coefficients greater than the critical (see fig. 62), but there were no significant effects of nozzle height on the critical momentum coefficient at 0° angle of attack (figs. 20 through 29). Data pertaining to the effects of nozzle height on the increment of lift coefficient obtained from reference 12 are shown in figure 62(c) for values of the height-chord ratio from 0.0005 to 0.009. These results show that increasing s/c from 0.0005 to 0.0015 brought about a much smaller loss in the lift increment than that shown in the present investigation by changing s/c from 0.00065 to 0.00110. The marked effect of nozzle height shown in figure 62(c) for increasing s/c from 0.0015 to 0.0050 is questionable because of changes that were made in the nozzle design and flap location. Since the limited amount of data presented herein indicates that the effects of changes in the nozzle height may depend partially on the particular nozzle and flap configuration used, the results obtained with flap A cannot be considered as general. However, for any particular blowing flap arrangement, the possibility of there being effects of nozzle height must be considered.

Effect of nose flap deflection.- Some of the effects of deflecting the nose flap are contained in the data of figures 12 and 13 for flap A, and in the data of figures 36 and 39 for flap C. The data obtained with the plain flap C were used to show the effects of nose flap deflection on the variation of the lift increment at the ideal angle of attack with momentum coefficient (fig. 63). The principal effect of deflecting the nose flap was to reduce the lift increment at small values of the momentum coefficient without affecting the critical momentum coefficient. As the momentum coefficient was increased, the difference in the lift increment caused by deflecting the nose flap continually decreased, and at values of the momentum coefficient larger than about 0.16, a somewhat larger lift increment was measured with the nose flap deflected than with it undeflected. The greater lift increments with the nose flap deflected were due mostly to a difference in the lift-curve slopes of the base curves which were used in the measurement of the lift increments. This effect of the different lift-curve slopes of the base curves was not

significant at low values of the momentum coefficient because the ideal angles of attack were small. (The base curves were those obtained without blowing, with the trailing-edge flap undeflected, and with the nose flap either undeflected or deflected 35°.)

In the following sections, comparisons will be made with the results of other investigations which employed airfoils having either no leading-edge device, or devices which differed from the nose flap of the present investigation. The data from the present investigation which will be used in the comparisons were obtained with the nose flap deflected. Although this practice resulted in smaller lift increments in the low range of momentum coefficient, it is believed to provide a more realistic comparison because thin airfoils, such as the one of the present investigation, would require some form of leading-edge device to delay leading-edge separation at high angles of attack.

Effect of blowing on the pitching moment and pressure distribution with flap A.- The data of figures 48 and 51(a) typify, for the flap in the extended and against-the-nozzle positions, respectively, the large changes that occur in the pitching moment as the momentum coefficient increases. However, as shown in the following table, the change in the pitching-moment coefficient due to a unit change in the lift coefficient was not significantly affected by blowing over the flap for either position of the flap. The values of the momentum coefficients are larger than the critical momentum coefficient in each instance.

Flap A										
Flap position	Extended						Against the nozzle			
δ	35°		50°		60°		50°		60°	
c_μ	0	0.12	0	0.27	0	0.175	0	0.03	0	0.03
$\frac{\Delta c_m}{\Delta c_l}$	-.20	-.22	-.26	-.22	-.22	-.22	-.19	-.20	-.18	-.19

The very great differences that occur in the pressure distributions for the no-blowing and for the high-quantity blowing cases are clearly shown by the data of figures 52 to 59. When the jet attached to the flap, a low pressure peak developed over the nose of the flap and the pressure coefficient near the trailing edge became positive in value (e.g., see figs. 55 and 58). Note that a positive pressure coefficient on the nose of the flap exceeding a value of 1.0 is indicated in figures 52(b) and (c) for the 75.10-percent-chord station. These high positive pressures on the nose of the flap result from the direct impingement of the jet on the flap and occurred with the flap undeflected or deflected in its position against the nozzle.

COMPARISONS AND EVALUATION OF THE EFFECTS OF BLOWING ON LIFT

The following comparisons of the effects of blowing on lift for the blowing-flap arrangements of the present and the referenced investigations are made in terms of quantities believed to be of most significance for the evaluation of relative flap effectiveness. These quantities are (1) the increment of lift coefficient at the ideal angle of attack, (2) the critical momentum coefficient and the increment of lift coefficient which was obtained at the critical momentum coefficient, (3) the rate of change of increment of lift coefficient with momentum coefficient $(d\Delta c_{l_i}/dc_\mu)_{\alpha_i,\delta}$ for values of the momentum coefficient which were greater than the critical value, and (4) the momentum coefficient required to obtain a lift increment equal to the theoretical increment of lift coefficient due to flap deflection without blowing. These quantities should be considered together, not individually, in order to form a complete picture of the relative lift effectiveness of blowing-flap arrangements. The airfoils of the referenced investigations were thicker than the airfoil of the present investigation and included types with and without leading-edge devices. It should be noted that differences exist in the value of the ratio of flap chord to wing chord for the various flaps of the present investigation as well as for the flaps of the referenced investigations (see fig. 64). Unfortunately, sufficient data are not contained in the reports of these investigations to clearly establish the effects of changes in the ratio of flap chord to wing chord.

Lift-Coefficient Increment at the Ideal Angle of Attack

In comparisons of the lift effectiveness of high-lift devices, the increment of lift coefficient obtained at a given angle of attack is usually presented as a function of the deflection of the device. This convention has been retained for the comparisons presented herein of the various arrangements of the flap and blowing system. However, an additional quantity, the jet-momentum coefficient has been included to show the effects of various amounts of blowing. The data of the present investigation and of references 4, 5, 9, and 12 (see fig. 64 for sketches showing the various arrangements of flaps and blowing-system nozzles) are summarized in this form in figures 65 through 71. The increments of lift coefficient presented herein for the present investigation were measured at the ideal angle of attack. The increments presented for the referenced investigations were measured at 0° angle of attack instead of at the ideal angle of attack because of insufficient data to define the latter angle. However, because the increment at 0° angle of attack was the largest that could be measured, and because it was thought that it would be essentially the same as that increment which would occur at the ideal angle of attack, it was decided for the

purposes of this report to refer to the increment of lift coefficient for the referenced data as $(\Delta c_l)_i$. Included in figures 65 through 71 are theoretical increments of lift coefficient due to flap deflection without blowing and, also, increments which have been obtained with conventional high-lift devices such as single and double slotted flaps. Because of the small amount of published data for these devices on airfoils having the same thickness ratios and the same ratios of flap chord to wing chord as the airfoils considered herein, it is difficult to make comparisons of these devices with all of the blowing-flap arrangements; thus, only data from the present investigation and from references 16 and 17 are considered. Consequently, these data for the single and double slotted flaps were included in these figures only where it was thought that comparisons with the blowing data would have some validity and interest.

The lift-coefficient increments obtained at the ideal angle of attack with the various blowing-flap arrangements on the thin airfoil of the present investigation are shown in figures 65 through 67; those obtained for the airfoils of the investigations of references 5, 9, 4, and 12, for which the airfoil thickness-chord ratios were 9, 10, 12, and 15 percent, respectively, are shown in figures 65 through 71.

It is evident from even a cursory examination of figures 65 through 71 that large differences exist among the various airfoils and blowing-flap arrangements in regard to their response to a given amount of blowing, and that with a sufficient amount of blowing the theoretical increments of lift coefficient were exceeded. A study of these figures reveals that with a given momentum coefficient an increment of lift coefficient could be obtained with the 6-percent-thick airfoil that equaled, or exceeded, the values obtained with the thicker airfoils of the referenced investigations. The data indicate that for some of the configurations additional lift effectiveness could be expected for flap deflections above 60° or 70°. This is particularly evident from the data for the thin airfoil of the present investigation with the small nozzle heights (see figs. 66(a) through 66(d)).

Critical Momentum Coefficient and Increment of Lift Coefficient

Presented in figure 72 is the variation of the critical momentum coefficient with trailing-edge flap deflection for the data from the present investigation and from the referenced investigations. As shown in this figure, the critical momentum coefficient generally increased with increasing flap deflection and with movement of the flap away from the nozzle exit. This increase with flap deflection was small in some cases but very rapid in others. The increase with movement of the flap away from the nozzle exit is shown by comparing the results for flap A in its position against the nozzle and in the extended position. The critical momentum coefficients obtained with flap A in its position

against the nozzle were smaller than those measured for any of the blowing-flap arrangements of the referenced investigations and did not exceed a value of about 0.03 for flap deflections up to 70°.

The increments of lift coefficient obtained at the critical momentum coefficients corresponding to those given in figure 72 are presented in figure 73 together with the theoretical lift increments due to flap deflection without blowing. An inspection of these two figures shows that there were large variations in the critical momentum coefficient and in the lift-coefficient increments measured at the critical momentum coefficient for the various blowing-flap arrangements. The differences between the measured lift increments and their corresponding theoretical lift increments also varied widely. For example, at 60° flap deflection the largest critical momentum coefficient for the data of the present investigation was about eight times greater than the smallest value, and the increments of lift coefficient varied from about 60 to 99 percent of their theoretical values. At first thought it might be expected that such differences in the increments of lift coefficient should not occur because, for the critical momentum coefficient, separation of the flow over the flap was prevented. Control of separation of the flow over the flap, however, is a necessary but not a sufficient condition for attainment of the theoretical lift increment. In addition, the amount of blowing in the experimental case must be controlled to provide a circulation strength around the airfoil equivalent to that of the potential flow solution. Since the amount of blowing required to prevent separation of the flow differed greatly for the various flaps, the circulation strengths, and hence the resulting lift increments, also differ greatly.

It is apparent from the preceding discussion and example that in evaluations of the relative lift effectiveness of blowing-flap arrangements, consideration must be given to both the critical momentum coefficient and to the increment of lift coefficient obtained for the critical momentum coefficient.

Examination of figures 72 and 73 shows, from the results of the present investigation, that the critical momentum coefficient and the associated increment of lift coefficient were unchanged for nozzle-height to wing-chord ratios of 0.00065 or less. They were also unchanged for the height-chord ratios of 0.00036 and 0.00072 which were investigated in reference 9. The data from reference 12 show a large effect of height-chord ratio, and the results obtained with the smallest nozzle heights indicated characteristics that differed from those obtained with the larger ones. It appears, therefore, that the effects of changes in the nozzle-height to wing-chord ratio are small for small values of this ratio (say, for values of s/c less than 0.001), but may be significant for larger values (say, for s/c greater than 0.001).

Rate of Change of Increment of Lift Coefficient With Momentum Coefficient

The rate of change of the increment of lift coefficient with momentum coefficient $(d\Delta c_{l_i}/dc_\mu)_{\alpha_i,\delta}$, measured at values of the momentum coefficient greater than the critical, is presented in figure 74 as a function of flap deflection for the flaps of the present and the reference investigations. A large value of $(d\Delta c_{l_i}/dc_\mu)_{\alpha_i,\delta}$ is, of course, desirable, but the significance of this parameter in assessing relative flap effectiveness depends also upon the critical momentum coefficient and the increment of lift coefficient at the critical momentum coefficient.

The effects of changes in the nozzle-height to wing-chord ratio on $(d\Delta c_{l_i}/dc_\mu)_{\alpha_i,\delta}$ were very small for flap A of the present investigation, but were large for the flap arrangement of reference 12, which had a much larger variation in the nozzle height. A considerably higher slope was measured for flap A in its position against the nozzle compared to that obtained in its extended position. It is of particular interest to note the superiority of plain flap C, which was hinged on the lower surface, compared to plain flap B, which was hinged on the airfoil center line. There was no marked effect of airfoil thickness ratio on $(d\Delta c_{l_i}/dc_\mu)_{\alpha_i,\delta}$ as evidenced by the fact that this parameter was as large, in general, for the various flaps on the thin airfoil of the present investigation as it was for the flaps on the thicker airfoils of the referenced investigations.

Momentum Coefficient for Theoretical Increment of Lift Coefficient

The value of the momentum coefficient required to achieve the theoretical lift increment is presented in figure 75.[3] The accuracy of measuring the momentum coefficient required to achieve the theoretical lift increment depends to a great extent upon the rate of change of the lift increment with momentum coefficient $(d\Delta c_{l_i}/dc_\mu)_{\alpha_i,\delta}$. Although the absolute value of the momentum coefficient in a particular case may be difficult to determine accurately, the values shown in figure 75 were all obtained in a similar manner providing a common basis for comparison.

In general, the values of the momentum coefficient required to attain the theoretical increment of lift coefficient with the 6-percent-thick airfoil were of the same order of magnitude as those measured for

[3]A similar presentation has been noted in reference 18. The larger values of the momentum coefficients presented herein are due to the inclusion of the airfoil thickness correction in computing the theoretical lift increments as previously mentioned.

thicker airfoil sections. In view of the variety of the blowing-flap arrangements considered, the data show very similar trends as a function of flap deflection, with but one exception - the data of reference 5. For this flap it is believed that the long overhang of the upper surface of the nozzle (see fig. 64) and the large distance from the nozzle exit to the flap resulted in a particularly poor blowing-flap arrangement. The advantages of the small nozzle-height to wing-chord ratios are evident from the reference data as well as the data of the present report. The values of the momentum coefficient required for the theoretical lift increment for values of s/c less than 0.00065 were not determined in the tests of the present investigation because of limitations of the available pressure ratio. However, on the basis of an examination of the limited amount of data available, no significant changes in the required momentum coefficient would be expected for the range of values of s/c from 0.00065 to 0.00017.

The data of figure 75 indicate that flap A in the extended position required a smaller momentum coefficient to achieve the theoretical lift increment than it did in its position against the nozzle. In practical applications where the available momentum coefficient may be limited, the small value of the momentum coefficient required to achieve the theoretical lift increment probably would not be as important as the undesirable large value of the critical momentum coefficient that occurs with the flap in the extended position. Flap F had a flap-chord to wing-chord ratio of 0.15 compared with 0.25 to 0.30 for the other flaps considered. Thus, the theoretical lift increment for flap F was smaller than for the other flaps. As previously shown (see fig. 61) the lift coefficients obtained (for momentum coefficients greater than the critical) with flap F compared very favorably with those of the other flaps. This combination of a smaller theoretical lift increment and the relatively good flap effectiveness resulted in a considerably smaller momentum coefficient required to achieve the theoretical lift increment for flap F compared to those of the other flaps of the present investigation. The superiority of plain flap C in this regard compared to plain flap B was due to a larger value of $(d\Delta c_{l_i}/dc_\mu)_{\alpha_i,\delta}$ obtained with flap C, since the critical momentum coefficients and the lift increments at the critical momentum coefficient were practically the same for these two flaps.

THEORETICAL FLOW AND POWER RELATIONSHIPS

Flow Relationships

The basic flow coefficients of interest for a blowing system are the mass-flow coefficient, c_Q, and the jet-momentum coefficient, c_μ. Figures 76 and 77 are presented to show the theoretical relationship among these coefficients and the operating pressure ratio, the ratio of

nozzle height to wing chord (proportional to A_j/S_w for the three-dimensional case), and the free-stream Mach number. Appendix A presents the derivation of the equations upon which the figures are based. The chart of figure 76 is applicable only where the pressure ratio is less than the critical. The chart of figure 77 presents the relationships for pressure ratios as high as 10, based on isentropic flow with an ideal nozzle.

It is to be noted that the definition of the jet-momentum coefficient is based on the assumption that the mass flow leaves the nozzle exit with the velocity that would be obtained by full isentropic expansion to free-stream static pressure. However, it should be realized that the momentum coefficients calculated on this basis do not always represent the true total momentum of the flow at the exit. A difference between the actual and the computed value of the momentum coefficient occurs when the exit pressure is not equal to the free-stream static pressure, or when the pressure ratio is supercritical and differs from the "design" value. The magnitude of the difference which may occur for pressure ratios above the critical is evident from the ratio of the jet-momentum coefficient for a convergent nozzle to that for a convergent-divergent nozzle for isentropic flow. The variation of the ratio of these momentum coefficients with pressure ratio is shown in figure 78 for pressure ratios less than 10. The derivation of the relationship is presented in Appendix A. It is apparent that as the pressure ratio increases, the ratio of the momentum coefficients decreases until, at a pressure ratio of 10, the jet-momentum coefficient that could be obtained with a convergent nozzle is 0.93 of that which could be obtained with a convergent-divergent nozzle.

A unique solution of the two equations shown in figures 76 and 77 is obtained by drawing a rectangle, such as the ones shown in these figures. The rectangle connects equal values of free-stream Mach number in the upper and lower halves of the figure with the corresponding values of c_μ and s/c for the associated values of c_Q and pressure ratio. For a particular solution, two of the parameters, in addition to the Mach number, must be specified.[4] A sequence of changes must occur among the various parameters shown in the figures whenever a change occurs in the value of any one of them. In the following examples the use of the charts is demonstrated. In general, certain changes dependent on the free-stream Mach number must occur in the values of the various parameters if the free-stream Mach number is changed. For example, consider the chart of figure 76 which applies for the range of subcritical pressure ratios. If the momentum coefficient and the nozzle height remain constant and the free-stream Mach number is changed, the mass-flow coefficient remains

[4]The lines of constant dynamic pressure, q_o (figs. 76 and 77), are based on an absolute free-stream total pressure equal to p_{std}, and they would be changed for other free-stream conditions. These lines are included in these figures for their general usefulness in problems concerned with sea-level atmospheric wind tunnels.

constant and the pressure ratio must change. Thus, assume the initial conditions indicated by the dashed rectangle (i.e., $c_\mu = 0.06$; $s/c = 0.0007$; $M_o = 0.10$; $p_{t_j}/p_o = 1.325$; and $c_Q = 0.0047$). Now assume the free-stream Mach number is increased to 0.14. By the process of successive approximations the required rectangle closure yields the results that the pressure ratio would have to increase to 1.73, and c_Q would remain the same. The fact that the mass-flow coefficient is invariant with free-stream Mach number for subcritical pressure ratios and for the conditions typified by this example (i.e., for a constant c_μ and s/c) can be proved by differentiating the equations shown in figure 76. For supercritical pressure ratios the mechanics of solving the equations shown in figure 77 are identical to those indicated above for the subcritical pressure ratios; that is, the required closed rectangle must be determined. With the assumption of the initial conditions indicated by the dashed rectangle in figure 77 ($c_\mu = 0.08$; $s/c = 0.00057$; $M_o = 0.14$; $p_{t_j}/p_o = 2.35$; and $c_Q = 0.0048$), a change in free-stream Mach number to 0.20 increases the pressure ratio to 3.85 and c_Q increases to 0.0053. For the range of supercritical pressure ratios the derivatives of the equations shown in figure 77 indicate that with a given momentum coefficient and nozzle geometry, the mass-flow coefficient will vary with free-stream Mach number. The preceding examples indicate how blowing-system data for particular free-stream Mach numbers can be properly modified and adapted for use at other free-stream Mach numbers.

The inserts in figures 76 and 77 showing typical scale changes are included to indicate the manner in which the range of values of c_μ, c_Q, and s/c can be modified, provided the range of values of free-stream Mach number and the pressure ratio remain the same. With this provision the values of c_μ, c_Q, and s/c can be multiplied or divided by powers of 10 as desired.

Power Relationships

The power required to operate a blowing system can be used as a basis for comparing various arrangements of a flap and blowing system. In Appendix B a power relationship is developed which is convenient for use in such comparisons. The final equation (eq. (B5)) relates the section mass-flow coefficient, free-stream Mach number, and pressure ratio, to the horsepower required per square foot of wing reference area. This horsepower relationship is based on the assumption of isentropic compression from free-stream total pressure to the jet total pressure, and is shown in figures 79 and 80 for pressure ratios up to 1.9 and 10, respectively. It should be noted that the pressure ratio in these figures p_{t_j}/p_{t_o} differs from the pressure ratio, p_{t_j}/p_o which is given in the flow charts. The lines of constant dynamic pressures shown in these figures are subject to the restrictions noted in footnote 4.

As an illustration of the application of the power and the flow charts, a comparison of the horsepower per square foot of wing reference area, the mass-flow coefficients, and the pressure ratios theoretically required at the value of the critical momentum coefficient for several of the arrangements of the flap and blowing system previously discussed is presented in figure 81. The value of the critical momentum coefficient for each arrangement and the corresponding lift increments have been presented in figures 72 and 73, respectively. It is evident from figure 81(a) that at a given Mach number there was a large variation in the power requirements for the various arrangements, and in some cases there were large effects of flap deflection. In general, there was an increase in the power required with an increase in Mach number, and the magnitude of the increase varied greatly among the various arrangements. If the air is provided by auxiliary compressing equipment, the power required is of greatest importance in the design of a blowing system. However, if the air is supplied by bleeding from a jet engine, the mass flow, or c_Q, is the more important quantity (fig. 81(b)). A large variation in the values of the mass-flow coefficients for the various flaps and blowing systems was evident, although for any particular case c_Q was invariant with Mach number. Figure 81(c) shows that the required pressure ratio generally increased with increasing Mach number, and, also, that at a given Mach number there was a large variation among the various arrangements. The advantage, from the standpoints of power and mass-flow coefficient, of positioning the flap against the nozzle and using small nozzle heights is apparent throughout the comparisons afforded by figure 81.

CONCLUDING REMARKS

The present report consists of (1) an experimental investigation made to determine the effects of blowing a jet of comparatively low-pressure air from a duct in the main portion of the wing over various types of trailing-edge flaps on an NACA 0006 airfoil, (2) a comparison and evaluation of the effects of blowing on lift, using the results of the present investigation and those of previous investigations, and (3) an analysis of the theoretical flow and power relationships of a blowing system.

Tests of flap A in various positions with respect to the nozzle showed that (1) the nose of the flap should protrude into the exiting nozzle flow, and (2) the critical momentum coefficient, and the lift obtained at the critical momentum coefficient, decreased as the gap between the flap and the wing was reduced.

Tests of flaps having different profiles indicated that the flaps whose profile enabled the exiting nozzle flow to be turned in a gradual manner had a smaller critical momentum coefficient than the flaps whose profile turned the exiting nozzle flow in an abrupt manner.

The lift obtained with blowing over a 15-percent-chord flap compared favorably with 25- and 30-percent-chord flaps at the higher values of the momentum coefficient. The critical momentum coefficient was large with the short chord flap but it could probably be reduced by changes in the flap profile.

Tests on flap A indicated that the effects of nozzle height on the increment of lift coefficient obtained for a given momentum coefficient were small in the range of nozzle-height to wing-chord ratios from 0.00017 to 0.00065. A further increase in the nozzle-height to wing-chord ratio to 0.00110, however, showed a considerable loss in the lift increment. There were no significant changes in the critical momentum coefficient with changes in the nozzle height.

The change in the pitching-moment coefficient due to a unit change in lift coefficient was not significantly affected by blowing.

Comparison of the data for the thin airfoil of the present investigation with other data for thicker airfoils and somewhat different blowing-flap arrangements showed that (1) the increments of lift coefficient obtained for a given momentum coefficient with the thin airfoil were comparable with, or exceeded, those values obtained with the thicker airfoil sections; (2) flap A positioned against the nozzle had smaller critical momentum coefficients than the flap arrangements used with the thicker airfoils; (3) the rate of change of the increment of lift coefficient with momentum coefficient (measured above the critical value) for the thin airfoil was comparable to that of the thicker airfoils; and (4) the momentum coefficient required to attain the theoretical increment of lift coefficient with the thin airfoil were of the same order of magnitude as those measured for the thicker airfoil sections.

A theoretical study was presented which established the relationship among the air flow and power parameters applicable to the general blowing case. Charts were presented showing these relationships. With the aid of these charts an analysis was made to show the magnitudes of the flow and power parameters for several blowing-flap arrangements operating at their critical momentum coefficients, and also, to show the effect of changes in the free-stream Mach number on these parameters. It was found that the horsepower per square foot of wing reference area, and the pressure ratio, increased with increasing Mach number, but that the mass-flow coefficient remained constant when the pressure ratio was subcritical.

Ames Aeronautical Laboratory
National Advisory Committee for Aeronautics
Moffett Field, Calif., Mar. 1, 1956

APPENDIX A

DERIVATION OF THE EQUATIONS RELATING THE GEOMETRIC AND AIR-FLOW PARAMETERS FOR A BLOWING SYSTEM

In the subsequent development of the various relationships involving the mass-flow coefficient, the jet-momentum coefficient, and the ratio of nozzle area to wing reference area (proportional to s/c for the two-dimensional case), it is assumed that the nozzle flow is for a perfect gas, that the flow is uniform, and that the compression from free-stream total pressure to the jet total pressure is isentropic.

By definition, the jet-mass-flow coefficient is

$$C_Q = \frac{\rho_j A_j V_j}{\rho_o S_w V_o} \tag{A1}$$

For adiabatic flow conditions and for $\gamma = 1.4$, this equation becomes

$$C_Q = \frac{p_j}{p_o}\frac{M_j}{M_o}\frac{A_j}{S_w}\left(\frac{T_{t_o}}{T_{t_j}}\right)^{1/2}\left(\frac{1 + 0.2M_j^2}{1 + 0.2M_o^2}\right)^{1/2} \tag{A2}$$

For the assumption of isentropic compression between the free stream and the jet reservoirs,

$$\left(\frac{T_{t_o}}{T_{t_j}}\right)^{1/2} = \left(\frac{p_{t_o}}{p_{t_j}}\right)^{\frac{\gamma-1}{2\gamma}} \tag{A3}$$

and, in general,

$$p_t = p(1 + 0.2M^2)^{\frac{\gamma}{\gamma-1}} \tag{A4}$$

then the mass-flow coefficient becomes

$$C_Q = \frac{A_j}{S_w}\frac{M_j}{M_o}\left(\frac{p_j}{p_o}\right)^{\frac{\gamma+1}{2\gamma}} \tag{A5}$$

In application, equation (A5) must be modified to suit particular conditions. With an ideal nozzle, complete expansion of the flow occurs to pressure p_o so that $p_j = p_o$. Also, for pressure ratios greater than

critical, the ideal nozzle must be convergent-divergent and for pressure ratios less than critical the nozzle must be convergent. Thus, for an ideal nozzle, and p_{t_j}/p_o greater than critical,

$$C_Q = \frac{A^*}{S_w}\frac{A_j}{A^*}\frac{M_j}{M_o} \tag{A6a}$$

(note that A_j/A^* and M_j are functions of p_{t_j}/p_o and their values are readily obtainable from tables such as those in reference 19). For the two-dimensional case, the section mass-flow coefficient becomes

$$c_Q = \frac{s}{c}\frac{f(p_{t_j}/p_o)}{M_o} \tag{A6b}$$

Also, for the ideal nozzle, and p_{t_j}/p_o less than critical,

$$C_Q = \frac{A_j}{S_w}\frac{M_j}{M_o} \tag{A7a}$$

or, for the two-dimensional case the section mass-flow coefficient is

$$c_Q = \frac{s}{c}\frac{M_j}{M_o} \tag{A7b}$$

With a convergent nozzle and pressure ratios greater than critical, the static pressure in the jet at the exit of the nozzle will not equal the free-stream static pressure ($p_j \neq p_o$), and the Mach number of the jet at the exit of the nozzle will be 1.0. By use of equation (A4) in (A5), the jet-mass-flow coefficient becomes

$$C_Q = \frac{A_j}{S_w}\left(\frac{p_{t_j}}{p_o}\right)^{\frac{\gamma+1}{2\gamma}}\frac{M_j}{M_o}\left[\frac{1}{(1 + 0.2M_j^2)^{\frac{\gamma+1}{2(\gamma-1)}}}\right] \tag{A8a}$$

where $M_j = 1.0$. As would be expected, equations (A6) and (A8a) provide equal values of C_Q at equal values of p_{t_j}/p_o, if A_j/S_w for the convergent nozzle equals A^*/S_w for the convergent-divergent nozzle. For the two-dimensional case the section mass-flow coefficient is

$$c_Q = \frac{s}{c}\left(\frac{p_{t_j}}{p_o}\right)^{6/7} \frac{M_j}{M_o}\left[\frac{1}{(1 + 0.2M_j^2)^3}\right] \tag{A8b}$$

By definition, the jet-momentum coefficient is

$$C_\mu = \frac{\text{total momentum of the flow at nozzle exit}}{q_o S_w}$$

$$= \frac{\rho_j A_j V_j^2}{q_o S_w} + \frac{A_j(p_j - p_o)}{q_o S_w} \tag{A9}$$

with the relationship

$$q_o = \frac{\gamma}{2} p_o M_o^2 \tag{A10}$$

equation (A9) becomes

$$C_\mu = \frac{2}{\gamma M_o^2} \frac{A_j}{S_w}\left[\frac{p_j}{p_o}(1 + \gamma M_j^2) - 1\right] \tag{A11}$$

If the nozzle expansion is to $p_j = p_o$, then for both subcritical and supercritical pressure ratios

$$C_\mu = 2 \frac{M_j^2}{M_o^2} \frac{A_j}{S_w} \tag{A12}$$

Combined with equation (A5), equation (A12) becomes for the case of isentropic flow

$$C_\mu = 2C_Q \frac{M_j}{M_o} \tag{A13a}$$

For the two-dimensional case the section jet-momentum coefficient is

$$c_\mu = 2c_Q \frac{M_j}{M_o} \tag{A13b}$$

By the use of equation (A11) a comparison can be made of the total momentum at the exit of an ideal convergent-divergent nozzle with that at the throat (which would be the total momentum for a convergent nozzle). Thus

$$\frac{C_\mu^*}{C_{\mu_j}} = \frac{A^*}{A_j} \frac{[p_j^*/p_o(1 + \gamma M^{*2}) - 1]}{[p_j/p_o(1 + \gamma M_j^2) - 1]} \tag{A14}$$

In the isentropic case for $p_j = p_o$, and using equation (A4),

$$\frac{C_\mu{}^*}{C_{\mu_j}} = \frac{A^*}{A_j} \frac{\left\{\frac{p_{t_j}{}^*}{p_o}\left[\frac{1+\gamma}{\left(1+\frac{\gamma-1}{2}\right)^{\frac{\gamma}{\gamma-1}}}\right]-1\right\}}{\gamma M_j{}^2} \tag{A15}$$

or

$$\frac{C_\mu{}^*}{C_{\mu_j}} = \frac{A^*}{A_j} \frac{1.268(p_{t_j}{}^*/p_o) - 1}{1.4M_j{}^2} \tag{A16}$$

(Note that $(p_{t_j}{}^*/p_o) = (p_{t_j}/p_o)$, and that both A^*/A_j and M_j are a function of (p_{t_j}/p_o).) Thus, equation (A16) gives the ratio of the total momentum at the exit of a convergent nozzle to that at the exit of an ideal convergent-divergent nozzle having the same throat area as the convergent nozzle.

The charts of figures 76 and 77 present a graphic solution of the equations interrelating the mass-flow coefficient, free-stream Mach number, the momentum coefficient, the ratio of nozzle area to wing reference area (proportional to s/c for the two-dimensional case), and the pressure ratio. For a nonisentropic process between the reservoirs of the free stream and the jet, it is necessary to take into account the changed reservoir conditions of the nozzle flow. It should be noted in connection with these charts that the theoretical momentum of the jet may differ considerably from the actual value. For example, this occurs when the pressure field into which the jet exhausts from the nozzle is less than the free-stream static pressure. Then the nozzle flow is subject to an effect similar to the Coanda effect for a jet exhausting into ambient air; that is, the actual pressure at the exit of the nozzle is reduced below the free-stream static value, thereby increasing the effective pressure ratio. Thus, for pressure ratios less than critical, a reduced nozzle-exit pressure would increase the mass flow and the momentum of the jet above the values that would be computed for a pressure ratio based on the free-stream static pressure. For pressure ratios above the critical there would be no effect on the mass flow, but the momentum of the jet would increase with an increase in the exit velocity. For pressure ratios less than critical the local pressure field at the exit of the nozzle is usually unknown, or difficult to obtain, so that it is much more convenient to base the momentum coefficient on the free-stream static condition; this was the case in the present report. For pressure ratios above the critical the local pressure field should only have a small effect on the over-all pressure ratio. However, as equation (A16) indicates, the momentum of the jet will depend on the nozzle design. Thus, particularly at pressure ratios much greater than critical, the computation of the momentum coefficient should be in accordance with whether the nozzle is convergent, or convergent-divergent.

APPENDIX B

DERIVATION OF THE POWER REQUIRED TO COMPRESS THE AIR FOR A BLOWING SYSTEM

In a steady-flow process the power required to maintain the flow is defined as the product of the mass flow and the work done per unit of mass flow. For isentropic flow relationships the horsepower required to compress the blowing-system air from free-stream total pressure to the jet total pressure is

$$hp = \frac{\rho_j A_j V_j}{550}\left\{\frac{\gamma}{\gamma - 1}\frac{p_{t_j}}{\rho_{t_j}}\left[1 - \left(\frac{p_{t_o}}{p_{t_j}}\right)^{\frac{\gamma-1}{\gamma}}\right]\right\} \tag{B1}$$

Substituting equation (A1) into (B1) and expressing the velocities and densities in terms of Mach number, total pressure, total temperature, and stagnation velocities of sound yields the following equation for the horsepower per square foot of wing reference area expressed in terms of the section mass-flow coefficient

$$\frac{hp}{S_w} = \frac{c_Q}{550}\frac{\gamma}{\gamma - 1}\frac{M_o}{(1 + 0.2M_o^2)^3}a_{std}\left(\frac{a_{t_o}}{a_{std}}\right)\left(\frac{p_{t_o}}{p_{t_j}}\right)\left(\frac{T_{t_j}}{T_{t_o}}\right)p_{t_j}\left[1 - \left(\frac{p_{t_o}}{p_{t_j}}\right)^{\frac{\gamma-1}{\gamma}}\right] \tag{B2}$$

With equation (A3), and noting that $(a_{t_o}/a_{std}) = (T_{t_o}/T_{std})^{1/2}$ equation (B2) becomes

$$\frac{hp}{S_w} = \frac{c_Q}{550}\frac{\gamma}{\gamma - 1}\frac{M_o}{(1 + 0.2M_o^2)^3}a_{std}\left(\frac{T_{t_o}}{T_{std}}\right)^{1/2}\left(\frac{p_{t_o}}{p_{t_j}}\right)^{1/\gamma}p_{t_j}\left[1 - \left(\frac{p_{t_o}}{p_{t_j}}\right)^{\frac{\gamma-1}{\gamma}}\right] \tag{B3}$$

Regrouping the terms to provide the pressure ratio p_{t_j}/p_{t_o} within the bracketed expression gives

$$\frac{hp}{S_w} = \frac{c_Q}{550}a_{std}p_{std}\frac{\gamma}{\gamma - 1}\frac{M_o}{(1 + 0.2M_o^2)^3}\left[\left(\frac{T_{t_o}}{T_{std}}\right)^{1/2}\left(\frac{p_{t_o}}{p_{std}}\right)\right]\left[\left(\frac{p_{t_j}}{p_{t_o}}\right)^{\frac{\gamma-1}{\gamma}} - 1\right] \tag{B4}$$

Equation (B4) is applicable for use in flight or atmospheric wind tunnels. However, the total-temperature ratio and the total-pressure ratio must be

evaluated differently in each application. If λ is a correction factor for ambient or atmospheric conditions differing from standard,

$$\lambda = \left[\left(\frac{T_a}{T_{std}}\right)^{1/2}\left(\frac{p_a}{p_{std}}\right)\right]$$

and by the use of the approximation that $(1 + 0.2M_o^2) = 1.0$ in equation (B4), the corrected horsepower per square foot of wing area becomes

$$\frac{hp}{\lambda S_w} = \frac{c_Q}{550} a_{std} p_{std} \frac{\gamma}{\gamma - 1} M_o \left[\left(\frac{p_{t_j}}{p_{t_o}}\right)^{\frac{\gamma-1}{\gamma}} - 1\right] \tag{B5}$$

A graphical solution of this equation is presented as figures 79 and 80. With the assumption that the Mach number function equals 1.0 there results a maximum error in the horsepower per square foot of wing area of about 1 and 3 percent for pressure ratios up to 10 for the flight, and for the wind-tunnel solutions, respectively. It will be noticed that the total-pressure ratio in equation (B5) $\left(p_{t_j}/p_{t_o}\right)^{\frac{\gamma-1}{\gamma}}$ could be put in the form $\left(p_{t_j}/p_o\right)^{\frac{\gamma-1}{\gamma}} [1/(1 + 0.2M_o^2]$, but in this case the assumption that $(1 + 0.2M_o^2) = 1.0$ results in increasingly large errors as the pressure ratio approaches 1.0. Thus, in using figures 79 or 80 to find the horsepower function, the total-pressure ratio p_{t_j}/p_{t_o} must be used. The flow charts of figures 76 and 77 give the pressure ratio in terms of p_{t_j}/p_o, which must be multiplied by p_o/p_{t_o} for the given Mach number to find p_{t_j}/p_{t_o} for use with the horsepower charts. The constant "q" lines on these power charts are restricted to wind-tunnel usage for the same reasons discussed in footnote 4 in regard to the flow charts.

REFERENCES

1. Seewald, F.: Increasing Lift by Releasing Compressed Air on Suction Side of Airfoil. NACA TM 441, 1927.

2. Reid, E. G., and Bamber, M. J.: Preliminary Investigation on Boundary Layer Control by Means of Suction and Pressure with the U.S.A. 27 Airfoil. NACA TN 286, 1928.

3. Wieland, K.: Experiments With a Wing From Which the Boundary Layer is Removed by Pressure or Suction. NACA TM 472, 1928.

4. Schwier, W.: Lift Increase by Blowing Out Air, Tests on Airfoil of 12-Percent Thickness, Using Various Types of Flap. NACA TM 1148, 1947.

5. Schwier, W.: Lift Increase Produced by Blowing a Wing of a Profile Thickness of 9 Percent, Equipped With a Slat and a Slotted Flap. Rep. No. F-TS-645-RE, Air Materiel Command Trans., Aug. 1946.

6. Boyer, Luther J.: Preliminary Investigation and Evaluation of the Coanda Effect. Tech Rep. No. F-TR-2207-ND, Air Materiel Command, Aug. 1948.

7. Nunemaker, John J., and Fisher, Jack W.: Two-Dimensional Wind Tunnel Investigation of Boundary-Layer Control by Blowing on an NACA 23015 Airfoil. Rep. No. 023, Municipal Univ. of Wichita Engr., Apr. 1950.

8. Rebuffet, P., and Poisson-Quinton, Ph.: Investigations of the Boundary-Layer Control on a Full Scale Swept Wing With Air Bled Off from the Turbojet. NACA TM 1331, 1952.

9. Harkleroad, E. L., and Murphy, R. D.: Two-Dimensional Wind-Tunnel Tests of a Model of an F9F-5 Airplane Wing Section Using a High-Speed Jet Blowing over the Flap; Part I - Tests of a 6-Foot Chord Model. Aero. Rep. 845, David W. Taylor Model Basin, May 1953.

10. Goldsmith, John: Boundary Layer Control for Various Modifications of Sweptback Wings. Rep. R-15037-5, East Hartford Research Dept., United Aircraft Co. Sept. 16, 1948.

11. Attinello, John S.: The Supersonic Blowing Jet for Wing-Lift Augmentation. Rep. No. DR-1706, Navy Dept. Res. Div., Oct. 1954.

12. Wallace, Richard E., and Stalter, J. L.: Systematic, Two-Dimensional Tests of an NACA 23015 Airfoil Section With a Single-Slotted Flap and Circulation Control. Aero. Rep. 120, Municipal University of Wichita, Aug. 1954.

13. Kelly, Mark W., and Tolhurst, William H., Jr.: Full-Scale Wind-Tunnel Tests of a 35° Sweptback Wing Airplane With High Velocity Blowing Over the Trailing-Edge Flaps. NACA RM A55I09, 1955.

14. Allen, Julian H., and Vincenti, Walter G.: Wall Interference in a Two-Dimensional-Flow Wind Tunnel With the Consideration of the Effect of Compressibility. NACA Rep. 782, 1944.

15. Ames, Milton B., Jr., and Sears, Richard I.: Determination of Control-Surface Characteristics from NACA Plain-Flap and Tab Data. NACA Rep. 721, 1941.

16. Kelly, John A., and Hayter, Nora-Lee F.: Lift and Pitching Moment at Low Speeds of the NACA 64A010 Airfoil Section Equipped With Various Combinations of a Leading-Edge Slat, Leading-Edge Flap, Split Flap, and Double-Slotted Flap. NACA TN 3007, 1953.

17. Wenzinger, Carl J., and Harris, Thomas A.: Wind-Tunnel Investigation of an NACA 23012 Airfoil With Various Arrangements of Slotted Flaps. NACA Rep. 664, 1939.

18. Williams, J.: An Analysis of Aerodynamic Data on Blowing Over Trailing Edge Flaps for Increasing Lift. Rep. No. 17,027, British A.R.C. Performance Sub-Committee, Sept. 6, 1954.

19. Ames Research Staff: Equations, Tables, and Charts for Compressible Flow. NACA Rep. 1135, 1953

TABLE I.- INDEX TO THE DATA FOR THE NACA 0006 AIRFOIL SECTION

Configuration					Results presented	Figure No.
Flap	Flap position	δ, deg	δ_n, deg	s/c		
Single slotted	See fig. 7(a)	50	Variable	---	c_l vs. α	8
		Variable	0, 30			9
A	---	0	---	0.00110		10
	Extended See fig. 7(b)	Variable	0			11
		50				12(a)
					c_l vs. c_Q, c_μ	12(b)
			Variable		c_l vs. α	13(a)
		60				13(b)
		0	35			14
		20				15
		35				16
		50				17(a)
					c_l vs. c_Q, c_μ	17(b)
		60			c_l vs. α	18(a)
					c_l vs. c_Q, c_μ	18(b)
		65			c_l vs. α	19
	Against nozzle. See fig. 7(b)	50				20(a)
					c_l vs. c_Q, c_μ	20(b)
		60			c_l vs. α	21(a)
					c_l vs. c_Q, c_μ	21(b)
		70			c_l vs. α	22(a)
					c_l vs. c_Q, c_μ	22(b)
	Against nozzle; slot sealed.	60			c_l vs. α	23(a)
					c_l vs. c_Q, c_μ	23(b)
	Against nozzle.	50		.00065	c_l vs. α	24(a)
					c_l vs. c_Q, c_μ	24(b)
		60			c_l vs. α	25
		50		.00036		26
		60				27
		50		.00017		28
				.00017		29
		60		.00017 (Partial span)		30
				.00110		31
B	---	Variable				32
		50				33(a)
		60			c_l vs. c_Q, c_μ	33(b)
					c_l vs. α	34
		70				35
C		Variable				36
		50				37(a)
		60			c_l vs. c_Q, c_μ	37(b)
					c_l vs. α	38
		70				39(a,b)
D		50	0			40
			35			41(a)
		60			c_l vs. c_Q, c_μ	41(b)
					c_l vs. α	42
		70				43
F		Variable				44
		50				45(a)
		60			c_l vs. c_Q, c_μ	45(b)
		70			c_l vs. α	46

Configuration					Results presented	Figure No.
Flap	Flap position	δ, deg	δ_n, deg	s/c		
A	Extended	Variable	35	0.00110	c_l vs. c_m $c_\mu = 0$	47(a)
					$c_\mu = 0.120$	47(b)
					$c_\mu = 0.270$	47(c)
		60			c_l vs. c_m c_μ = variable	48
	Against nozzle.	Variable			c_l vs. c_m $c_\mu = 0$	49(a)
					$c_\mu \cong 0.03$	49(b)
				0.00065	c_l vs. c_m $c_\mu \cong 0.03$	50(a)
				.00036		50(b)
						50(c)
				.00017	c_l vs. c_m c_μ = variable	51(a) to (d)
	---	0	0	.00110	P vs. percent c $c_\mu = 0$	52(a)
					P vs. percent c $c_\mu = 0.117$	52(b)
					P vs. percent c $c_\mu = 0.273$	52(c)
			35		P vs. percent c $c_\mu = 0$	53(a)
					P vs. percent c $c_\mu = 0.265$	53(b)
	Extended	35			P vs. percent c $c_\mu = 0$	54(a)
					P vs. percent c $c_\mu = 0.05$	54(b)
					P vs. percent c $c_\mu = 0.270$	54(c)
		50			P vs. percent c $c_\mu = 0$	55(a)
					P vs. percent c $c_\mu = 0.097$	55(b)
					P vs. percent c $c_\mu = 0.274$	55(c)
		60			P vs. percent c $c_\mu = 0$	56(a)
					P vs. percent c $c_\mu = 0.101$	56(b)
					P vs. percent c $c_\mu = 0.276$	56(c)
		50			P vs. percent c c_μ = variable	57(a) to (c)
	Against nozzle.				P vs. percent c $c_\mu = 0$	58(a)
					P vs. percent c $c_\mu = 0.110$	58(b)
					P vs. percent c $c_\mu = 0.066$	58(c)
					P vs. percent c $c_\mu = 0.160$	58(d)
		60			P vs. percent c $c_\mu = 0$	59(a)
					P vs. percent c $c_\mu = 0.015$	59(b)
					P vs. percent c $c_\mu = 0.060$	59(c)
					P vs. percent c $c_\mu = 0.246$	59(d)
	Variable	50			$c_{l(\alpha=0)}$ vs. c_m	60(a)
		60				60(b)

[redacted]

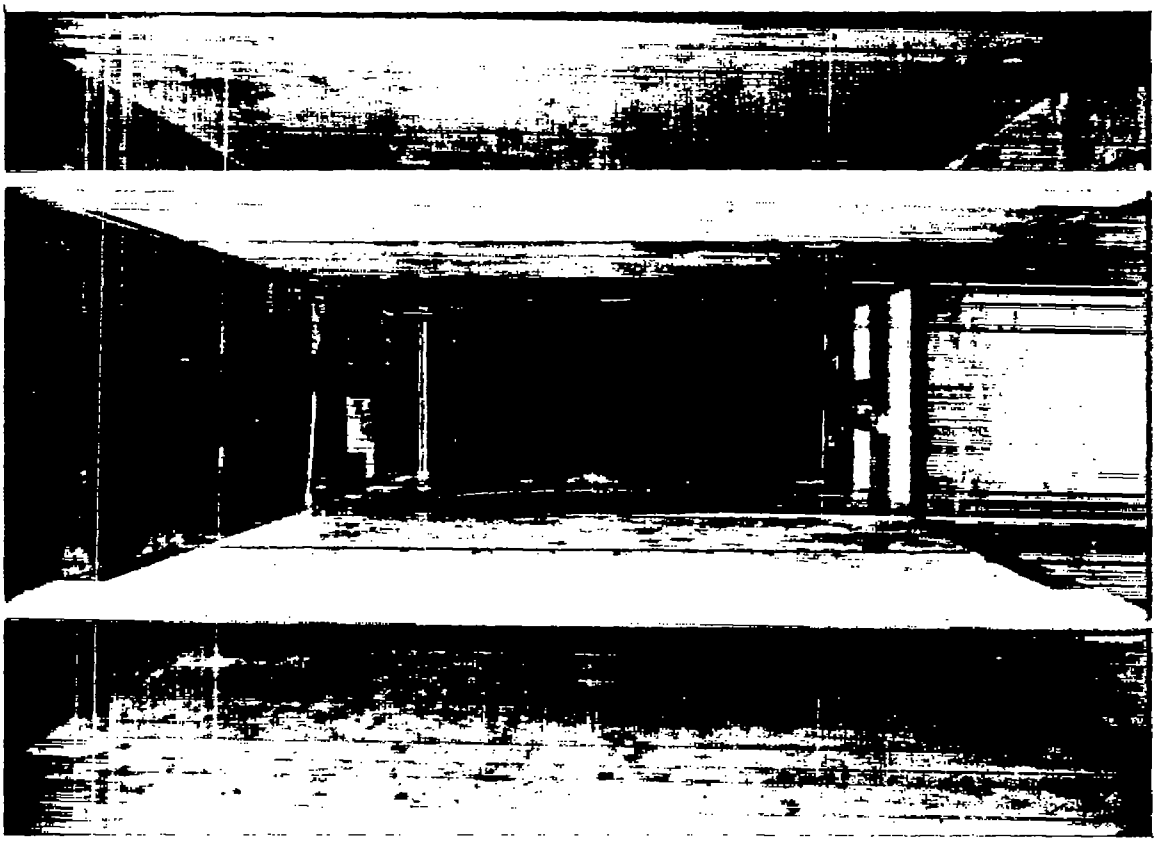

A-19240

Figure 1.- The horizontal dividers installed in the 7- by 10-foot wind tunnel to provide a 4- by 10 foot test section; view downstream.

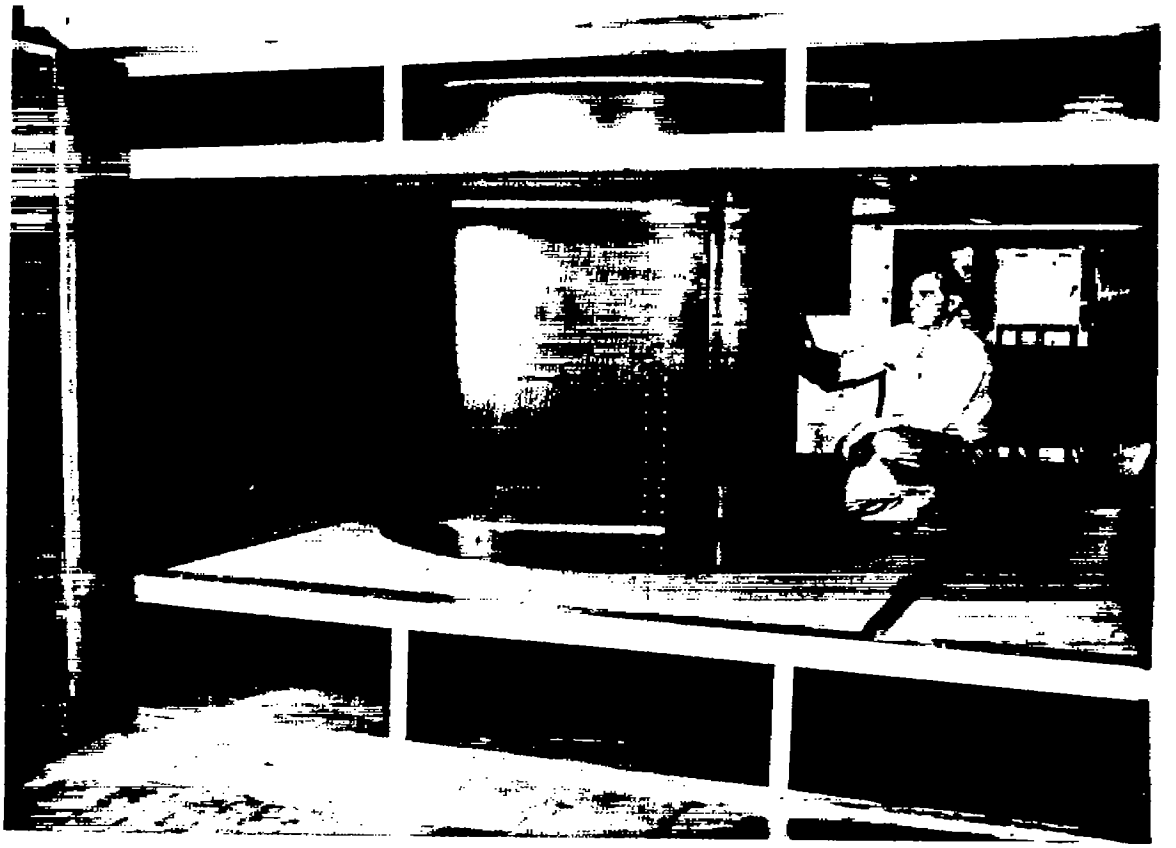

A-19300

Figure 2.- The model installed in the 4- by 10-foot test section.

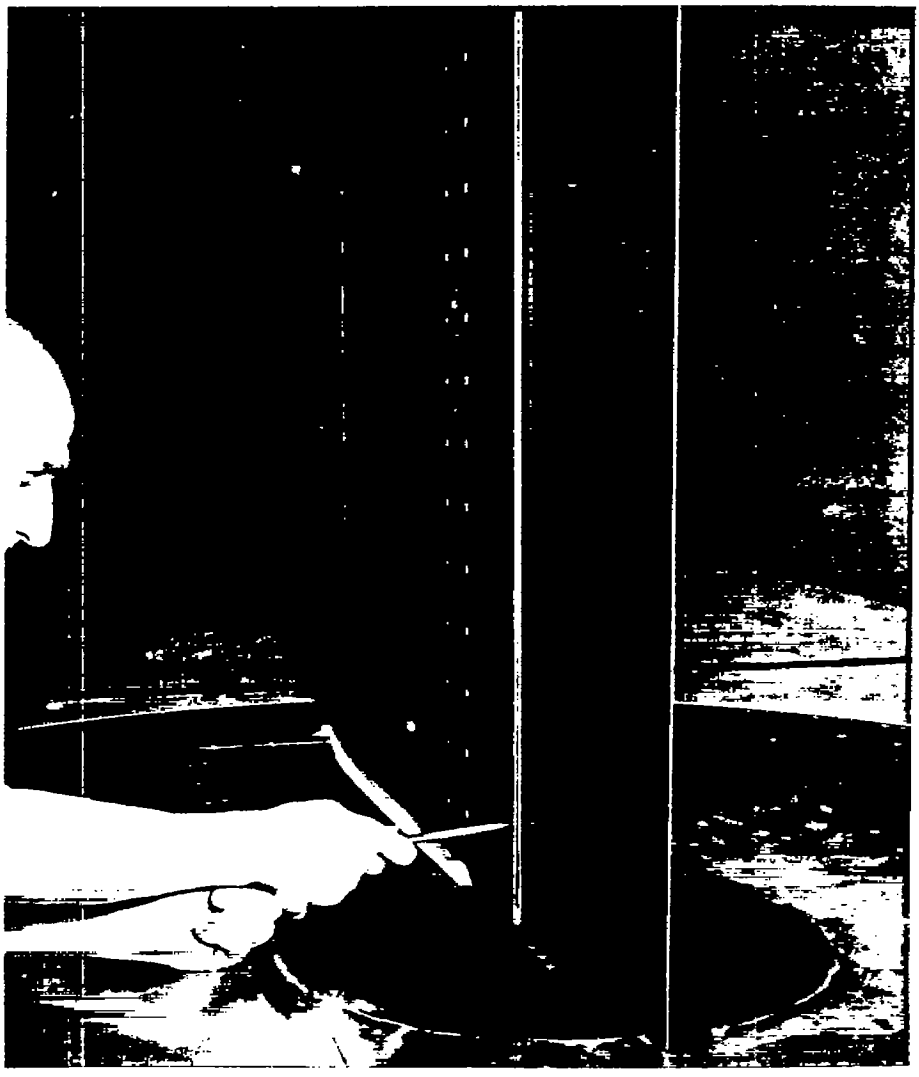

A-19301

Figure 3.- A detailed view of the model with flap A showing the exit of the nozzle.

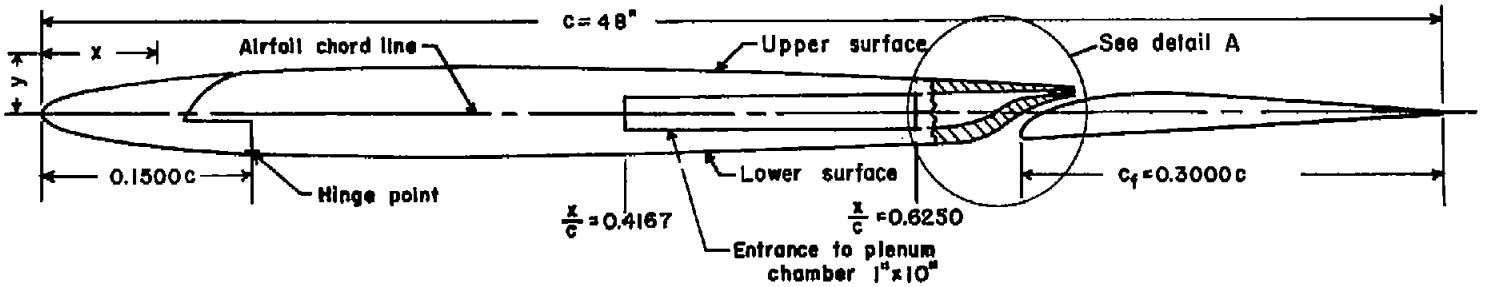

FLAP COORDINATES (Percent flap chord)			
Upper		Lower	
Sta.	Ord.	Sta.	Ord.
0	--	0	--
0.77	-3.30	0.69	-5.63
2.62	-1.75	1.39	-5.87
5.17	-0.27	2.08	-5.96
7.71	0.83	2.78	-5.97
10.27	1.74	17.70	-5.20
15.30	3.19	33.33	-4.38
20.34	4.05	66.65	-2.42
25.34	4.46	83.35	-1.34
30.34	4.51	100.00	-0.21
33.33	4.38		
66.65	2.42		
83.35	1.34		
100.00	0.21		
L.E.R. = 0.89			
Center of radius at			
Sta. 0.83; Ord. -4.59			

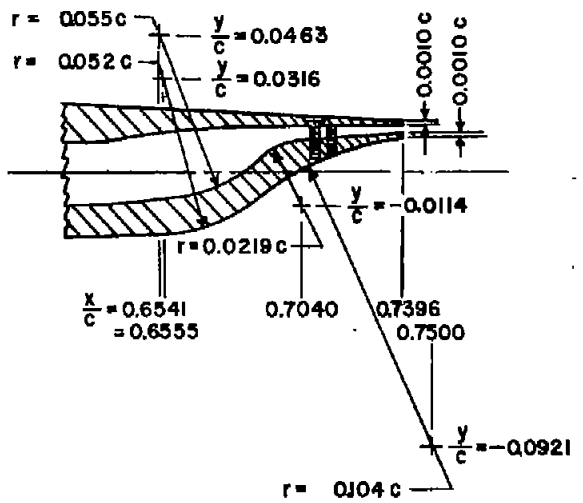

Detail A

Figure 4.- The NACA 0006 airfoil showing the 30-percent-chord flap A, the 15-percent-chord leading-edge flap, and the nozzle details.

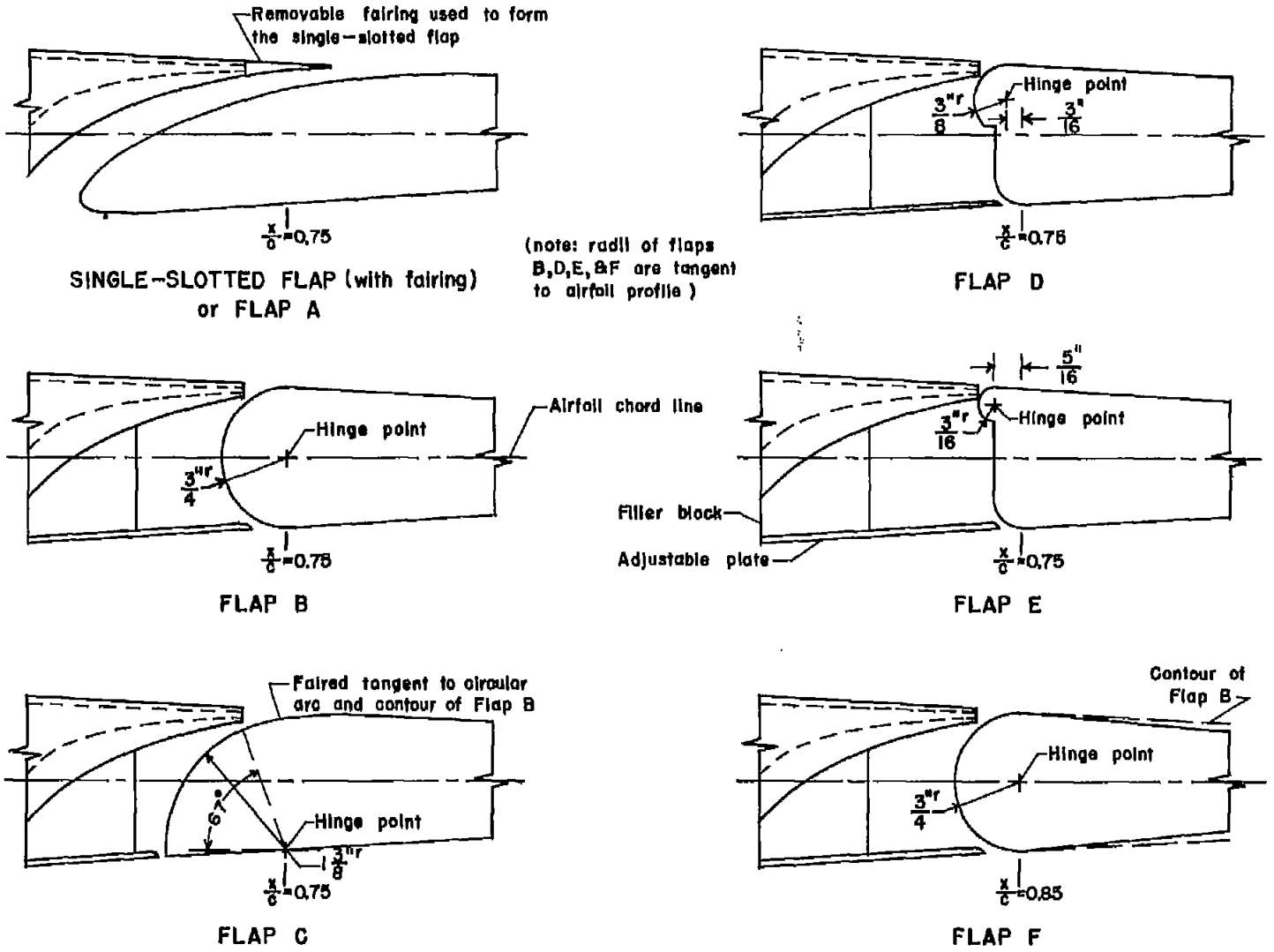

Figure 5.- The various flap configurations tested.

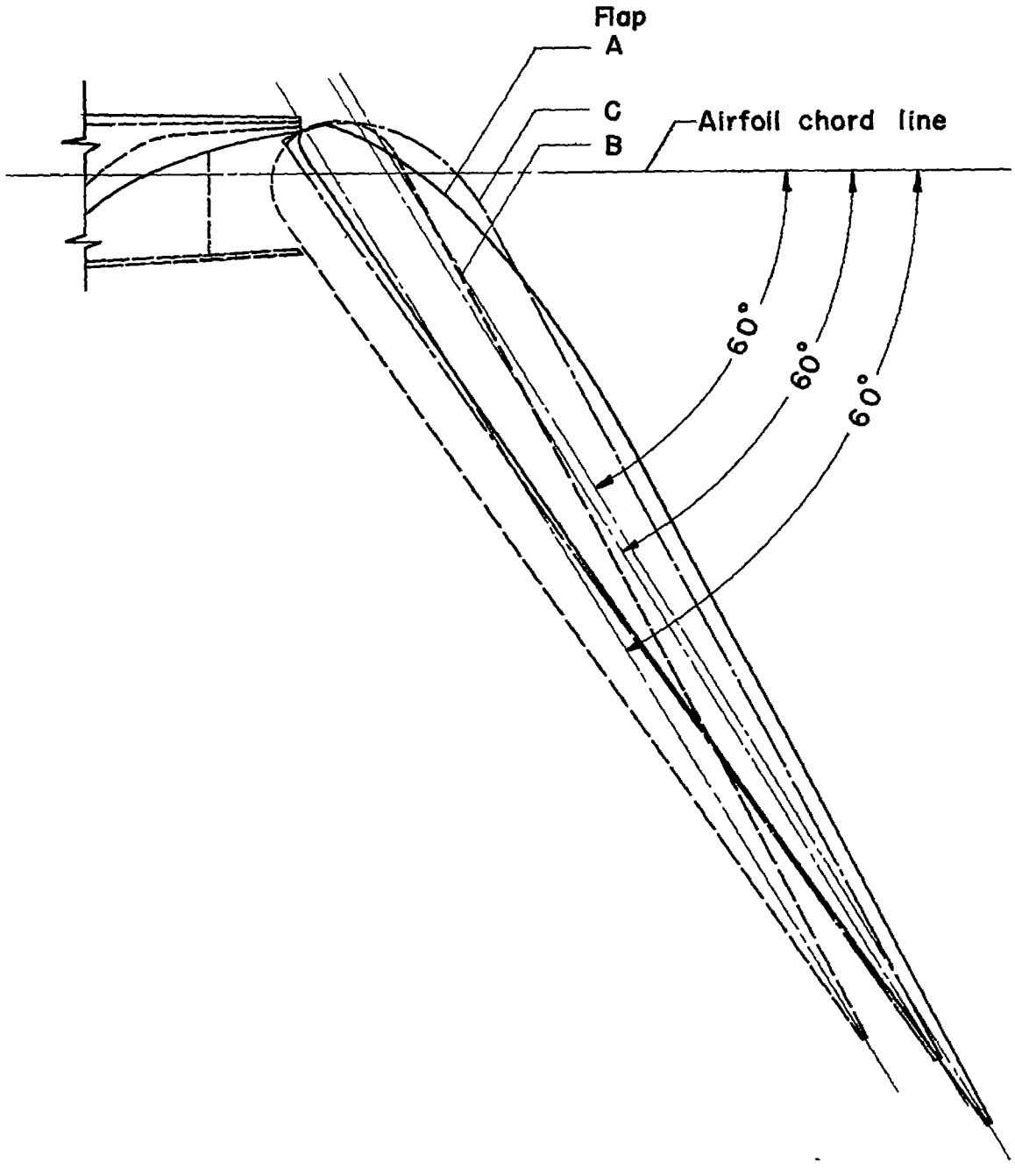

Figure 6.- Sketch of flaps A, B, and C deflected 60°.

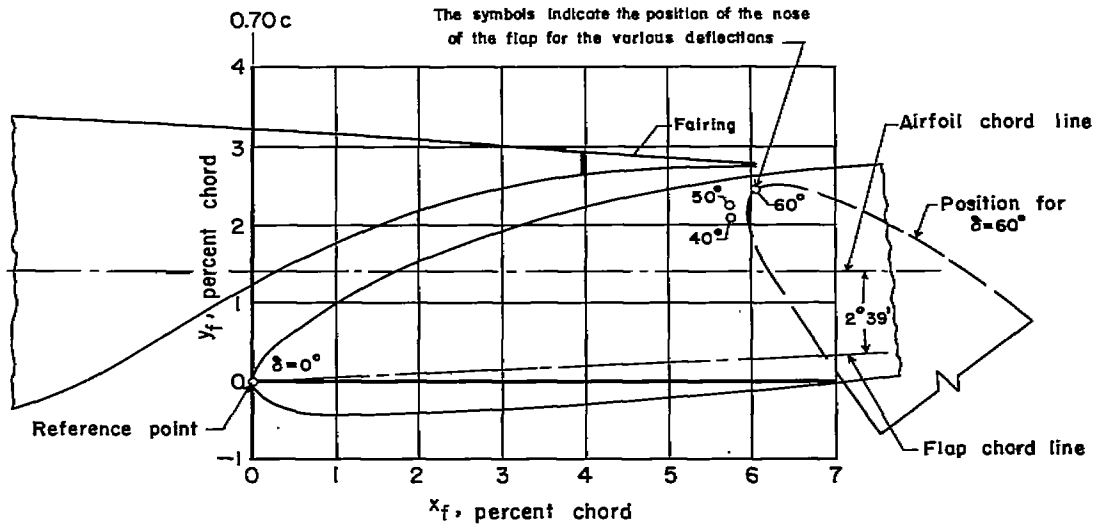

(a) Single-slotted flap.

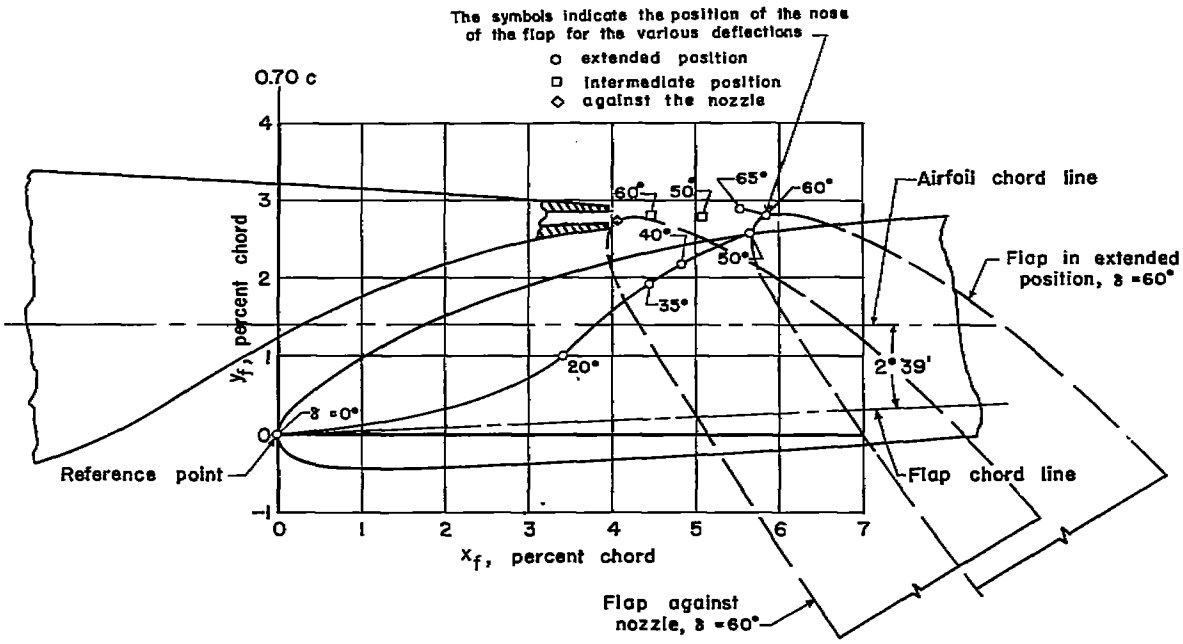

(b) Flap A.

Figure 7.- The selected locations of the nose of the single-slotted flap and of flap A for various flap deflections.

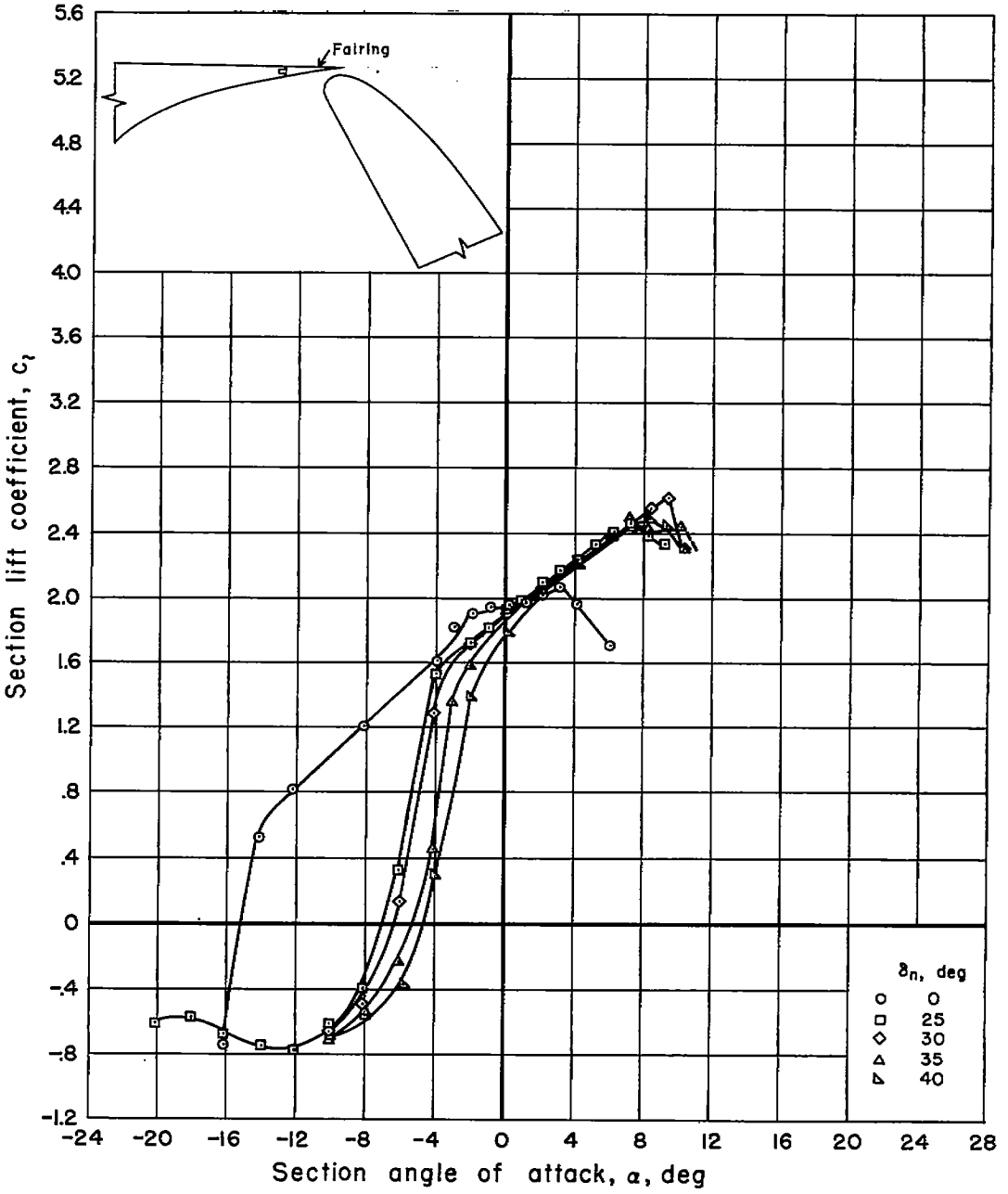

Figure 8.- Effect of nose-flap deflection on the lift of the model with the single-slotted flap deflected 50°; R = 4.0×10^6.

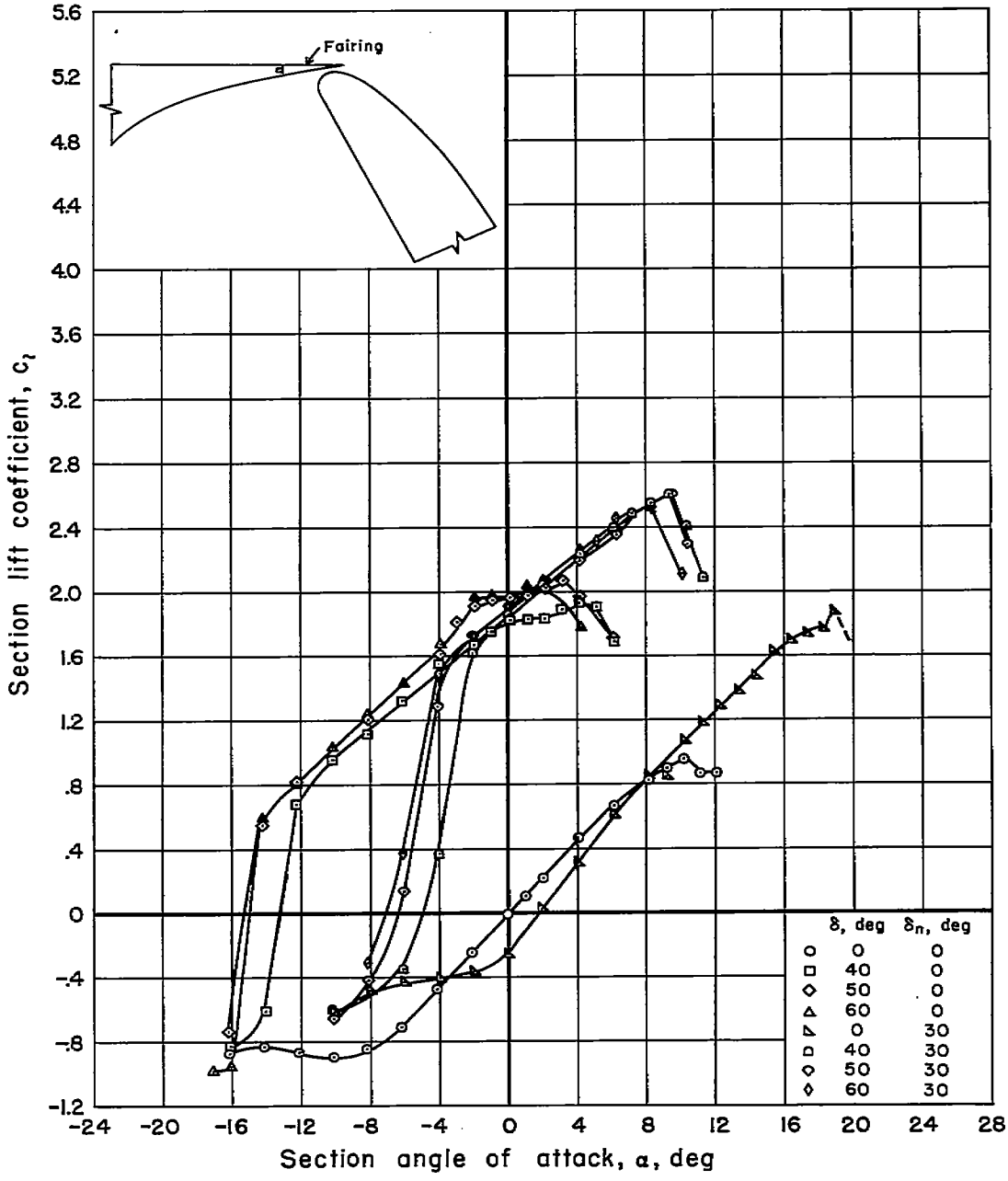

Figure 9.- Effect of slotted-flap deflection on the lift of the model with the nose flap deflected 0° and 30°; R = 4.0×10^6.

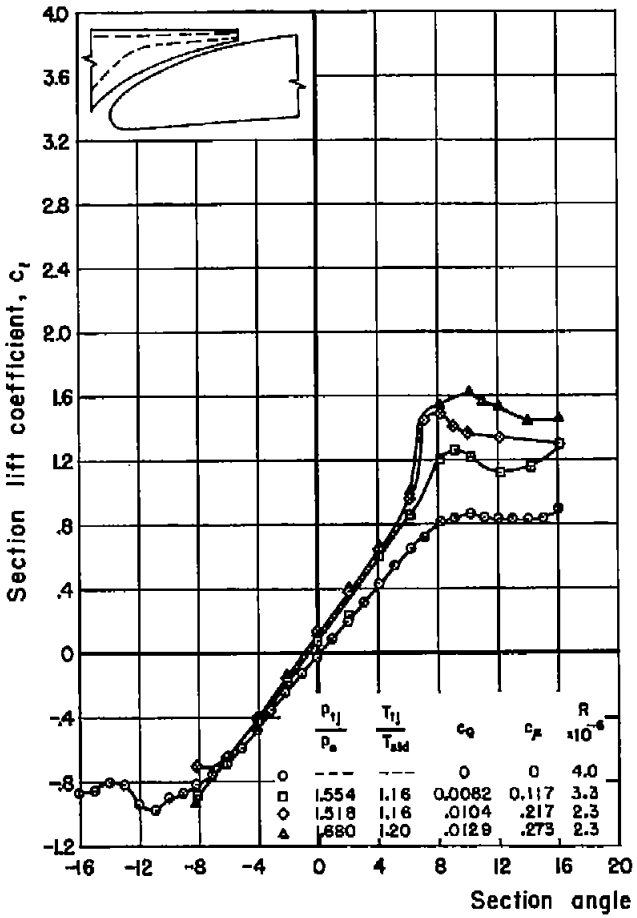

Figure 10.- Effect of blowing on the lift of the model with flap A undeflected; $s/c = 0.00110$; $\delta_n = 0^{\circ}$.

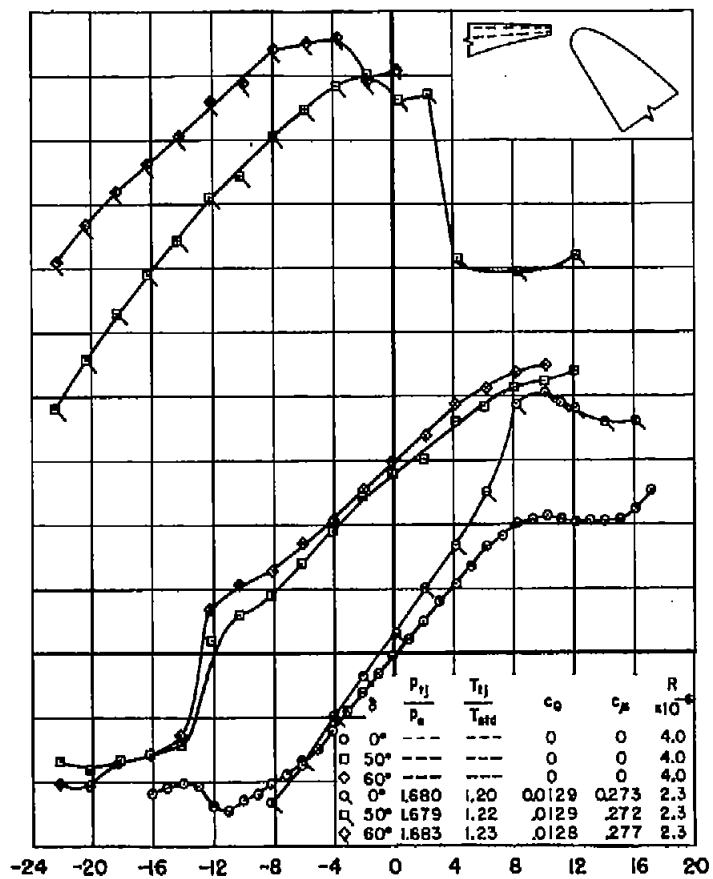

Figure 11.- Effect of trailing-edge flap deflection on the lift of the model with flap A in the extended position with and without blowing; $s/c = 0.00110$; $\delta_n = 0^{\circ}$.

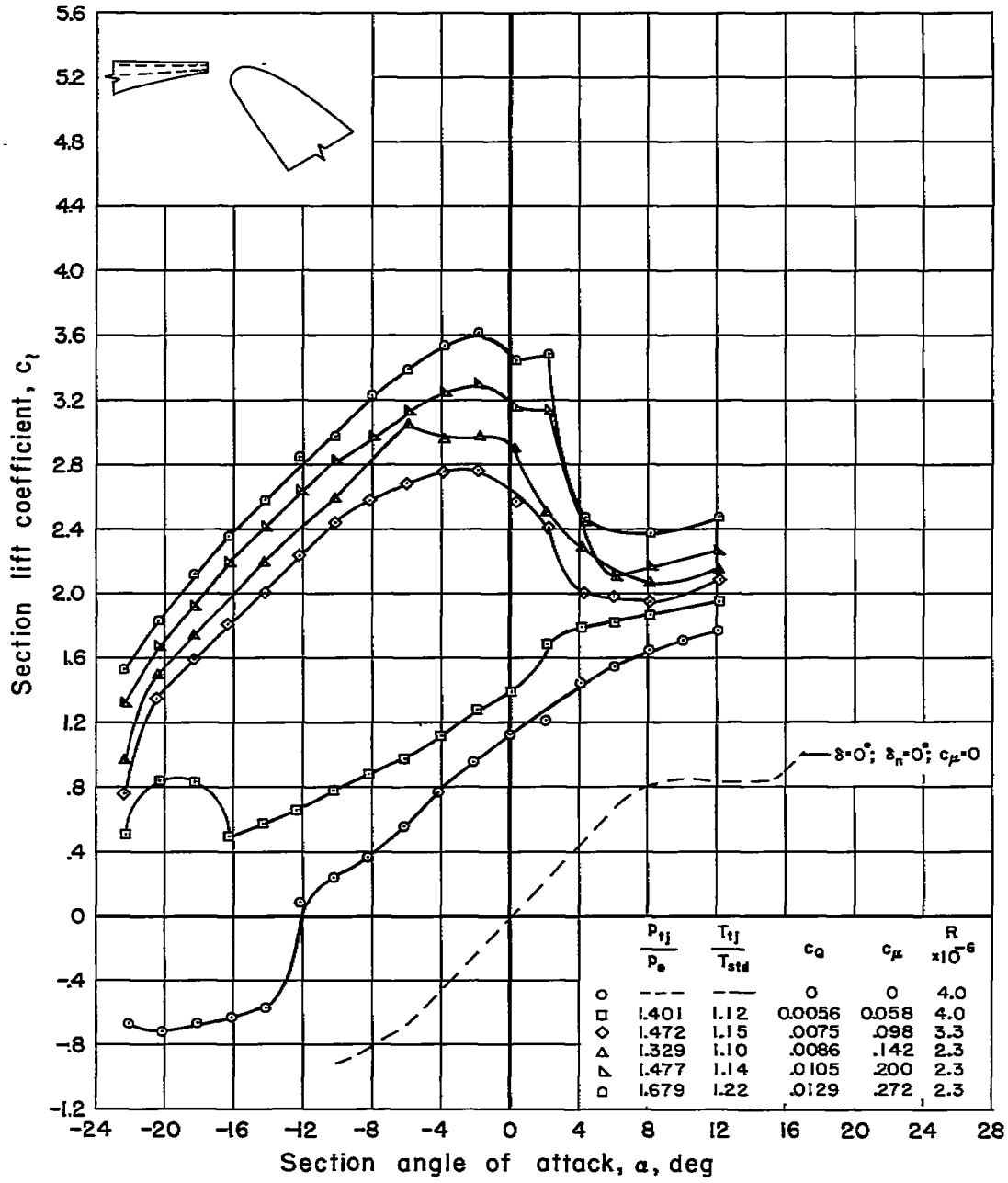

(a) Variable α.

Figure 12.- Effect of blowing on the lift of the model with flap A in the extended position; s/c = 0.00110; δ = 50°; δ_n = 0°.

[redacted]

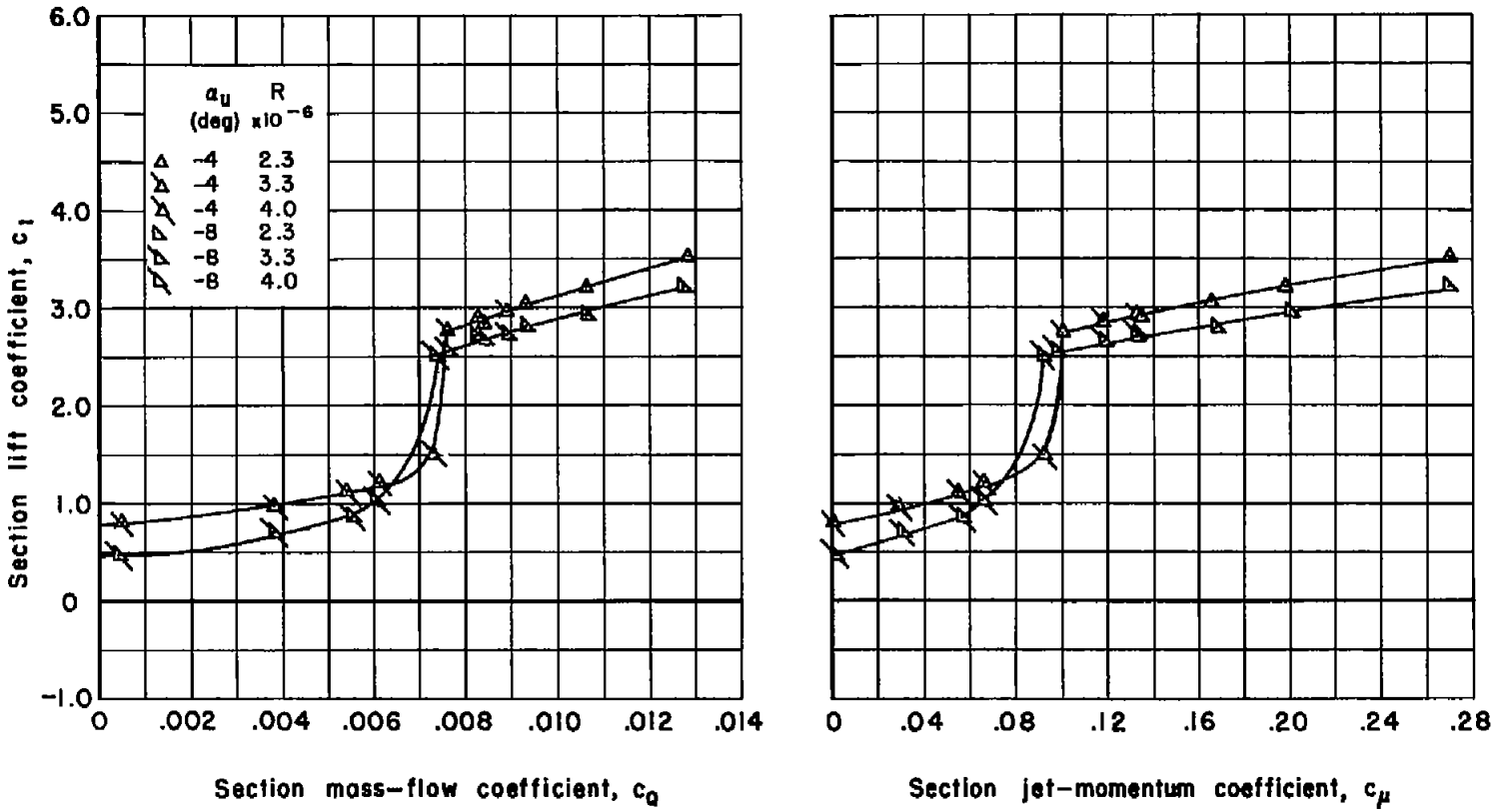

(b) Variable nozzle flow.

Figure 12.- Concluded.

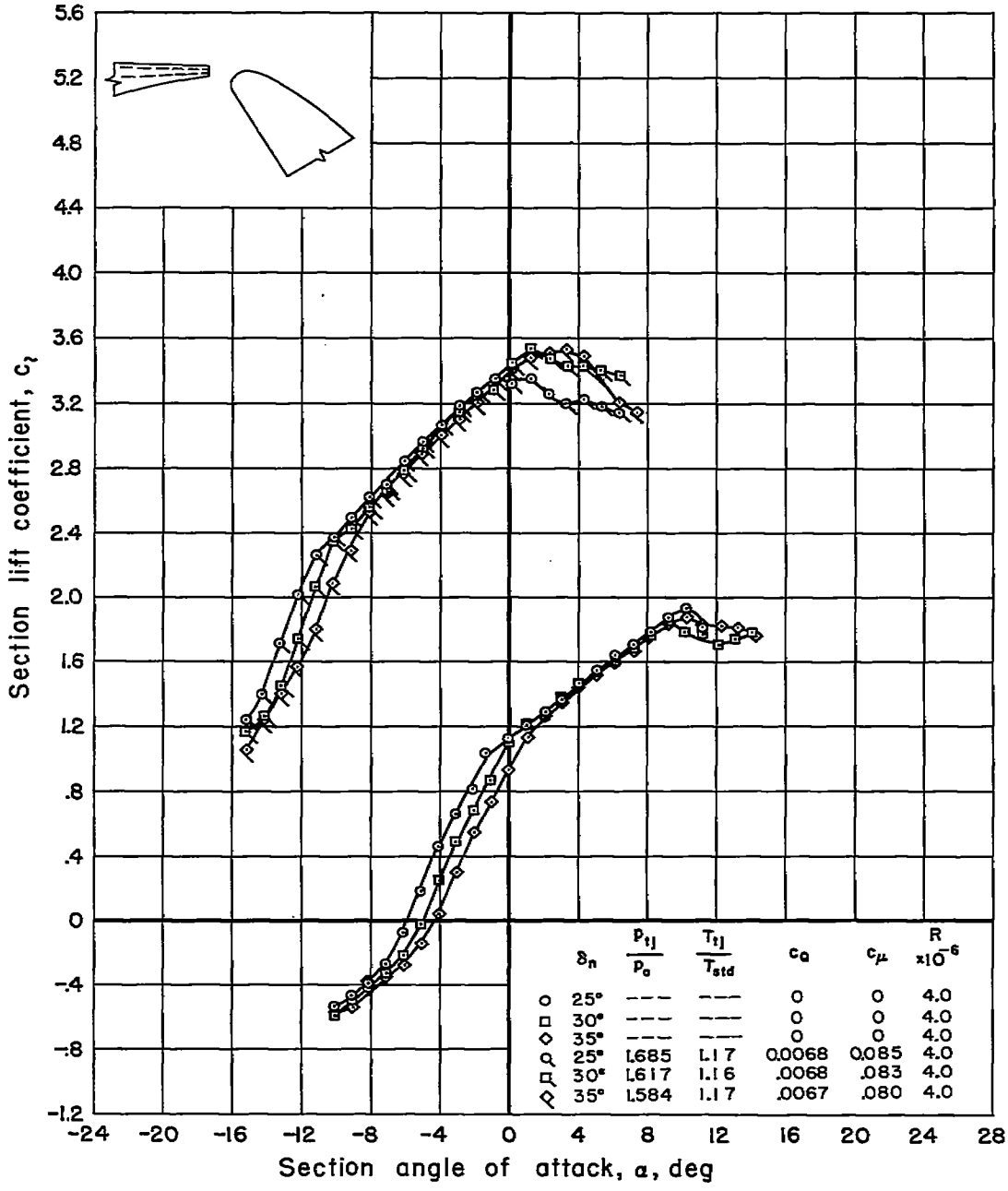

(a) $\delta = 50^{\circ}$

Figure 13.- Effect of nose-flap deflection on the lift of the model with flap A in the extended position with and without blowing; s/c = 0.00110.

[redacted]

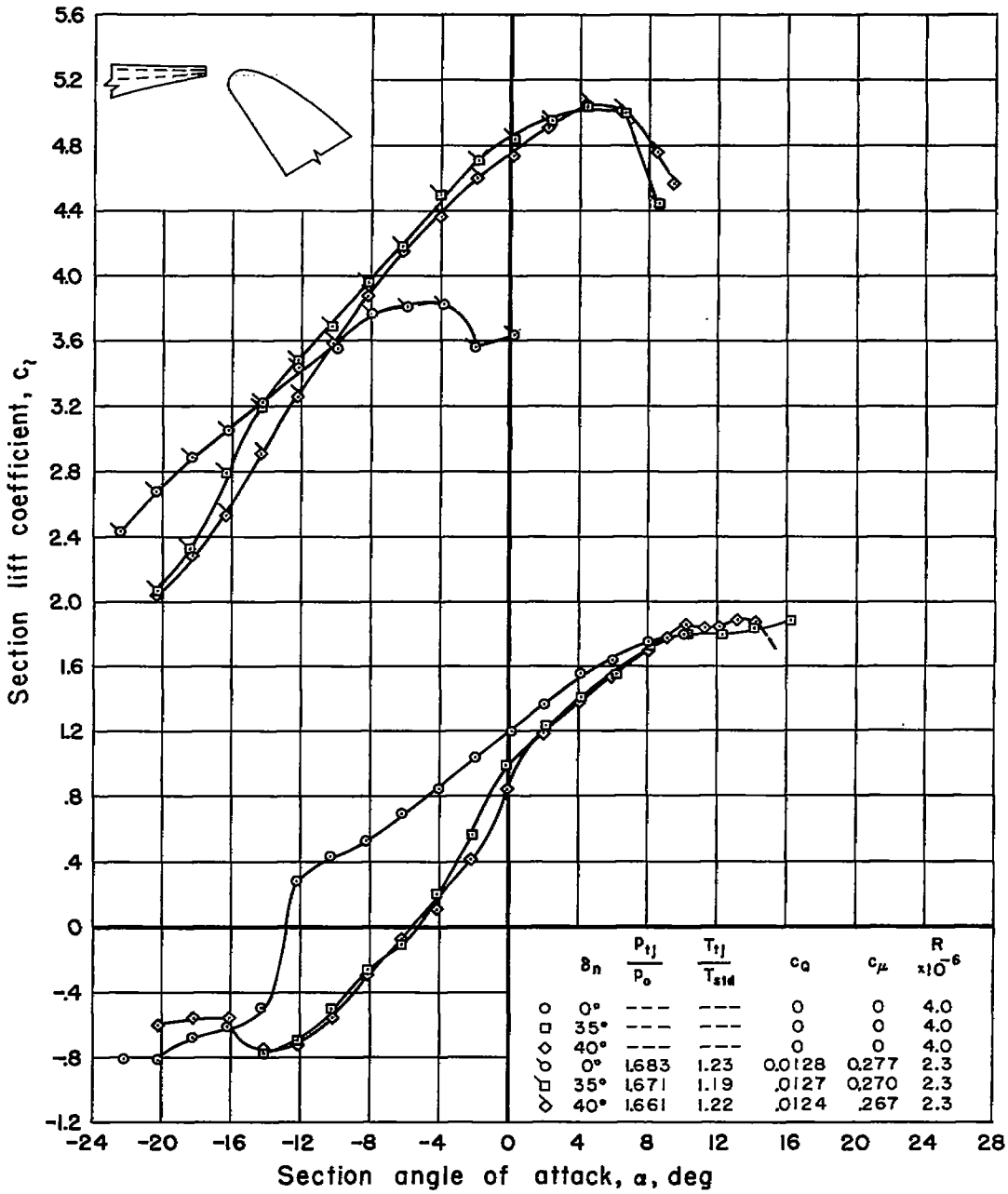

(b) $\delta = 60^{\circ}$

Figure 13.- Concluded.

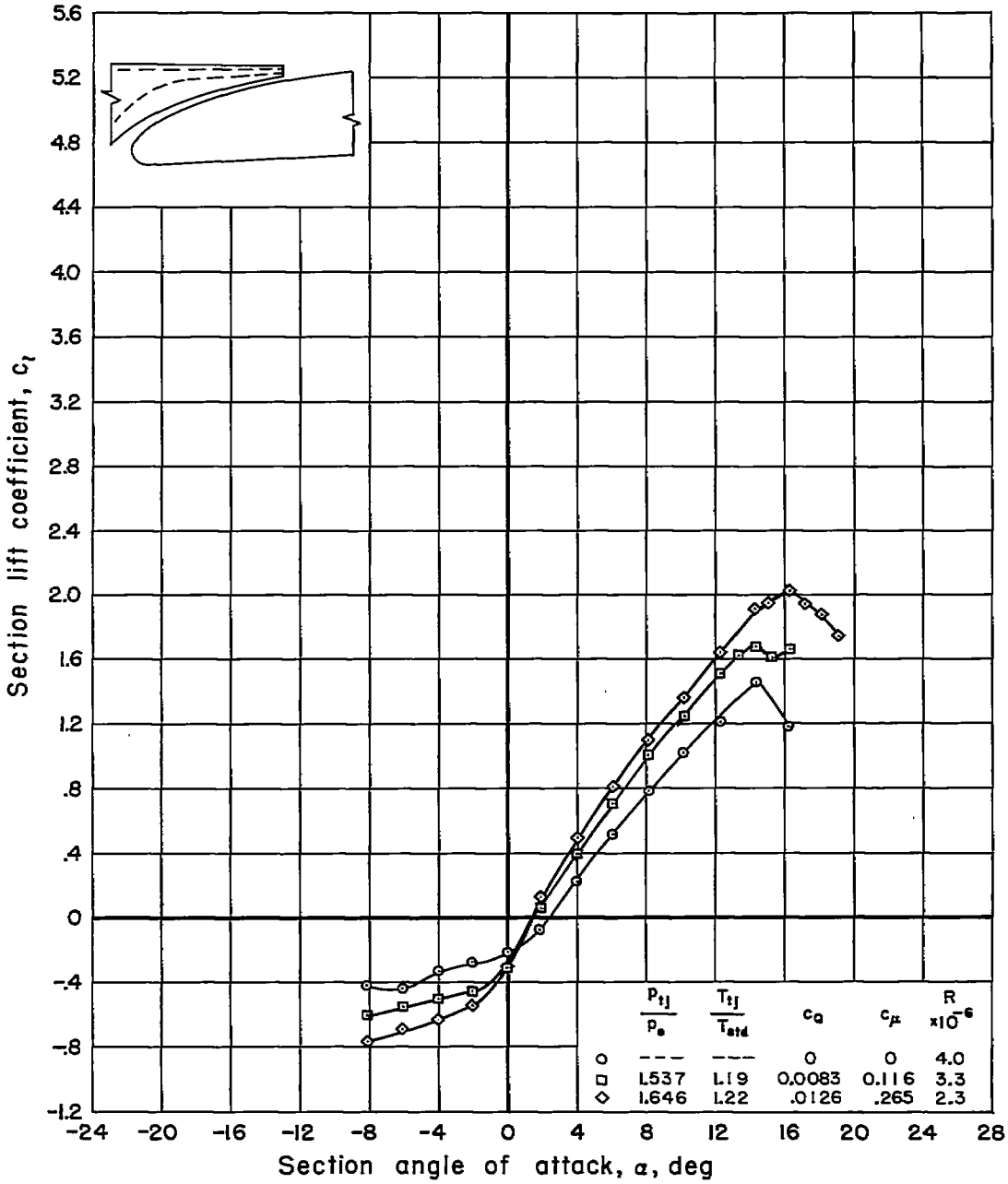

Figure 14.- Effect of blowing on the lift of the model with flap A undeflected; s/c = 0.00110; $\delta_n = 35^\circ$.

[redacted]

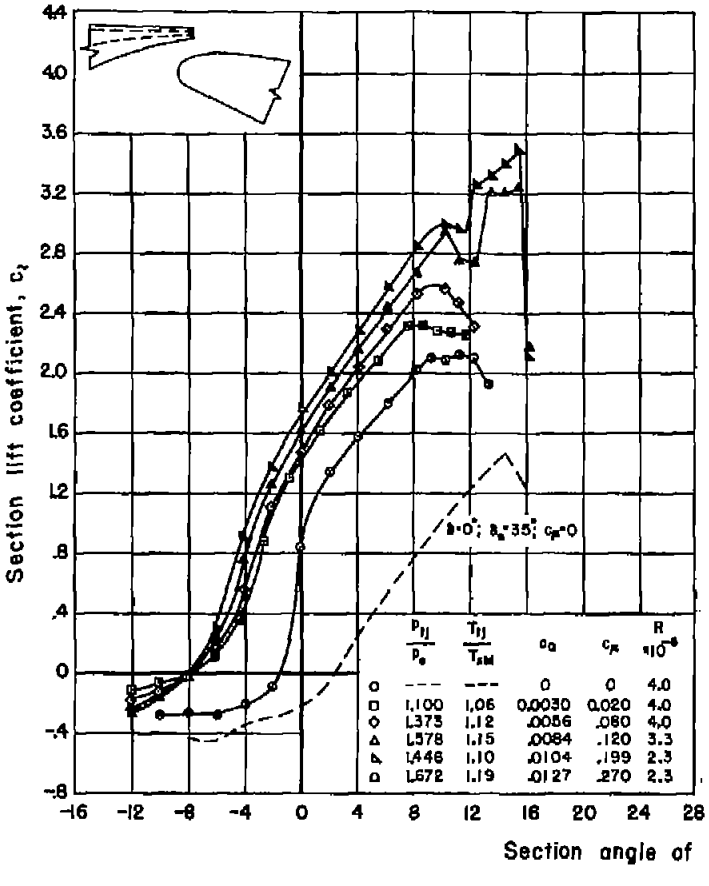

Figure 15.- Effect of blowing on the lift of the model with flap A deflected 20° in the extended position; $s/c = 0.00110$; $\delta_n = 35°$.

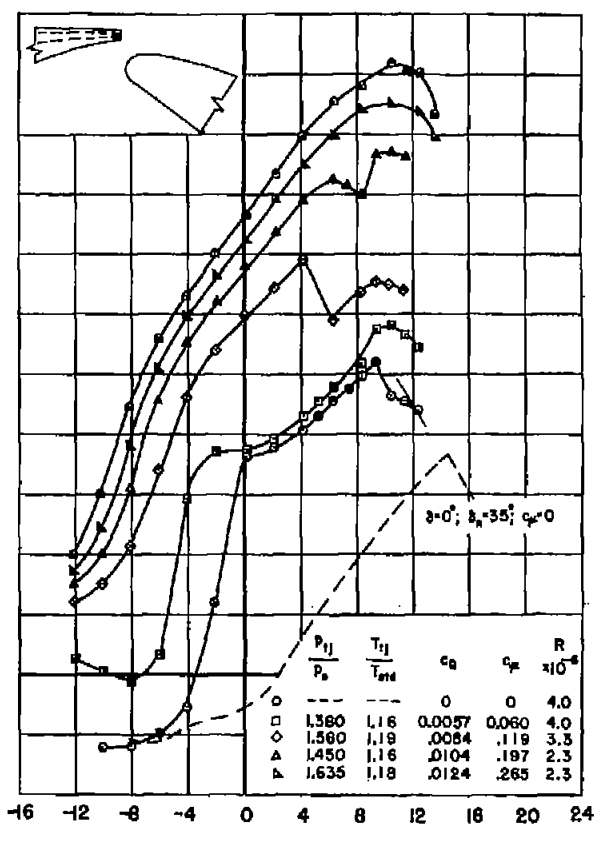

Figure 16.- Effect of blowing on the lift of the model with flap A deflected 35° in the extended position; $s/c = 0.00110$; $\delta_n = 35°$.

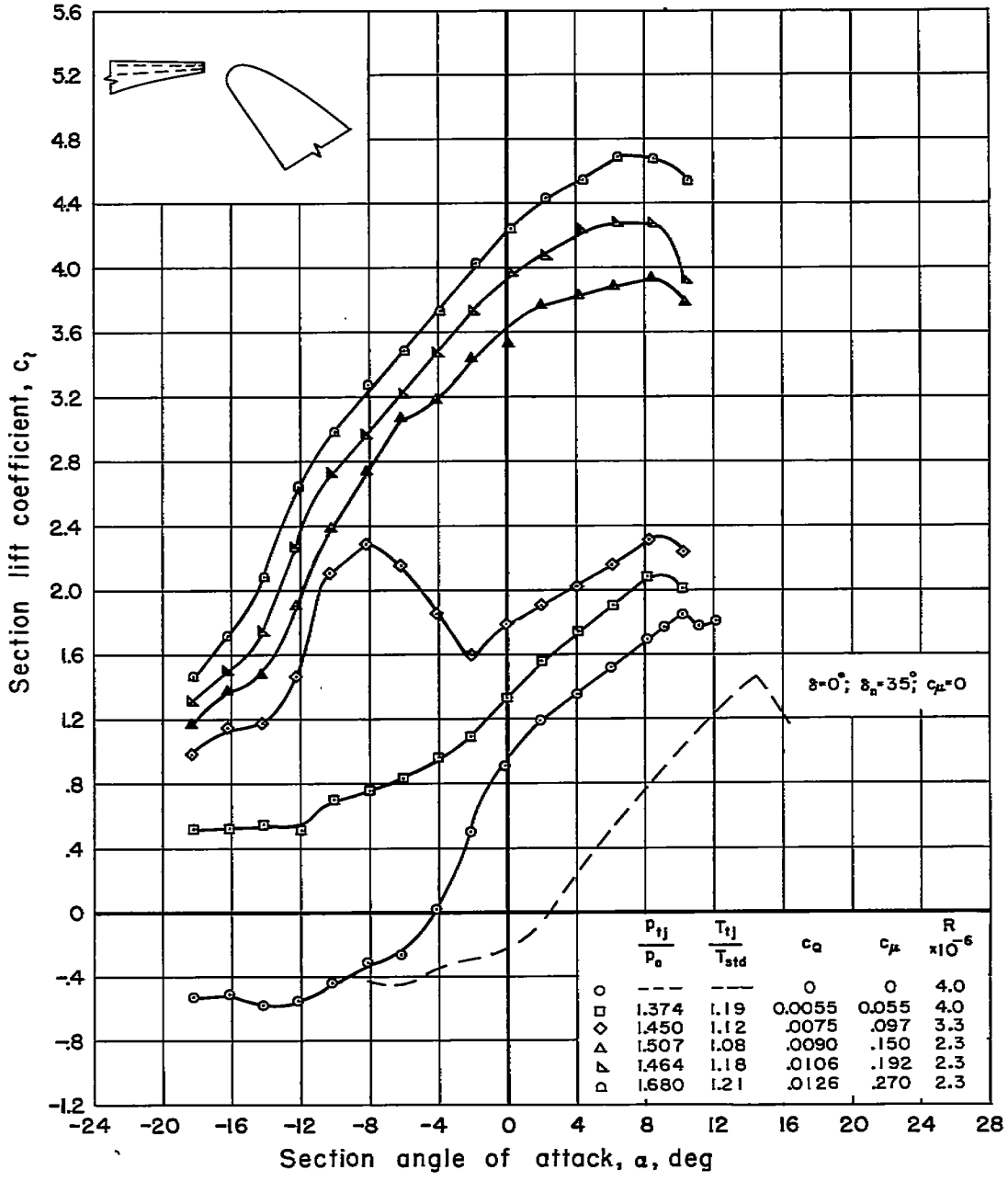

(a) Variable α.

Figure 17.- Effect of blowing on the lift of the model with flap A deflected 50° in the extended position; s/c = 0.00110; δ_n = 35°.

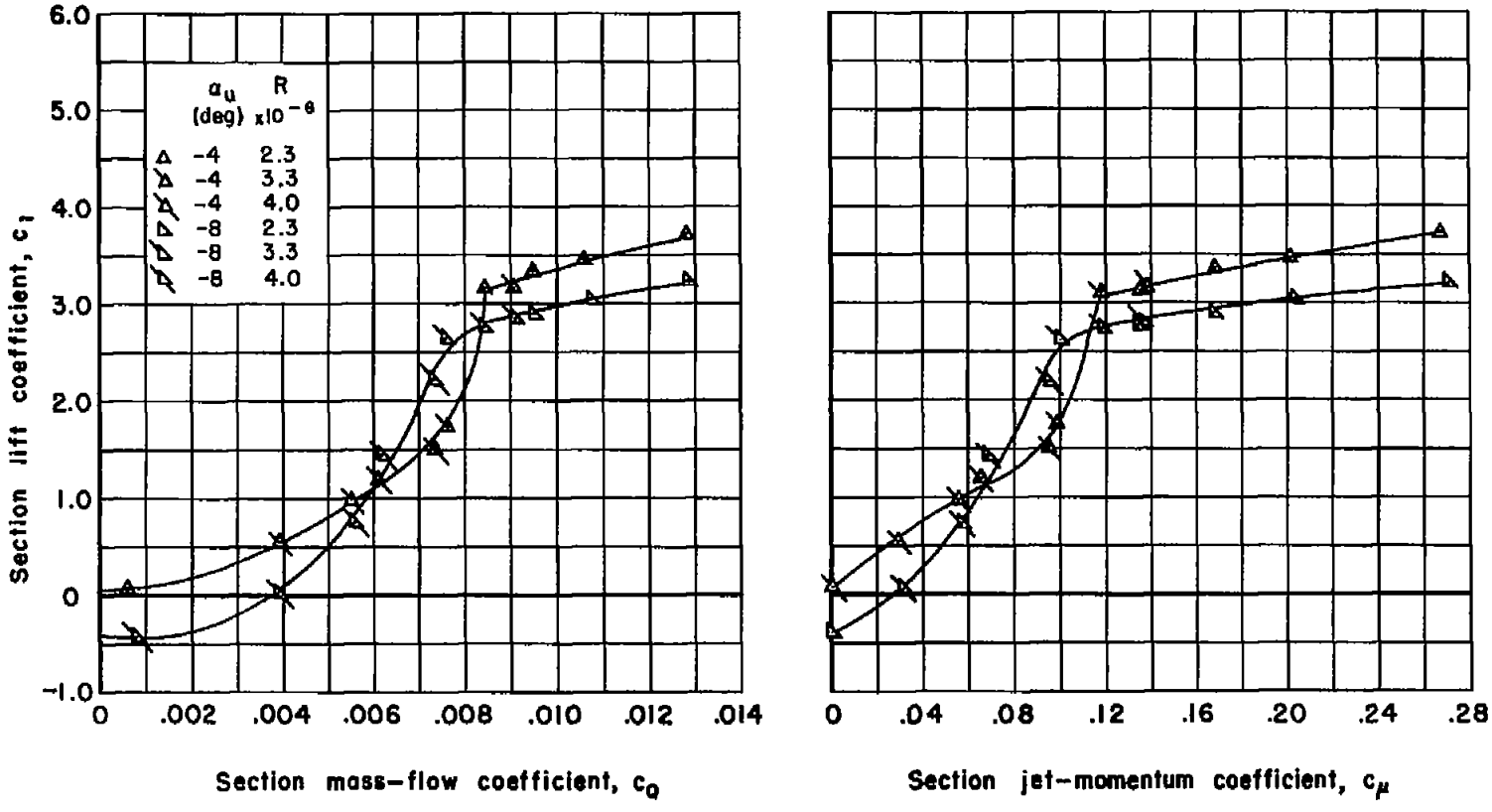

(b) Variable nozzle flow.

Figure 17.- Concluded.

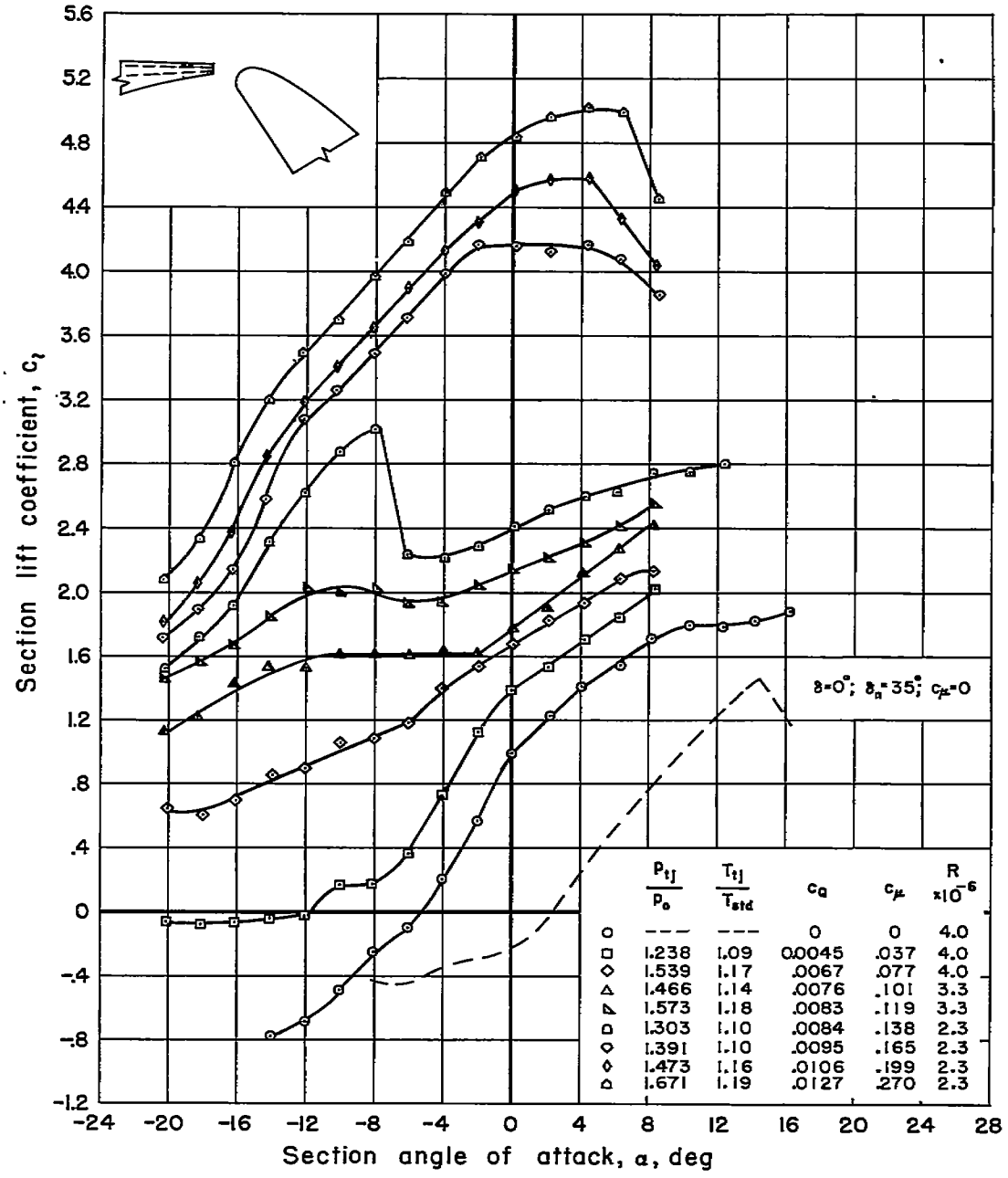

(a) Variable α.

Figure 18.- Effect of blowing on the lift of the model with flap A deflected 60° in the extended position; s/c = 0.00110; δ_n = 35°.

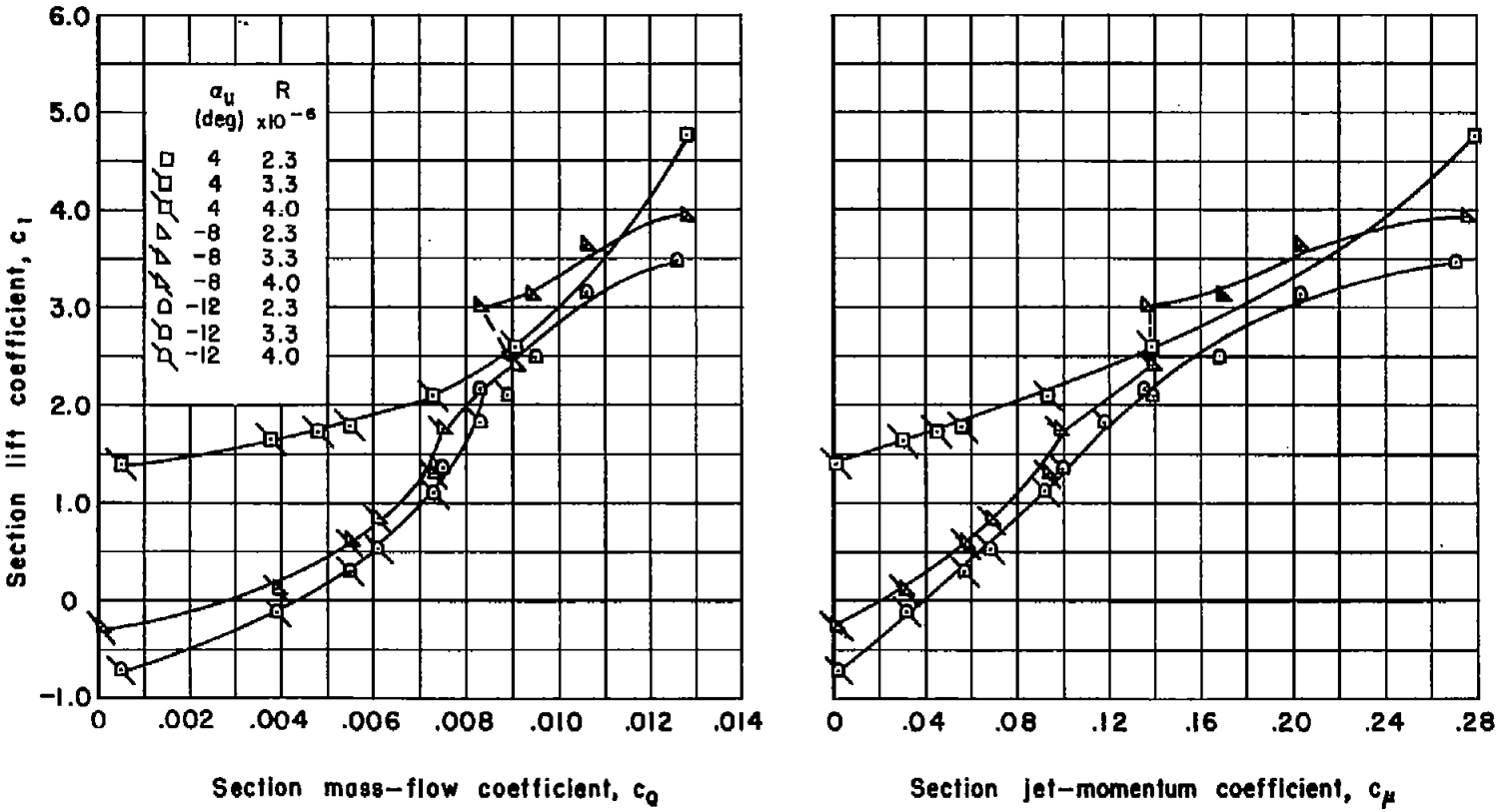

(b) Variable nozzle flow.

Figure 18.- Concluded.

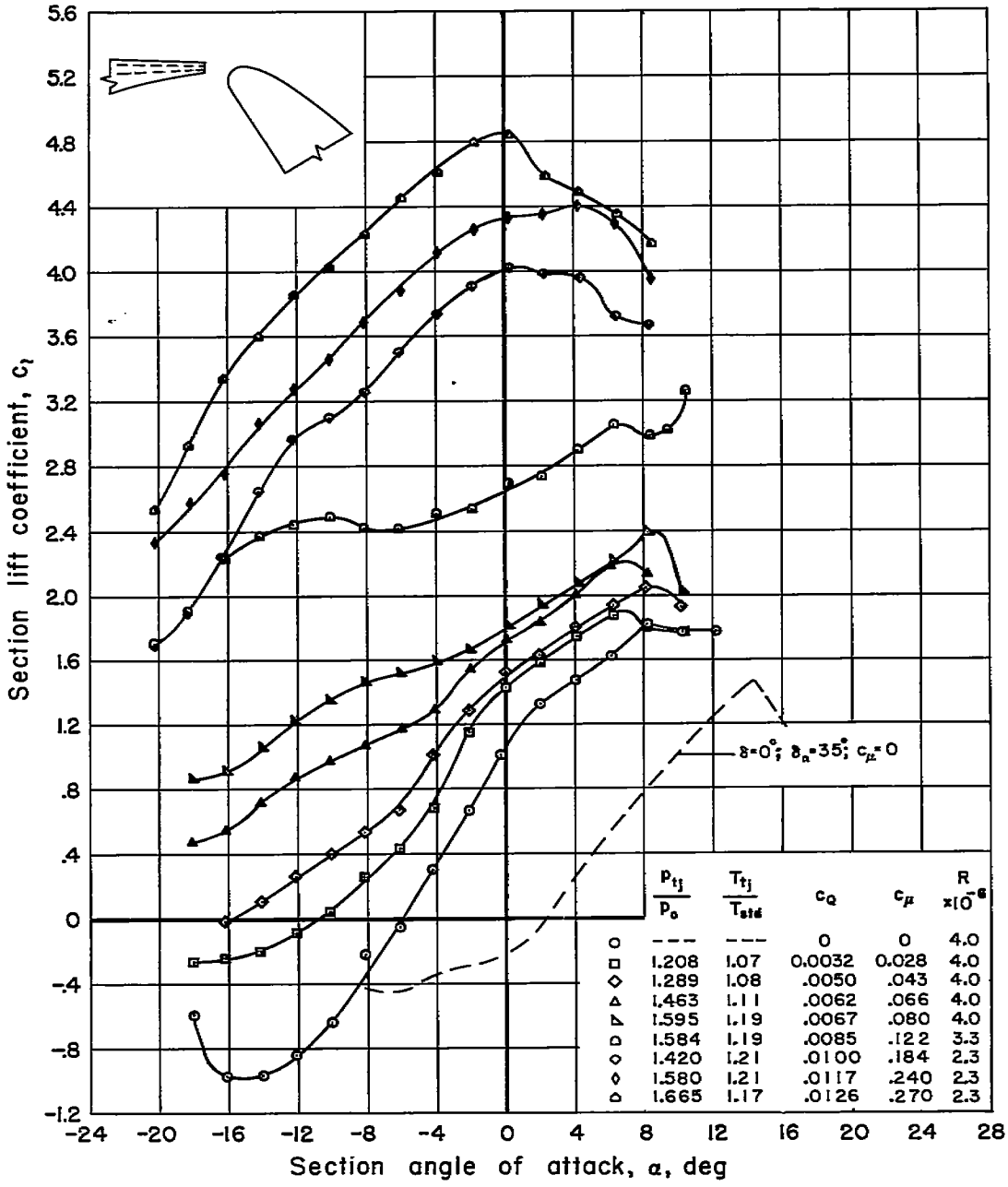

Figure 19.- Effect of blowing on the lift of the model with flap A deflected 65° in the extended position; s/c = 0.00110; δ_n = 35°.

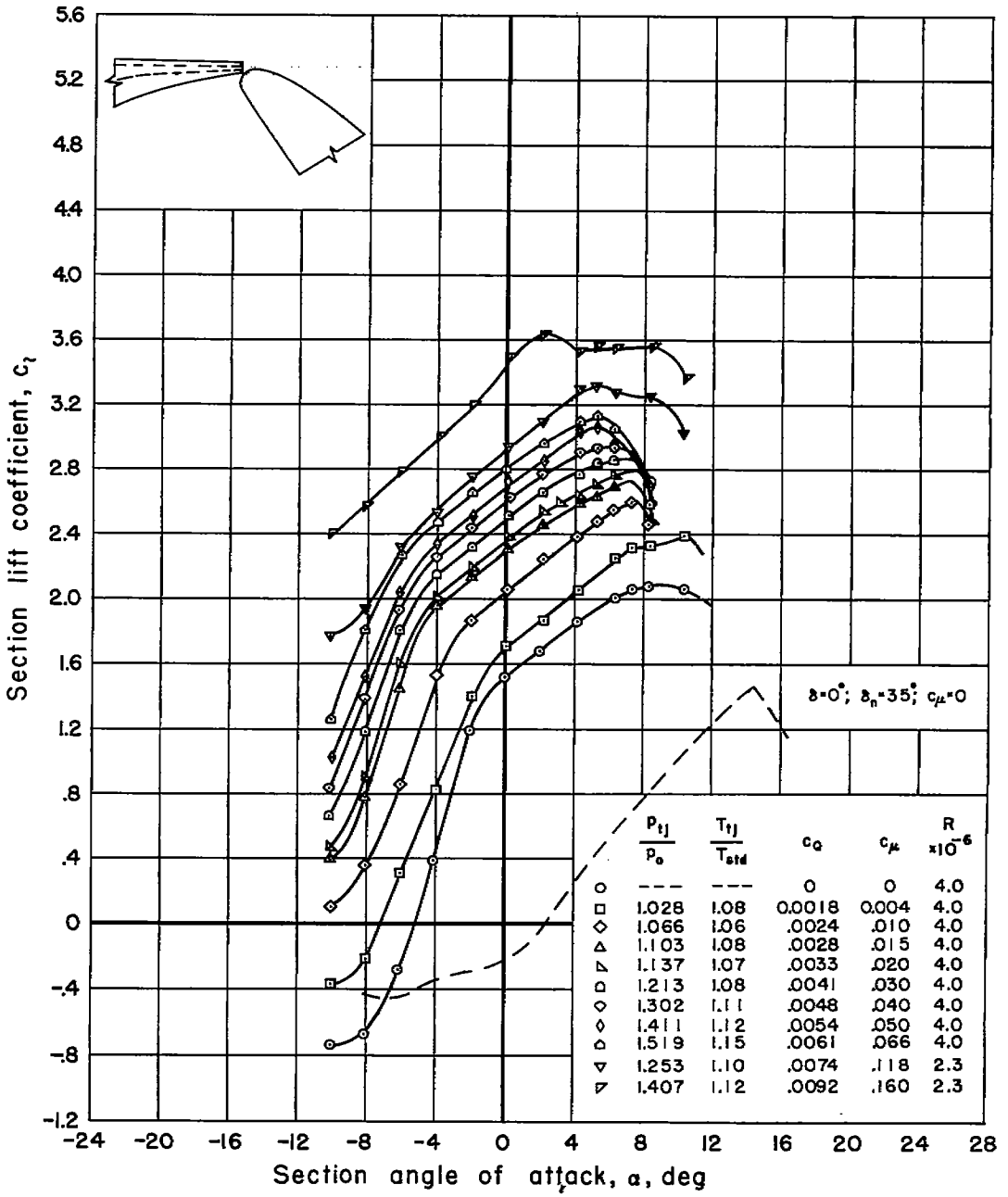

(a) Variable α.

Figure 20.- Effect of blowing on the lift of the model with flap A deflected 50° in the position against the nozzle; s/c = 0.00110; δ_n = 35°.

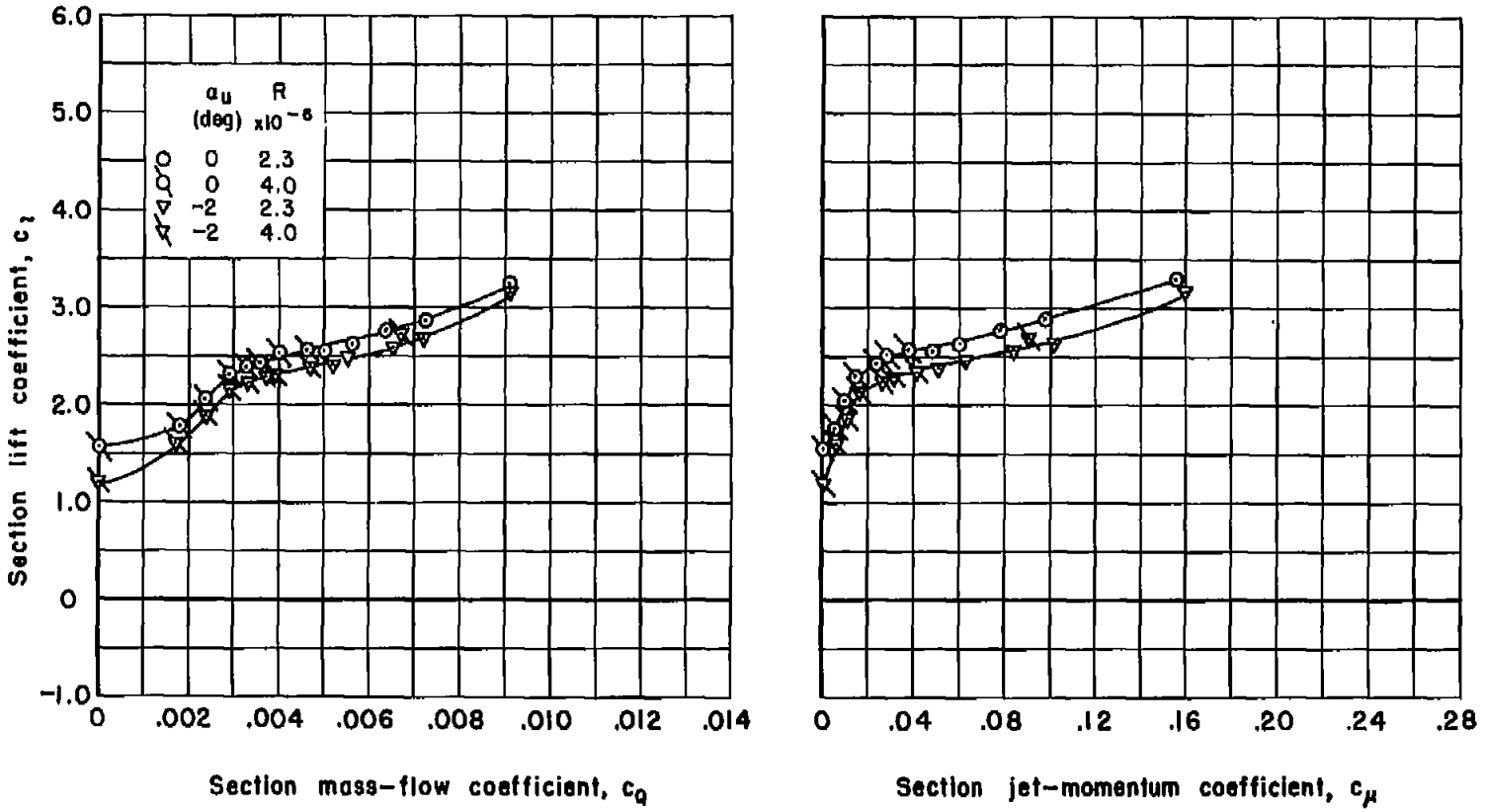

(b) Variable nozzle flow.

Figure 20.- Concluded.

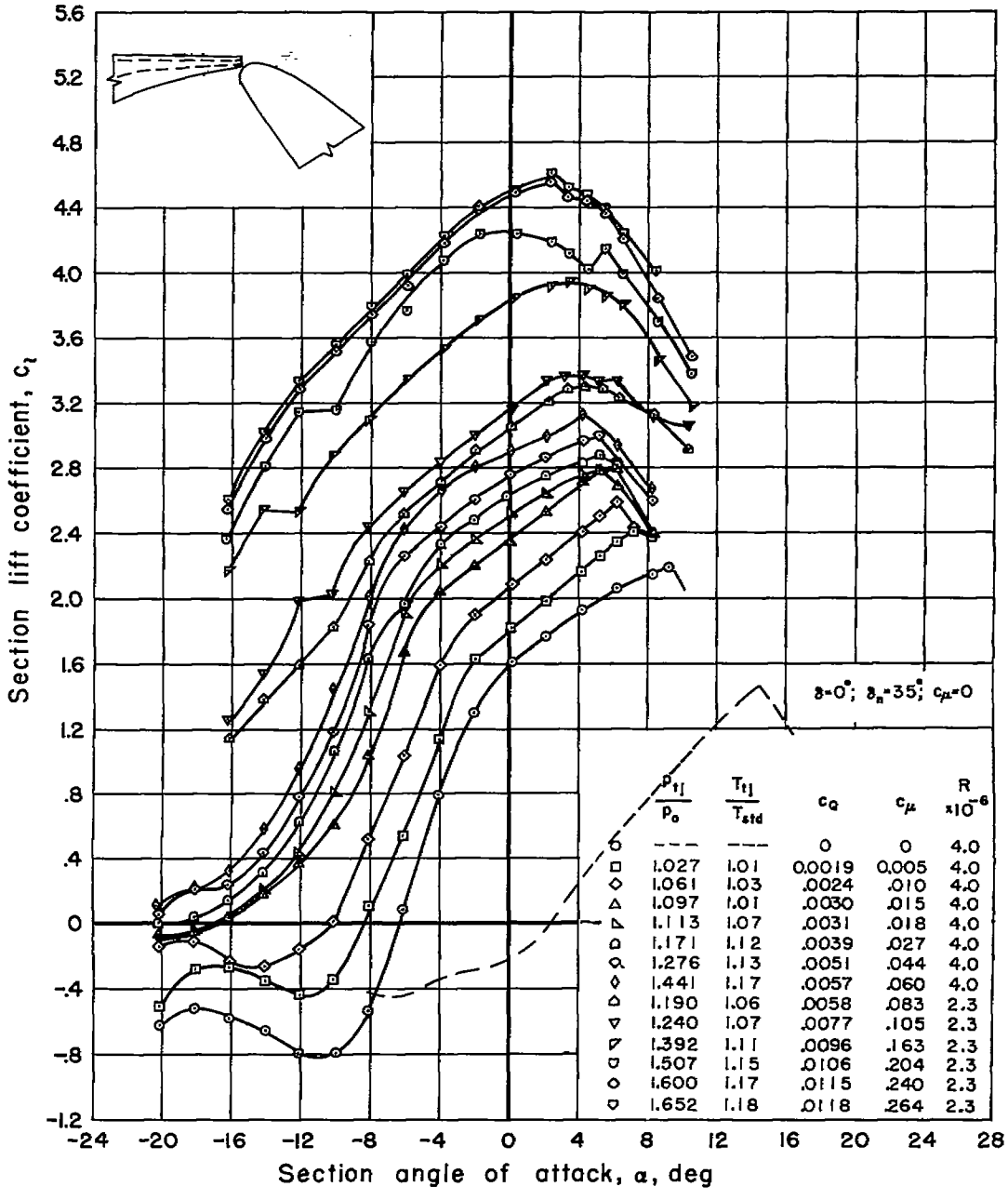

(a) Variable α.

Figure 21.- Effect of blowing on the lift of the model with flap A deflected 60° in the position against the nozzle; s/c = 0.00110; δ_n = 35°.

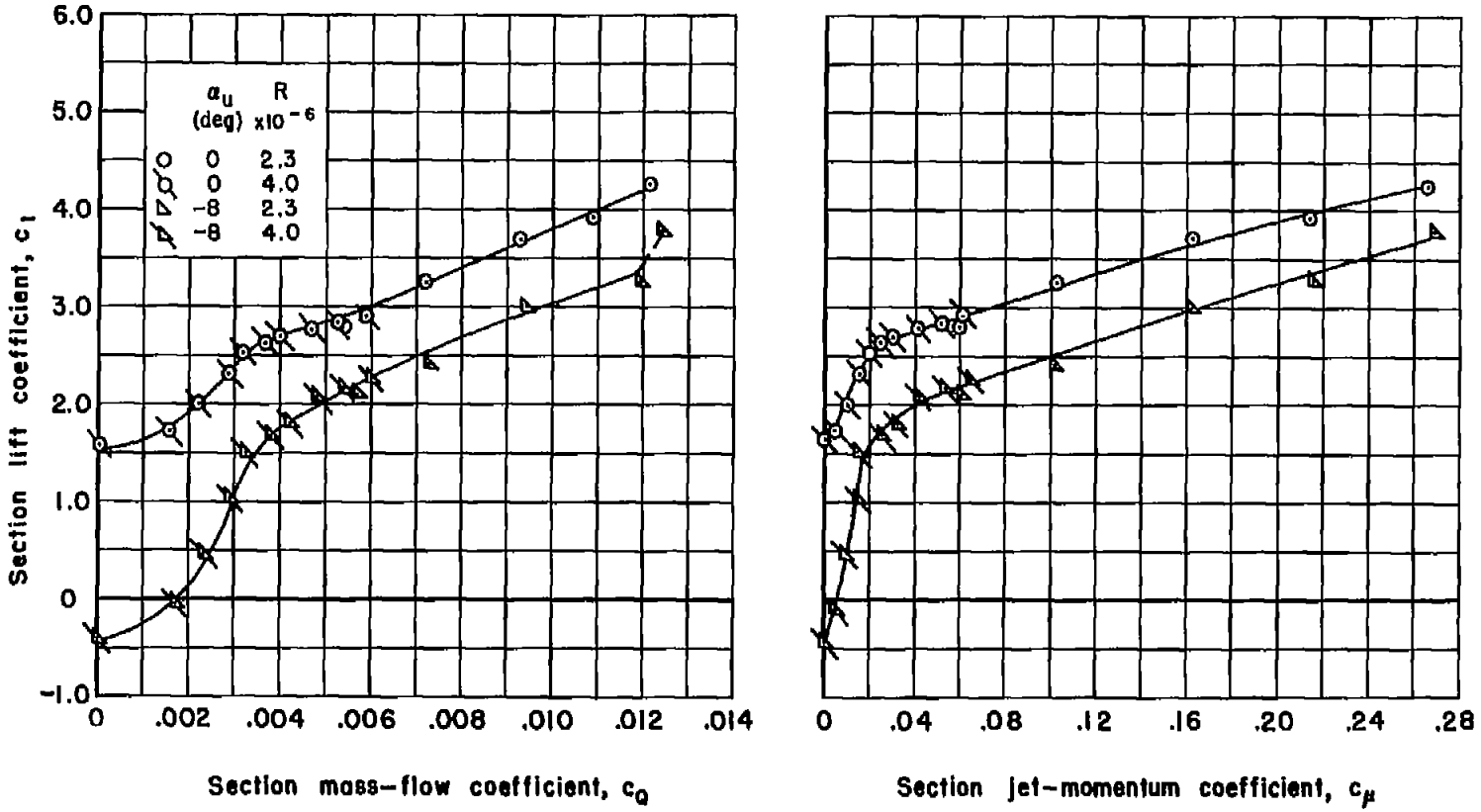

(b) Variable nozzle flow.

Figure 21.- Concluded.

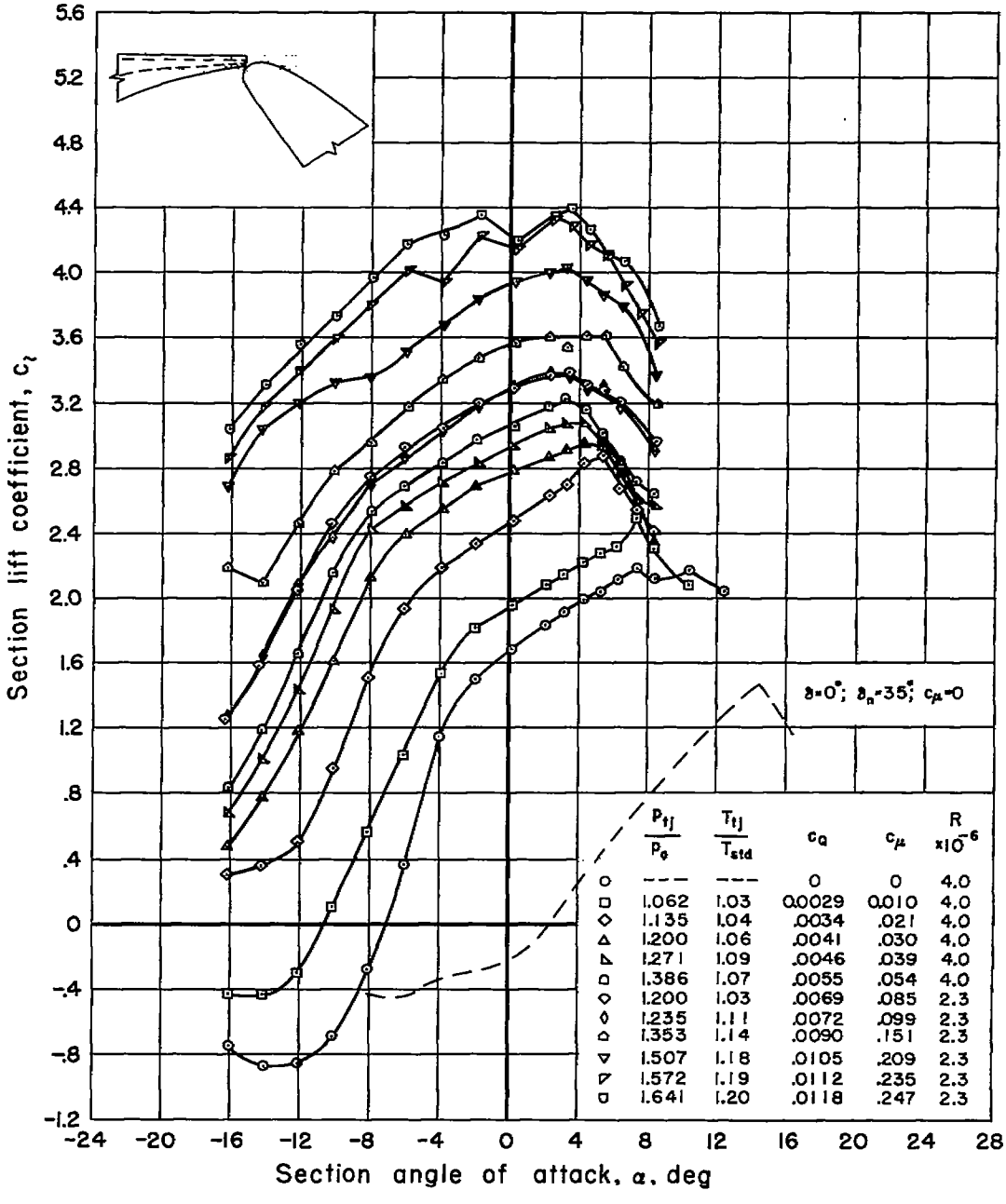

(a) Variable α.

Figure 22.- Effect of blowing on the lift of the model with flap A deflected 70° in the position against the nozzle; s/c = 0.00110; δ_n = 35°.

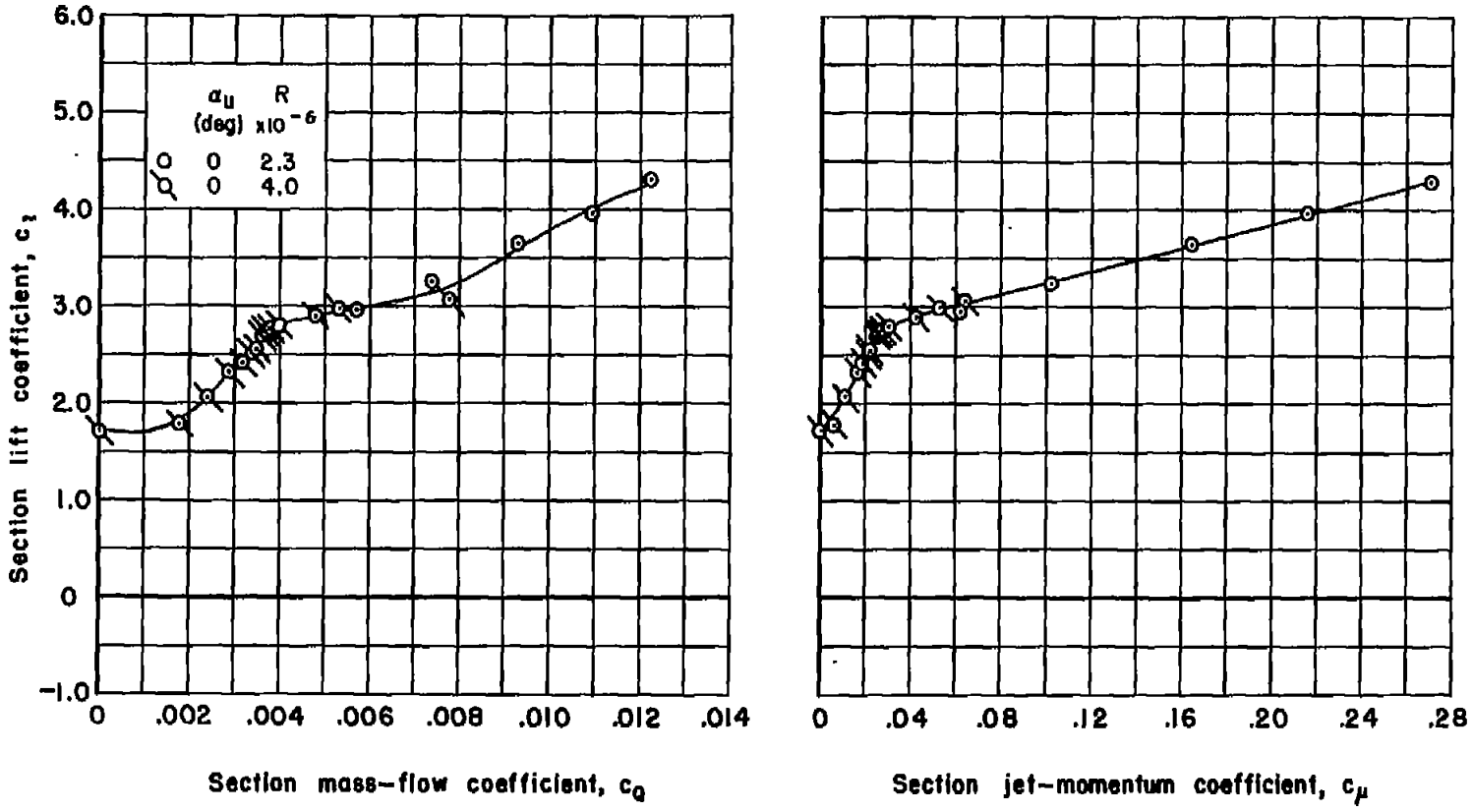

(b) Variable nozzle flow.

Figure 22.- Concluded.

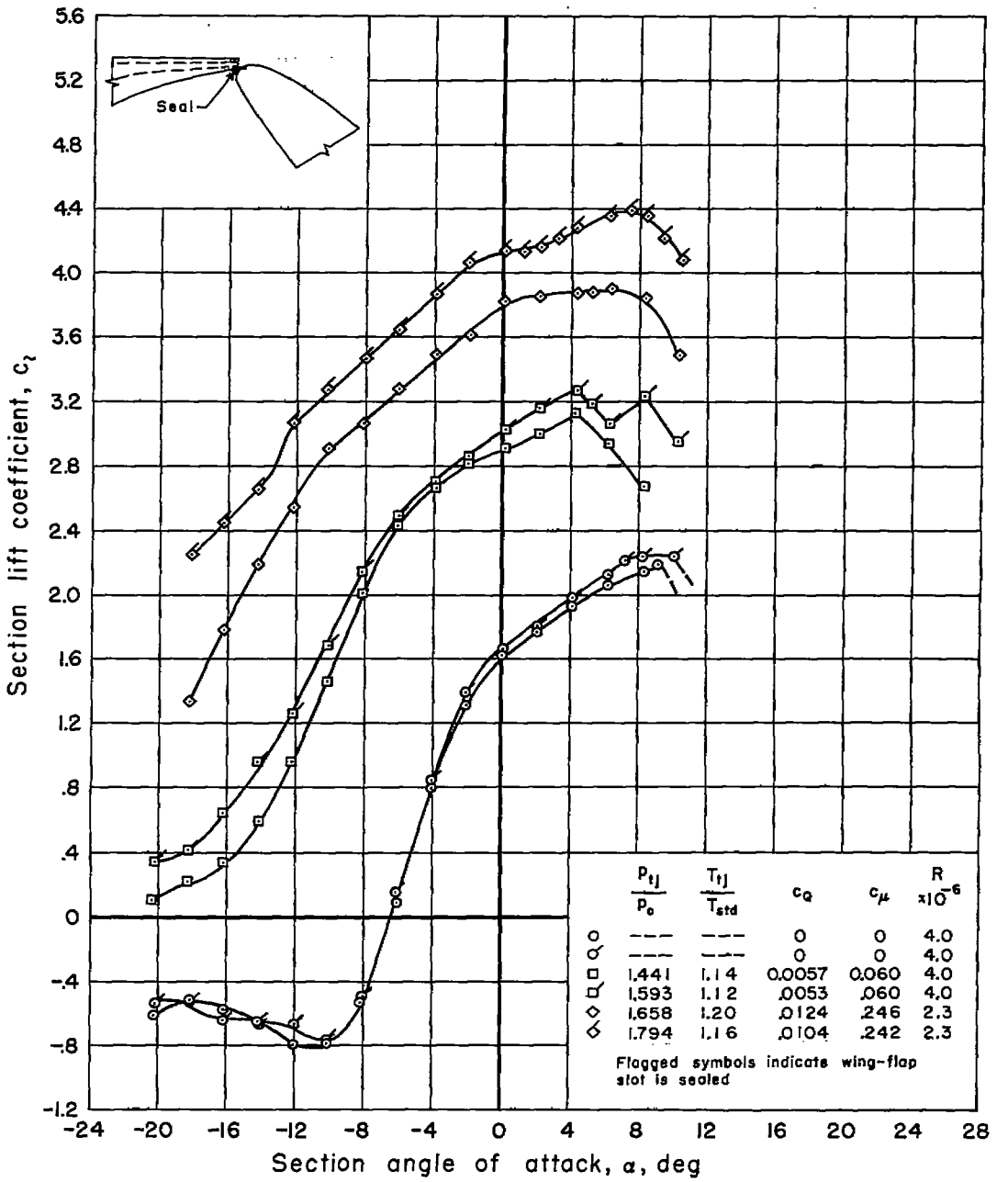

(a) Variable α.

Figure 23.- Effect of sealing the wing-flap slot on the lift of the model with flap A deflected 60° in the position against the nozzle; s/c = 0.00110; δ_n = 35°.

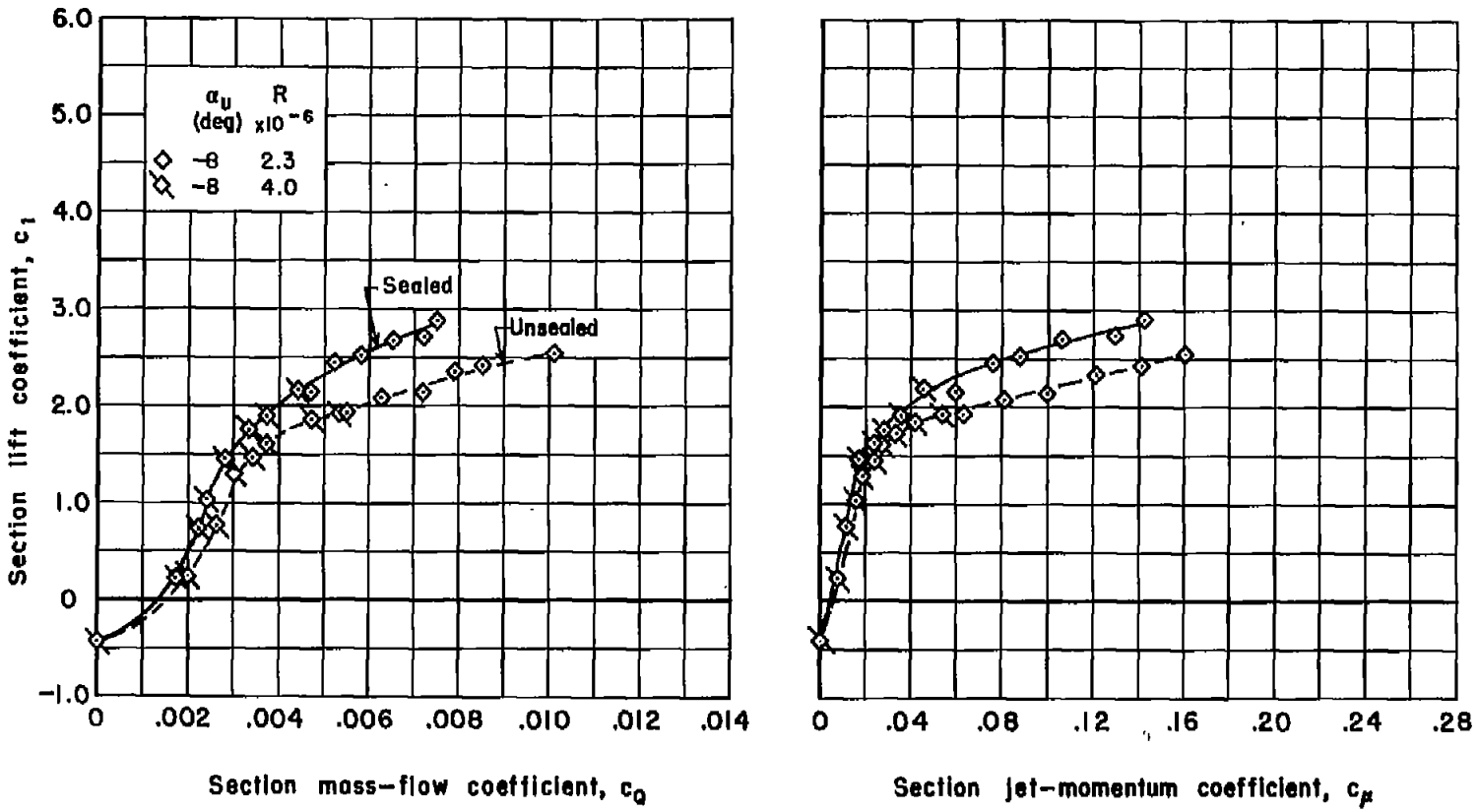

(b) Variable nozzle flow.

Figure 23.- Concluded.

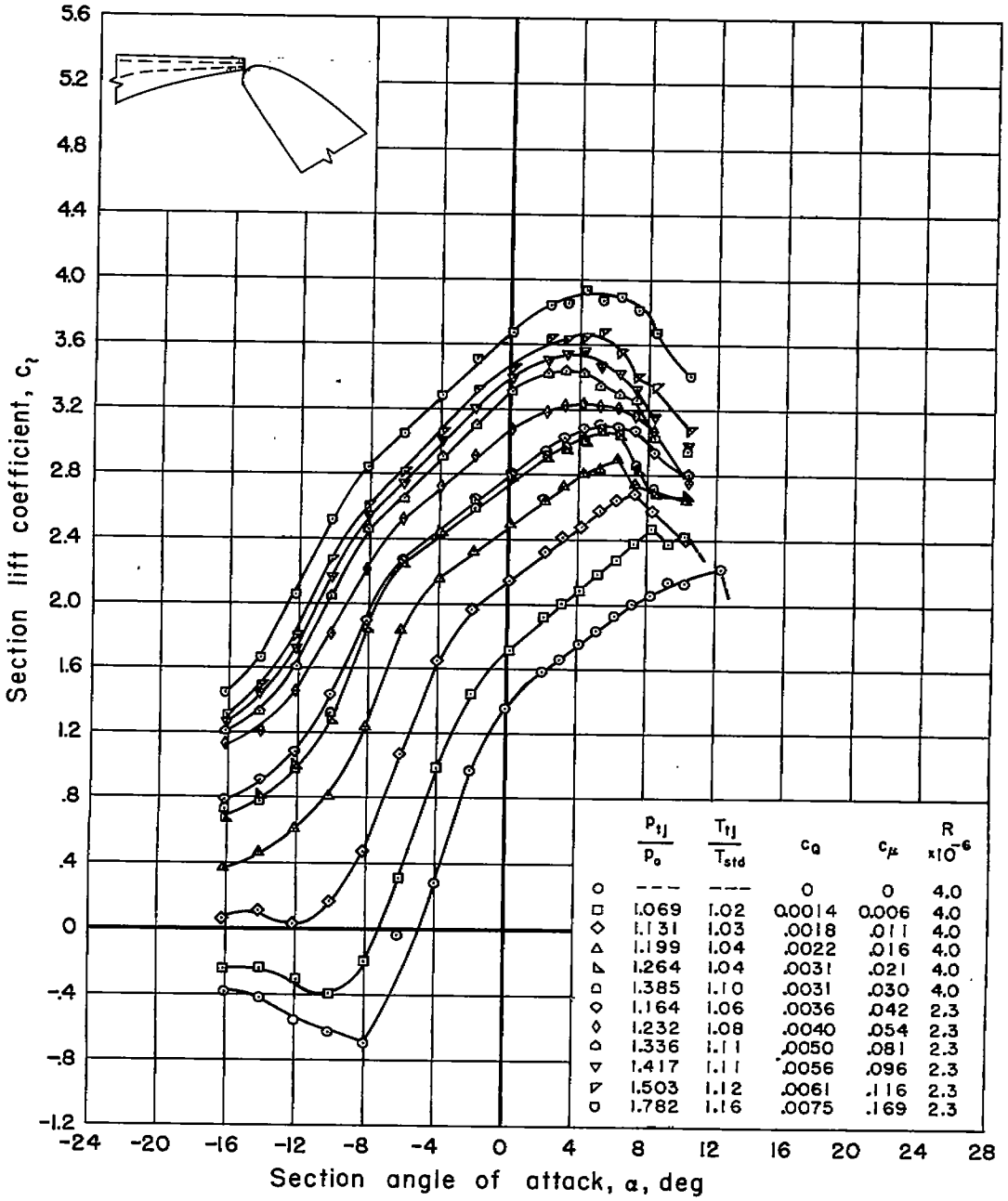

(a) Variable α.

Figure 24.- Effect of blowing on the lift of the model with flap A deflected 50° in the position against the nozzle; s/c = 0.00065; δ_n = 35°.

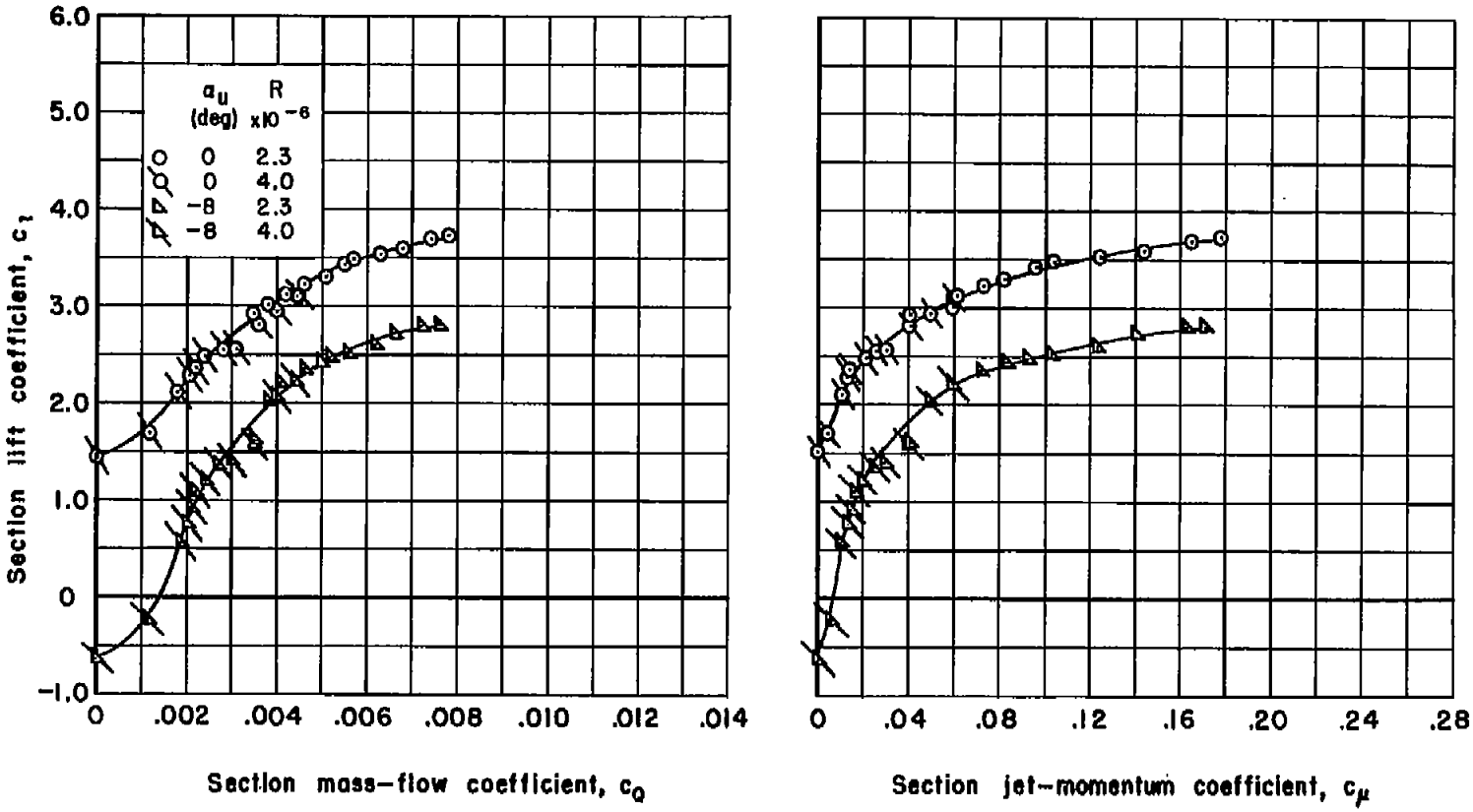

(b) Variable nozzle flow.

Figure 24.- Concluded.

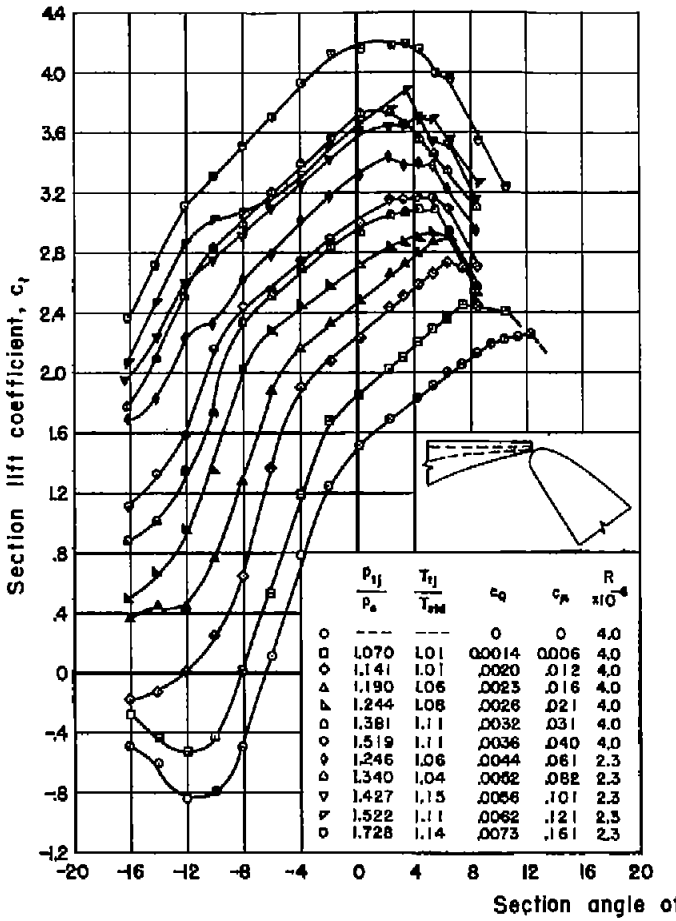

Figure 25.- Effect of blowing on the lift of the model with flap A deflected 60° in the position against the nozzle; s/c = 0.00065; δ_n = 35°.

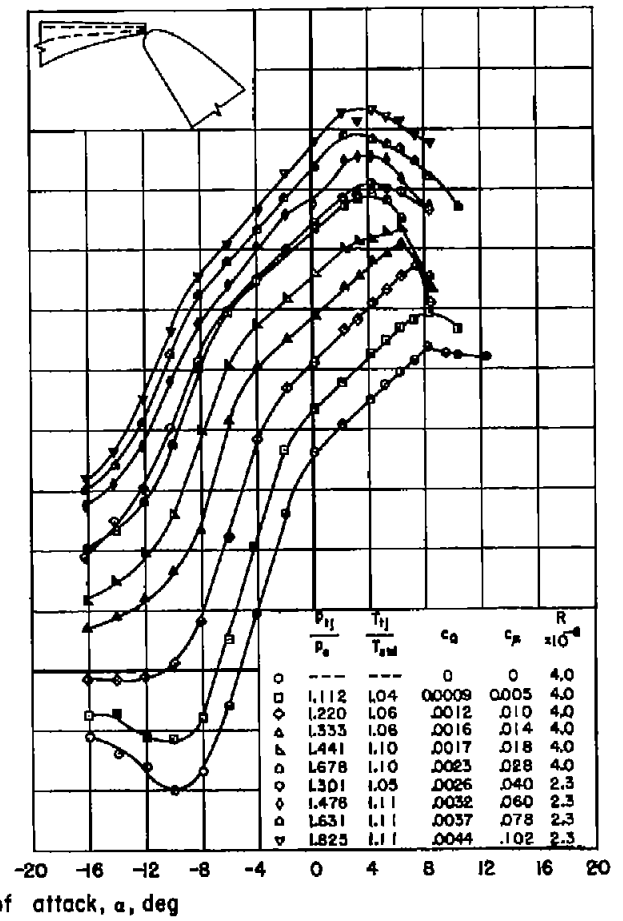

Figure 26.- Effect of blowing on the lift of the model with flap A deflected 50° in the position against the nozzle; s/c = 0.00036; δ_n = 35°.

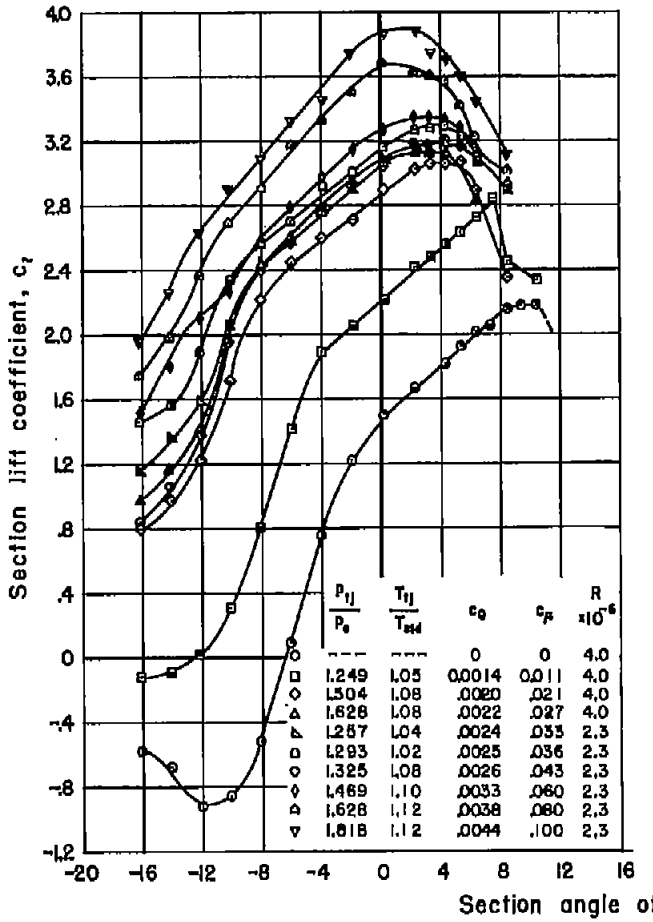

Figure 27.- Effect of blowing on the lift of the model with flap A deflected 60° in the position against the nozzle; s/c = 0.00036; δ_n = 35°.

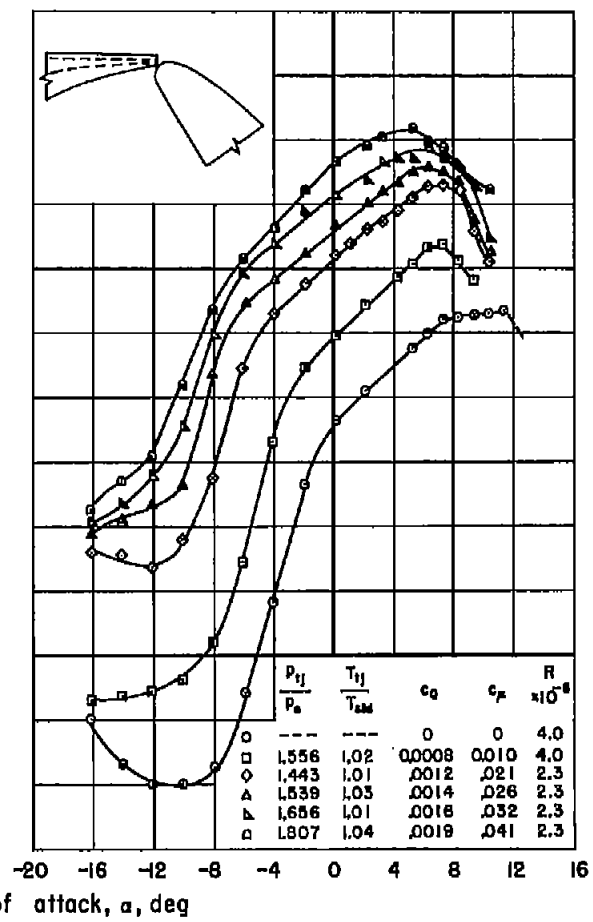

Figure 28.- Effect of blowing on the lift of the model with flap A deflected 50° in the position against the nozzle; s/c = 0.00017; δ_n = 35°.

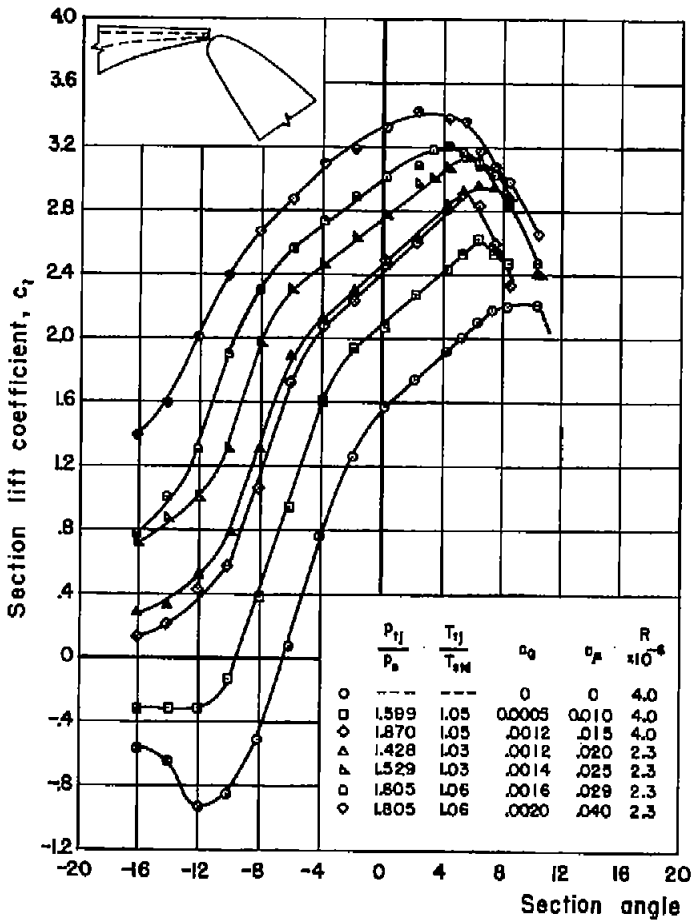

Figure 29.- Effect of blowing on the lift of the model with flap A deflected 60° in the position against the nozzle; s/c = 0.00017; δ_n = 35°.

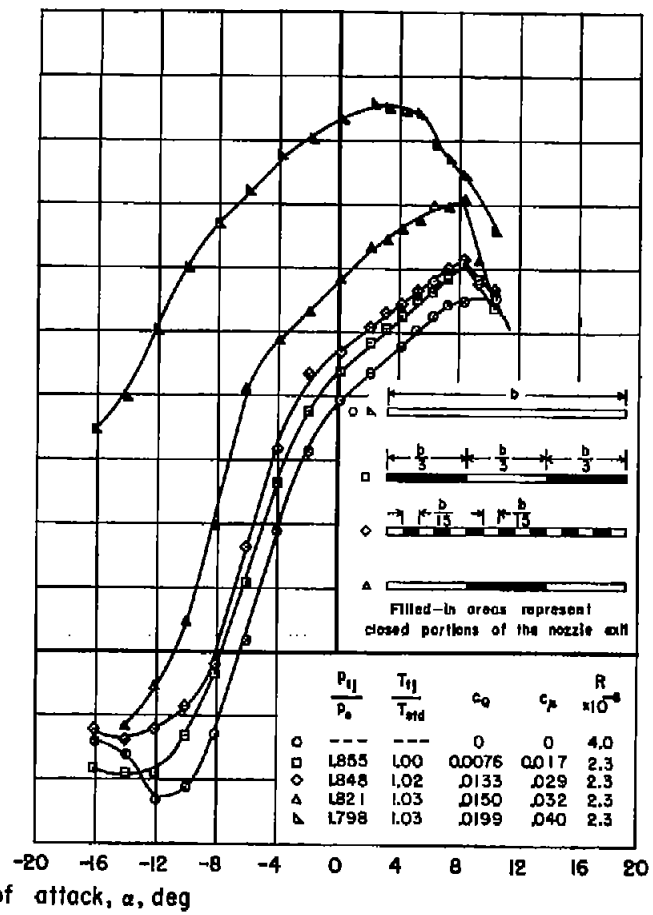

Figure 30.- Effect of spanwise extent of blowing on the lift of the model with flap A against the nozzle; s/c = 0.0017; δ = 60°; δ_n = 35°.

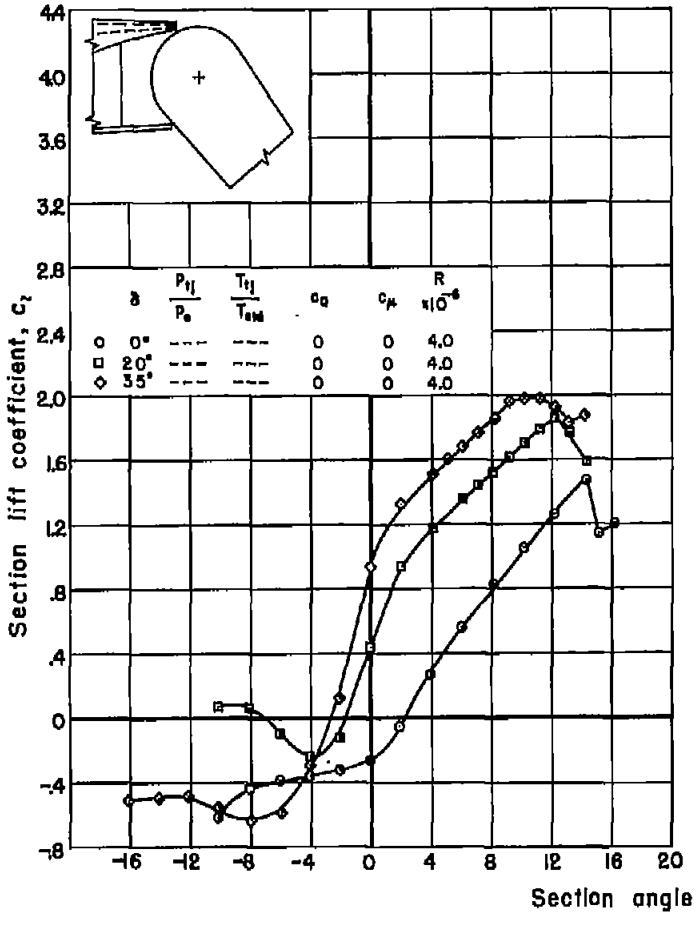

Figure 31.- Effect of trailing-edge flap deflection on the lift of the model with flap B; s/c = 0.00110; $\delta_n = 35^\circ$.

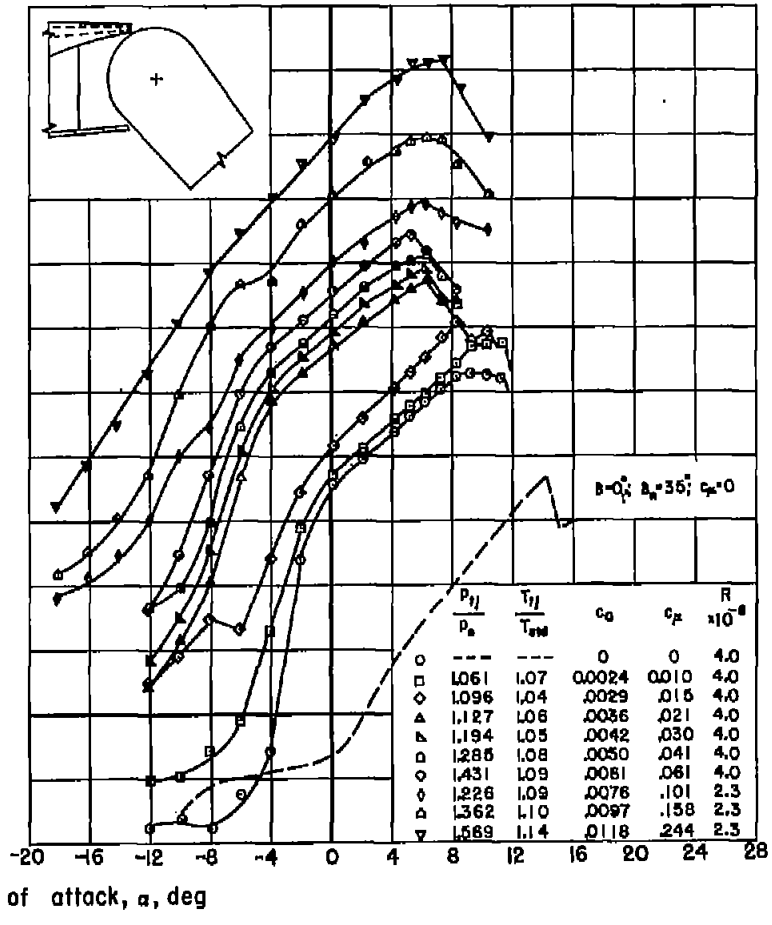

Figure 32.- Effect of blowing on the lift of the model with flap B deflected 50°; s/c = 0.00110; $\delta_n = 35^\circ$.

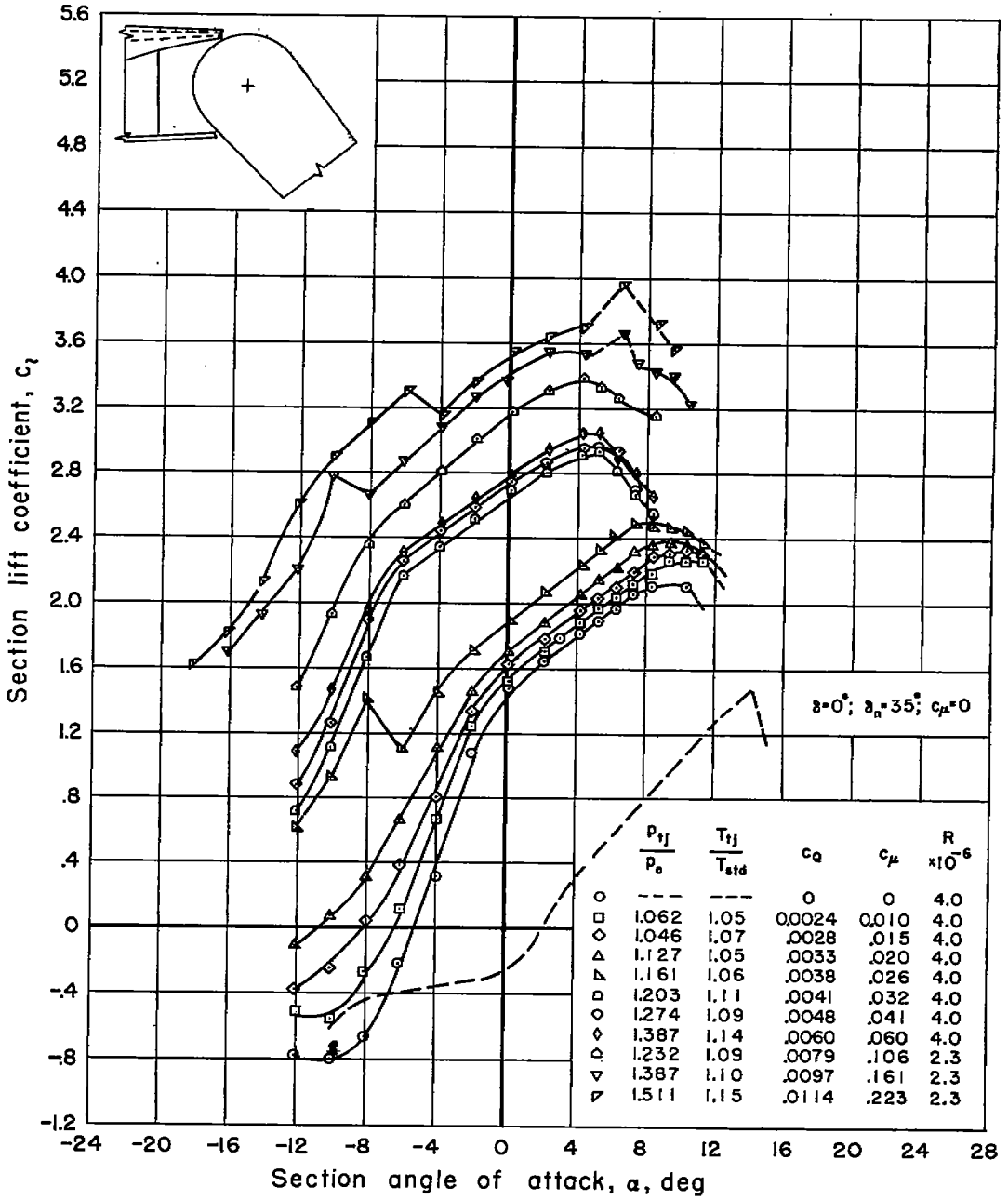

(a) Variable α.

Figure 33.- Effect of blowing on the lift of the model with flap B deflected 60°; s/c = 0.00110; δ_n = 35°.

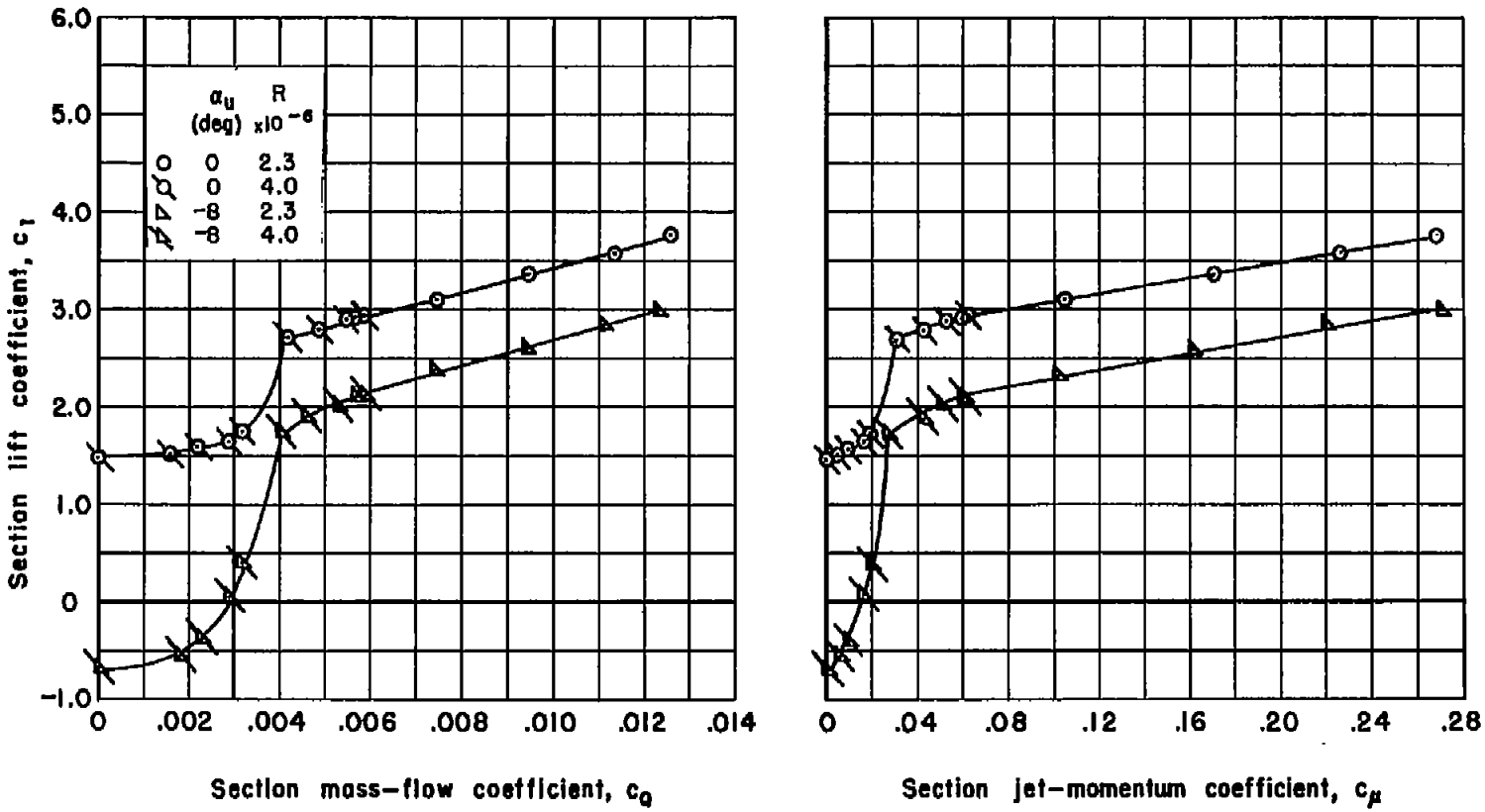

(b) Variable nozzle flow.

Figure 33.- Concluded.

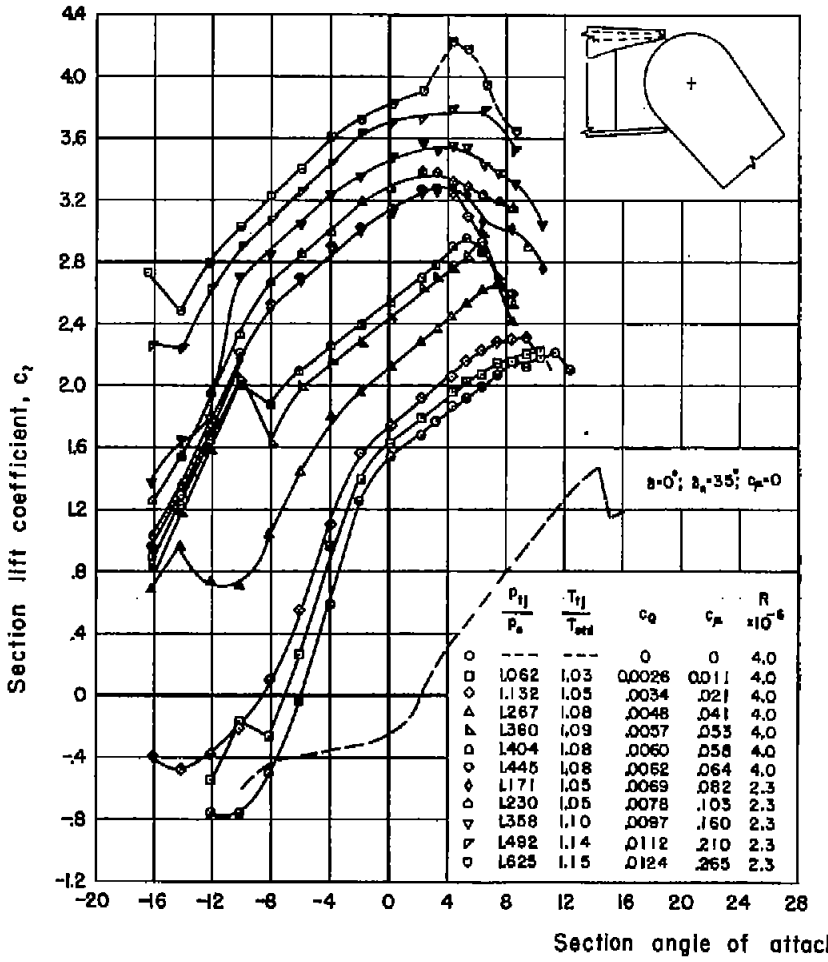

Figure 34.- Effect of blowing on the lift of the model with flap B deflected 70°; s/c = 0.00110; δ_n = 35°.

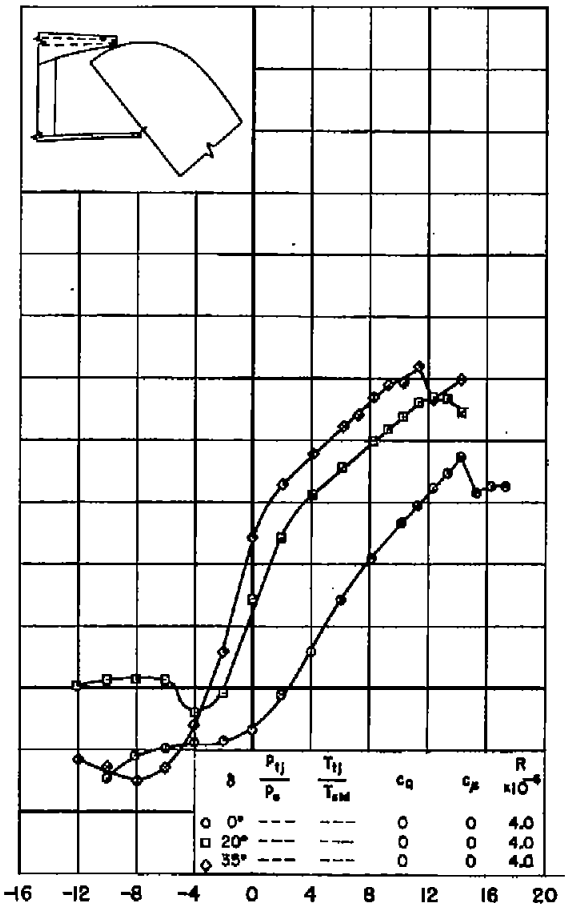

Figure 35.- Effect of trailing-edge flap deflection on the lift of the model with flap C; s/c = 0.00110; δ_n = 35°.

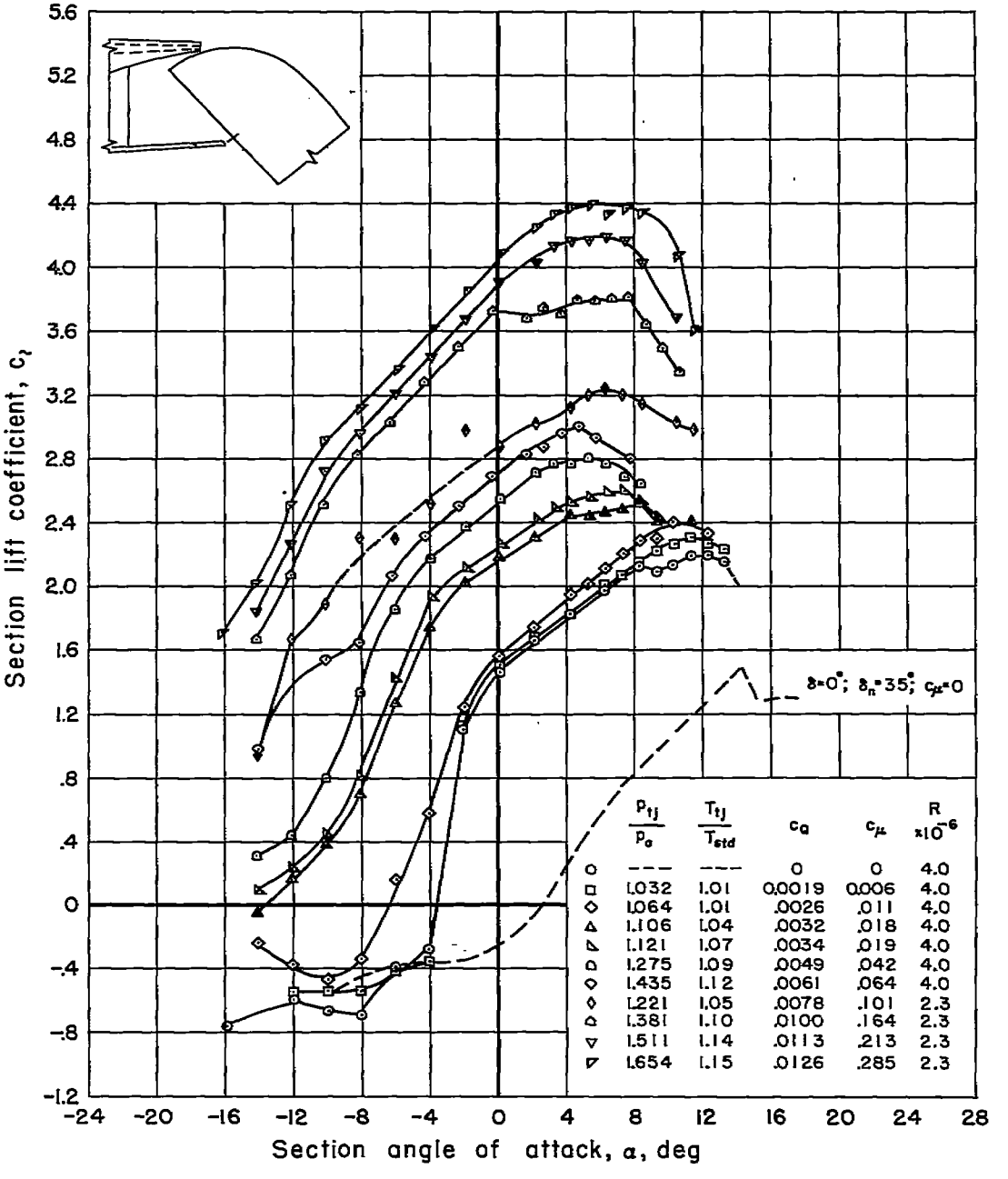

Figure 36.- Effect of blowing on the lift of the model with flap C deflected 50°; s/c = 0.00110; δ_n = 35°.

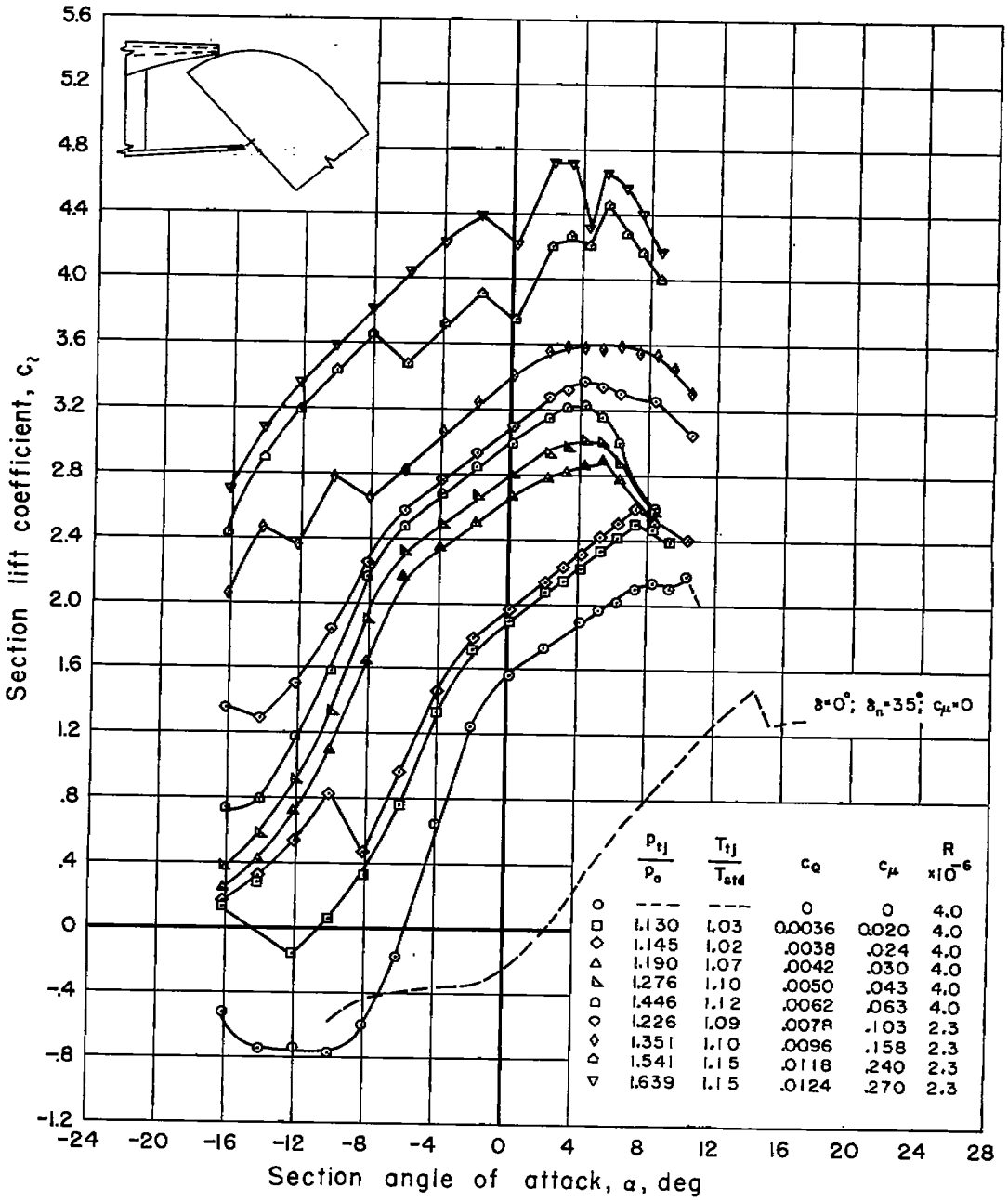

(a) Variable α.

Figure 37.- Effect of blowing on the lift of the model with flap C deflected 60°; s/c = 0.00110; δ_n = 35°.

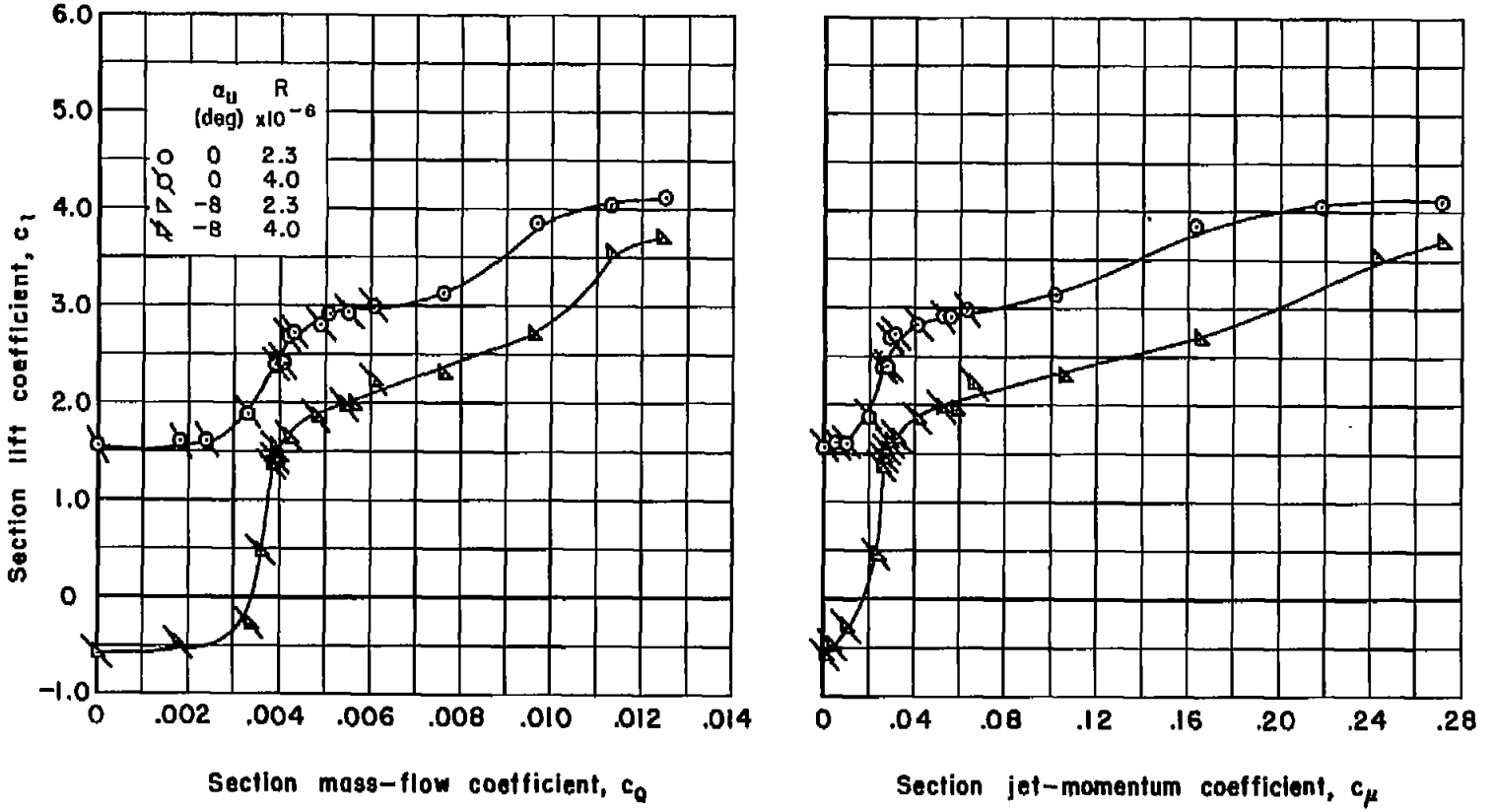

(b) Variable nozzle flow.

Figure 37.- Concluded.

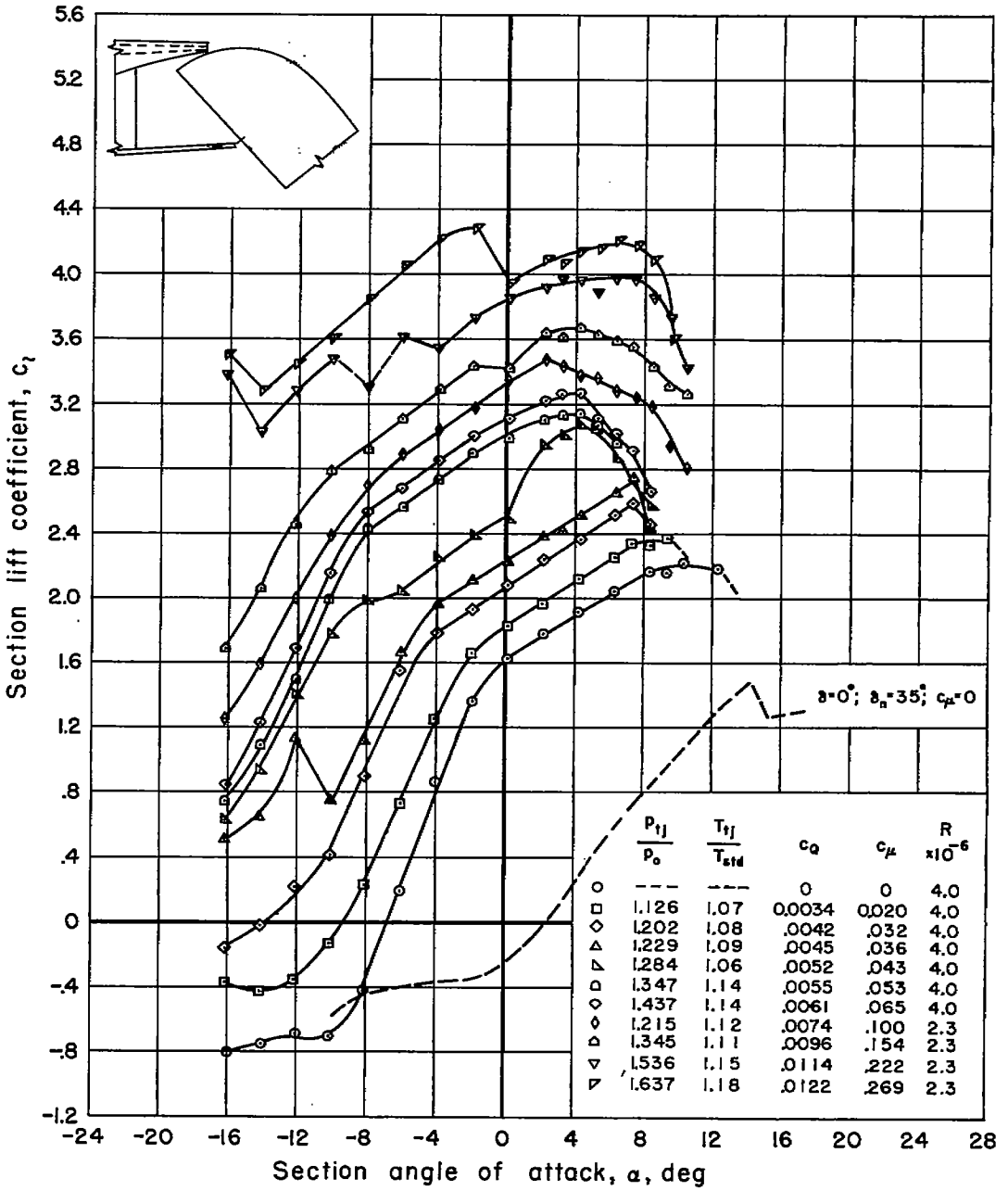

Figure 38.- Effect of blowing on the lift of the model with flap C deflected 70°; s/c = 0.00110; δ_n = 35°.

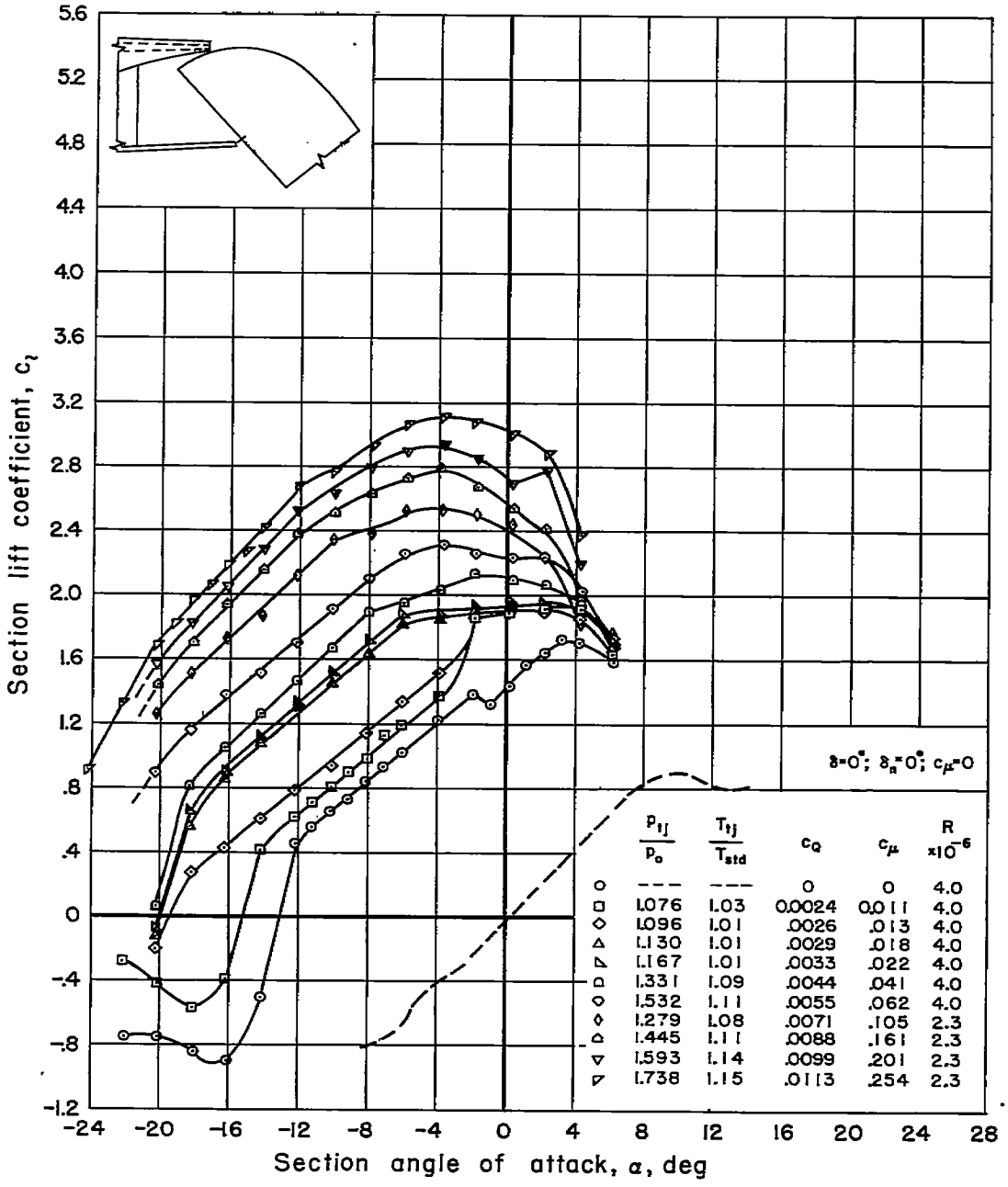

(a) Variable α.

Figure 39.- Effect of blowing on the lift of the model with flap C deflected 50° and $\delta_n = 0^\circ$; $s/c = 0.00110$.

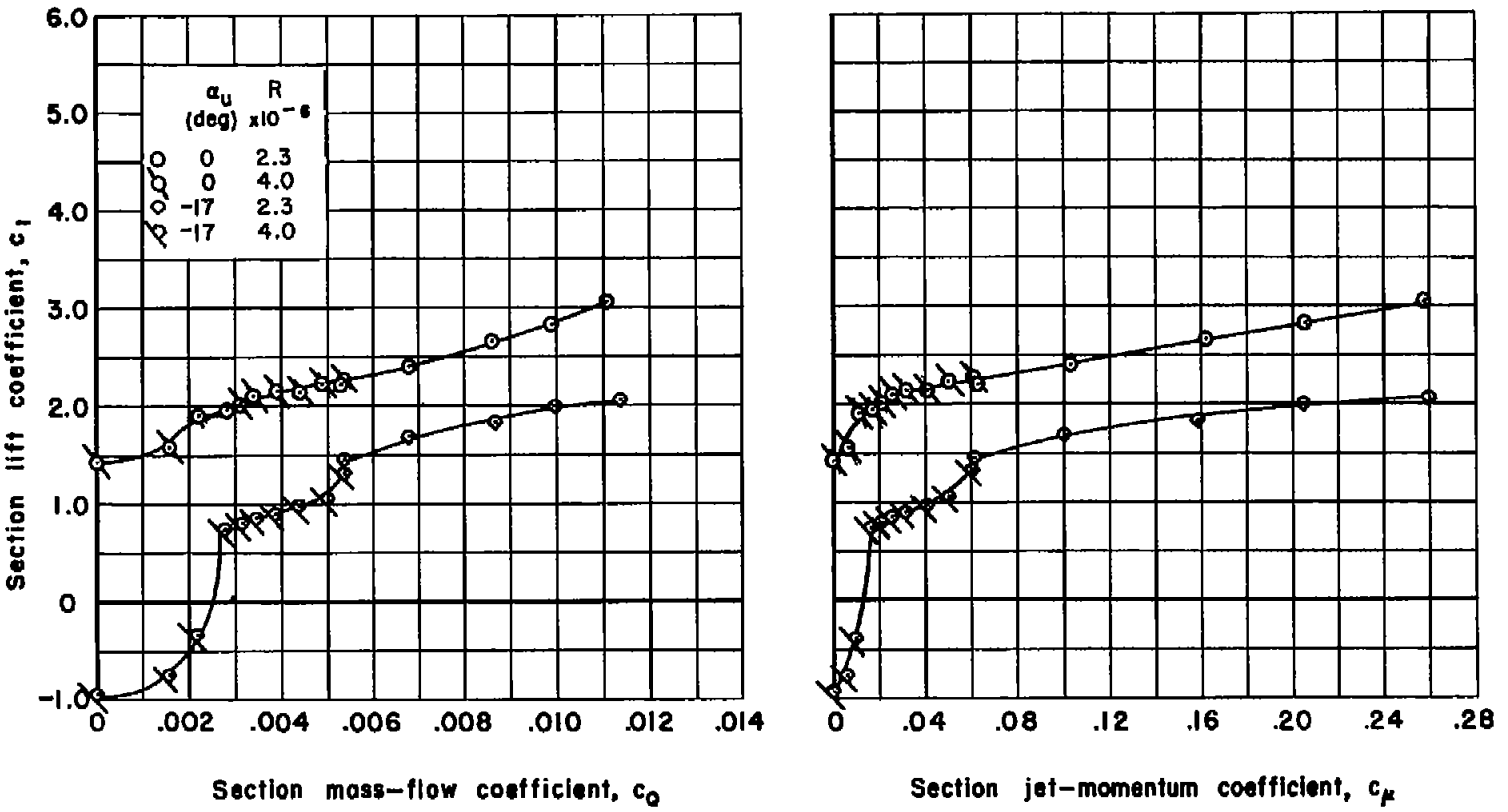

(b) Variable nozzle flow.

Figure 39.- Concluded.

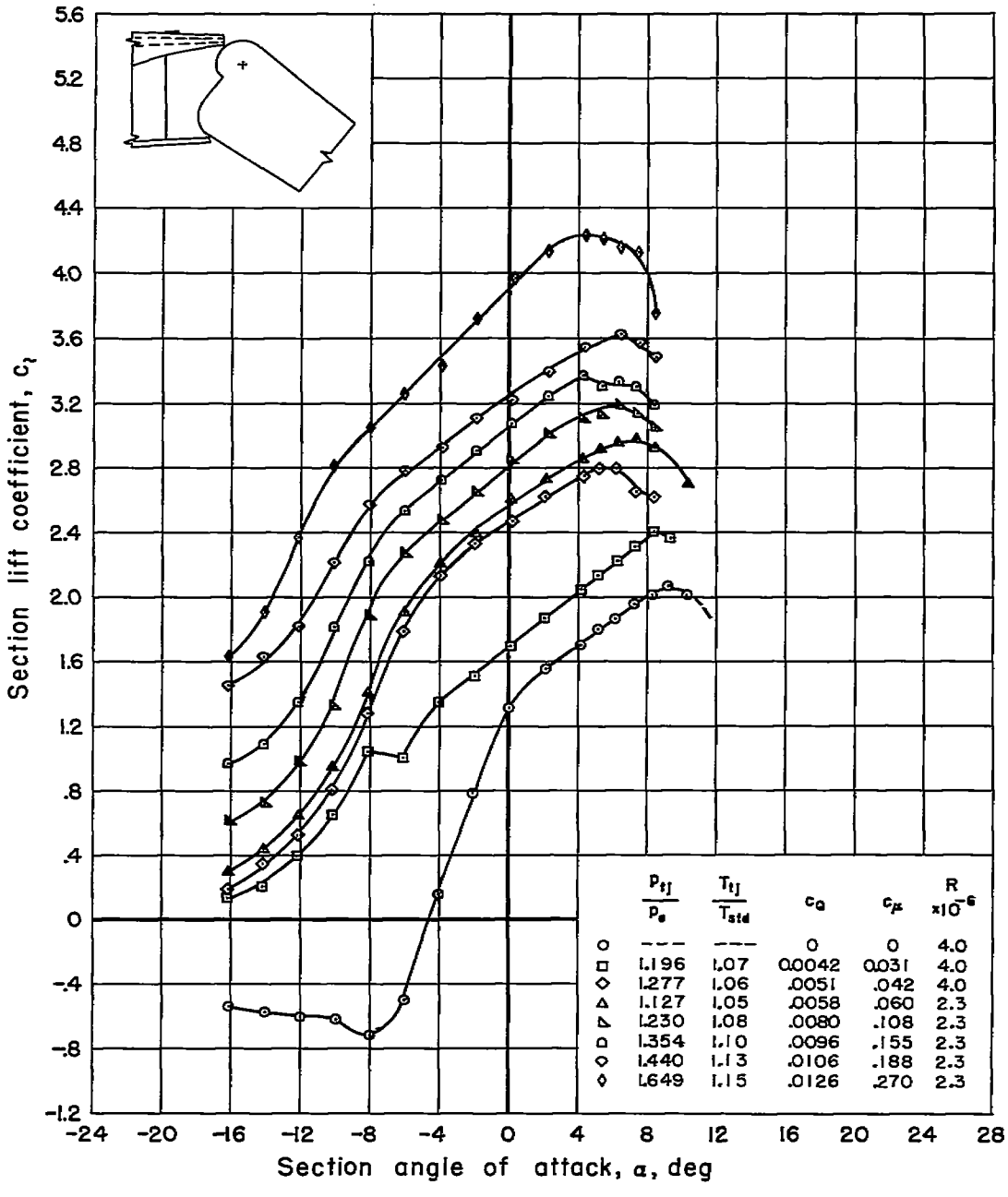

Figure 40.- Effect of blowing on the lift of the model with flap D deflected 50°; s/c = 0.00110; δ_n = 35°.

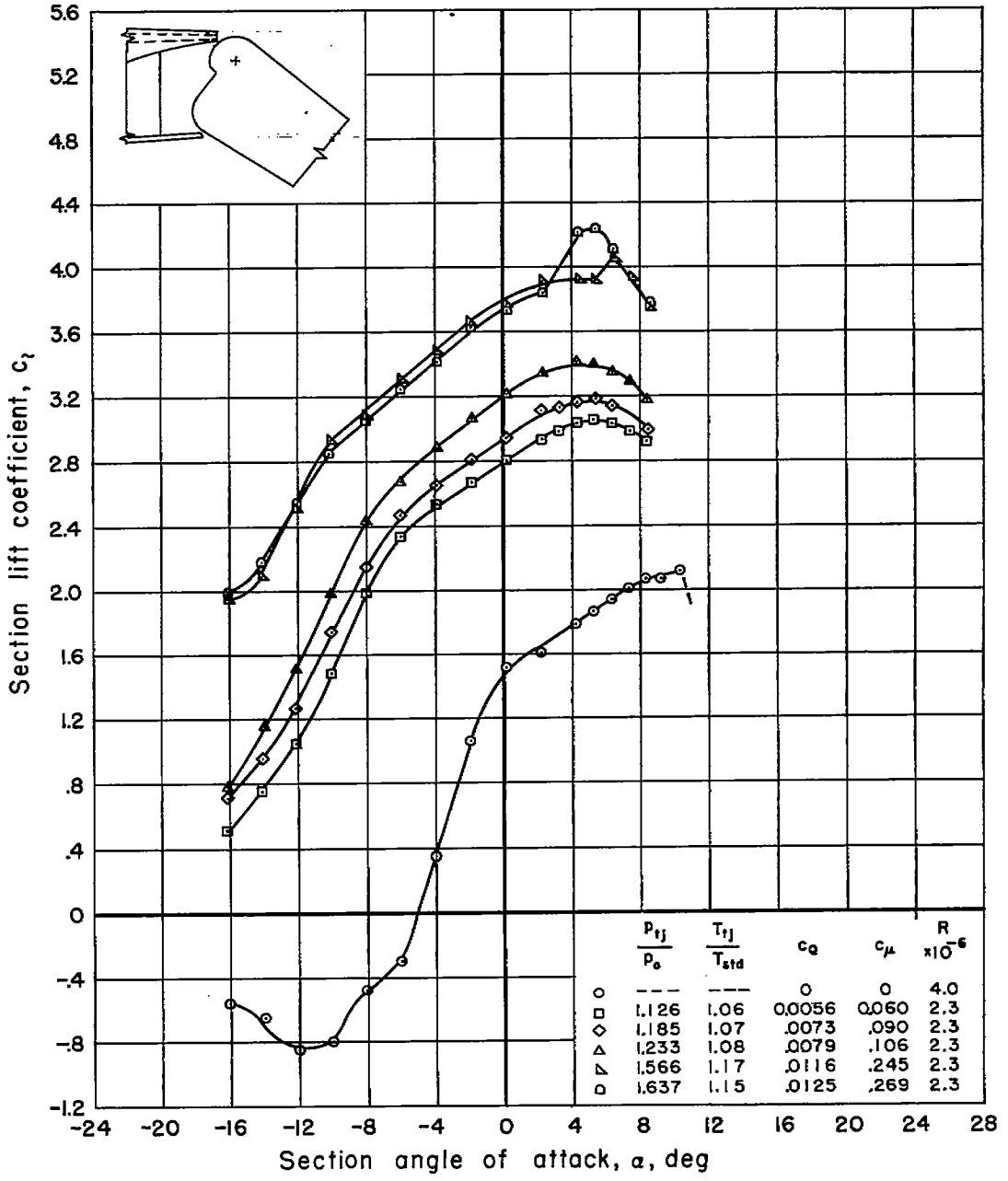

(a) Variable α.

Figure 41.- Effect of blowing on the lift of the model with flap D deflected 60°; s/c = 0.00110; δ_n = 35°.

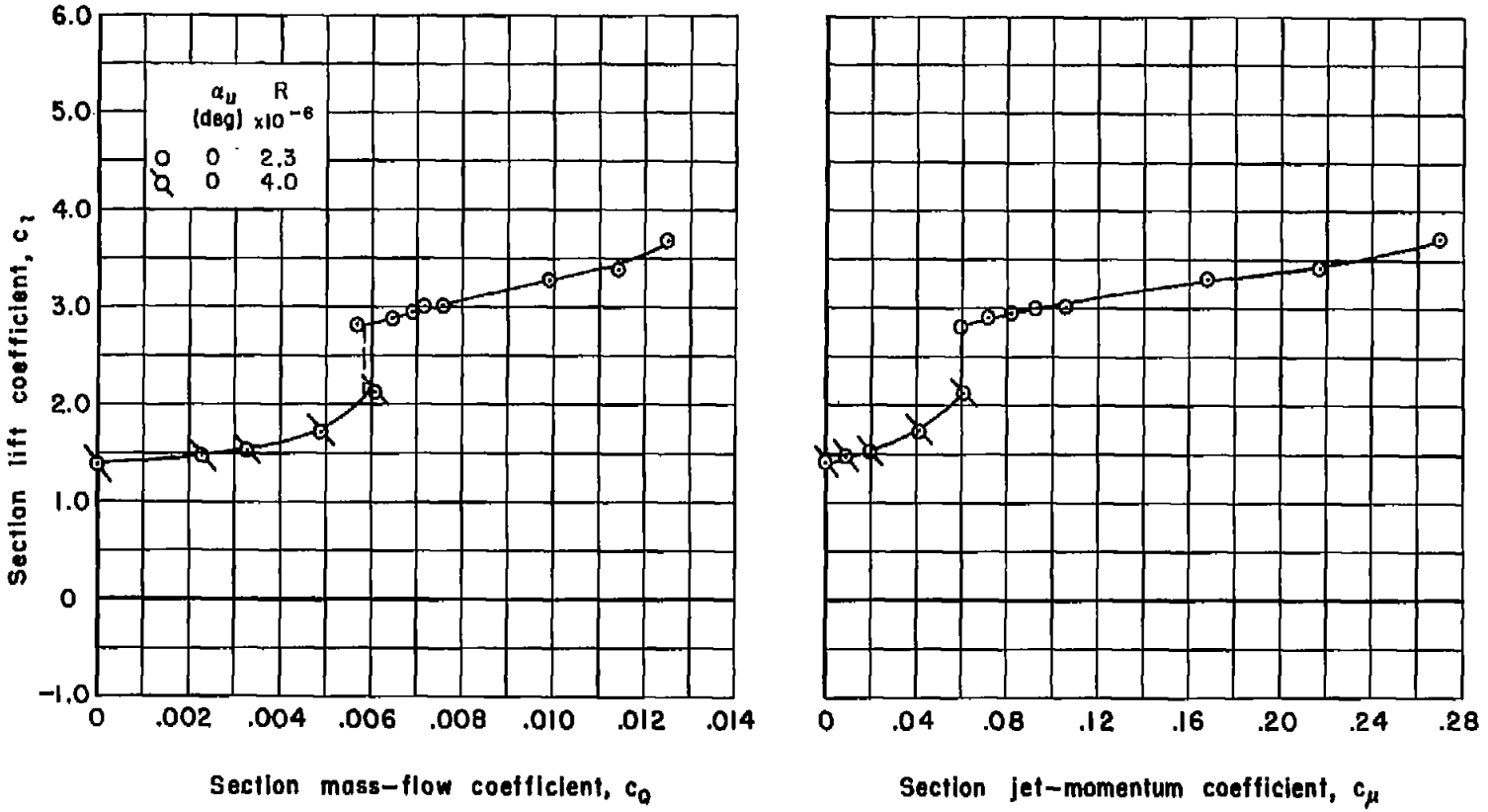

(b) Variable nozzle flow.

Figure 41.- Concluded.

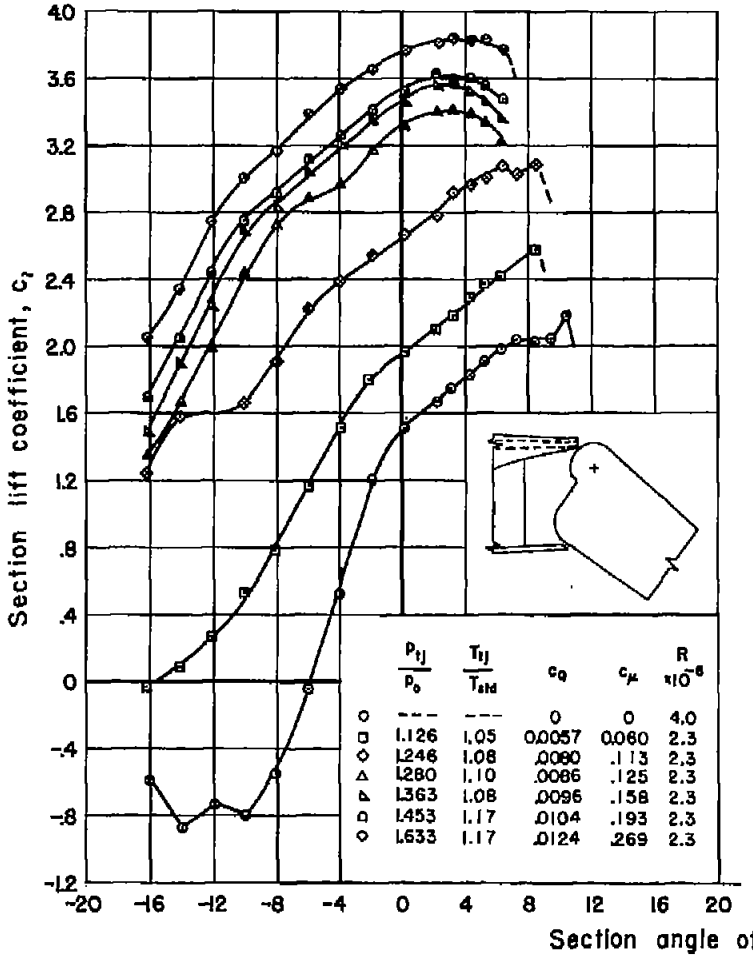

Figure 42.- Effect of blowing on the lift of the model with flap D deflected 70°; s/c = 0.00110; δ_n = 35°.

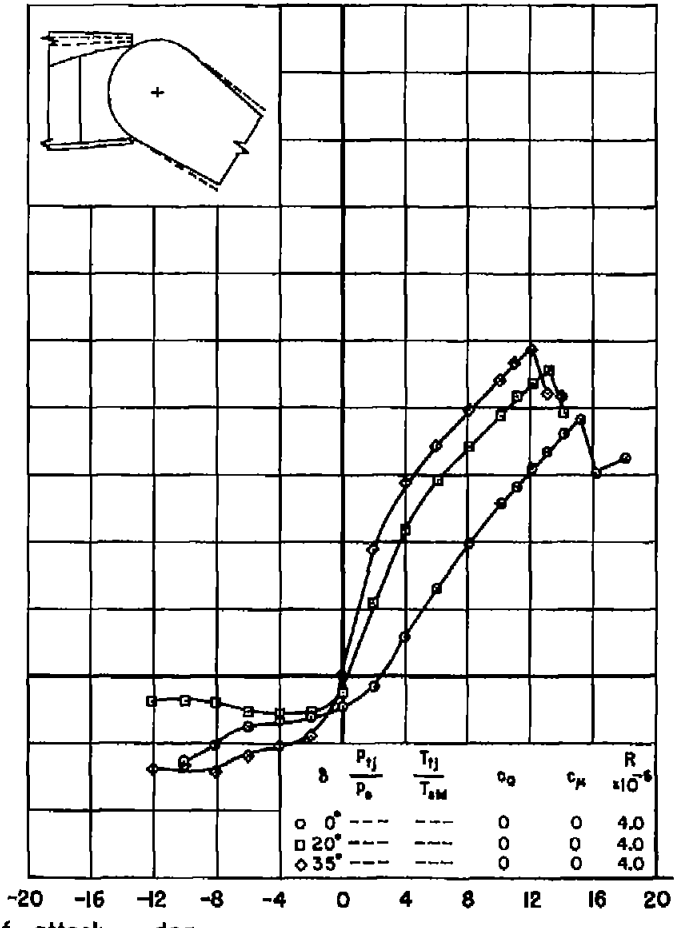

Figure 43.- Effect of trailing-edge flap deflection on the lift of the model with flap F; s/c = 0.00110; δ_n = 35°.

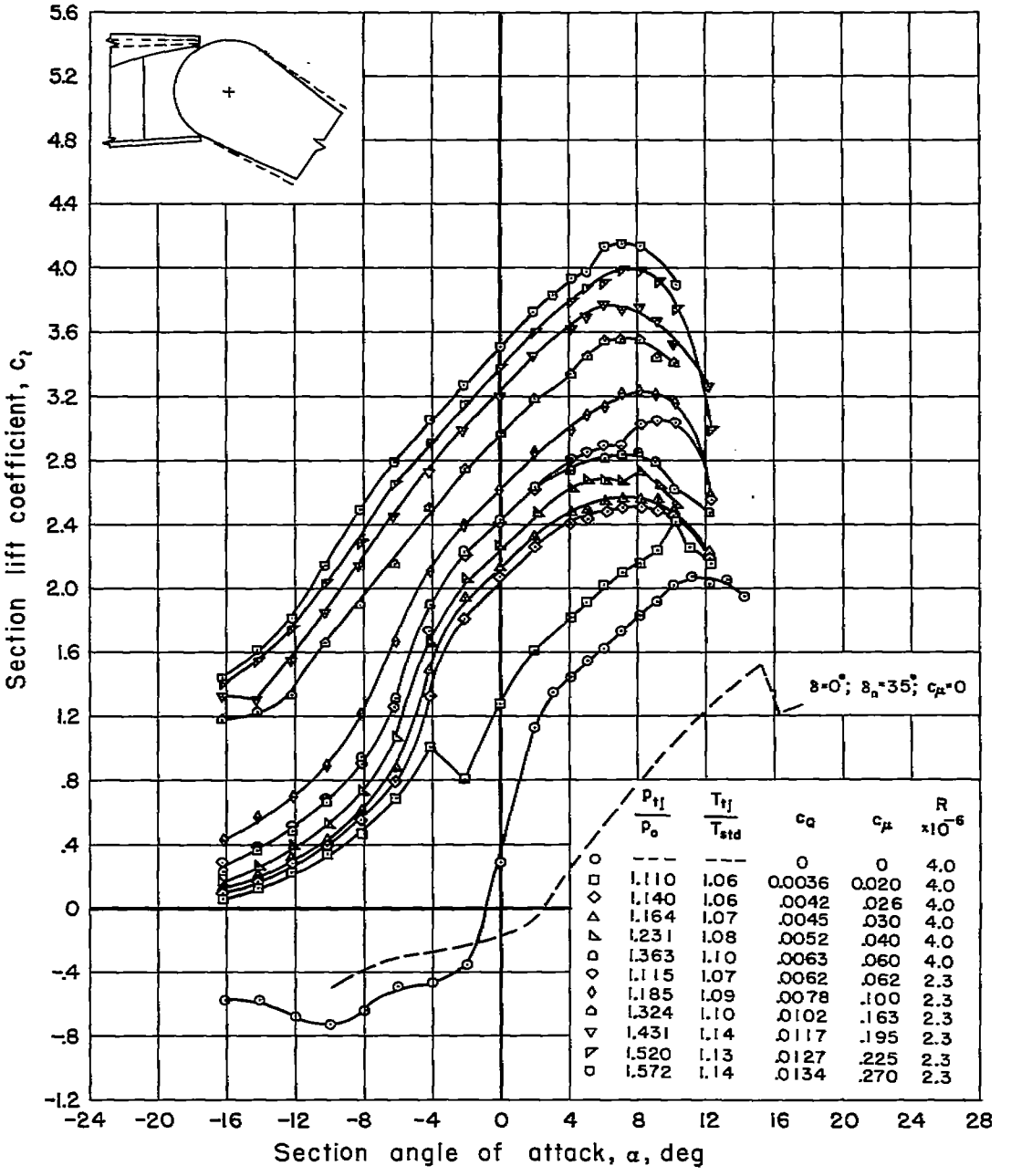

Figure 44.- Effect of blowing on the lift of the model with flap F deflected 50°; s/c = 0.00110; δ_n = 35°.

[redacted]

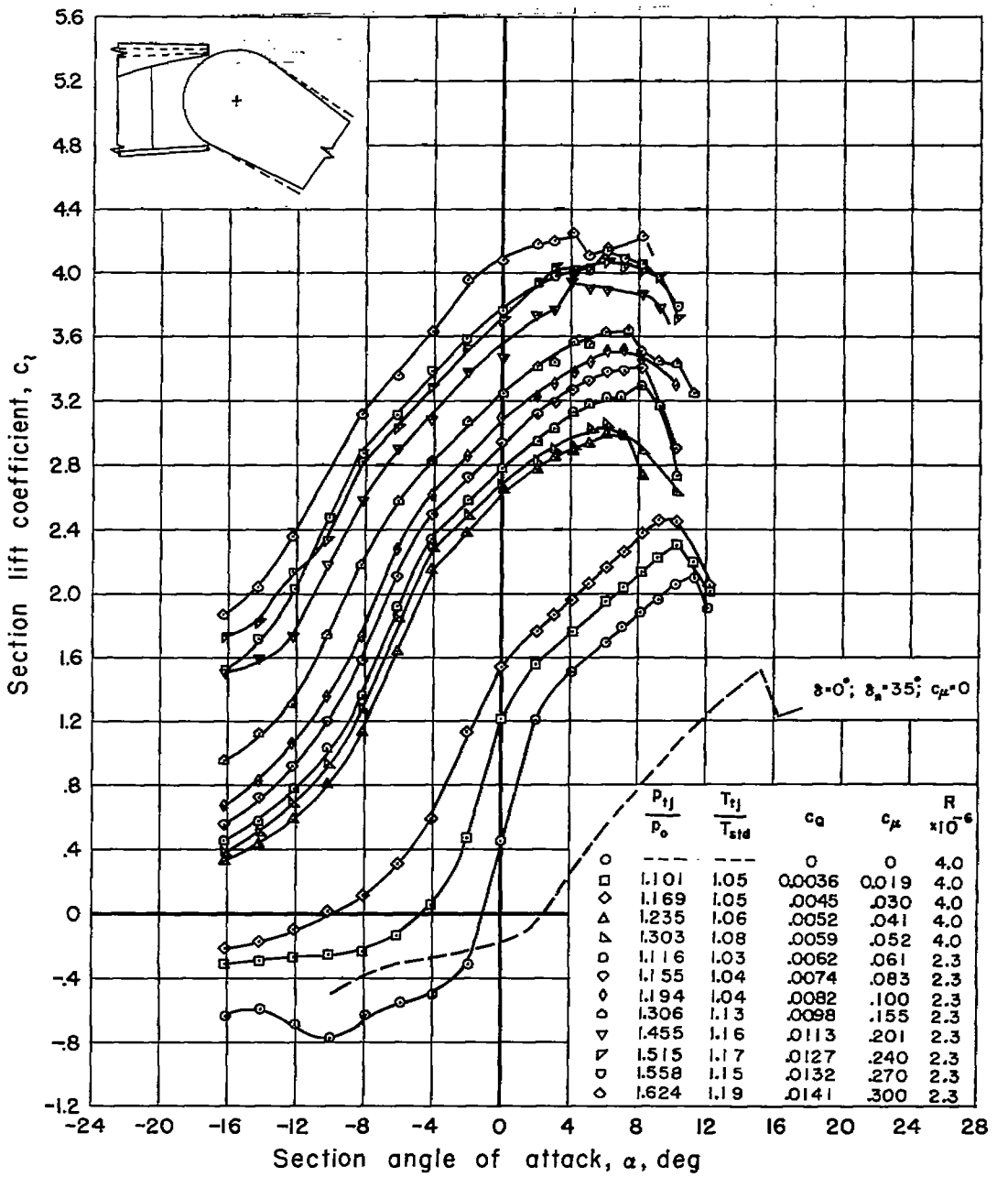

(a) Variable α.

Figure 45.- Effect of blowing on the lift of the model with flap F deflected 60°; s/c = 0.00110; δ_n = 35°.

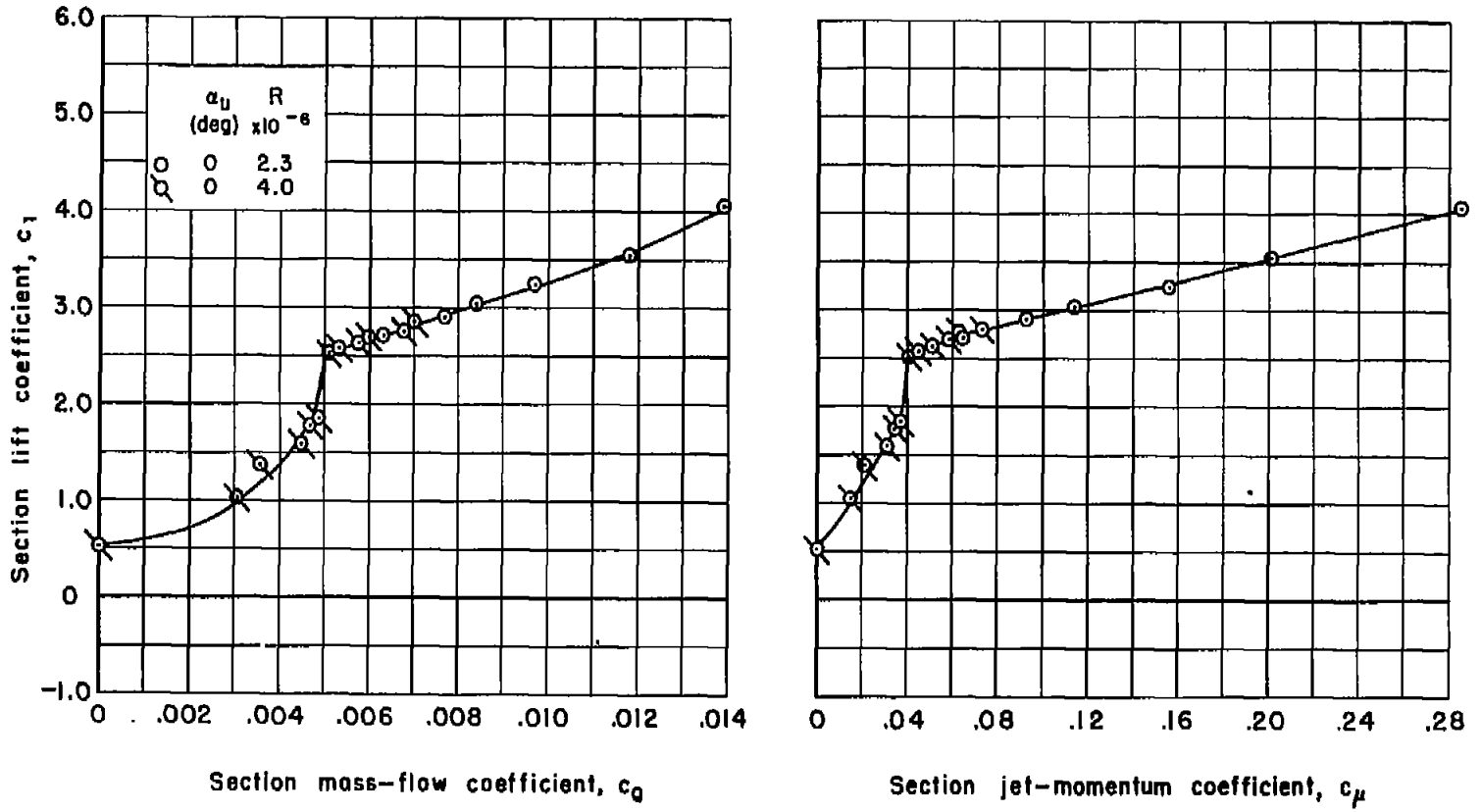

(b) Variable nozzle flow.

Figure 45.- Concluded.

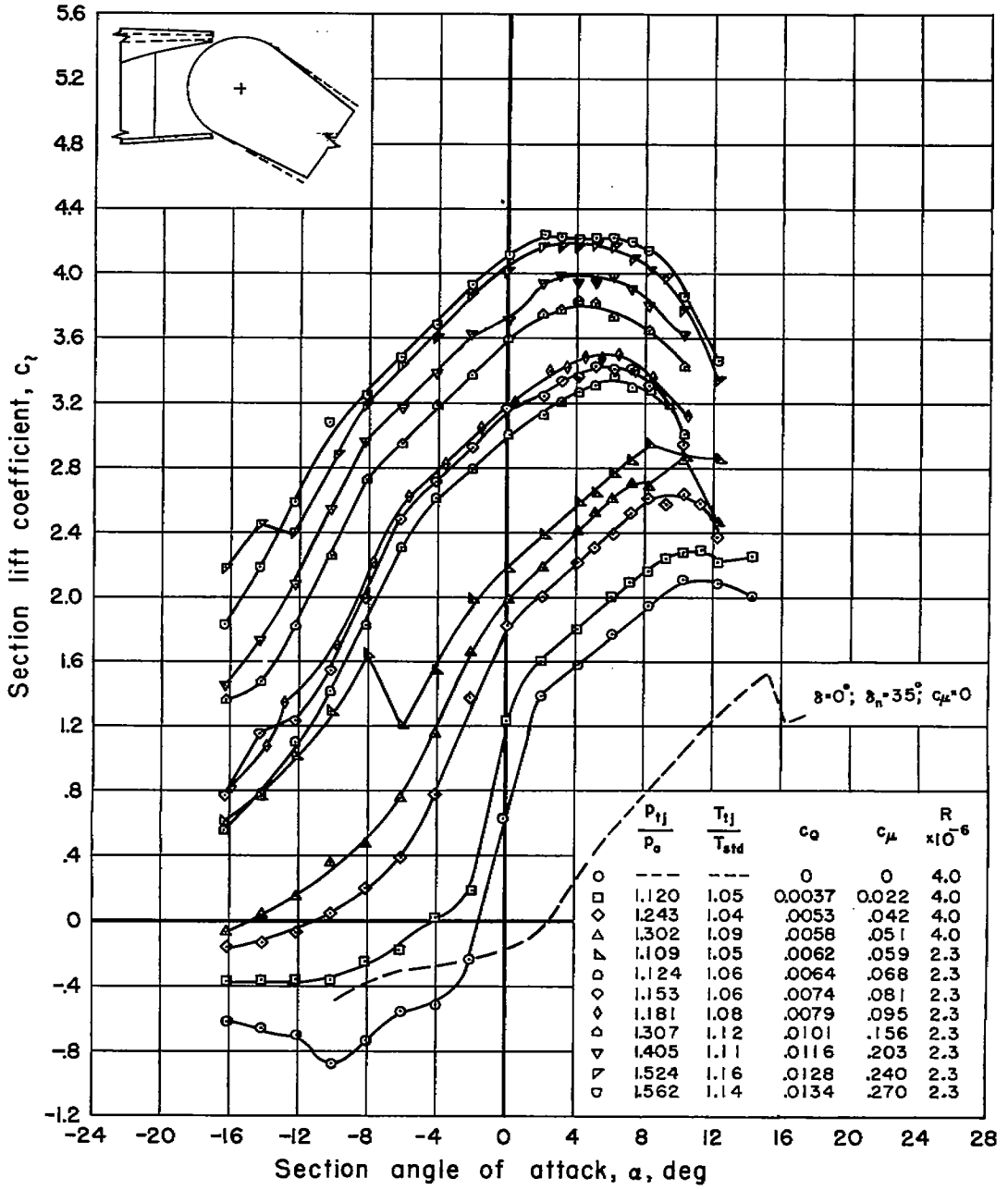

Figure 46.- Effect of blowing on the lift of the model with flap F deflected 70°; s/c = 0.00110; δ_n = 35°.

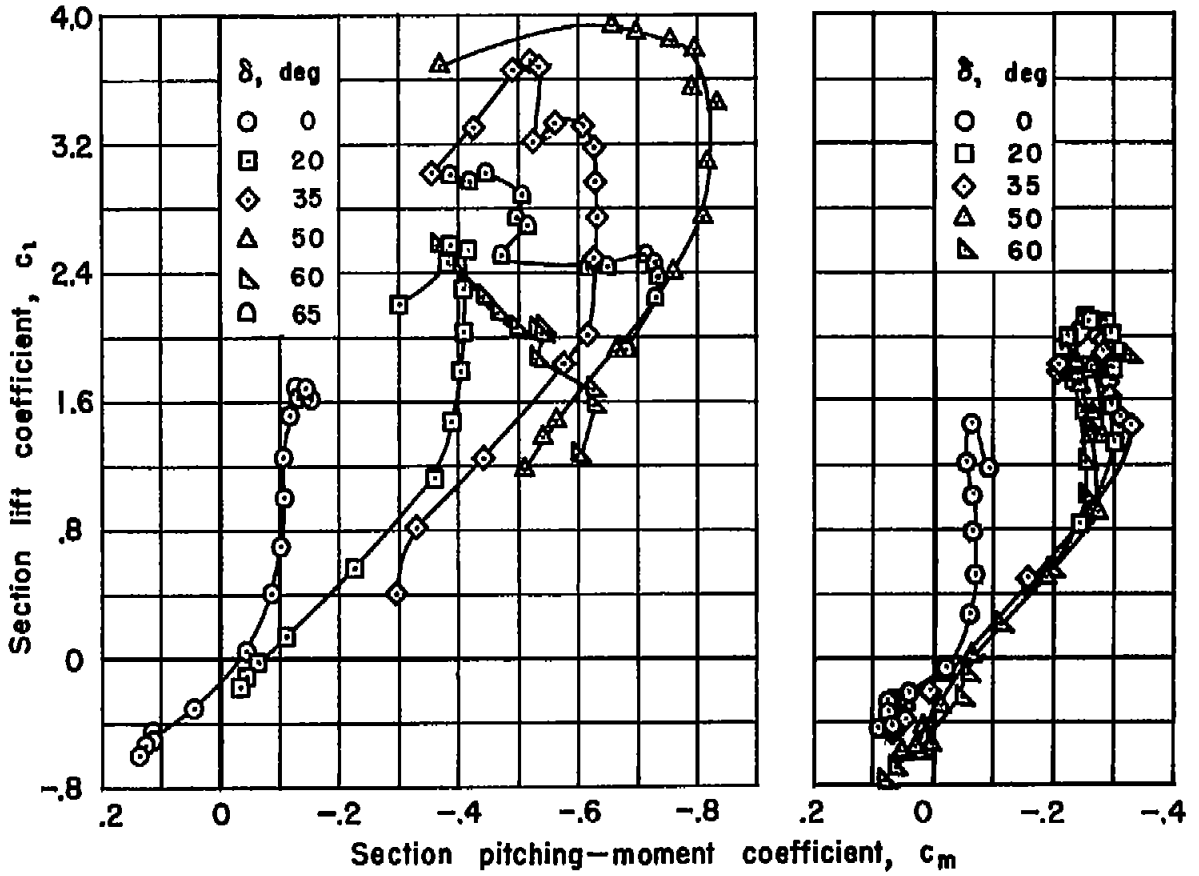

(a) $c_\mu = 0$

(b) $c_\mu \cong 0.12$

Figure 47.- Effect of blowing and of flap deflection on the pitching-moment characteristics of the model with flap A in the extended position; $s/c = 0.00110$; $\delta_n = 35^\circ$.

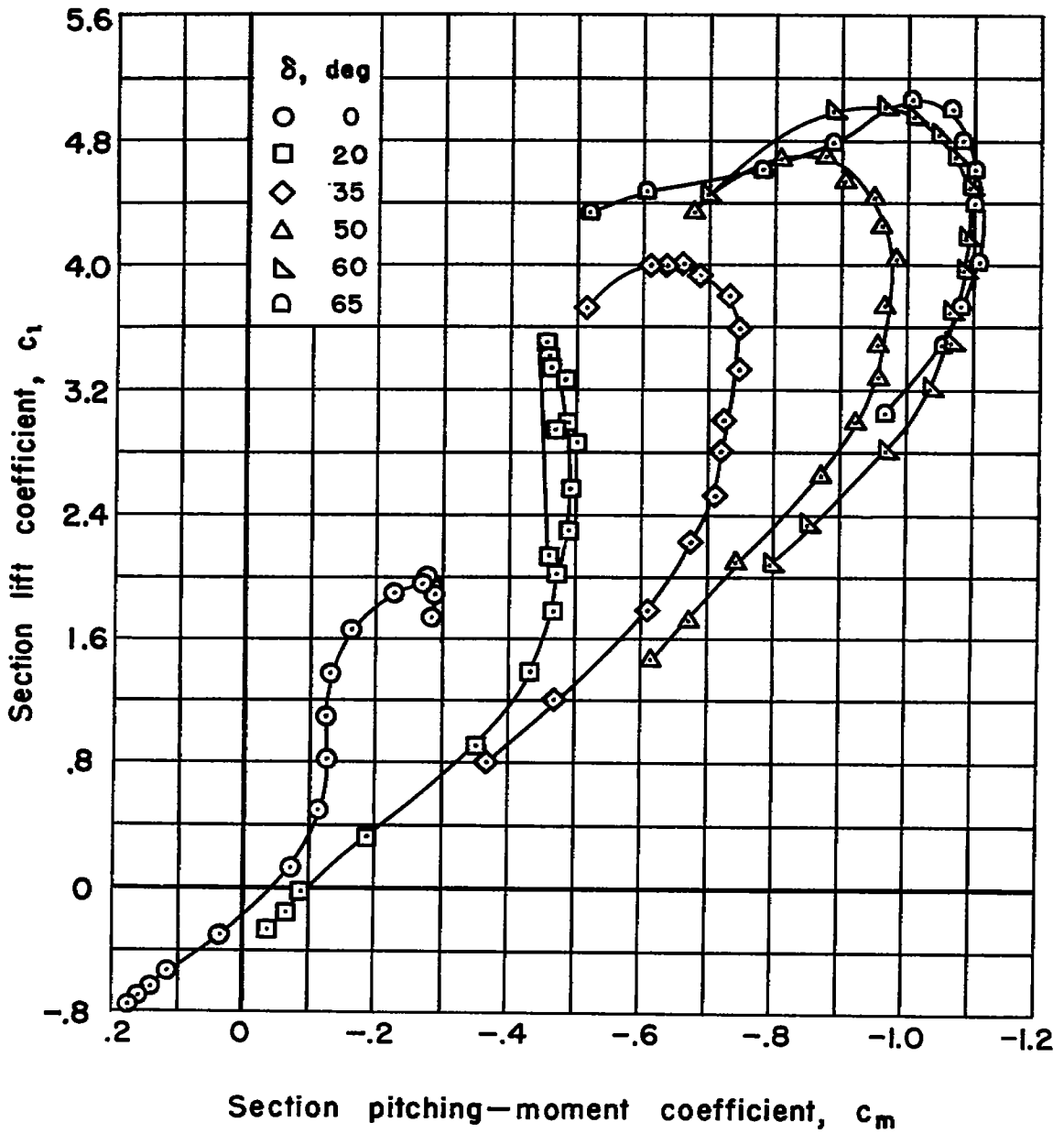

(c) $c_\mu \cong 0.27$

Figure 47.- Concluded.

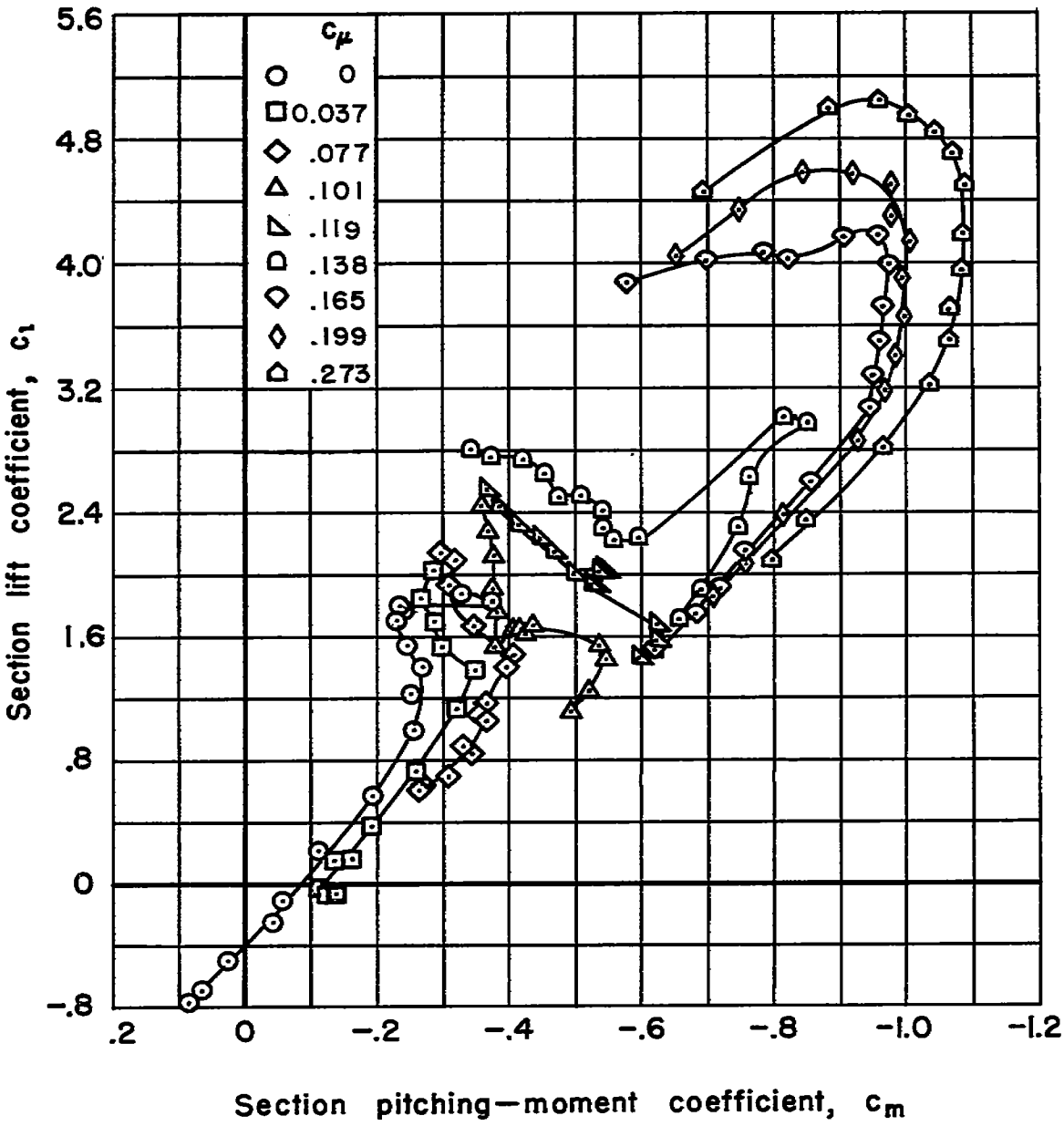

Figure 48.- Effect of blowing on the pitching-moment characteristics of the model with flap A deflected 60° in the extended position; s/c = 0.00110; δ_n = 35°.

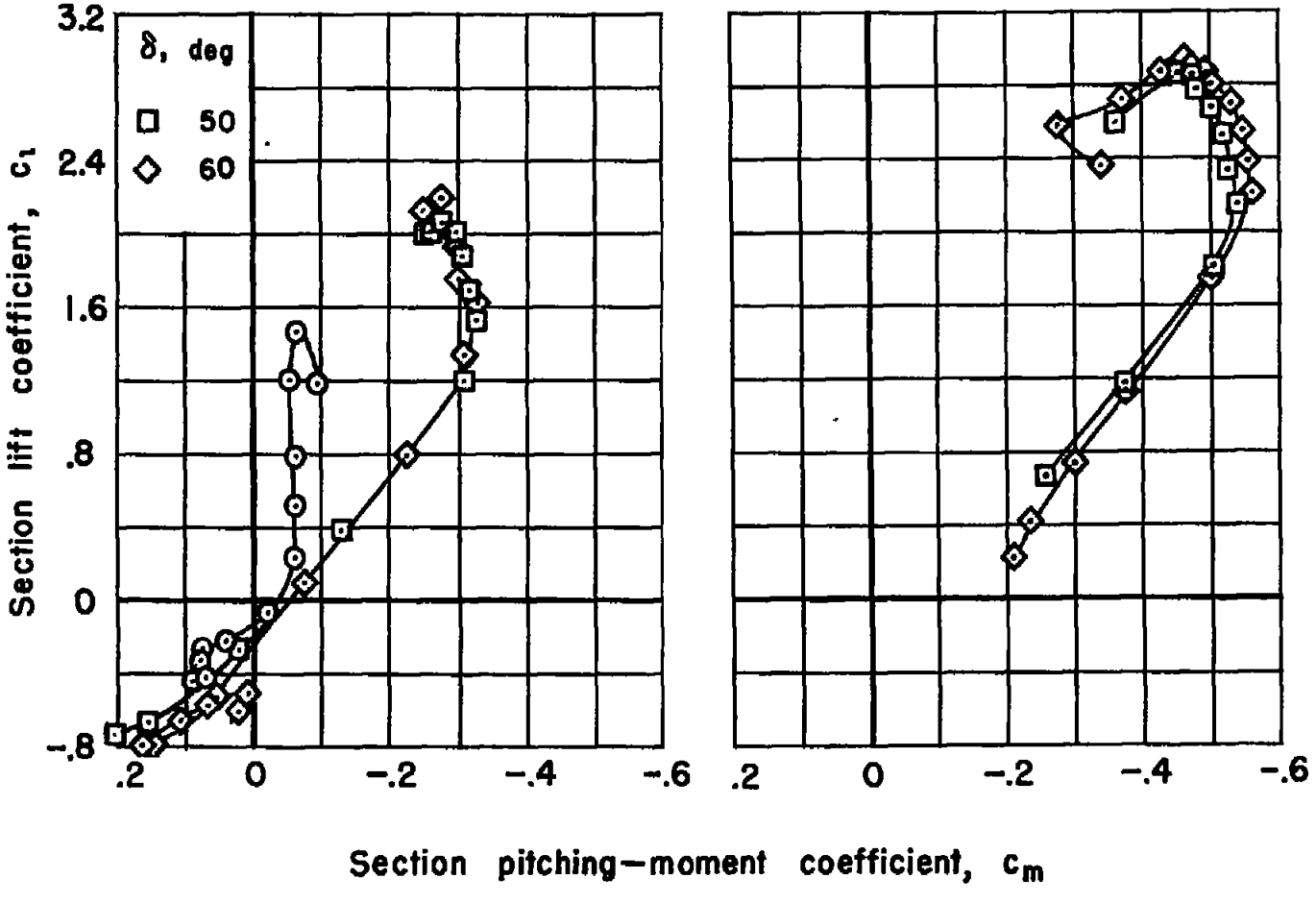

(a) $c_\mu = 0$

(b) $c_\mu \cong 0.03$

Figure 49.- Effect of blowing and of flap deflection on the pitching-moment characteristics of the model with flap A against the nozzle; $s/c = 0.00110$; $\delta_n = 35^\circ$.

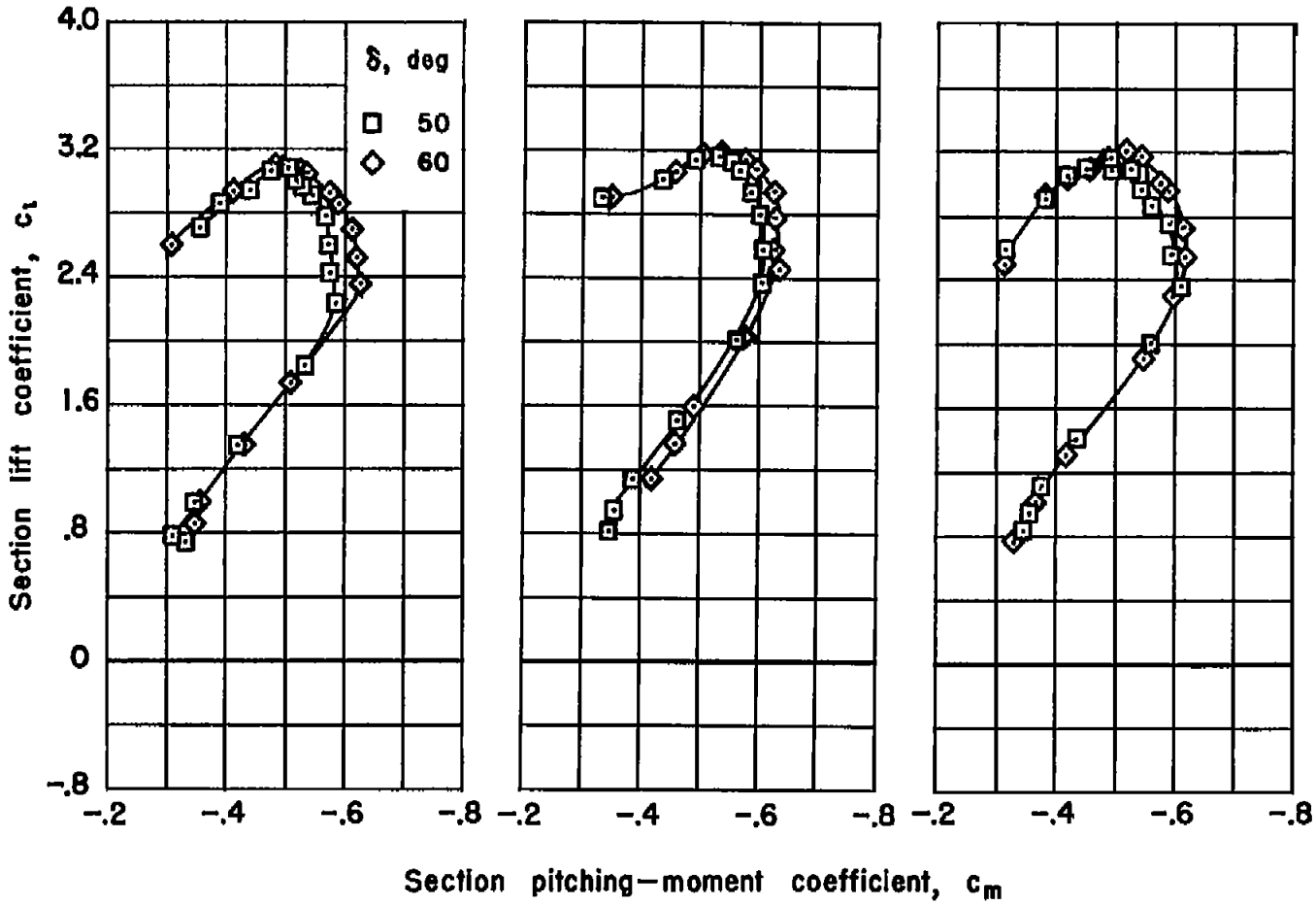

(a) s/c = 0.00065 (b) s/c = 0.00036 (c) s/c = 0.00017

Figure 50.- Effect of nozzle height and of flap deflection on the pitching-moment characteristics of the model with flap A against the nozzle; $c_\mu \cong 0.03$; $\delta_n = 35^\circ$.

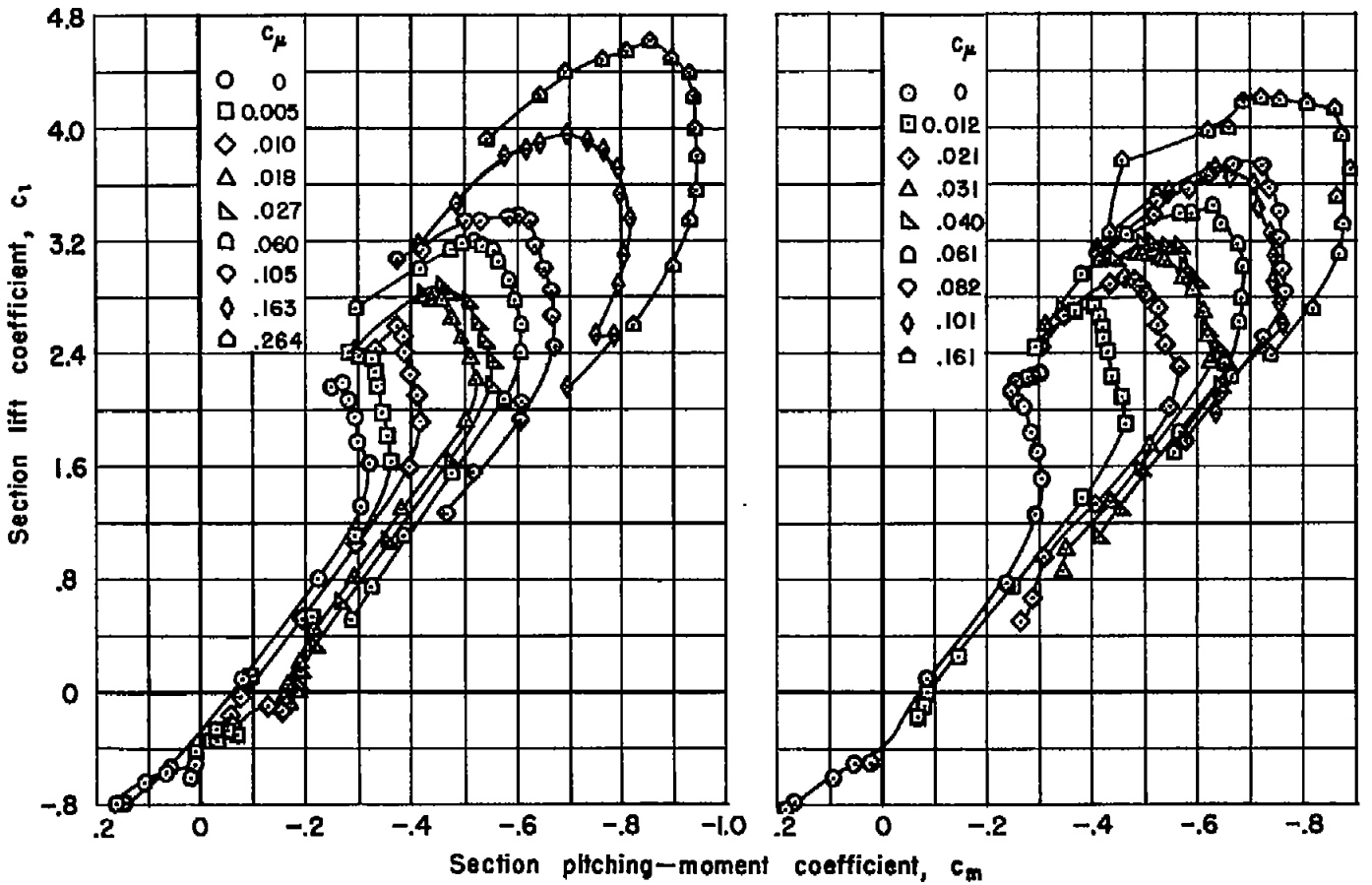

(a) s/c = 0.00110

(b) s/c = 0.00065

Figure 51.- Effect of blowing and of nozzle height on the pitching-moment characteristics of the model with flap A deflected 60° against the nozzle; $\delta_n = 35°$.

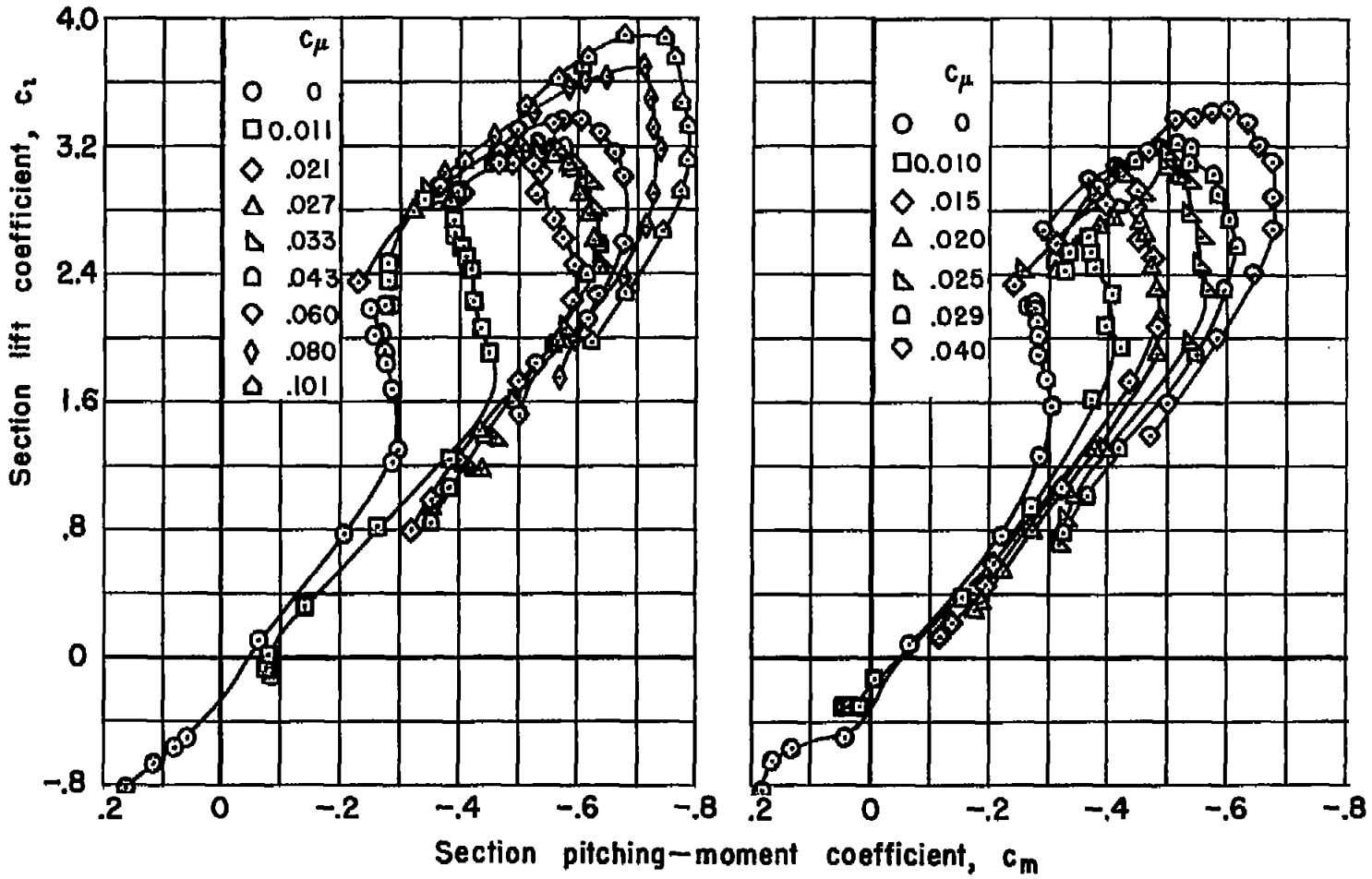

(c) s/c = 0.00036

(d) s/c = 0.00017

Figure 51.- Concluded.

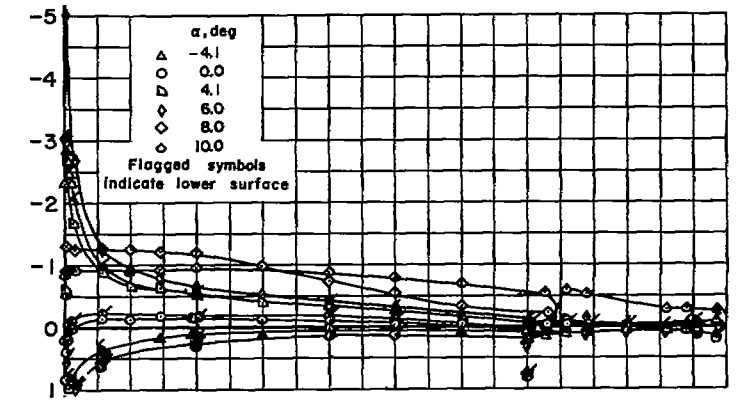

(a) $c_Q = 0$; $c_\mu = 0$; $R = 4.0 \times 10^6$

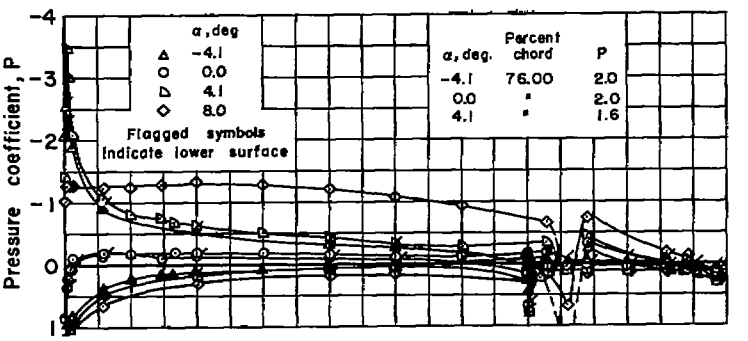

(b) $c_Q = 0.0082$; $c_\mu = 0.117$; $R = 3.3 \times 10^6$

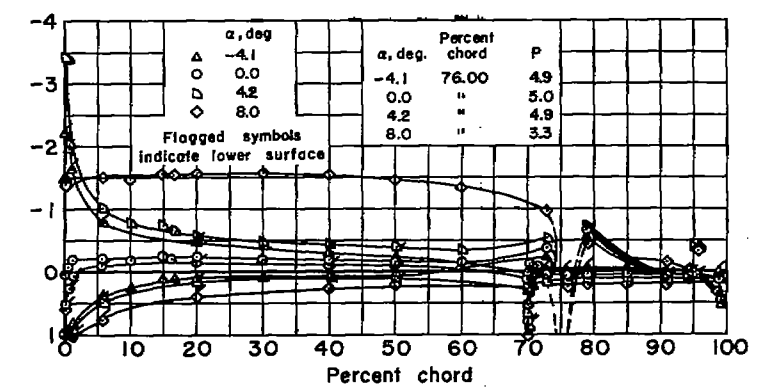

(c) $c_Q = 0.0129$; $c_\mu = 0.273$; $R = 2.3 \times 10^6$

Figure 52.- Effect of angle of attack and of blowing on the chordwise distribution of pressure of the model with flap A undeflected; $s/c = 0.00110$; $\delta_n = 0$.

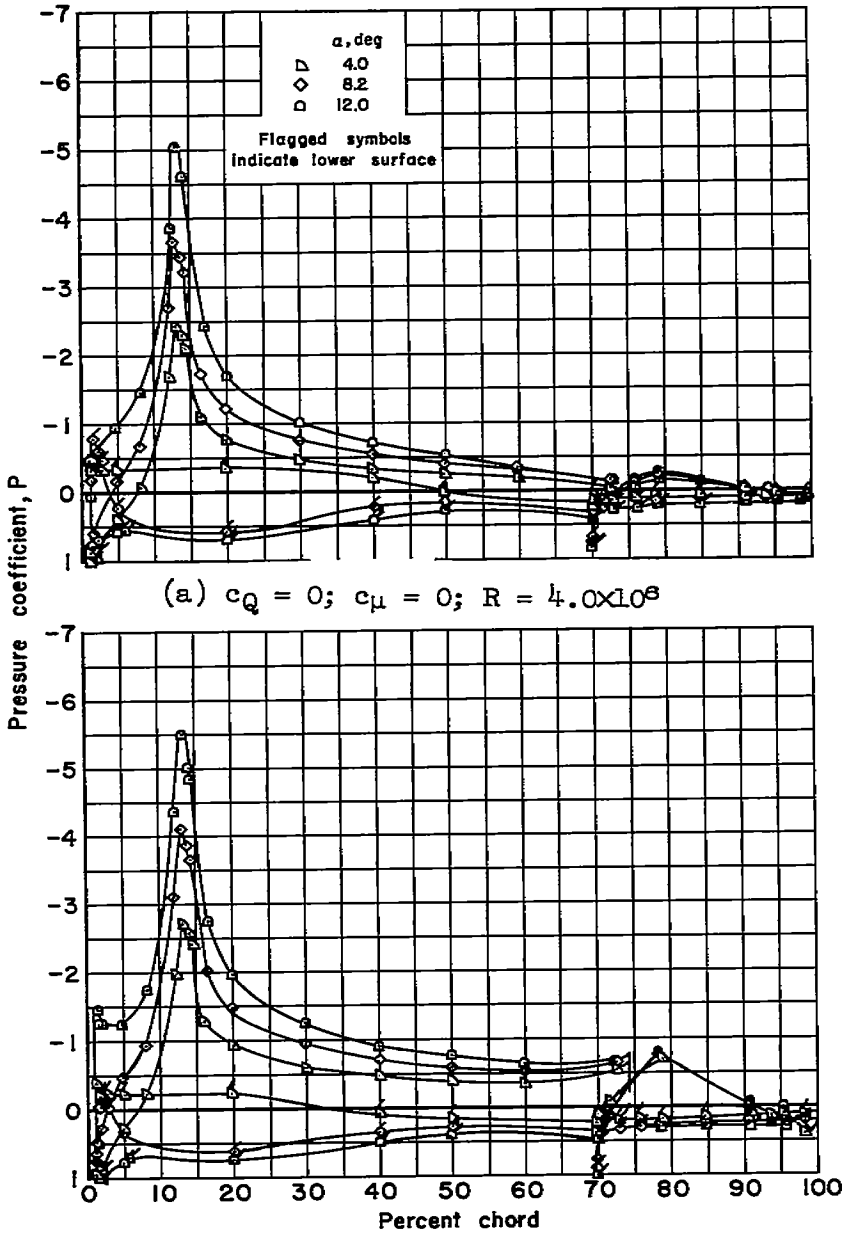

(a) $c_Q = 0$; $c_\mu = 0$; $R = 4.0 \times 10^6$

(b) $c_Q = 0.0126$; $c_\mu = 0.265$; $R = 2.3 \times 10^6$

Figure 53.- Effect of angle of attack and of blowing on the chordwise distribution of pressure of the model with flap A undeflected; $s/c = 0.00110$; $\delta_n = 35^\circ$.

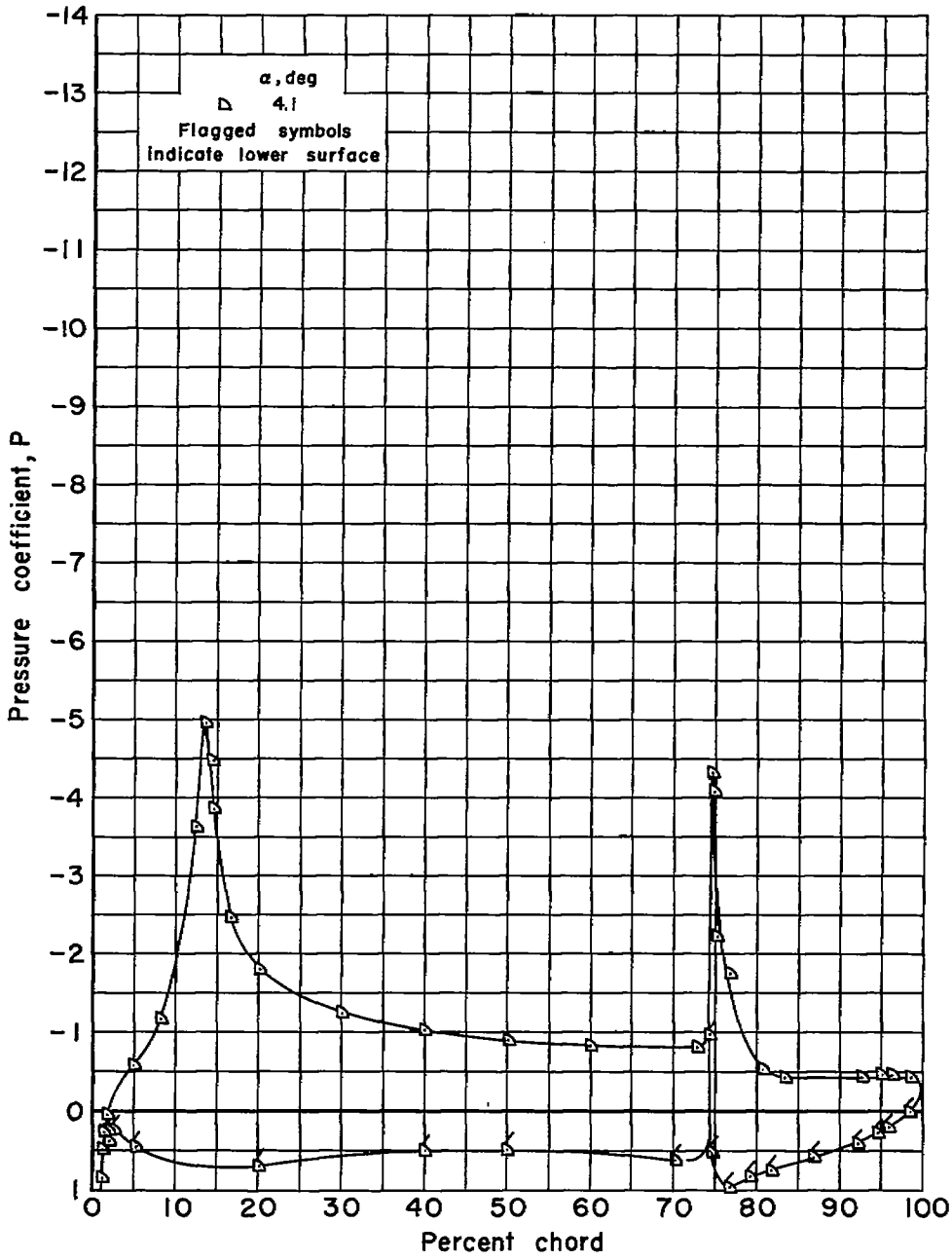

(a) $c_Q = 0$; $c_\mu = 0$; $R = 4.0 \times 10^6$

Figure 54.- Effect of angle of attack and of blowing on the chordwise distribution of pressure of the model with flap A deflected 35° in the extended position; $s/c = 0.00110$; $\delta_n = 35°$.

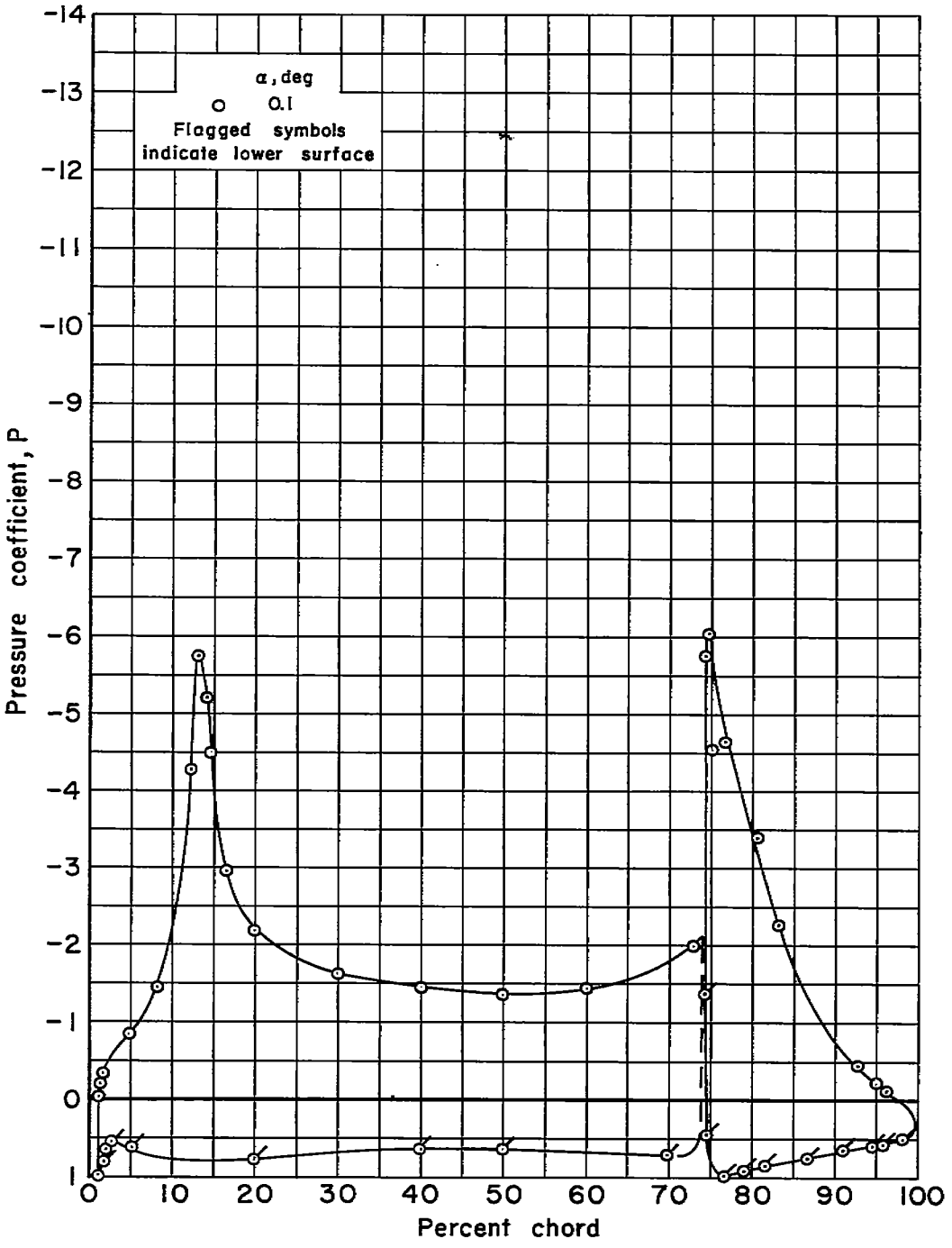

(b) $c_Q = 0.0056$; $c_\mu = 0.060$; $R = 4.0 \times 10^6$

Figure 54.- Continued.

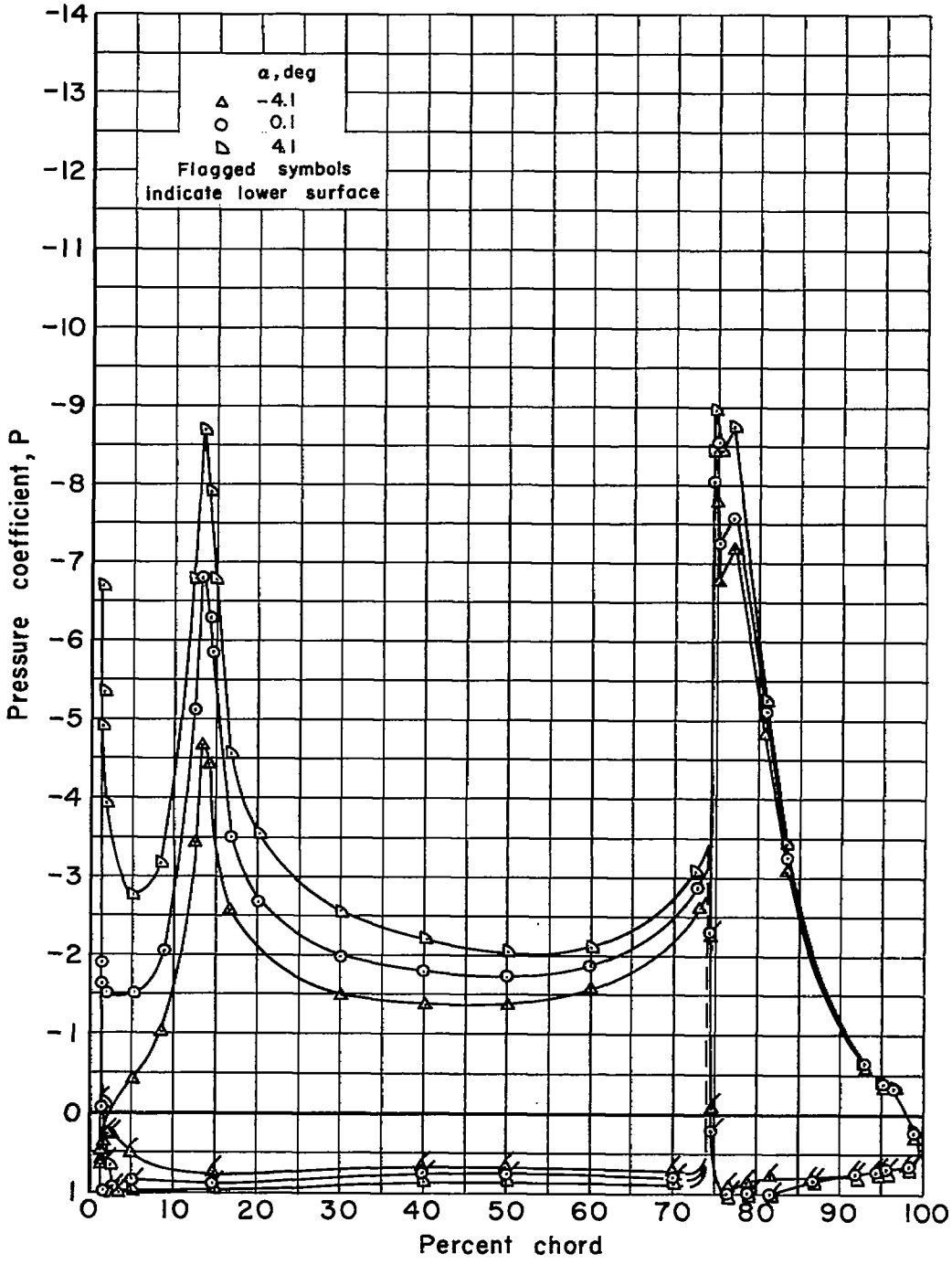

(c) $c_Q = 0.0127$; $c_\mu = 0.270$; $R = 2.3 \times 10^6$

Figure 54.- Concluded.

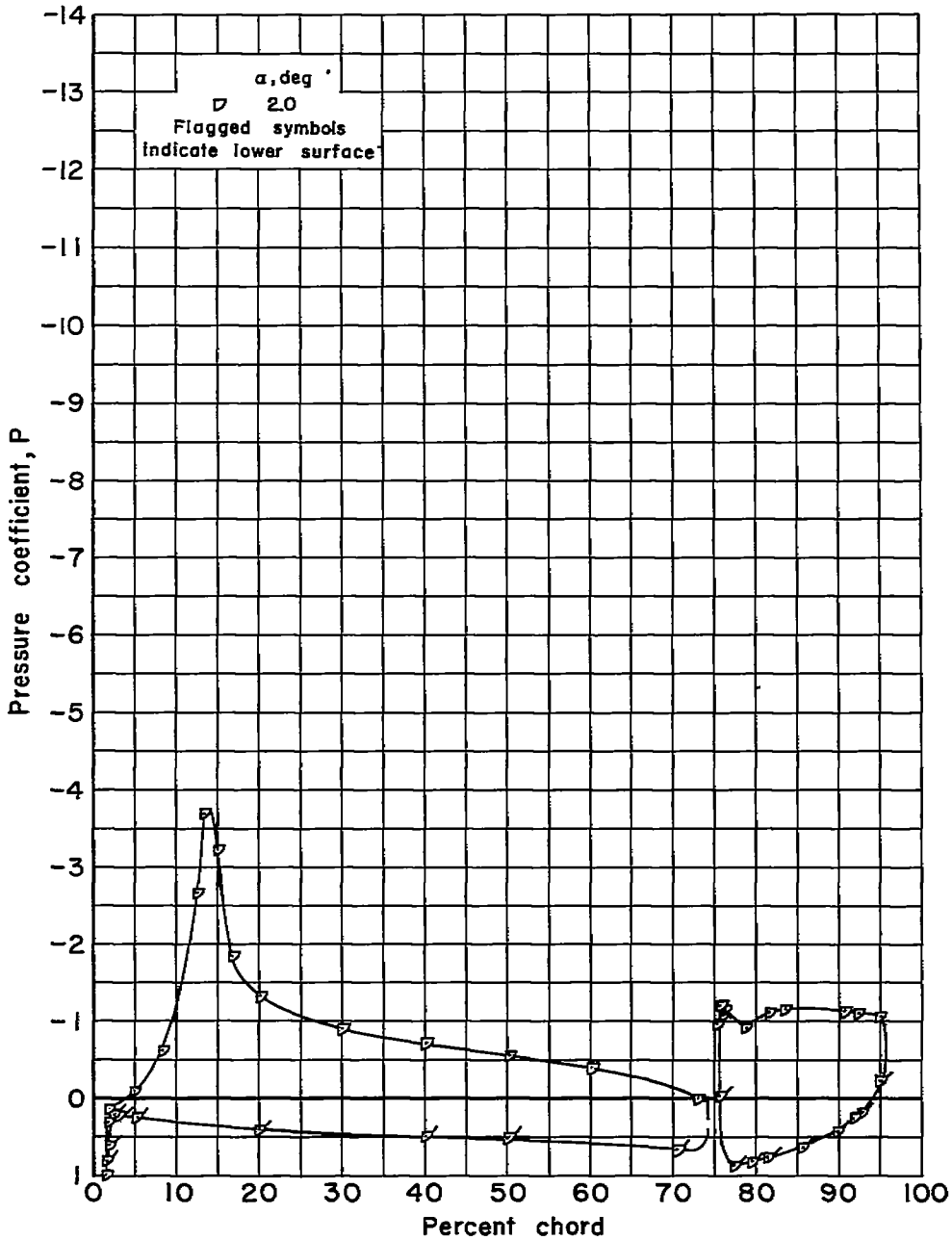

(a) $c_Q = 0$; $c_\mu = 0$; $R = 4.0 \times 10^6$

Figure 55.- Effect of angle of attack and of blowing on the chordwise distribution of pressure of the model with flap A deflected 50° in the extended position; $s/c = 0.00110$; $\delta_n = 35°$.

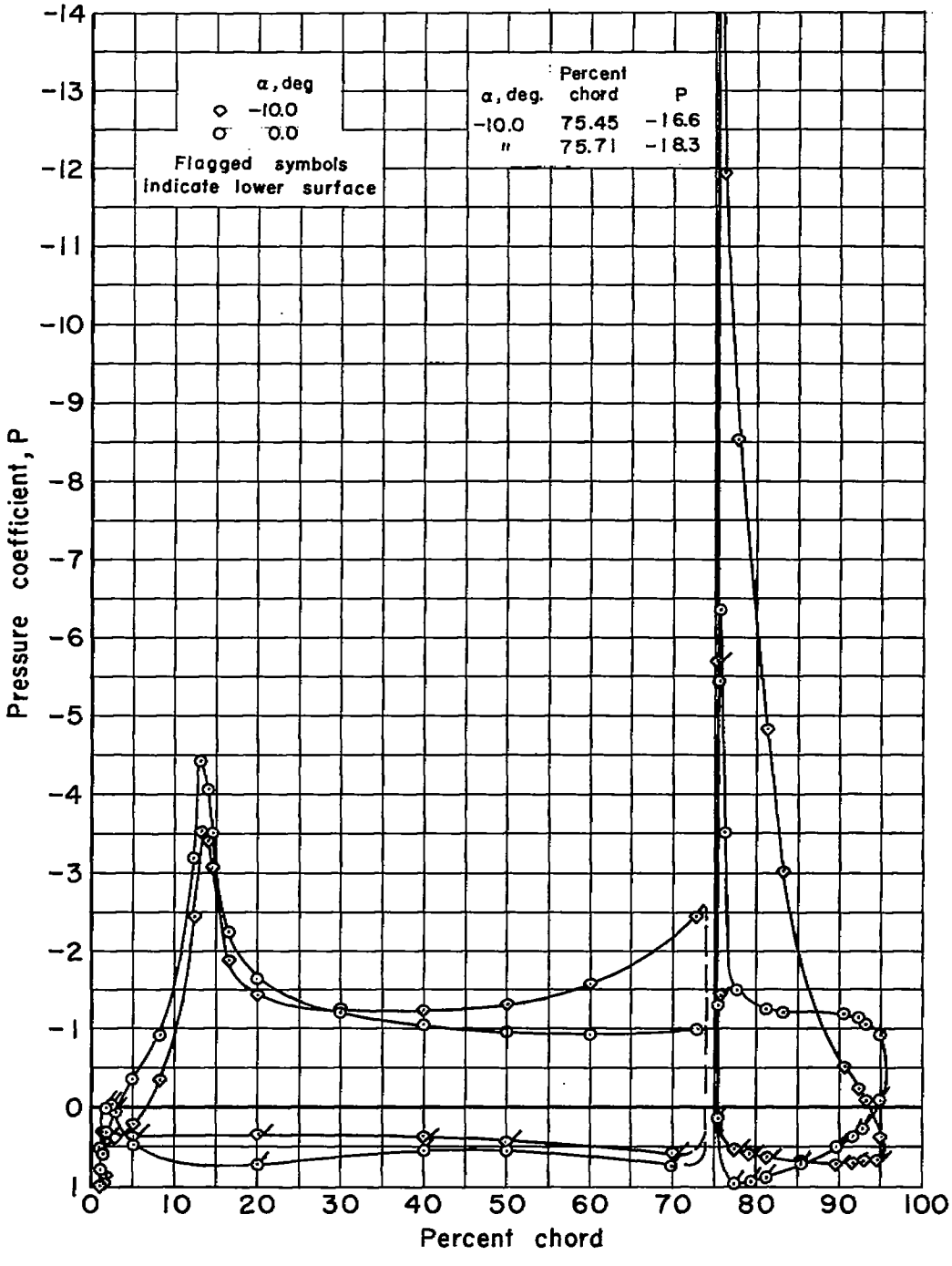

(b) $c_Q = 0.0075$; $c_\mu = 0.097$; $R = 3.3 \times 10^6$

Figure 55.- Continued.

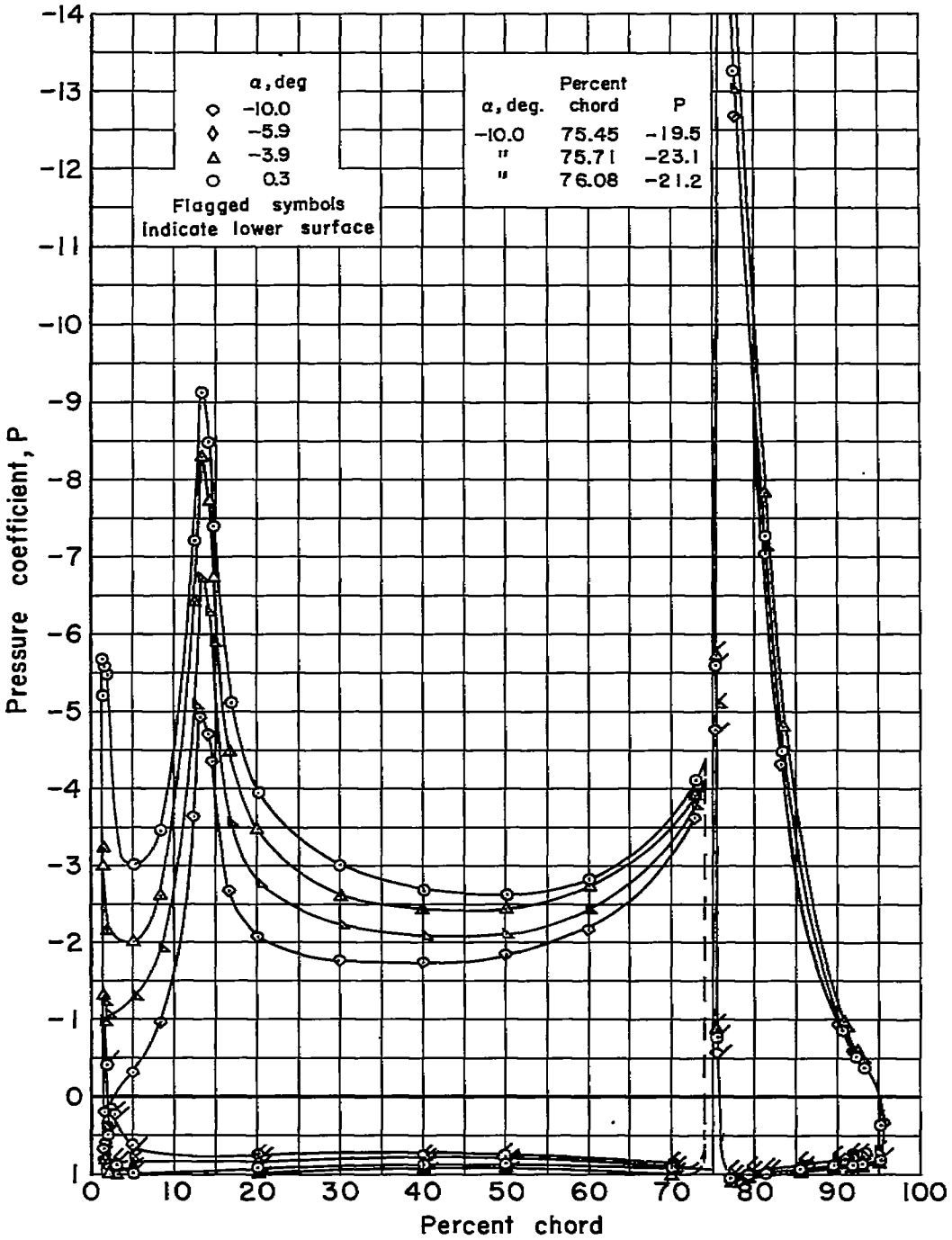

(c) $c_Q = 0.0126$; $c_\mu = 0.274$; $R = 2.3 \times 10^6$

Figure 55.- Concluded.

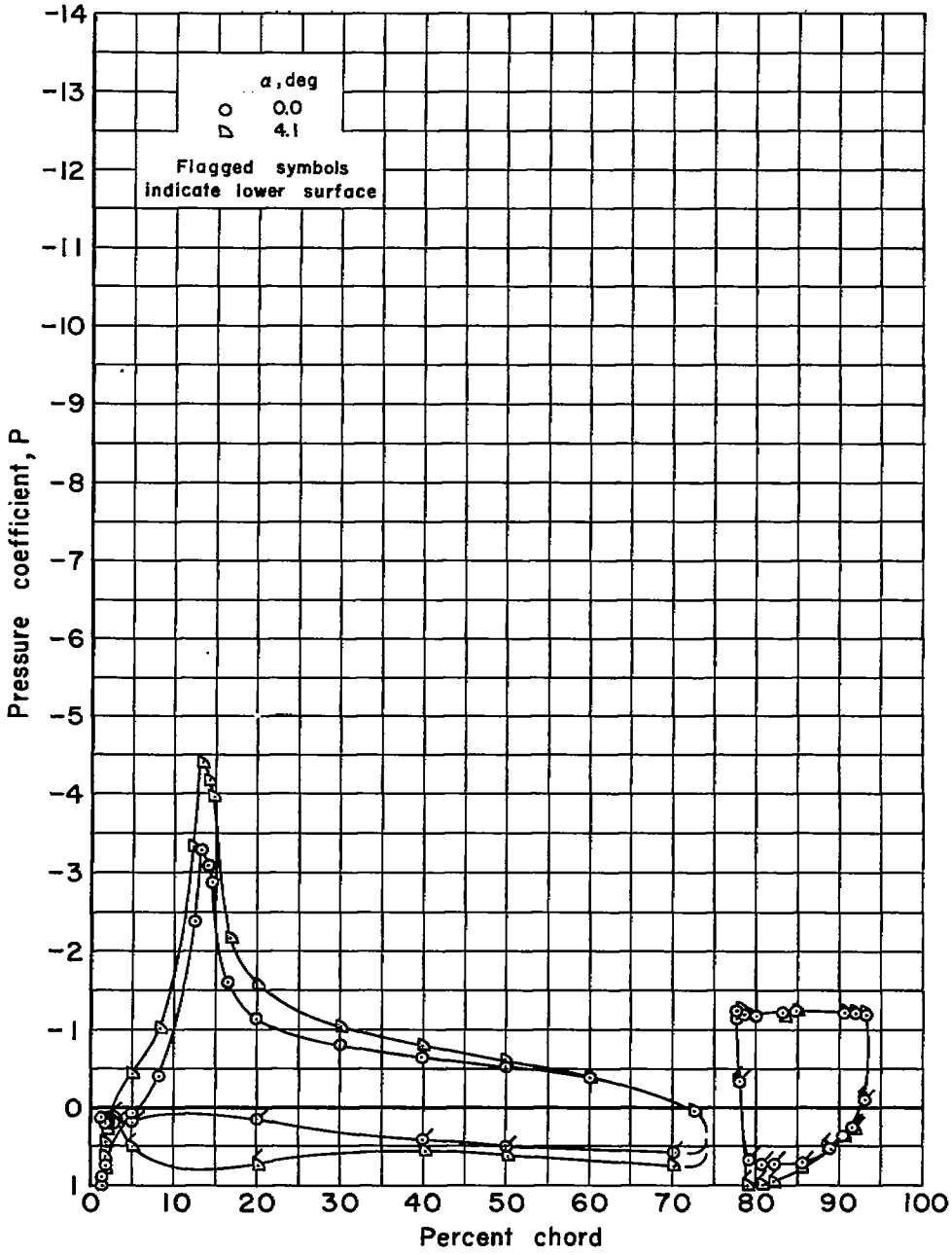

(a) $c_Q = 0$; $c_\mu = 0$; $R = 4.0 \times 10^6$

Figure 56.- Effect of angle of attack and of blowing on the chordwise distribution of pressure of the model with flap A deflected 60° in the extended position; $s/c = 0.00110$; $\delta_n = 35°$.

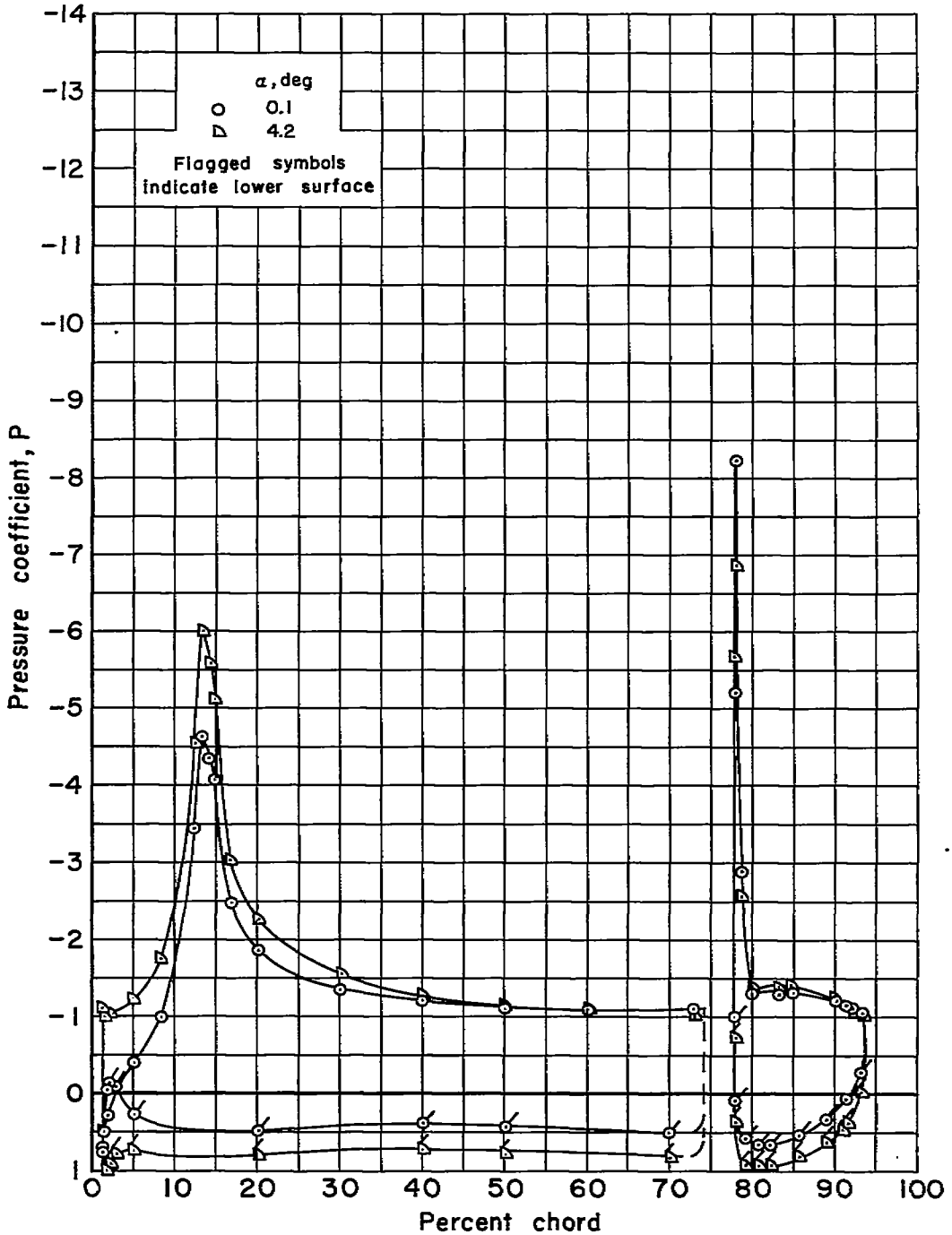

(b) $c_Q = 0.0076$; $c_\mu = 0.101$; $R = 3.3 \times 10^6$

Figure 56.- Continued.

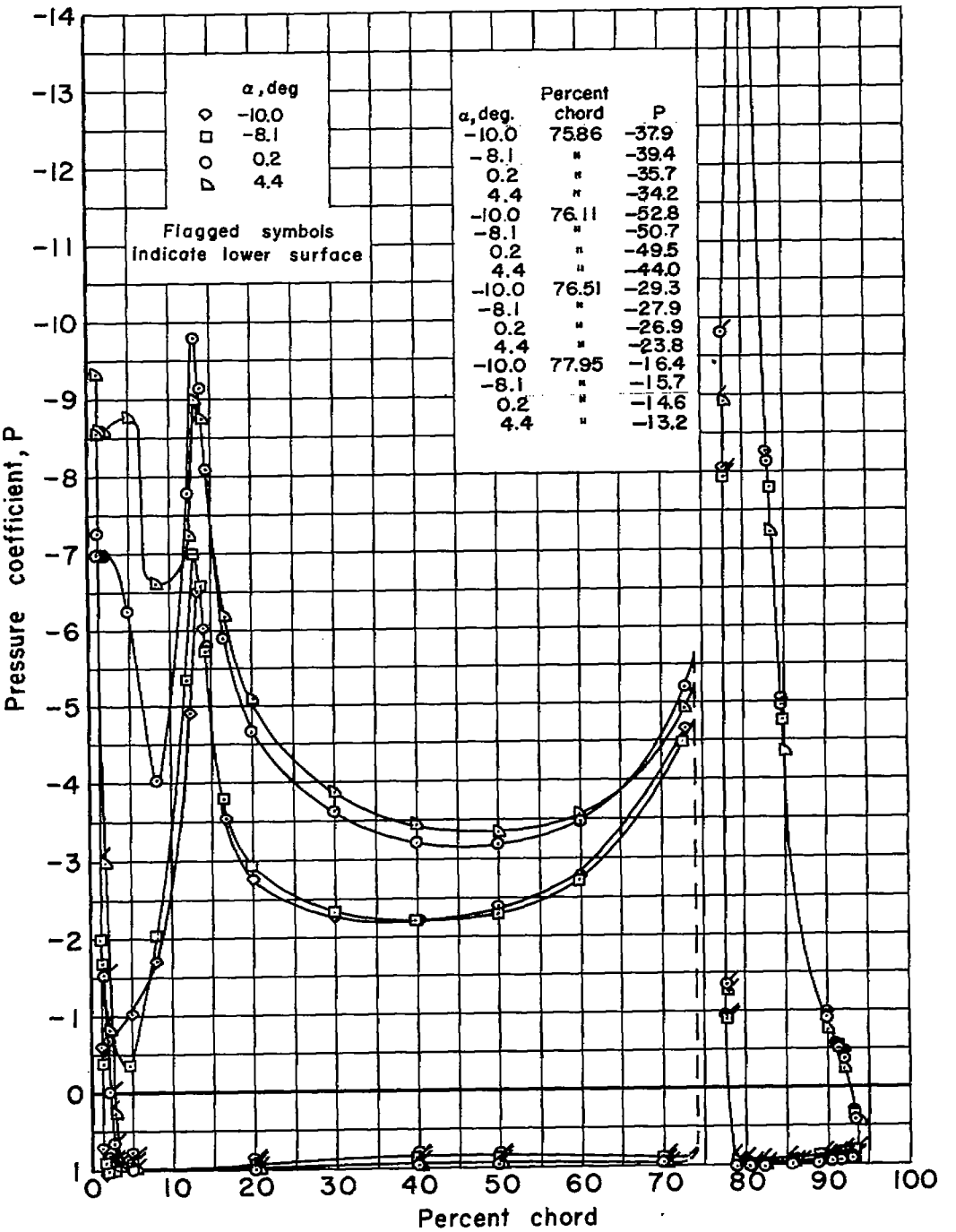

(c) $c_Q = 0.0127$; $c_\mu = 0.276$; $R = 2.3 \times 10^6$

Figure 56.- Concluded.

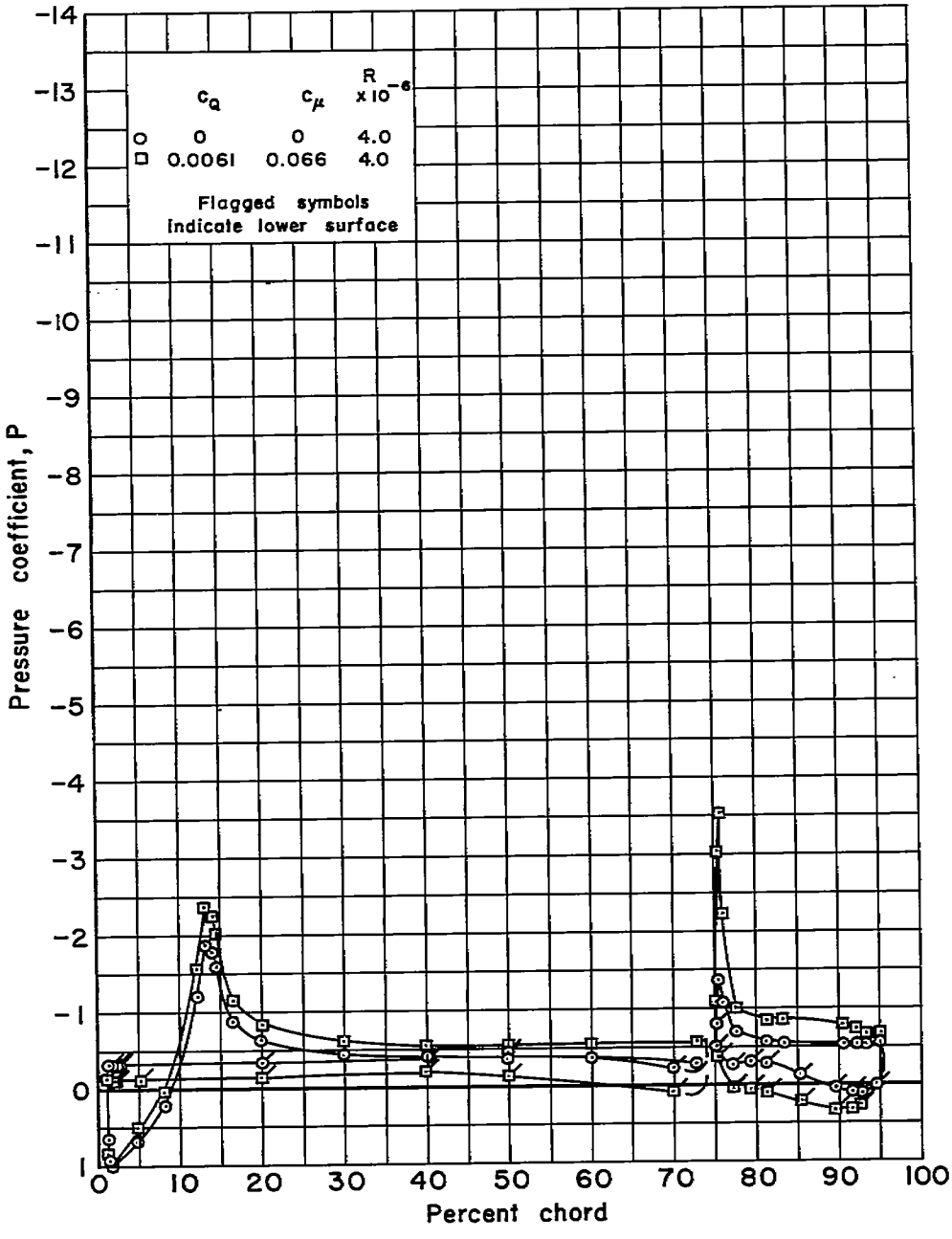

(a) c_Q = 0 and 0.0061

Figure 57.- Effect of blowing on the chordwise distribution of pressure of the model at a constant angle of attack ($\alpha_u = -4.0^\circ$) with flap deflected 50° in the extended position; s/c = 0.00110; $\delta_n = 35^\circ$.

[redacted]

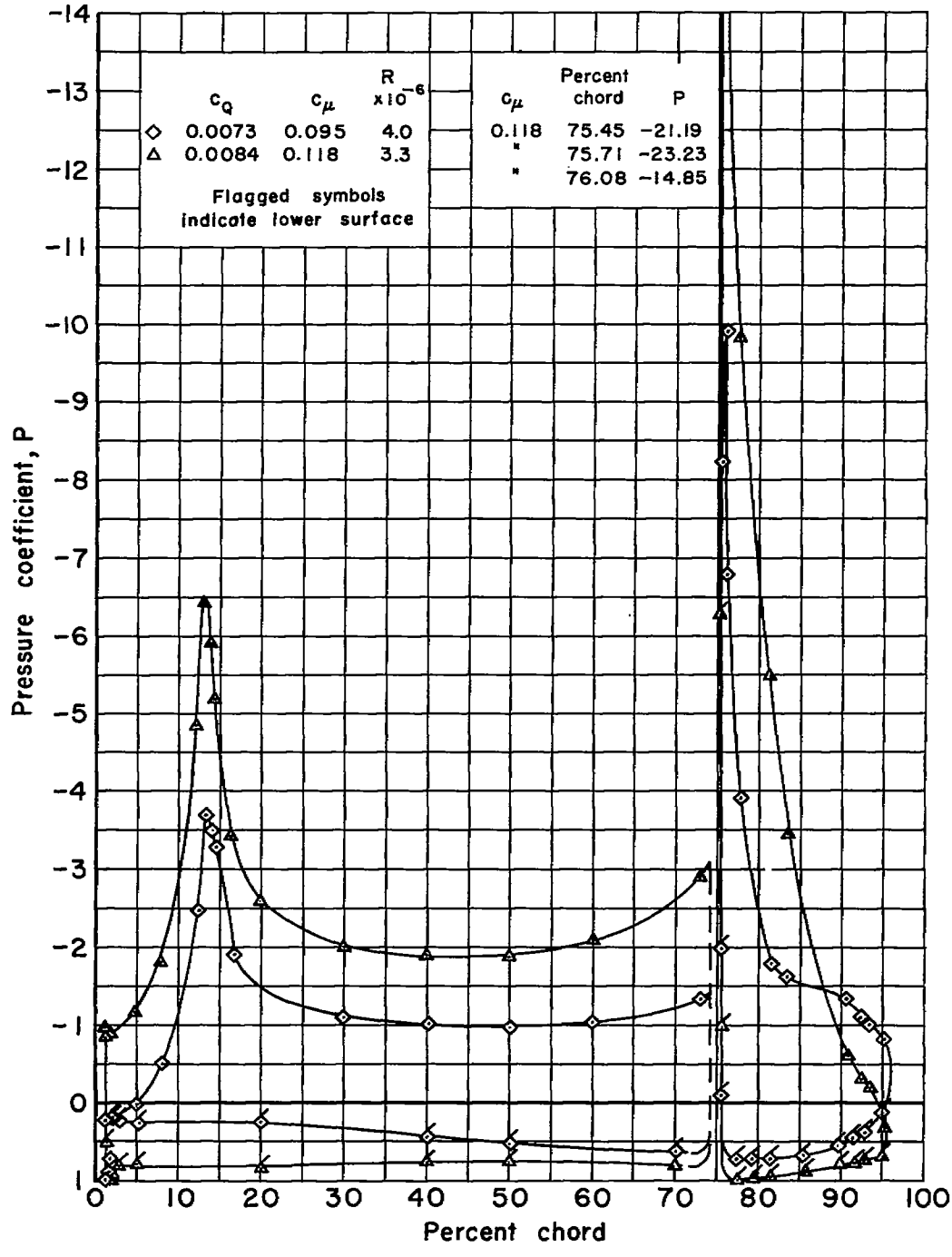

(b) c_Q = 0.0073 and 0.0084

Figure 57.- Continued.

[redacted]

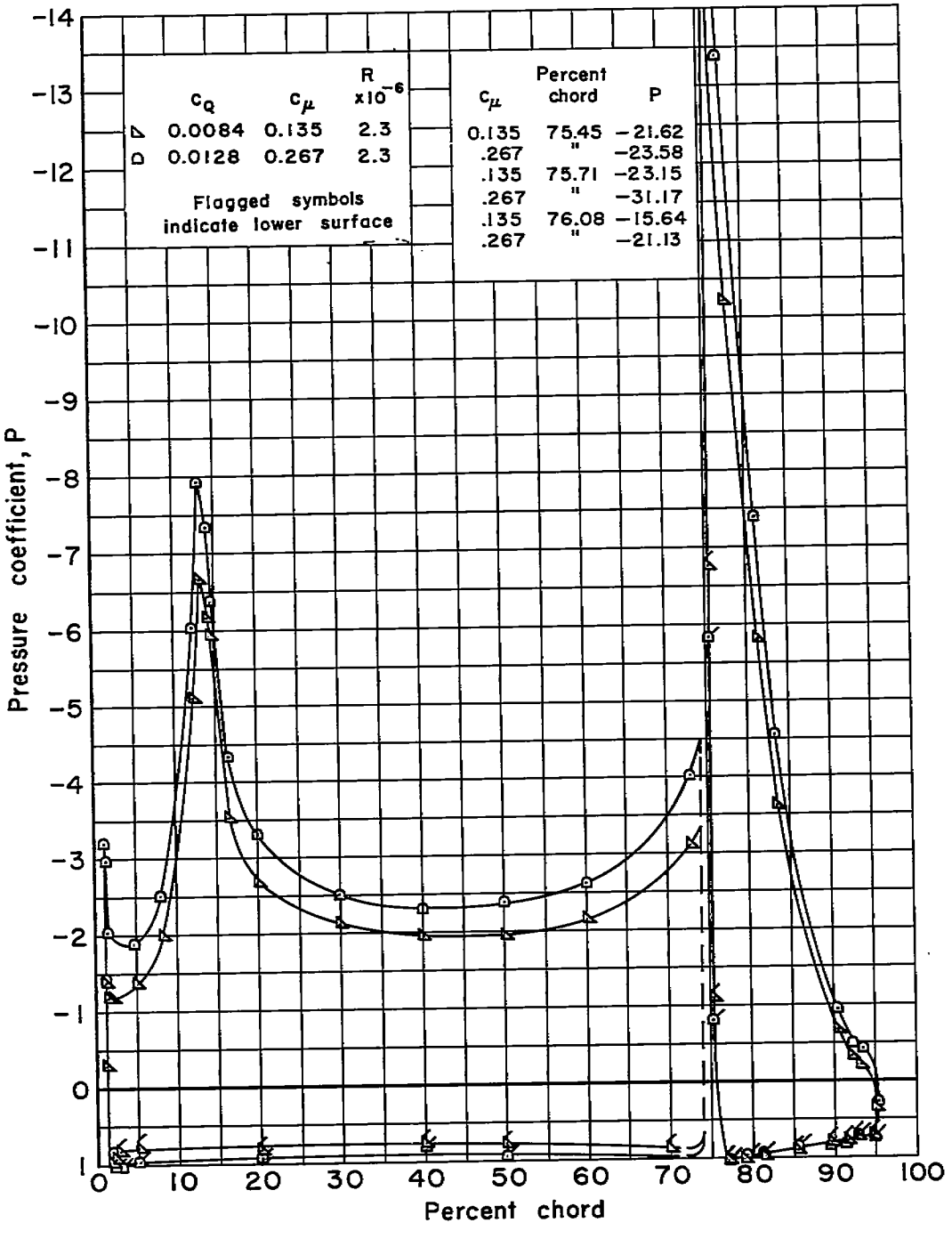

(c) c_Q = 0.0084 and 0.0128

Figure 57.- Concluded.

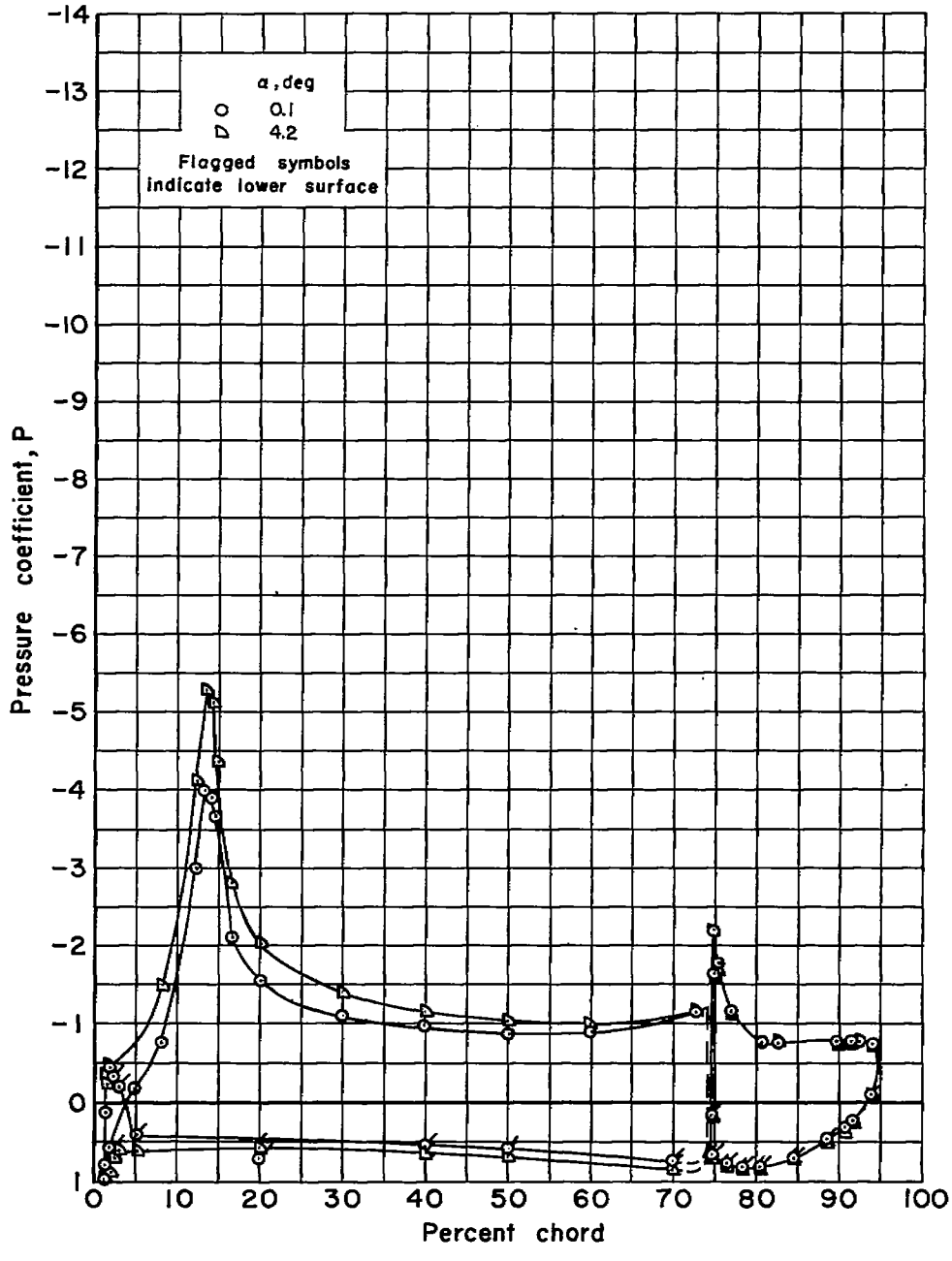

(a) $c_Q = 0$; $c_\mu = 0$; $R = 4.0 \times 10^6$

Figure 58.- Effect of angle of attack and of blowing on the chordwise distribution of pressure of the model with flap A deflected 50° against the nozzle; $s/c = 0.00110$; $\delta_n = 35°$.

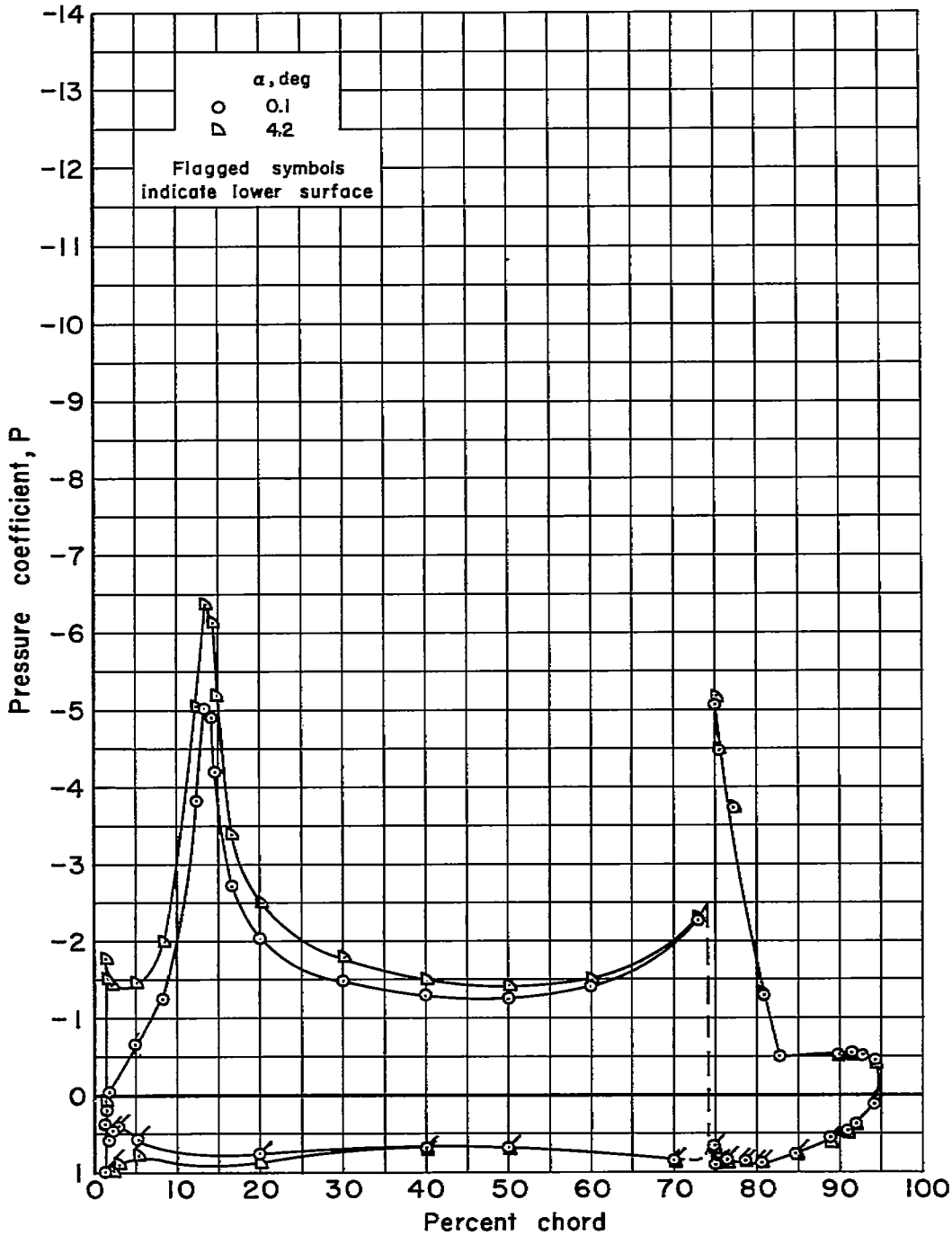

(b) $c_Q = 0.0024$; $c_\mu = 0.010$; $R = 4.0 \times 10^6$

Figure 58.- Continued.

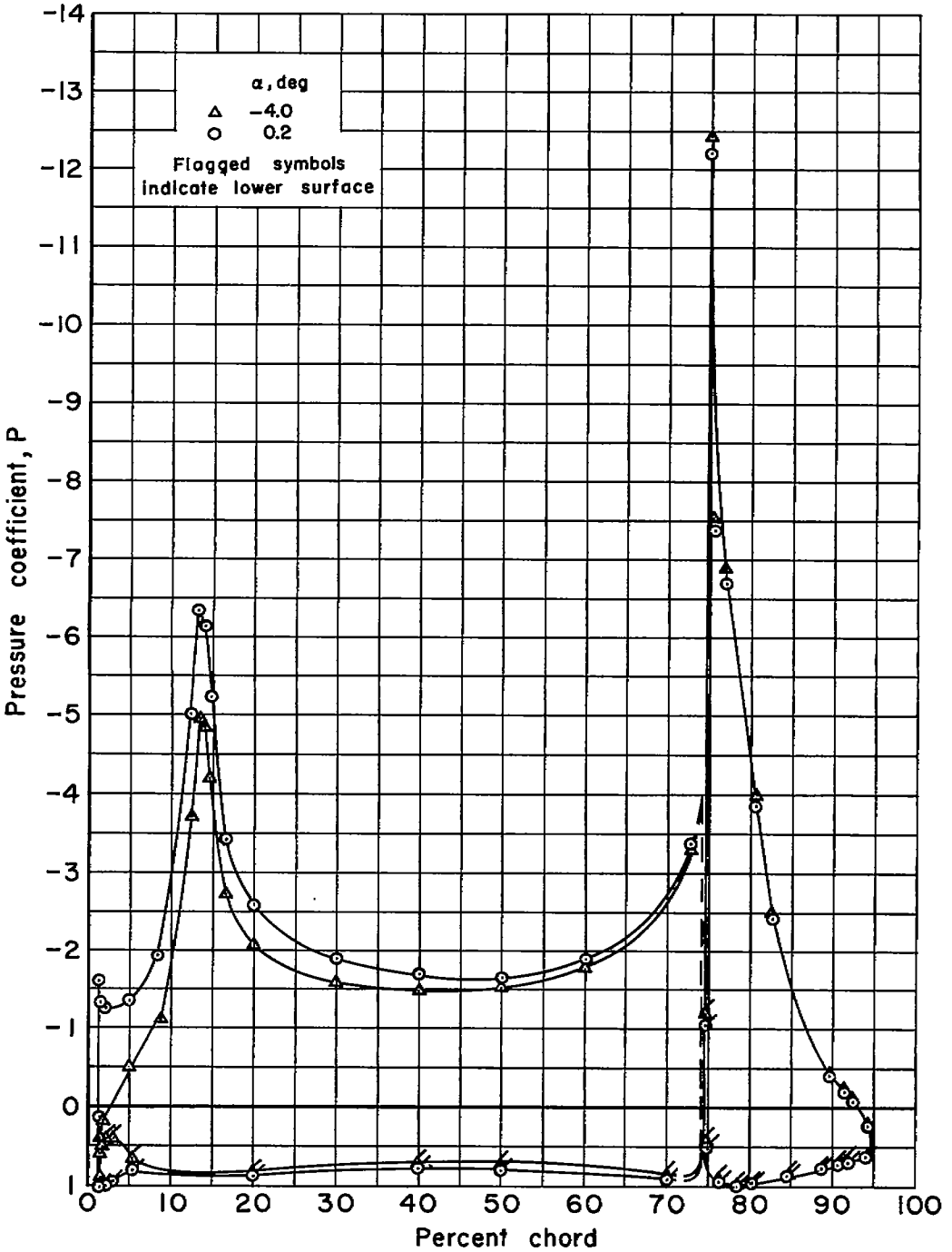

(c) $c_Q = 0.0061$; $c_\mu = 0.066$; $R = 4.0 \times 10^6$

Figure 58.- Continued

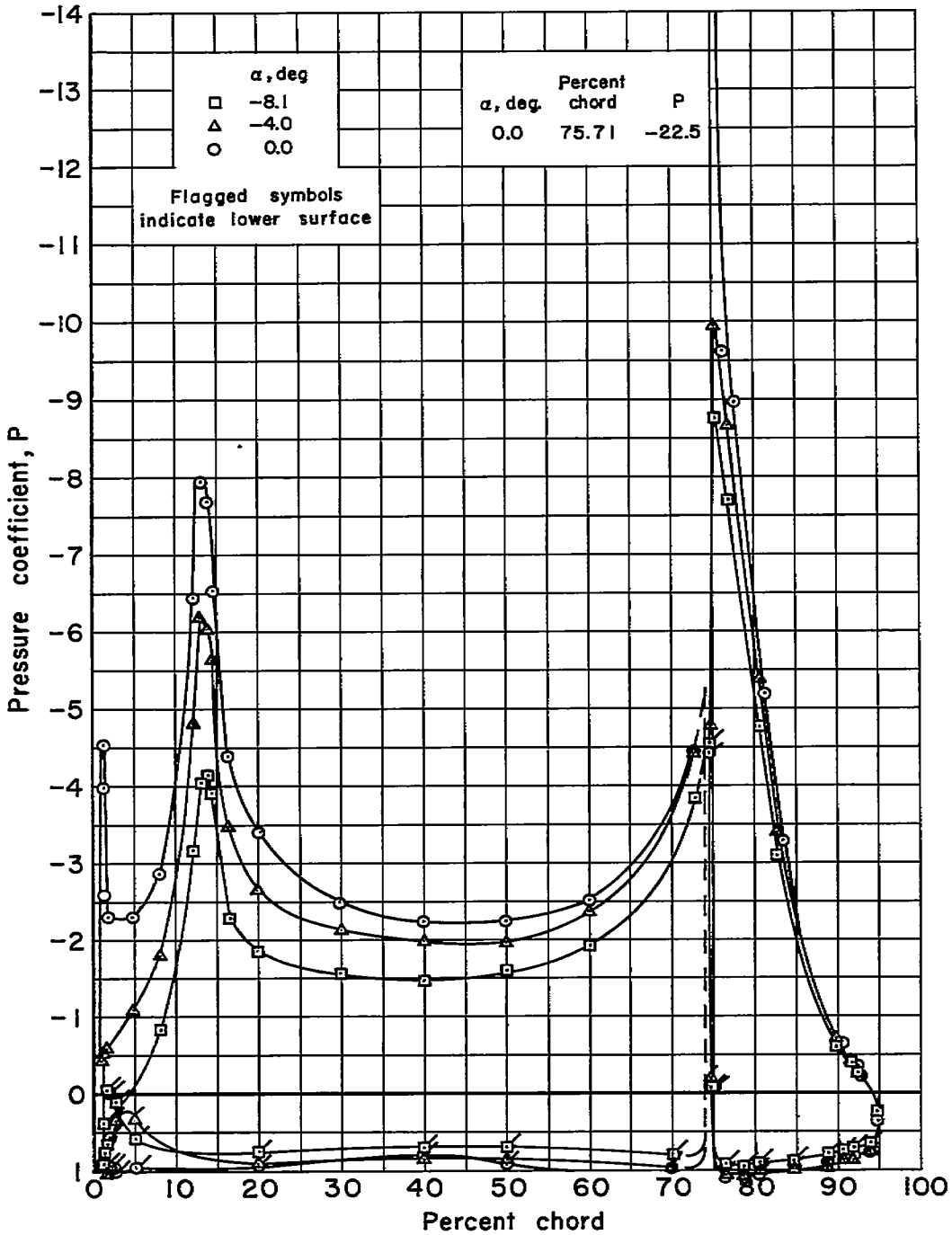

(d) $c_Q = 0.0092$; $c_\mu = 0.160$; $R = 2.3 \times 10^6$

Figure 58.- Concluded.

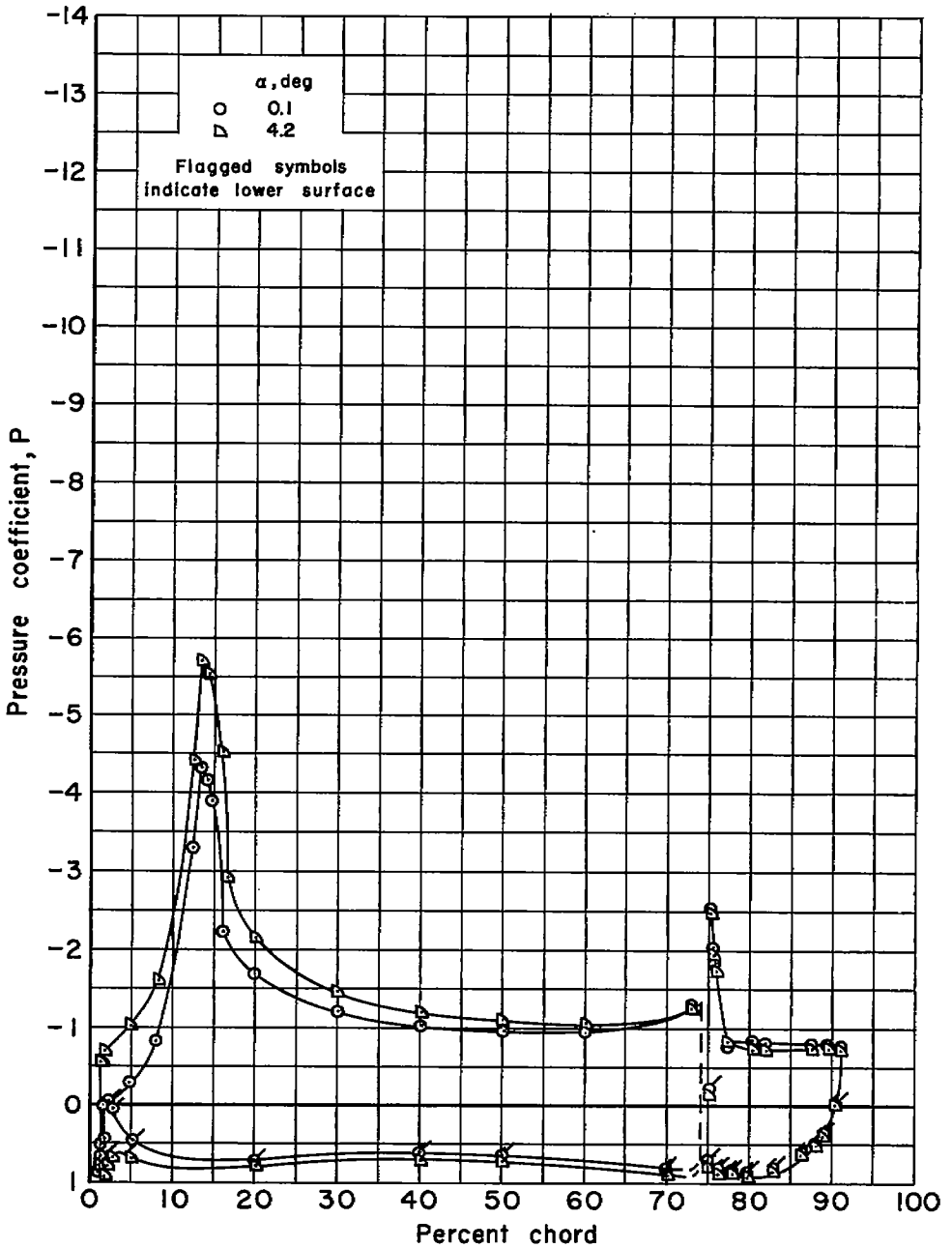

(a) $c_Q = 0$; $c_\mu = 0$; $R = 4.0 \times 10^6$

Figure 59.- Effect of angle of attack and of blowing on the chordwise distribution of pressure of the model with flap A deflected 60° against the nozzle; $s/c = 0.00110$; $\delta_n = 35°$.

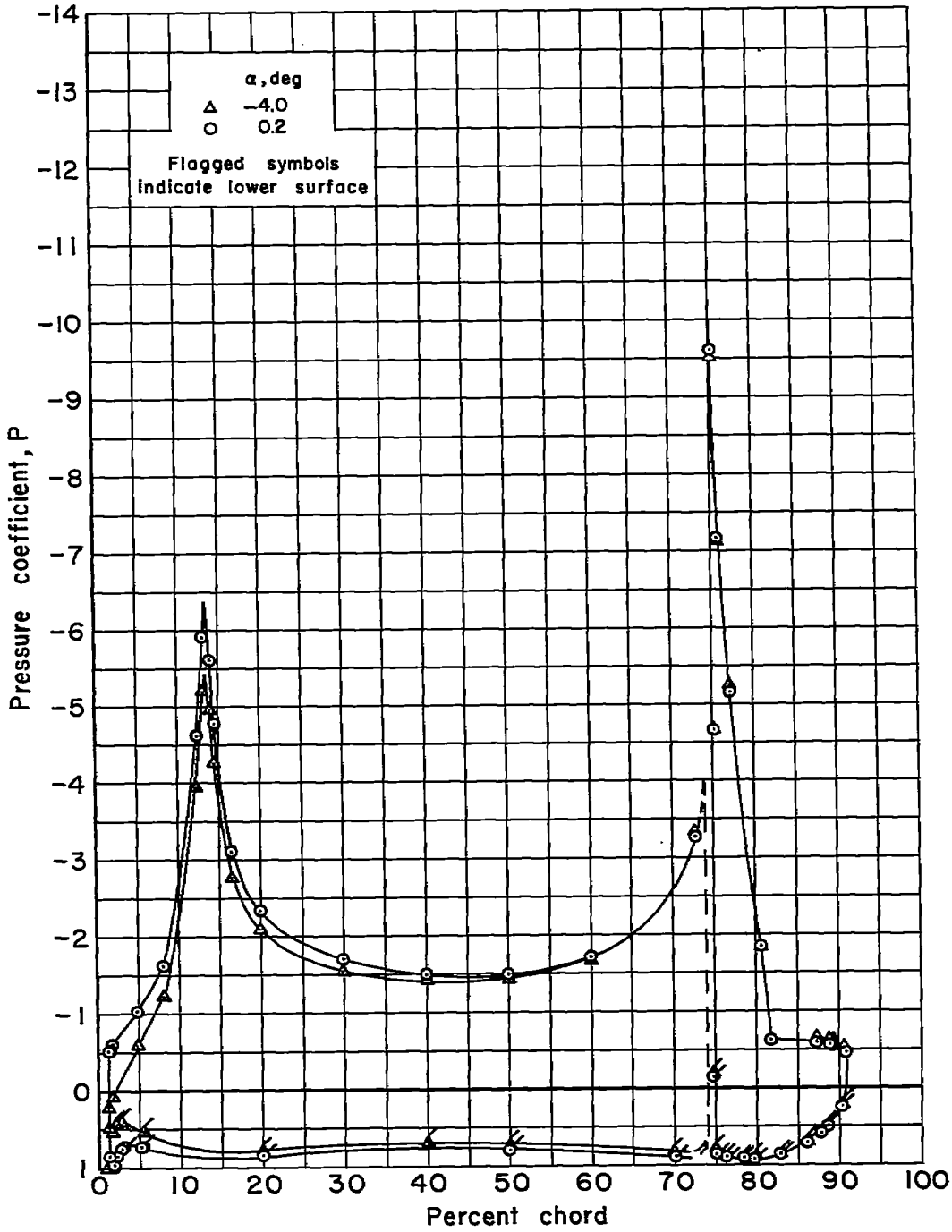

(b) $c_Q = 0.0030$; $c_\mu = 0.015$; $R = 4.0 \times 10^6$

Figure 59.- Continued.

[redacted]

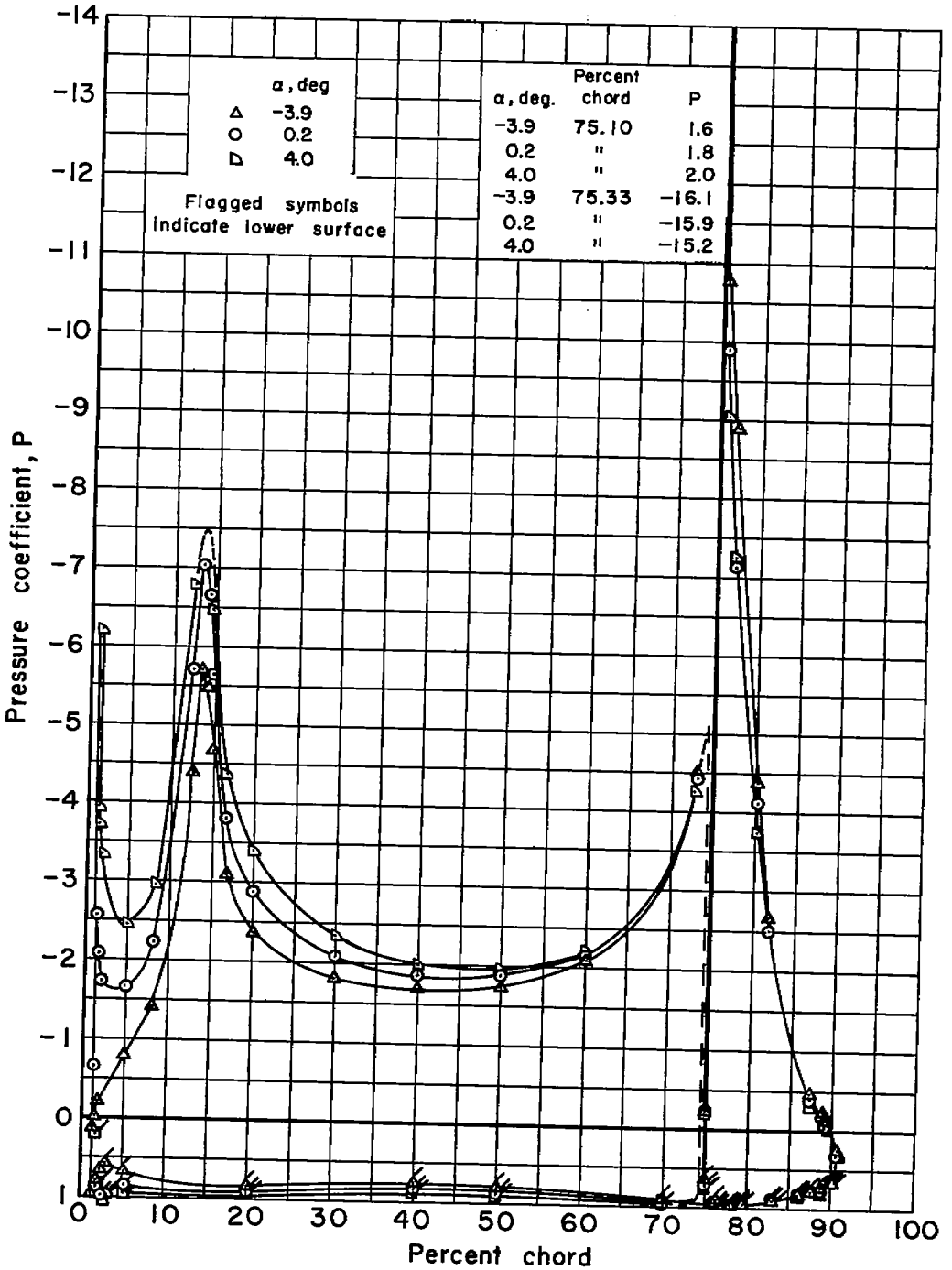

(c) $c_Q = 0.0059$; $c_\mu = 0.060$; $R = 4.0 \times 10^6$

Figure 59.- Continued.

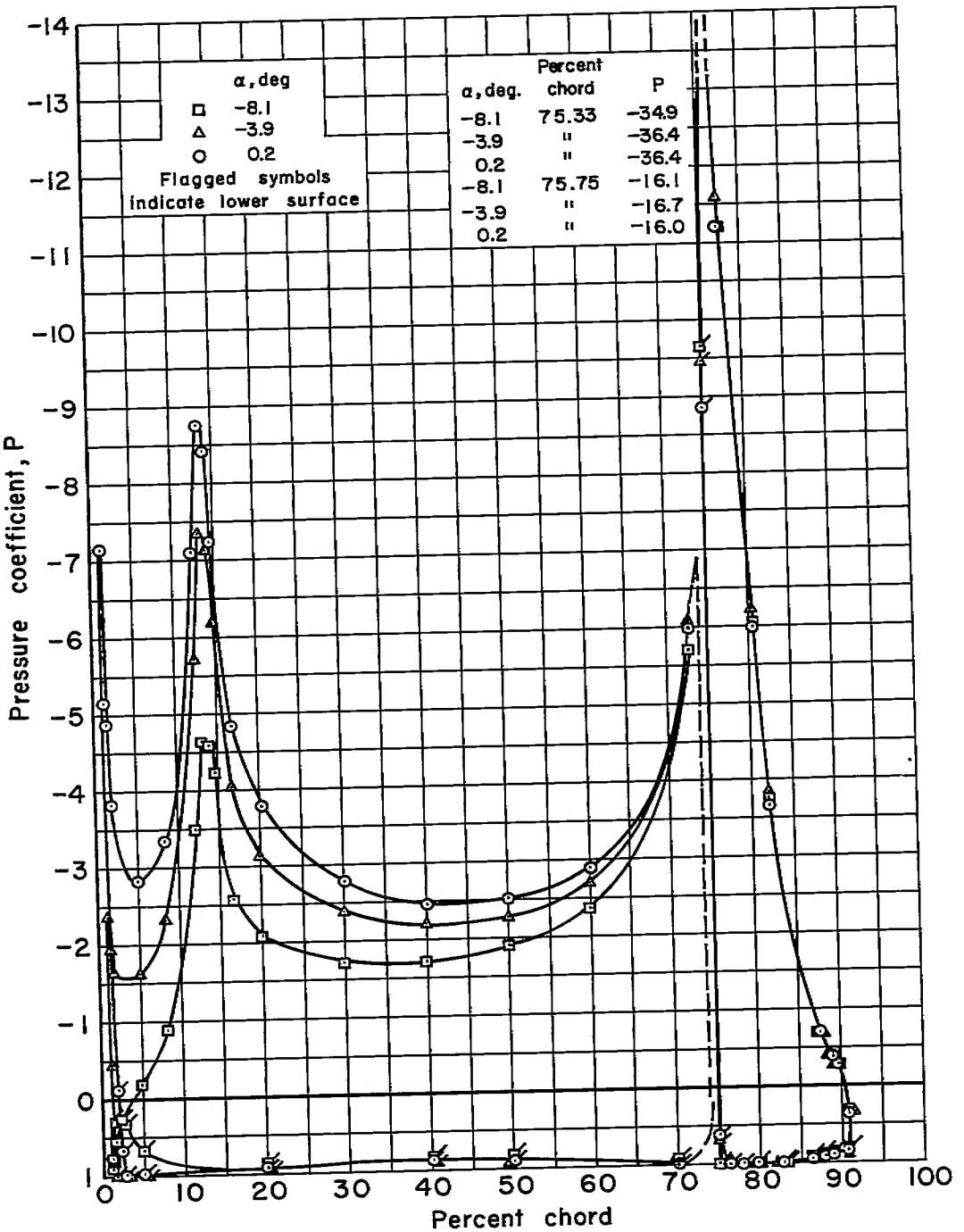

(d) $c_Q = 0.0124$; $c_\mu = 0.246$; $R = 2.3 \times 10^6$

Figure 59.- Concluded.

[redacted]

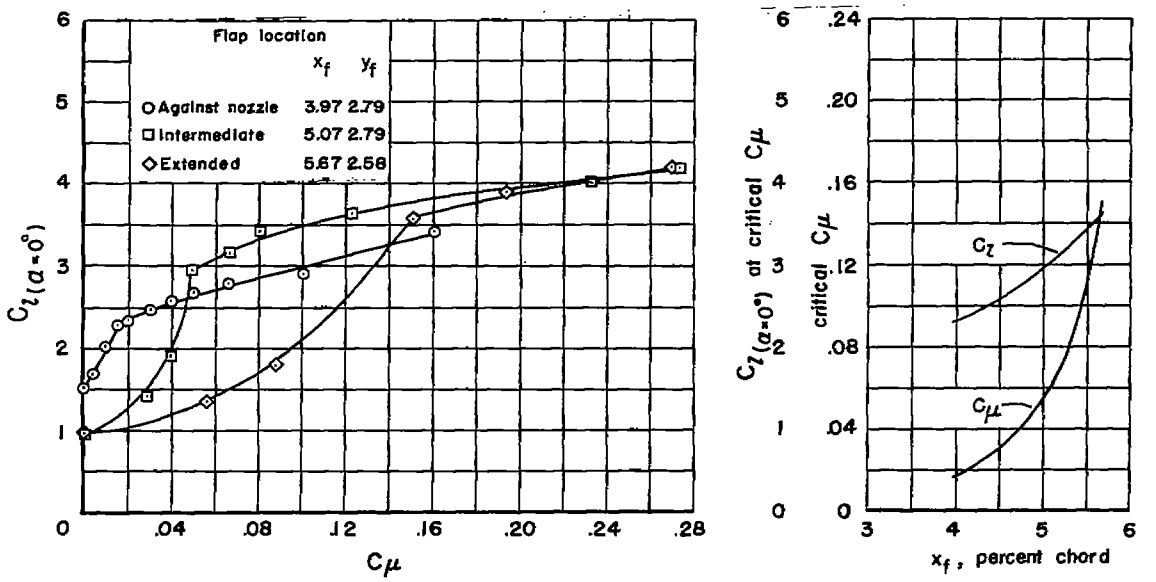

(a) $\delta = 50°$

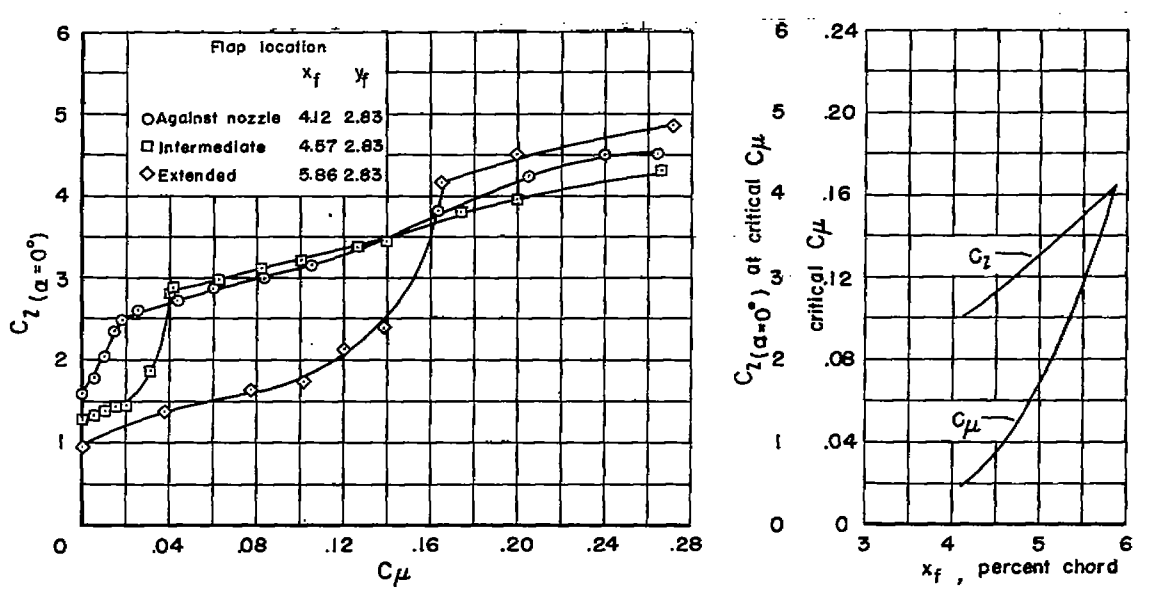

(b) $\delta = 60°$

Figure 60.- Effect of flap position on the lift of the model with flap A; $s/c = 0.00110$; $\delta_n = 35°$.

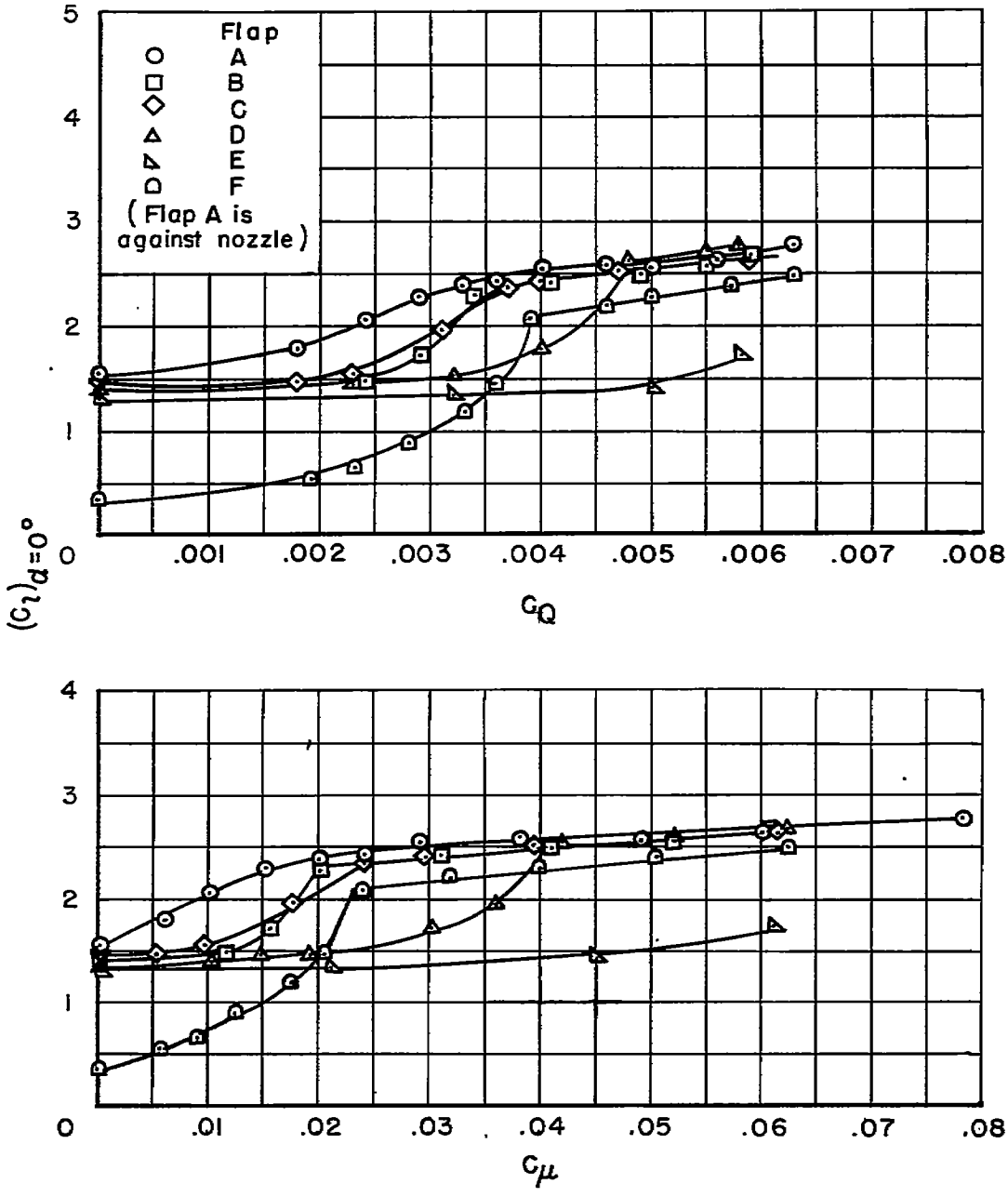

(a) $\delta = 50°$

Figure 61.- The variation of the lift coefficient at zero degrees angle of attack with the mass-flow and the jet-momentum coefficients for the various flaps tested; $s/c = 0.00110$; $\delta_n = 35°$.

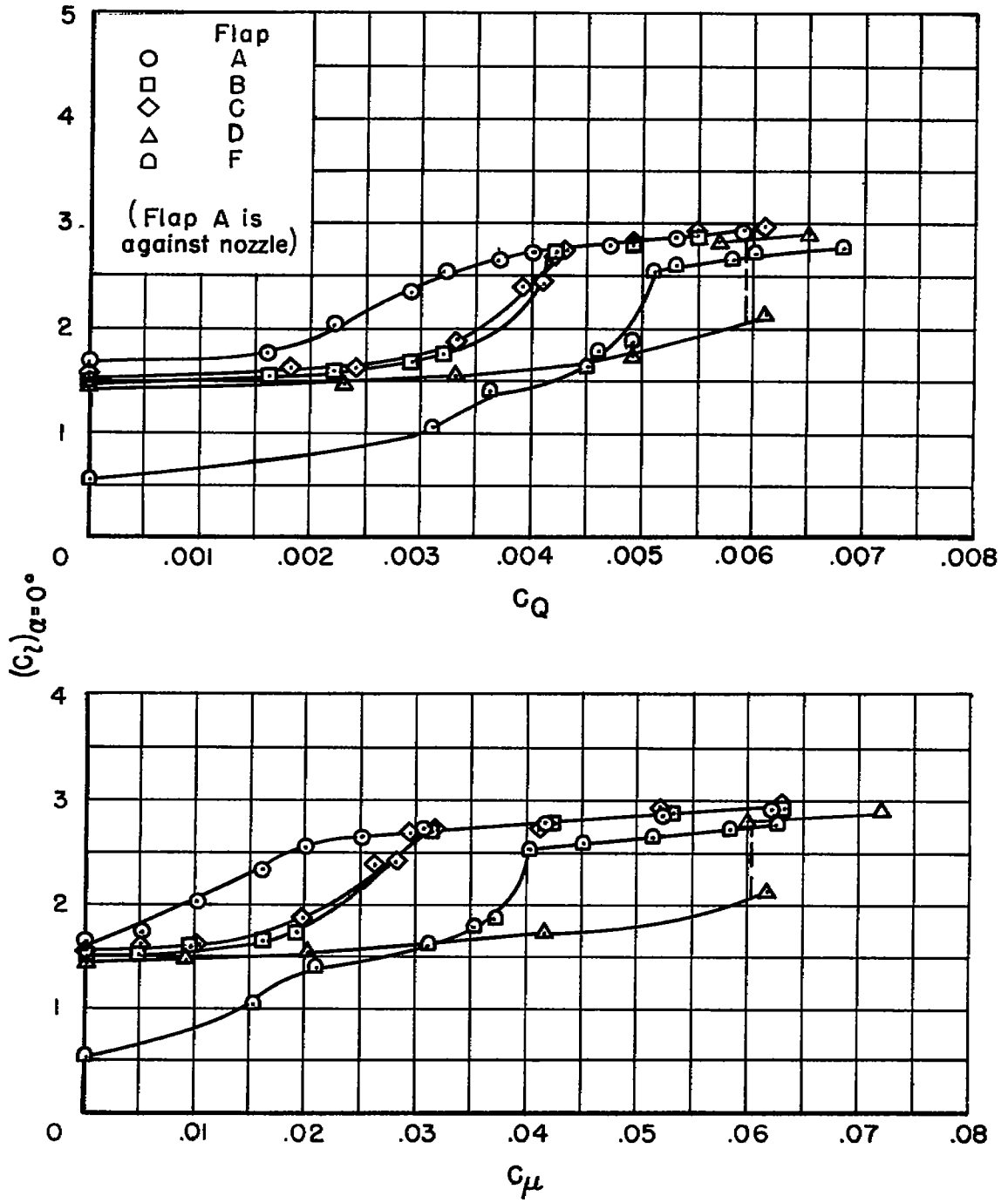

(b) $\delta = 60°$

Figure 61.- Continued.

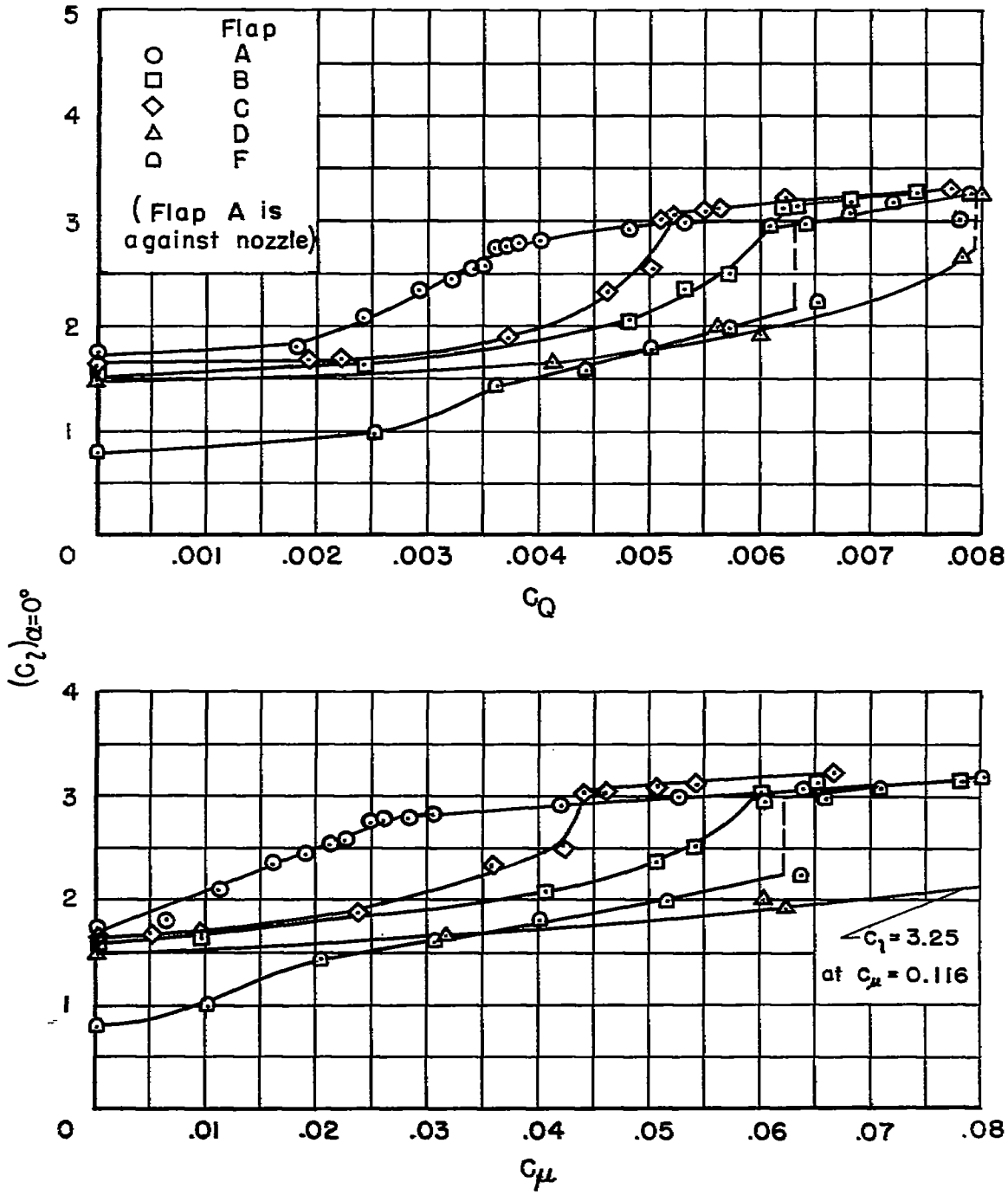

(c) $\delta = 70°$

Figure 61.- Concluded.

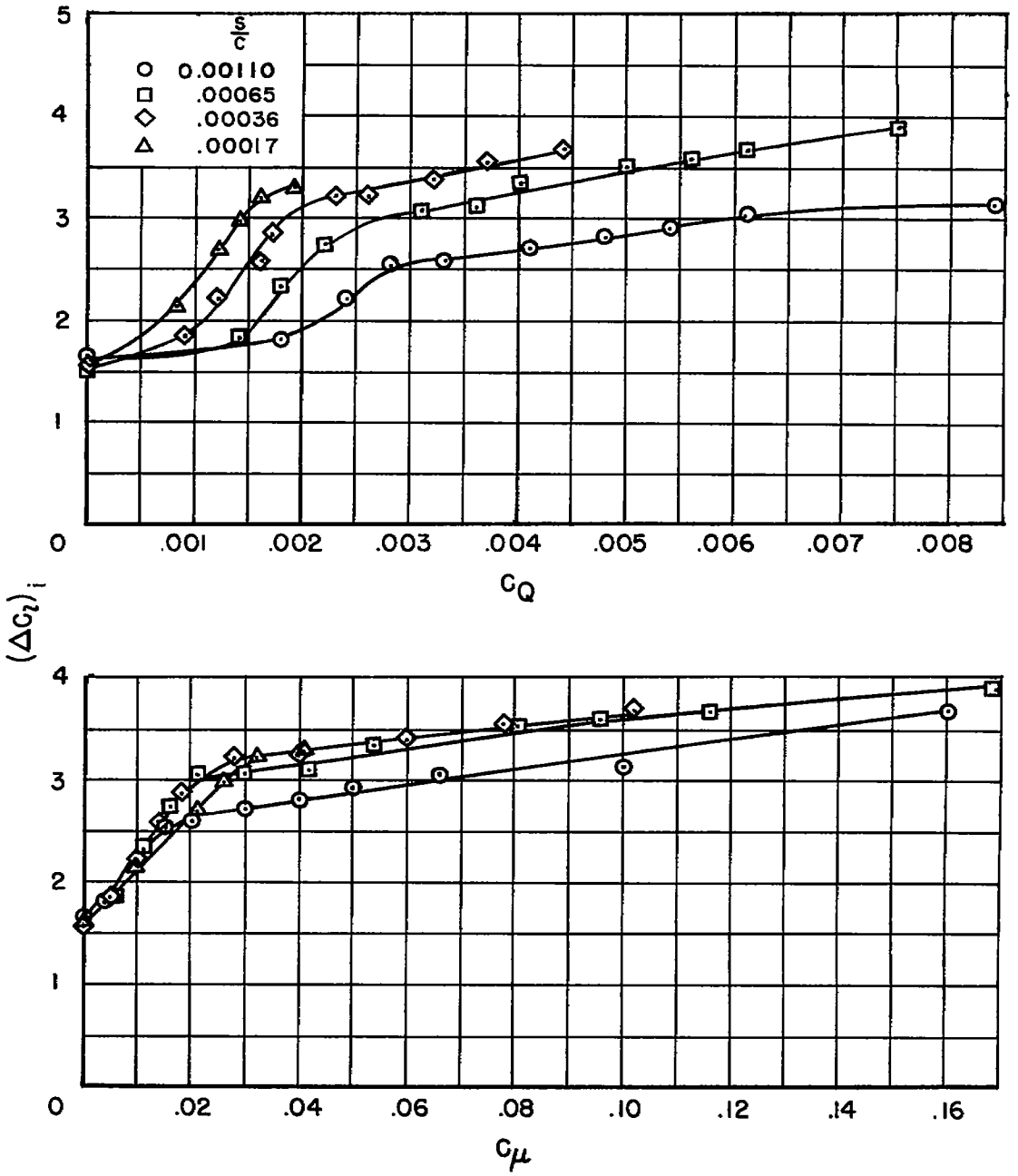

(a) Flap A against the nozzle; $\delta = 50^\circ$; $\delta_n = 35^\circ$.

Figure 62.- The effect of nozzle height on the variation of the increment of lift coefficient with the mass-flow and jet-momentum coefficients.

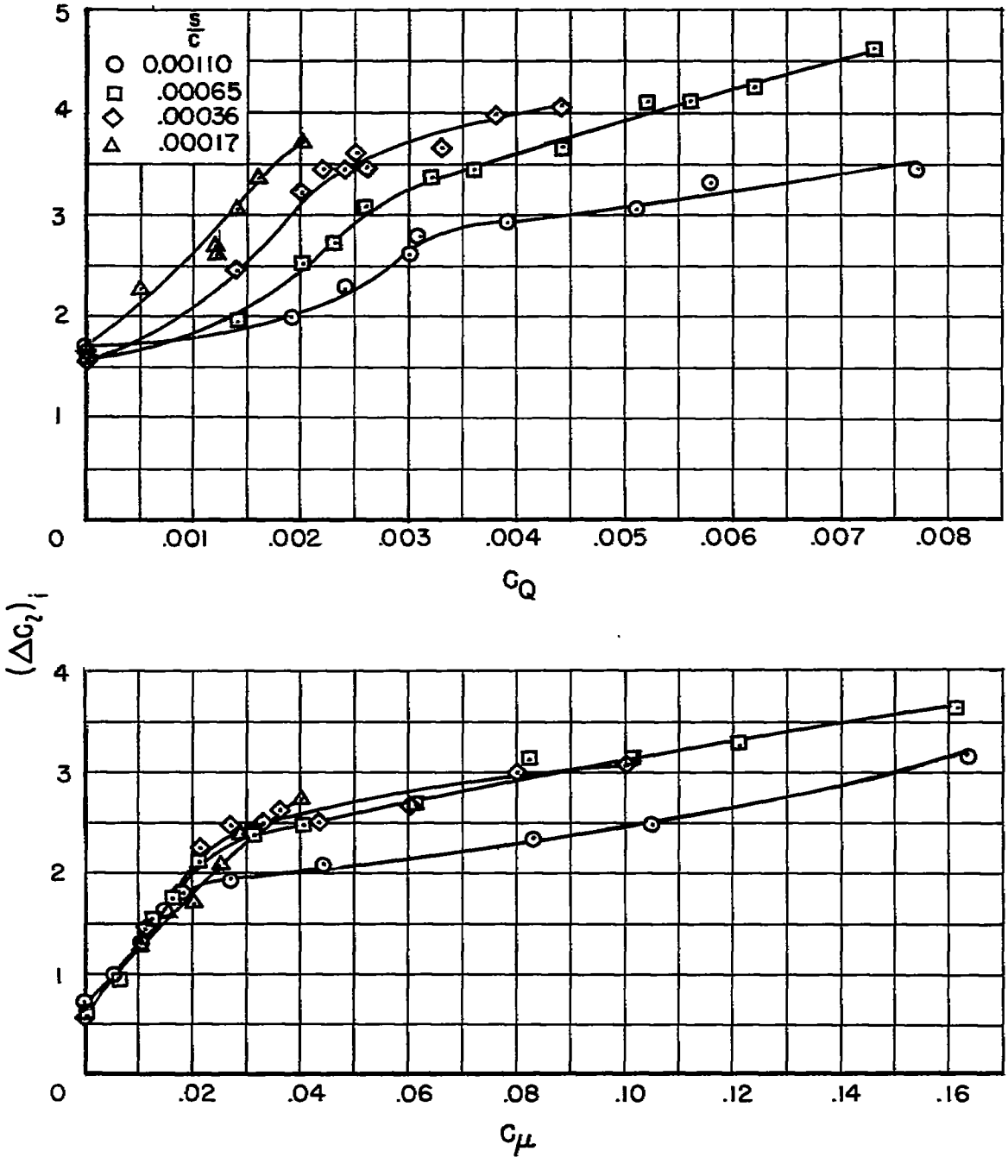

(b) Flap A against the nozzle; $\delta = 60^\circ$; $\delta_n = 35^\circ$.

Figure 62.- Continued.

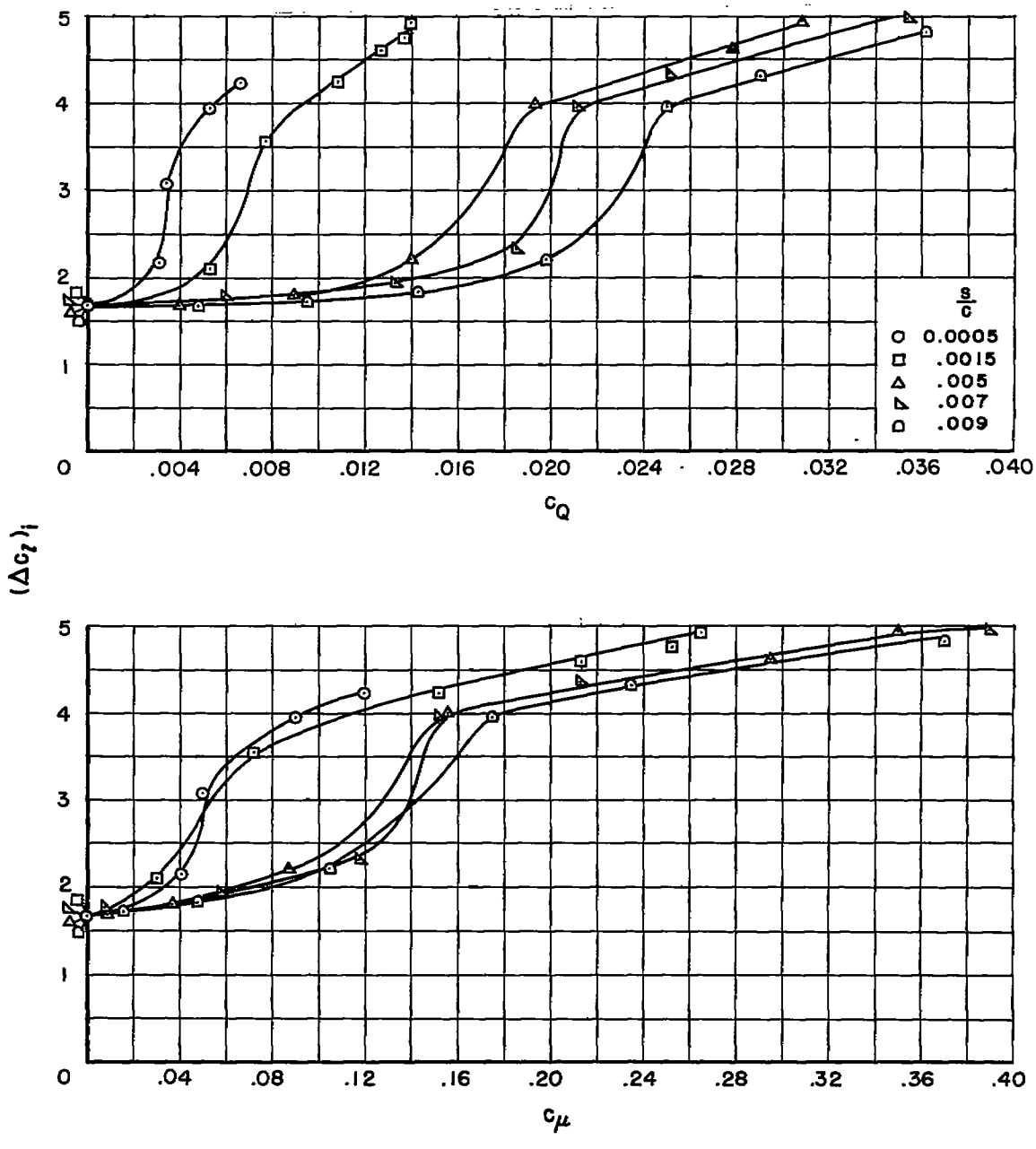

(c) Flap of reference 12; $\delta = 60^{\circ}$; no leading-edge device.

Figure 62.- Concluded.

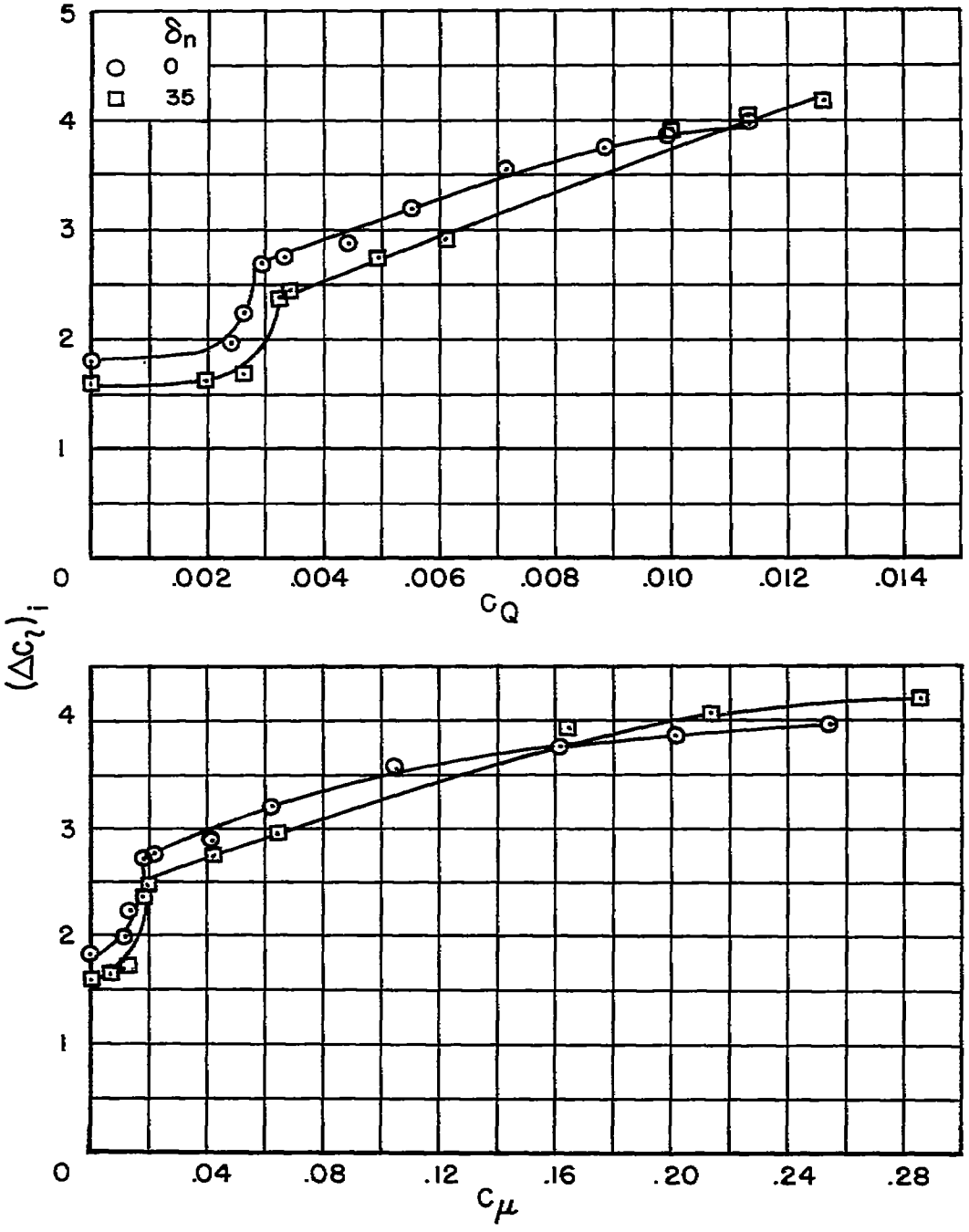

Figure 63.- The effect of nose-flap deflection on the variation of the increment of lift coefficient with the mass-flow and jet-momentum coefficients; flap C; s/c = 0.00110; $\delta = 50^\circ$.

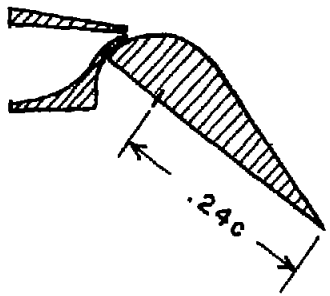

(Flap type e)
Ref. 4

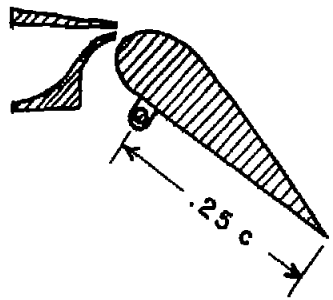

(Flap type f)
Ref. 4

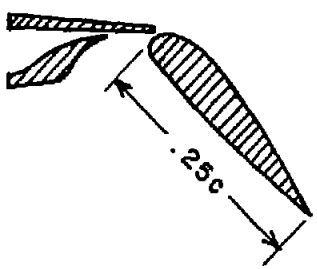

Ref. 5

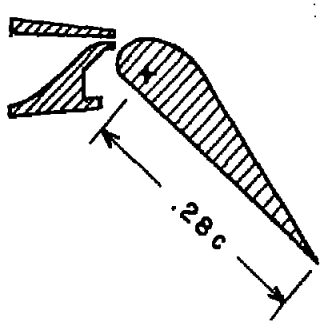

Ref. 9

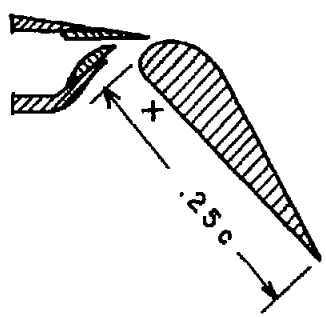

Ref. 12

Figure 64.- Sketches showing the arrangement of the flap and blowing systems for each of the referenced investigations.

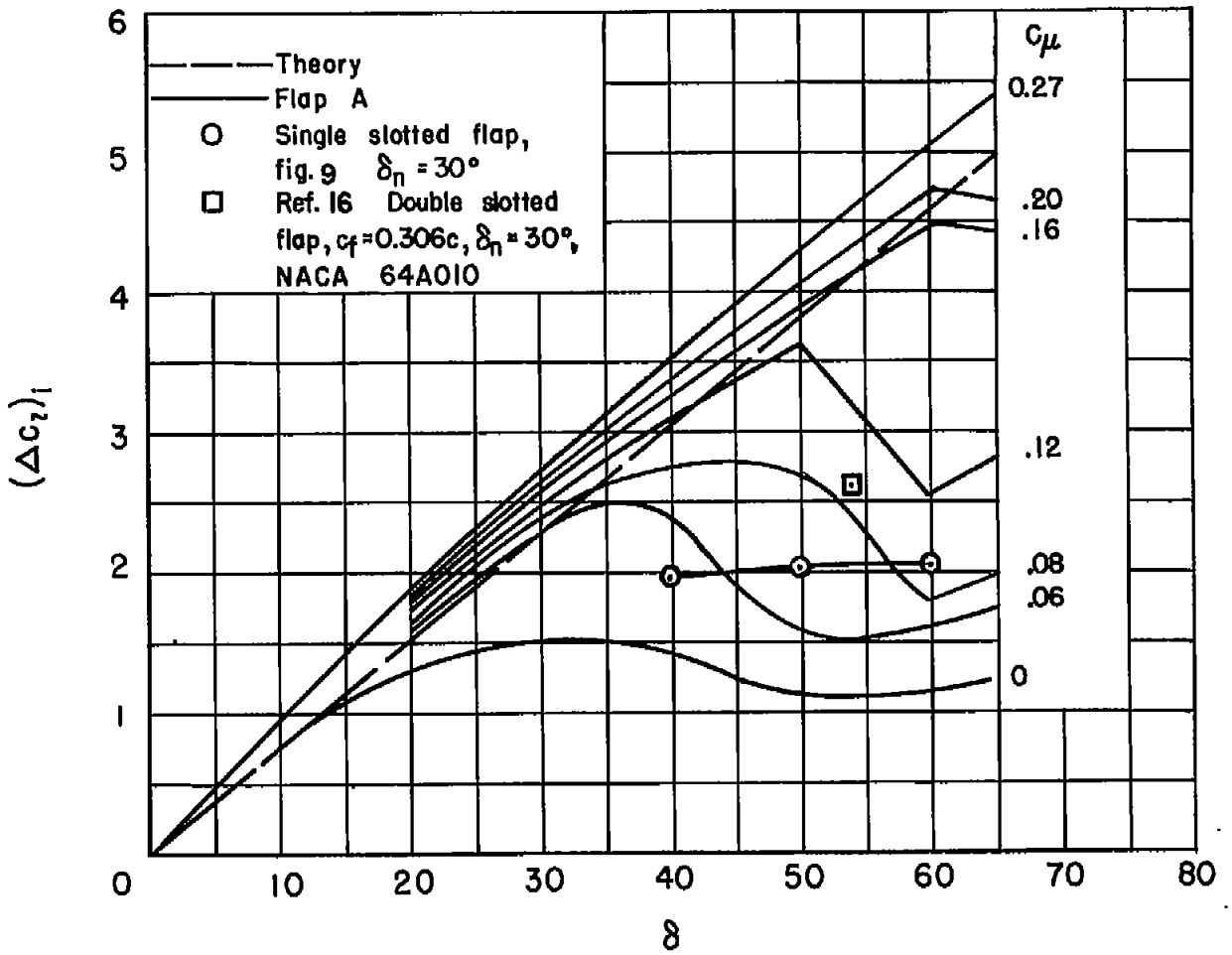

Figure 65.- The effect of the jet-momentum coefficient, c_μ, on the variation of the increment of lift coefficient with flap deflection; flap A extended; NACA 0006 airfoil section; $s/c = 0.00110$; $\delta_n = 35°$.

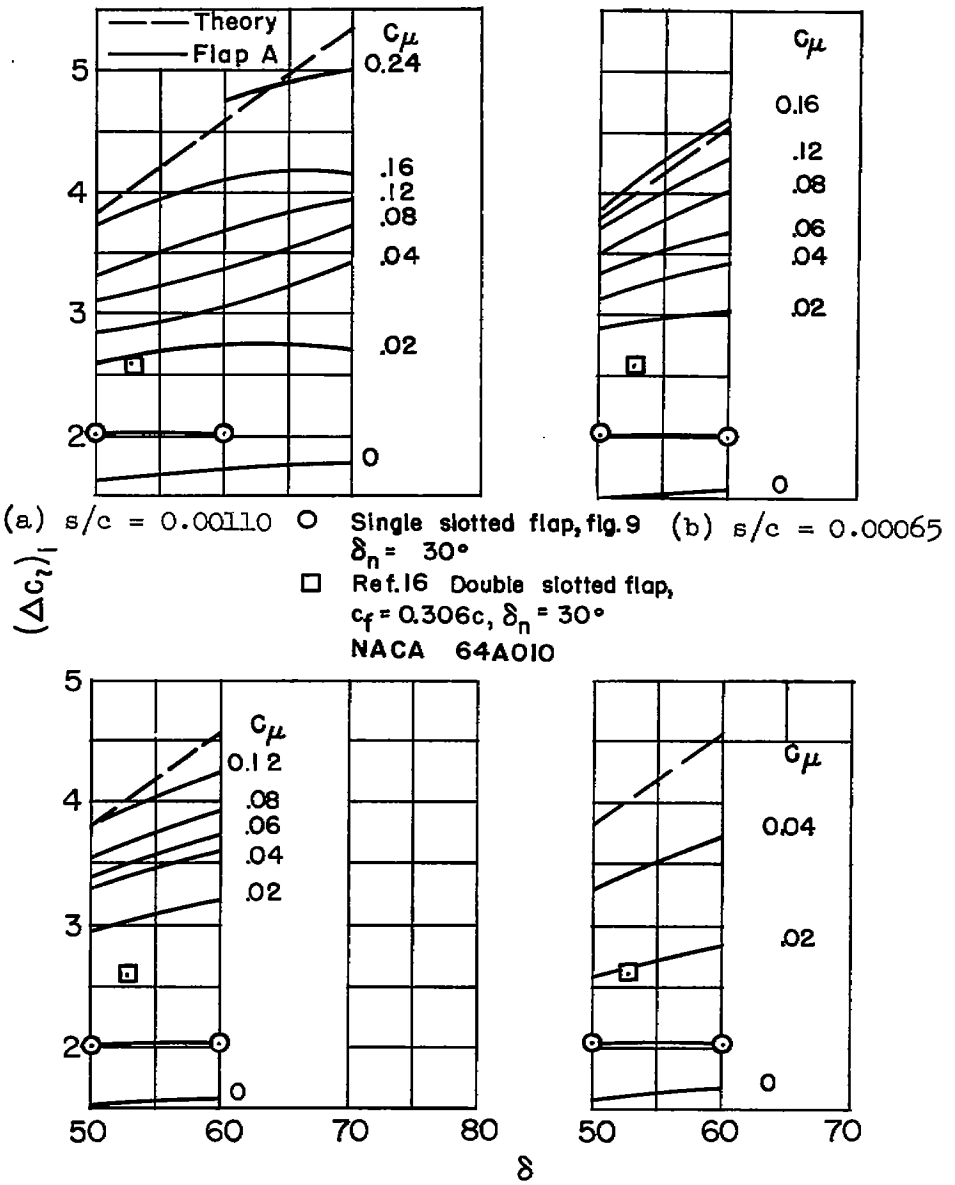

Figure 66.- The effect of the jet-momentum coefficient, c_μ, on the variation of the increment of lift coefficient with flap deflection; flap A against nozzle; NACA 0006 airfoil section; $\delta_n = 35^\circ$.

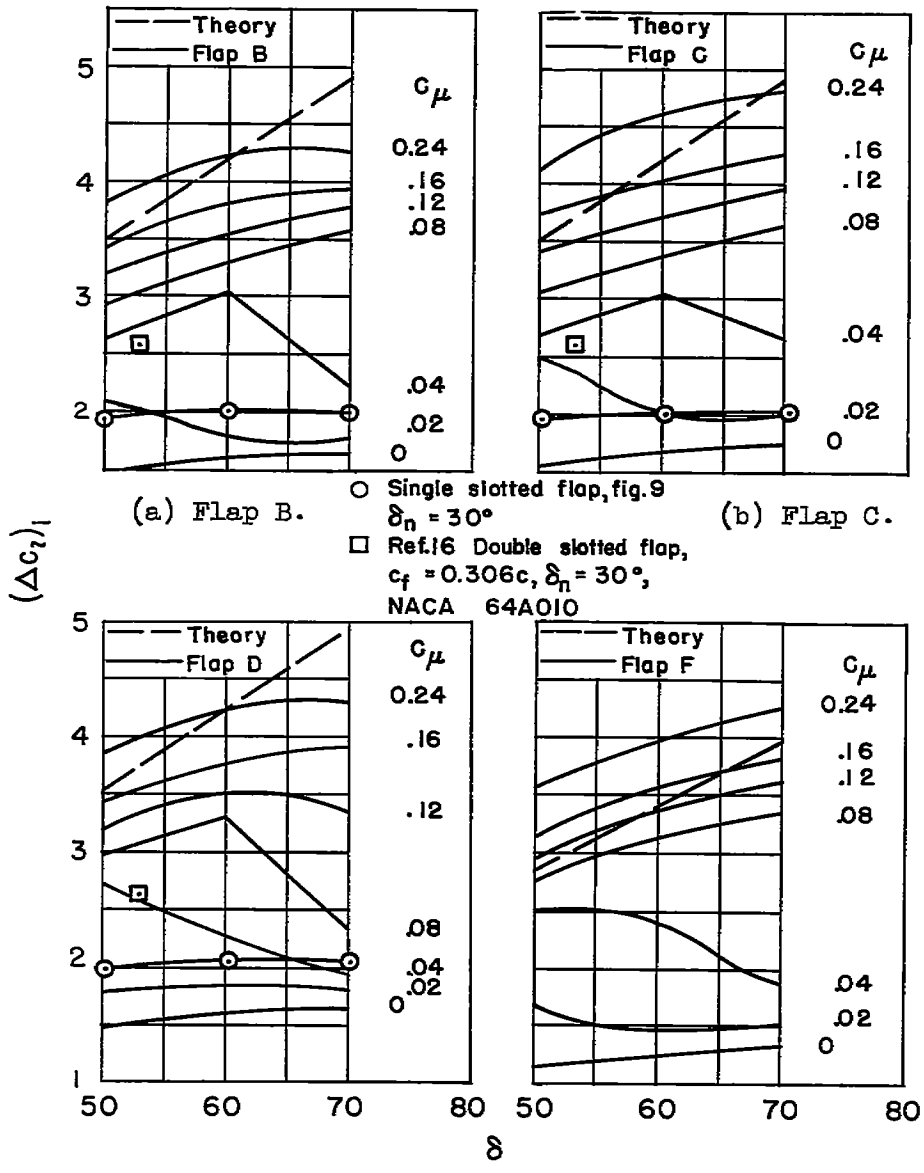

Figure 67.- The effect of the jet-momentum coefficient, c_μ, on the variation of the increment of lift coefficient with flap deflection; NACA 0006 airfoil section; s/c = 0.00110; $\delta_n = 35^\circ$.

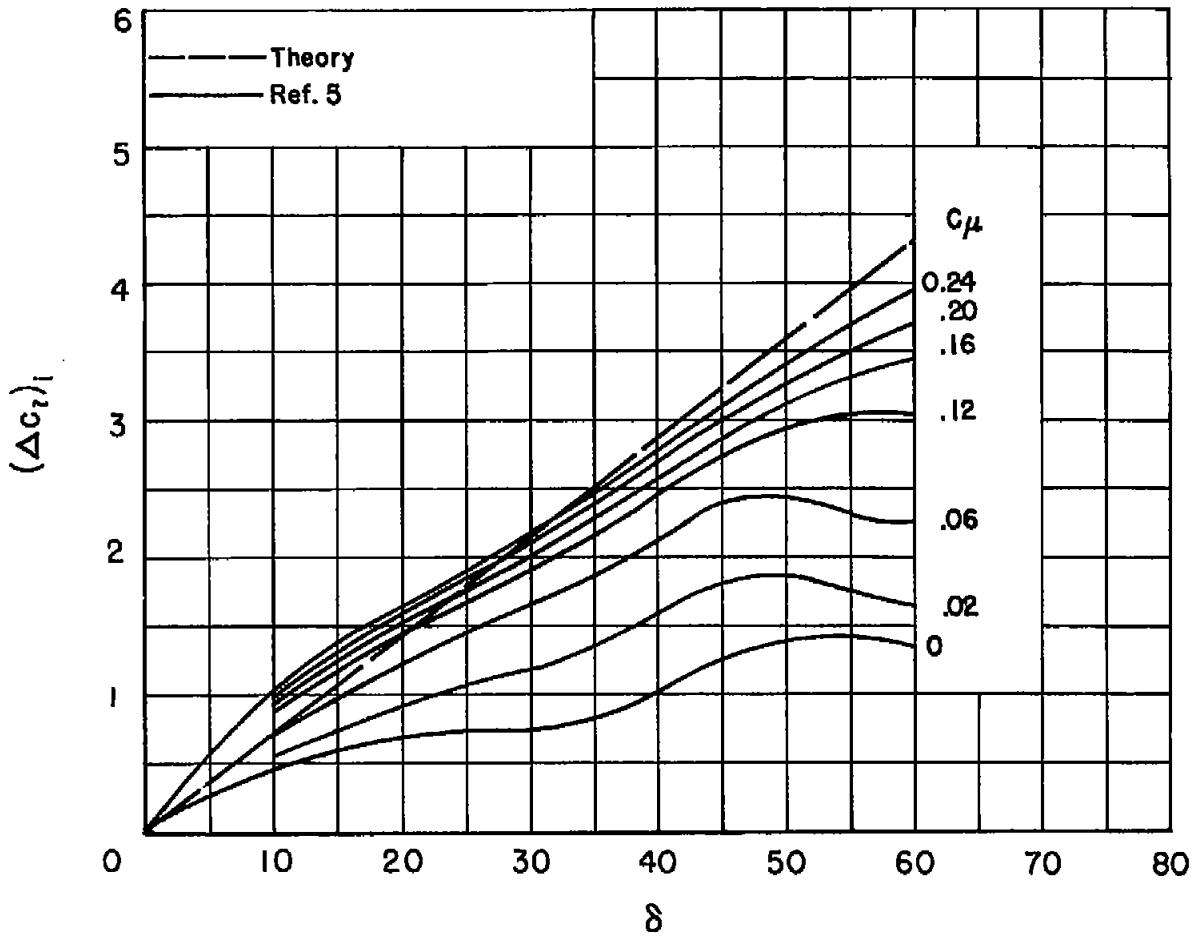

Figure 68.- The effect of the jet-momentum coefficient, c_μ, on the variation of the increment of lift coefficient with flap deflection for the flap of reference 5; 0009-E4 airfoil section; slat position 4d (10); s/c = 0.0050.

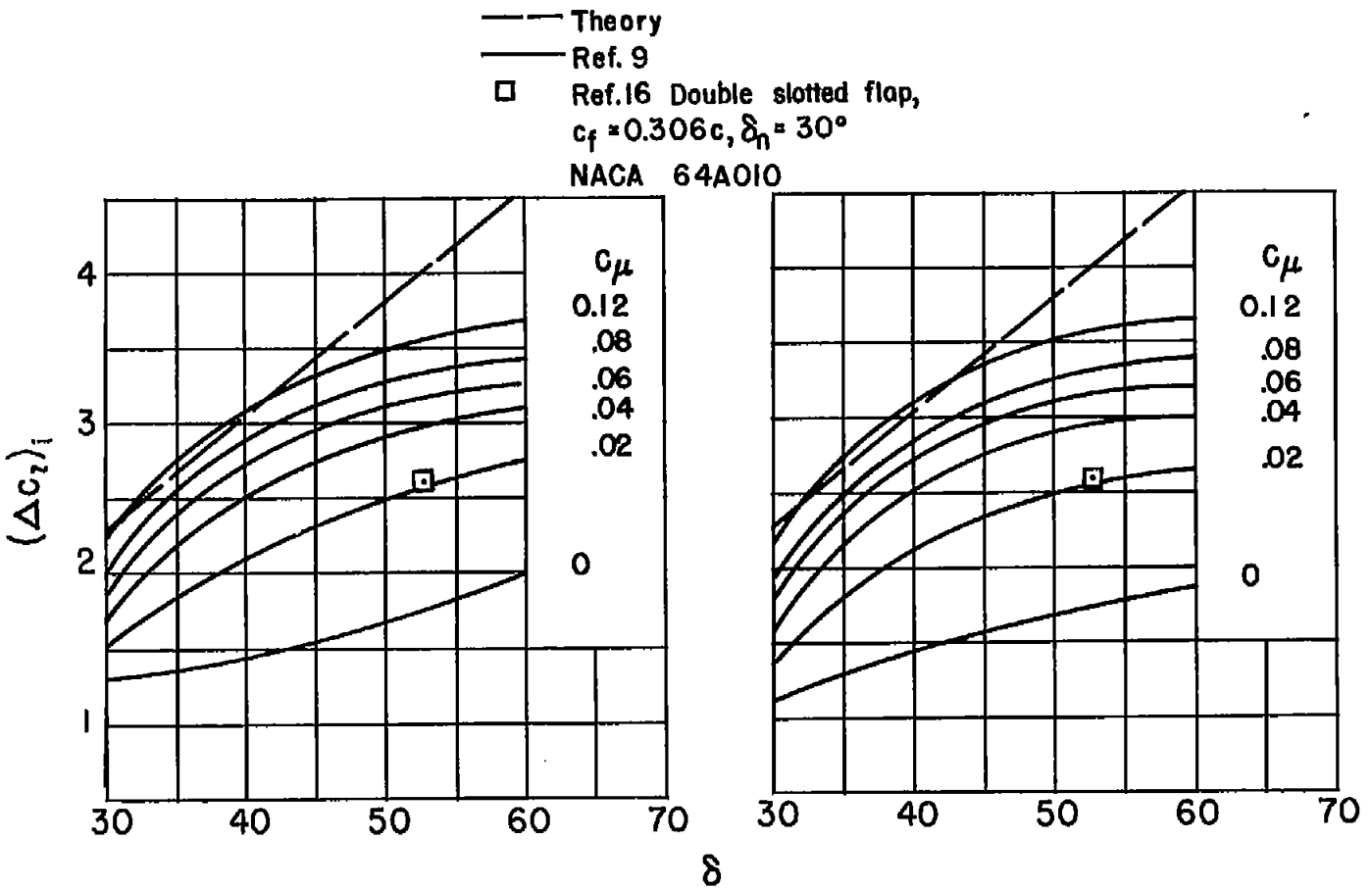

(a) s/c = 0.00072.

(b) s/c = 0.00036.

Figure 69.- The effect of the jet-momentum coefficient, c_μ, on the variation of the increment of lift coefficient with flap deflection for the flap of reference 9. NACA 64A010 airfoil section; flap position D; δ_n = 20°.

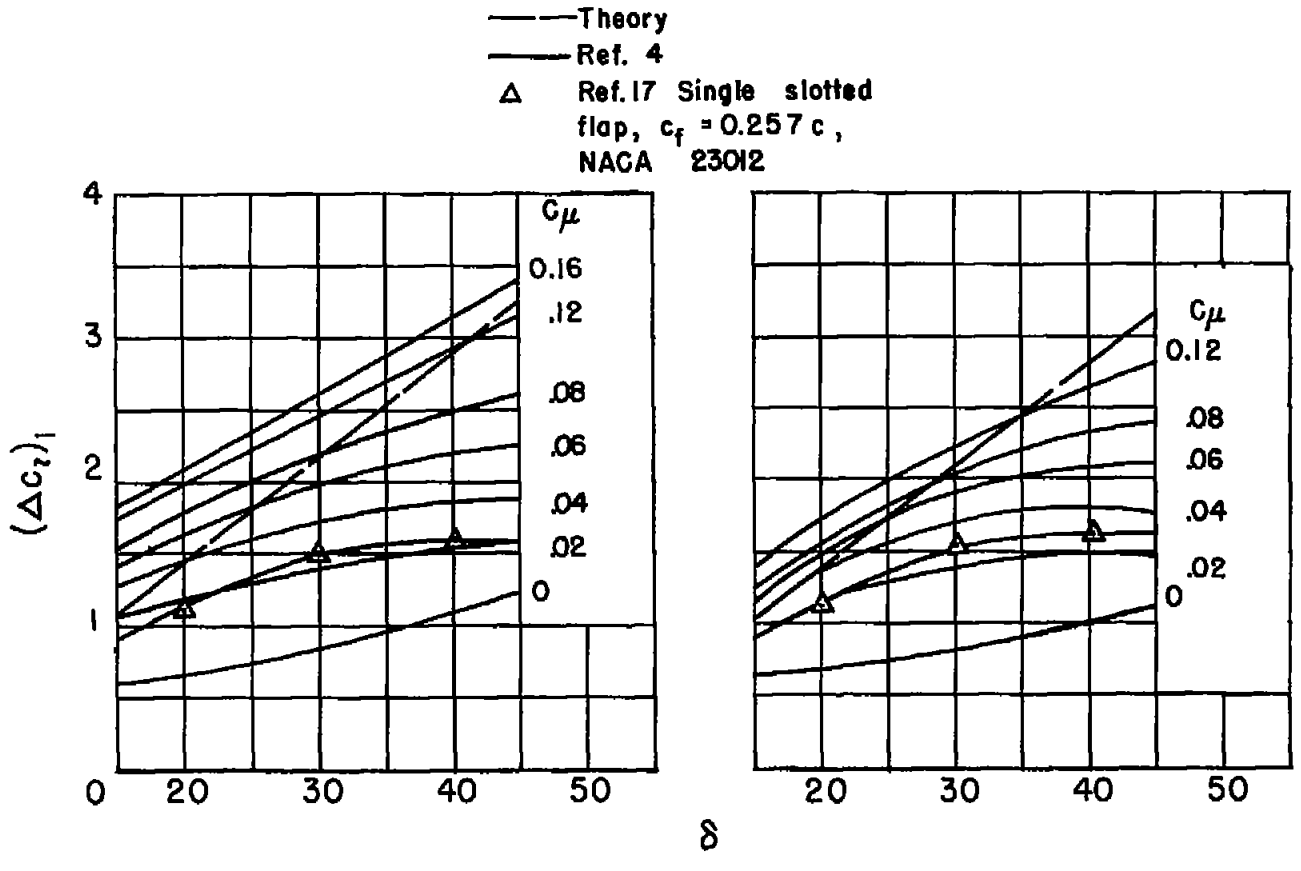

(a) Flap type f; slat position 6e; s/c = 0.0050.

(b) Flap type e; slat position 6e; s/c = 0.00667.

Figure 70.- The effect of the jet-momentum coefficient, c_μ, on the variation of the increment of lift coefficient with flap deflection for the flaps of reference 4; NACA 23012-64 airfoil section.

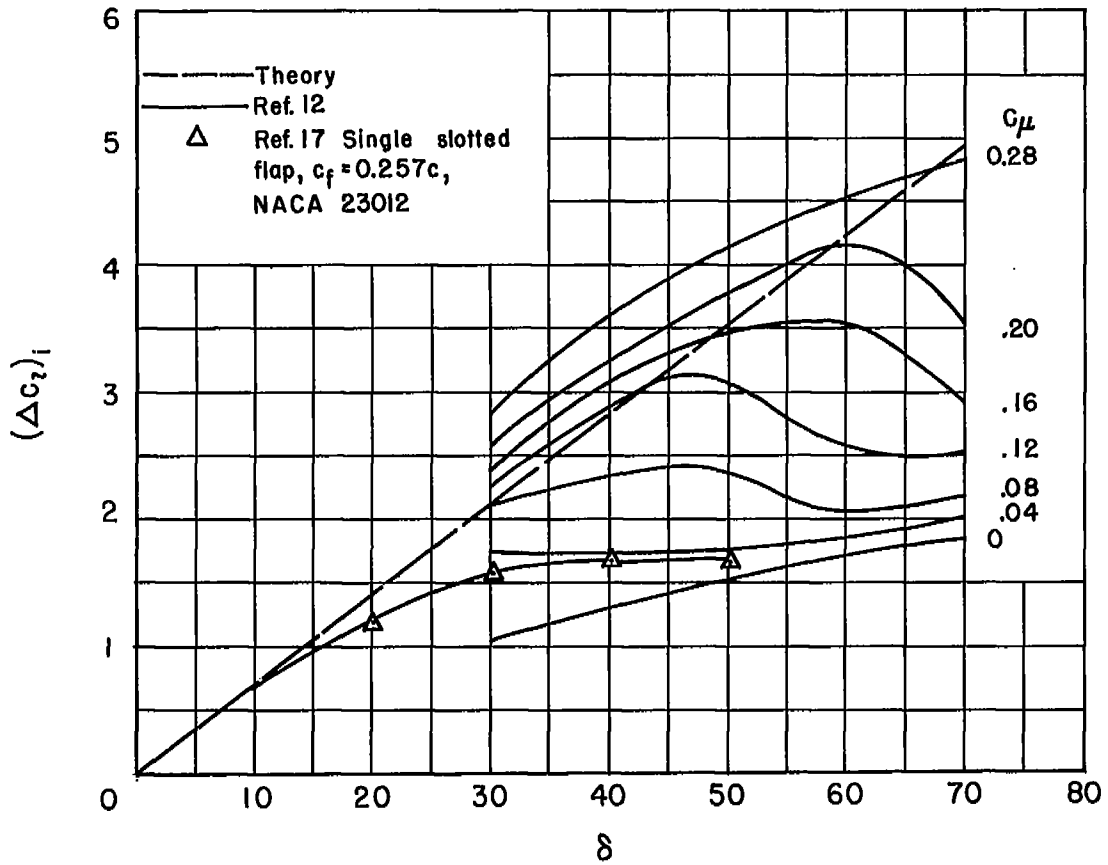

(a) s/c = 0.0090

Figure 71.- The effect of the jet-momentum coefficient, c_μ, on the variation of the increment of lift coefficient with flap deflection for the flap of reference 12; NACA 23015 airfoil section; no leading-edge high-lift device.

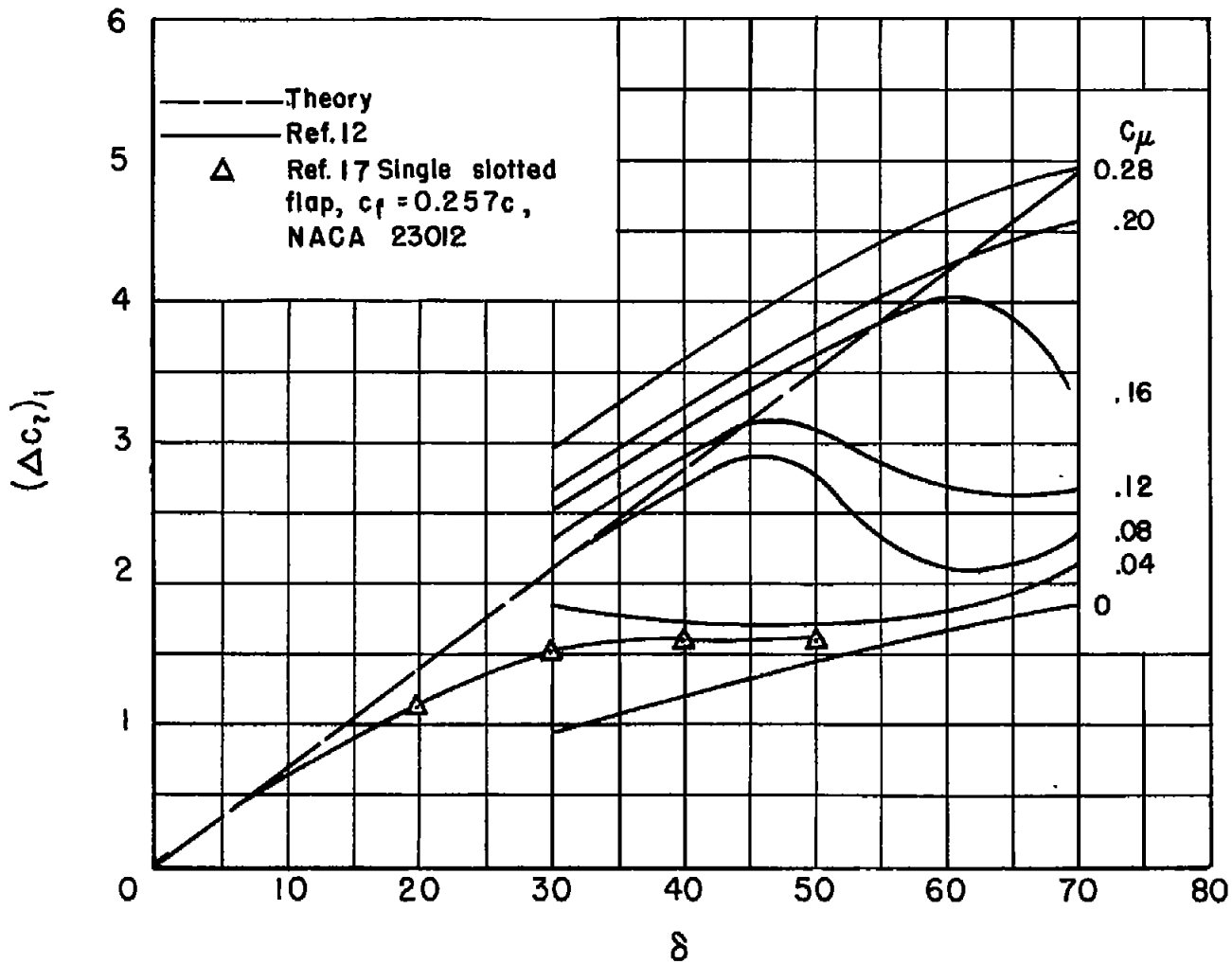

(b) s/c = 0.0070

Figure 71.- Continued.

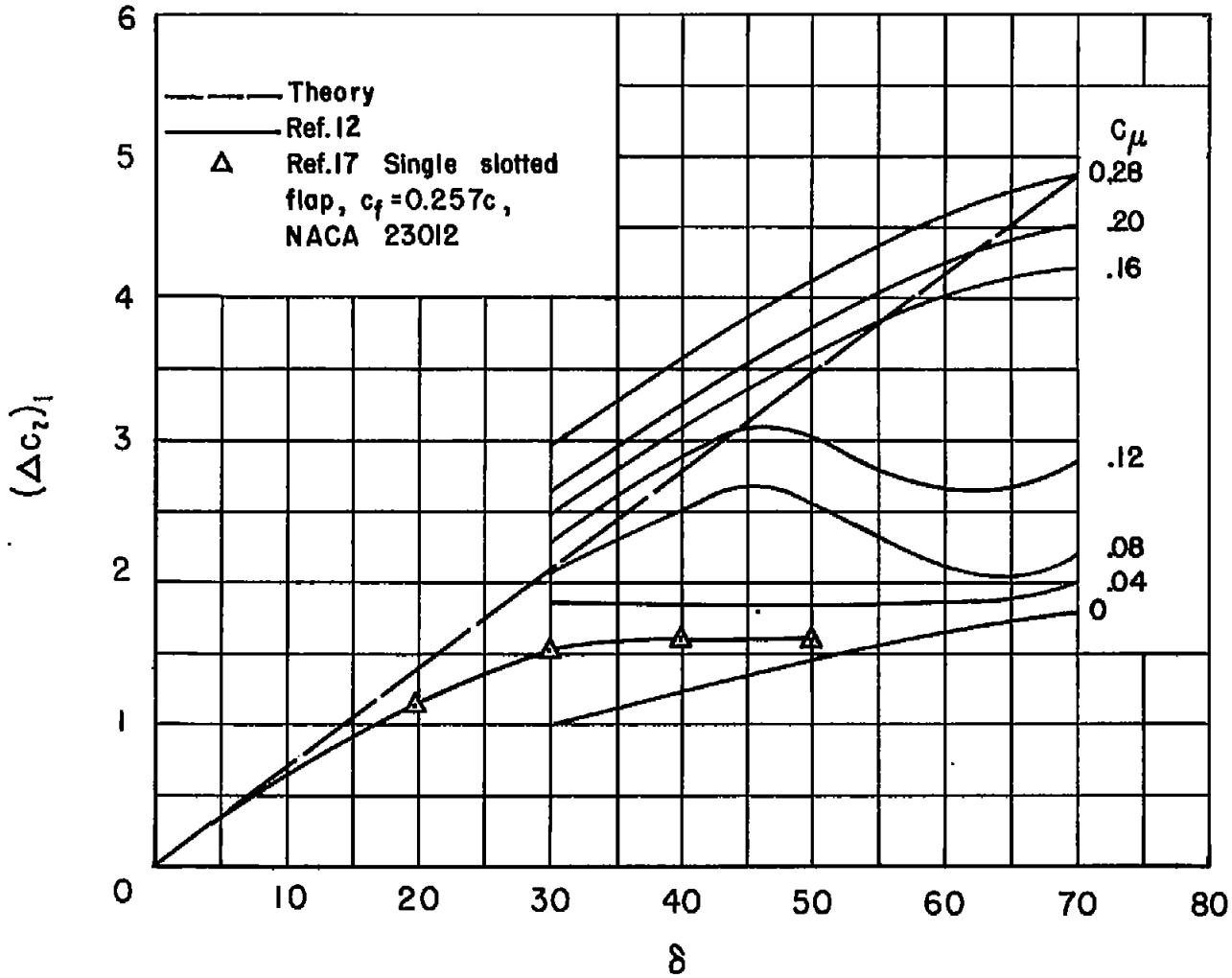

(c) s/c = 0.0050

Figure 71.- Continued.

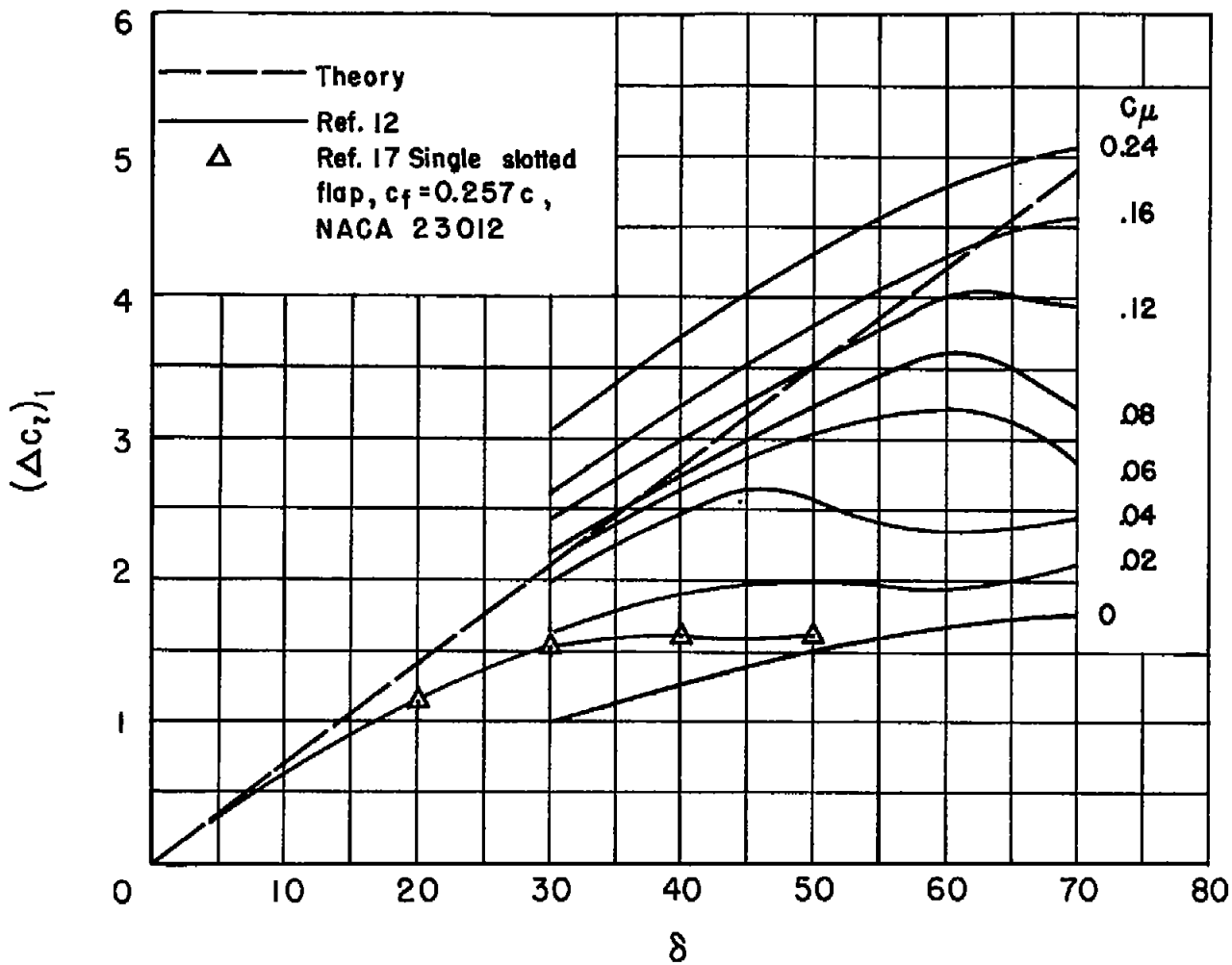

(d) s/c = 0.0015

Figure 71.- Continued.

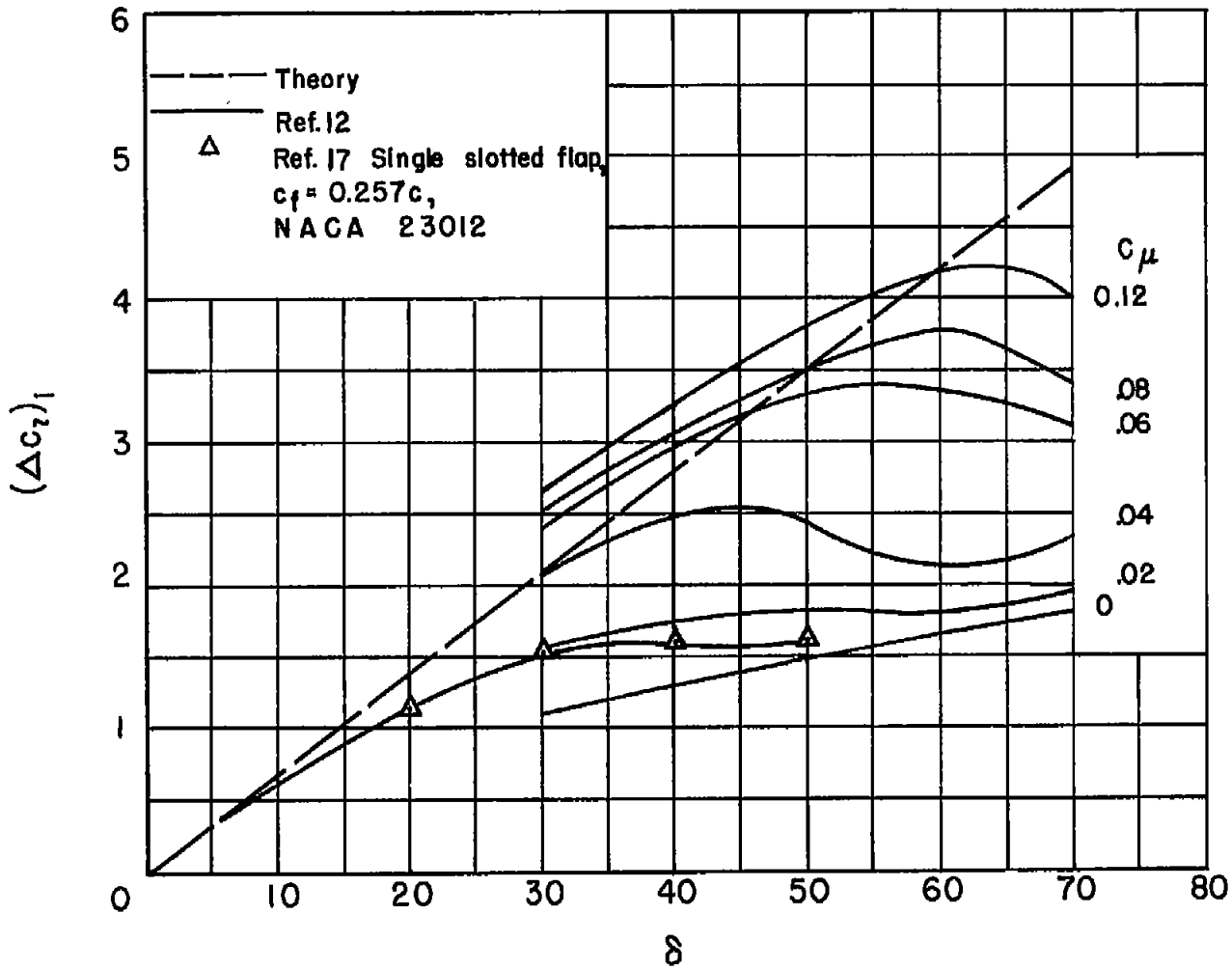

(e) s/c = 0.0005

Figure 71.- Concluded.

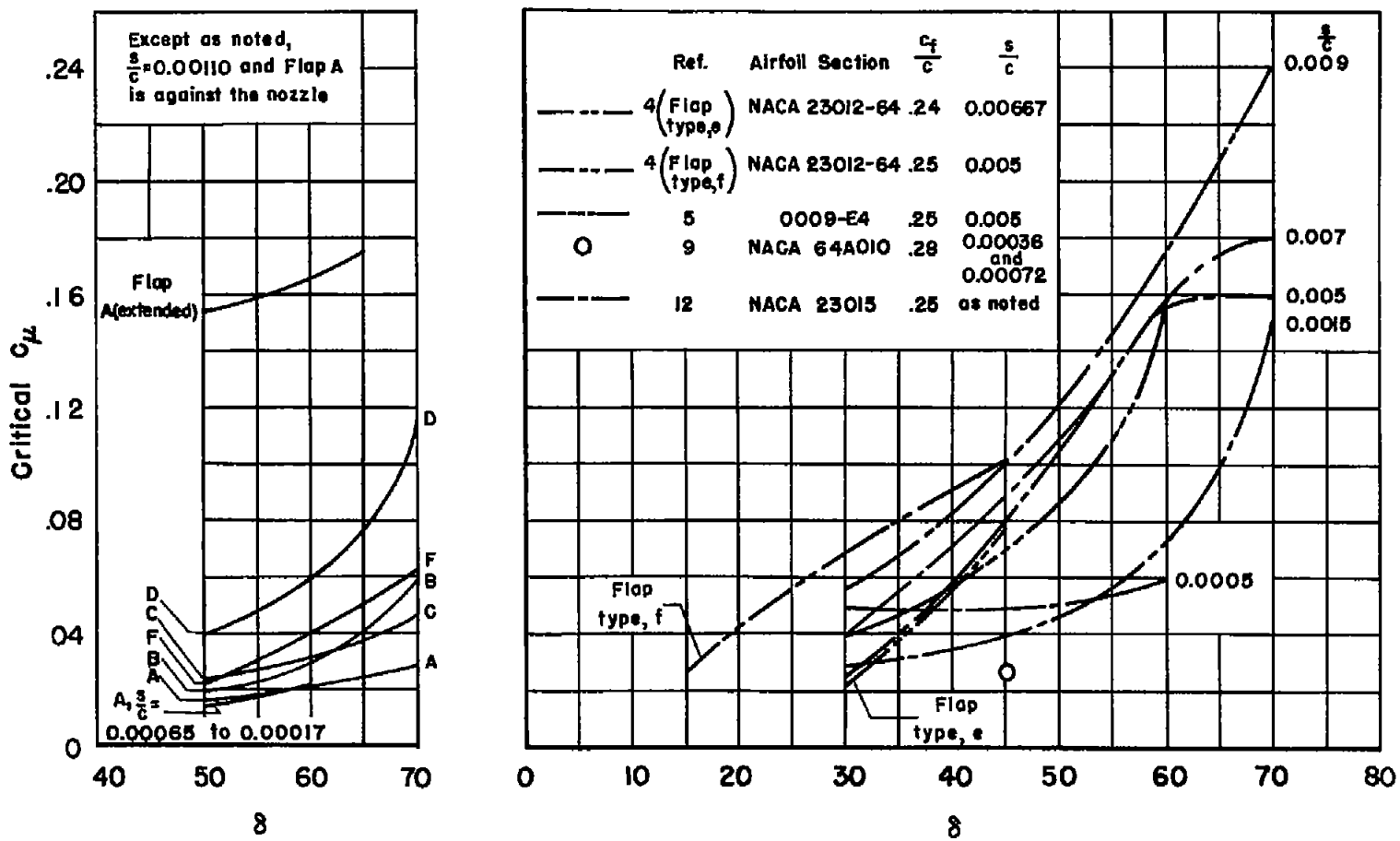

(a) Present investigation.

(b) Reference investigations.

Figure 72.- The critical jet-momentum coefficients for the models of the present and the referenced investigations; $\alpha = 0$.

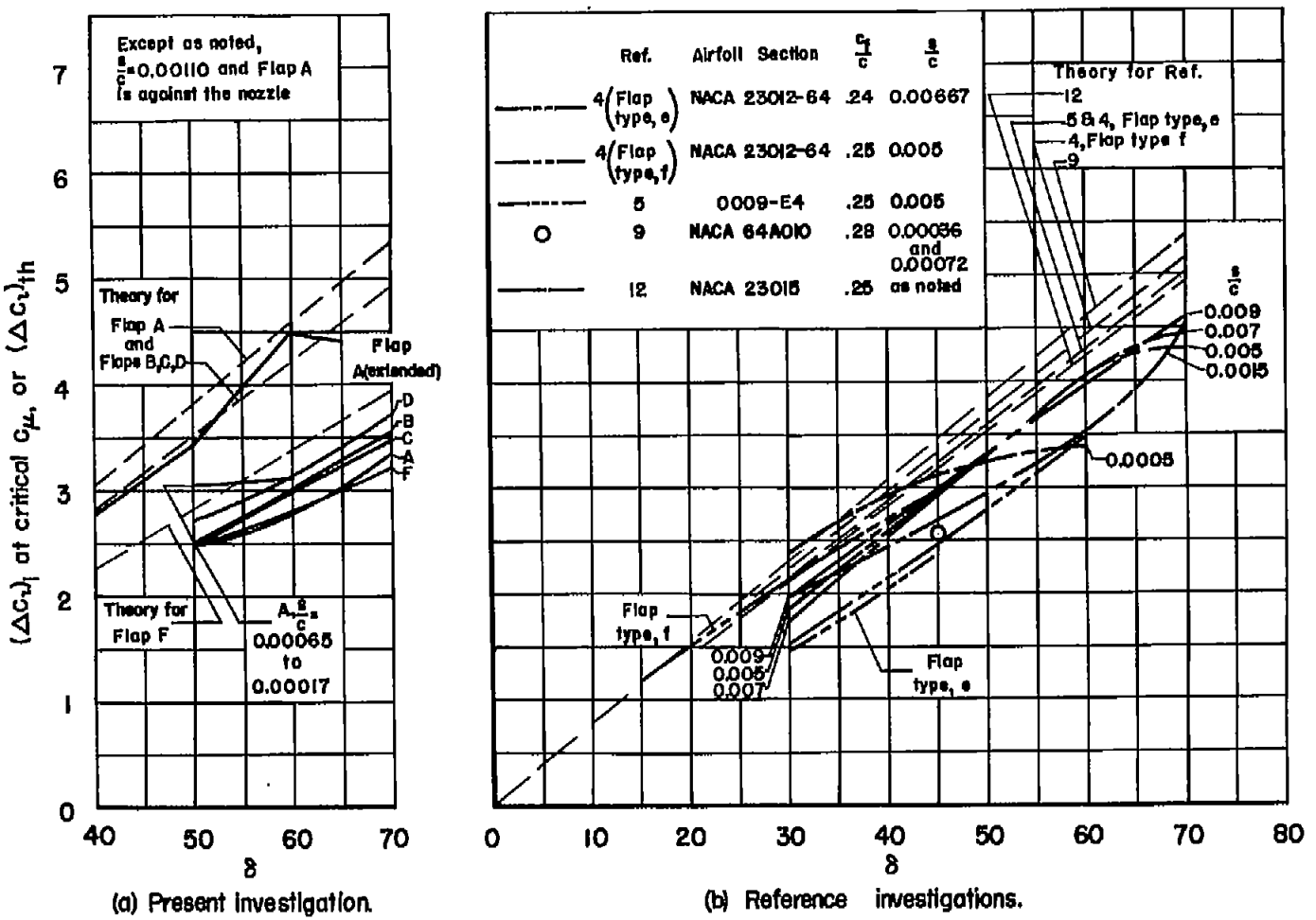

Figure 73.- The theoretical increments of lift coefficient, and the measured increments at the critical jet-momentum coefficient for the models of the present and the referenced investigations.

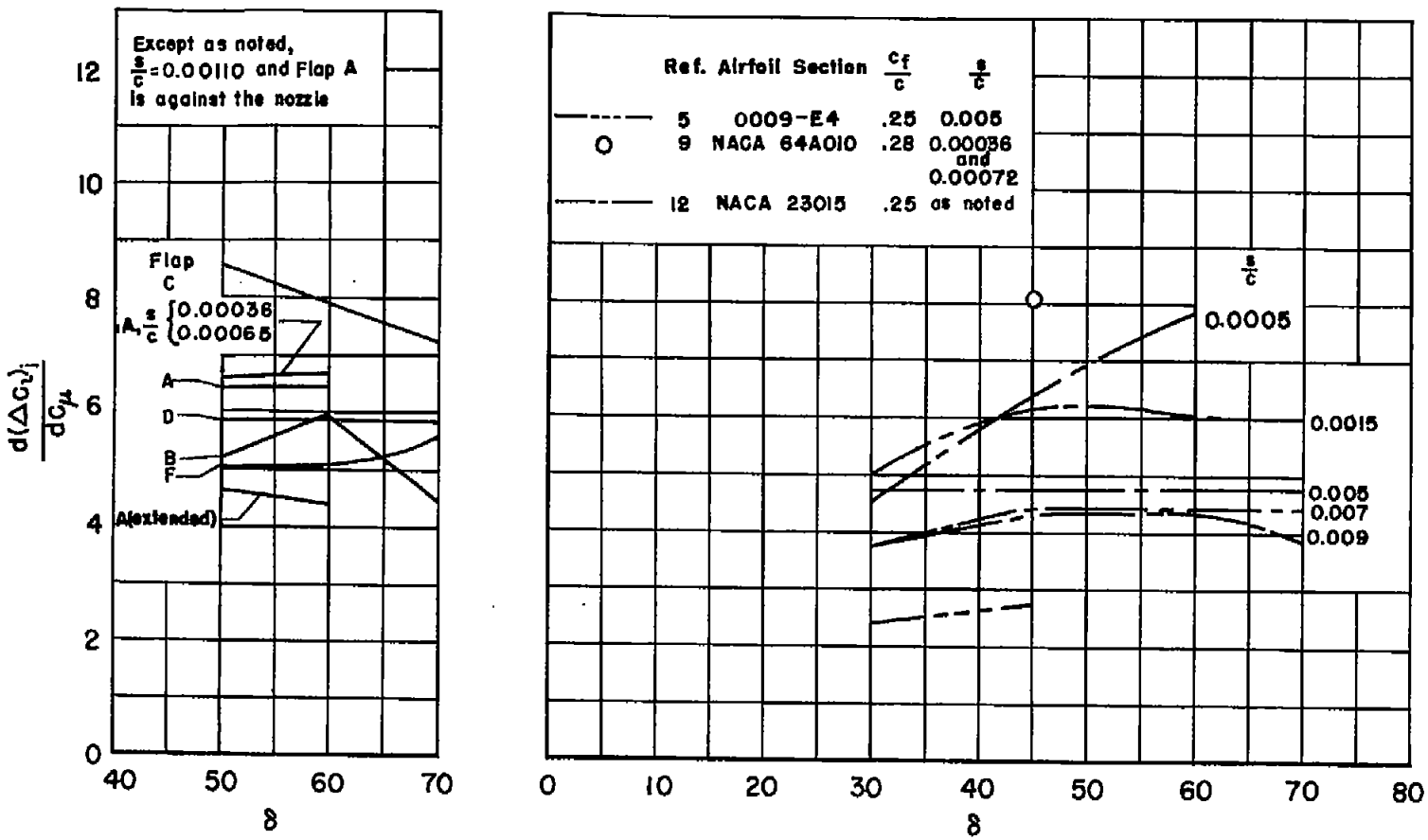

(a) Present investigation.

(b) Reference investigations.

Figure 74.- The rate of change of the increment of lift coefficient with jet-momentum coefficient for values of the momentum coefficient greater than the critical value for the models of the present and the referenced investigations.

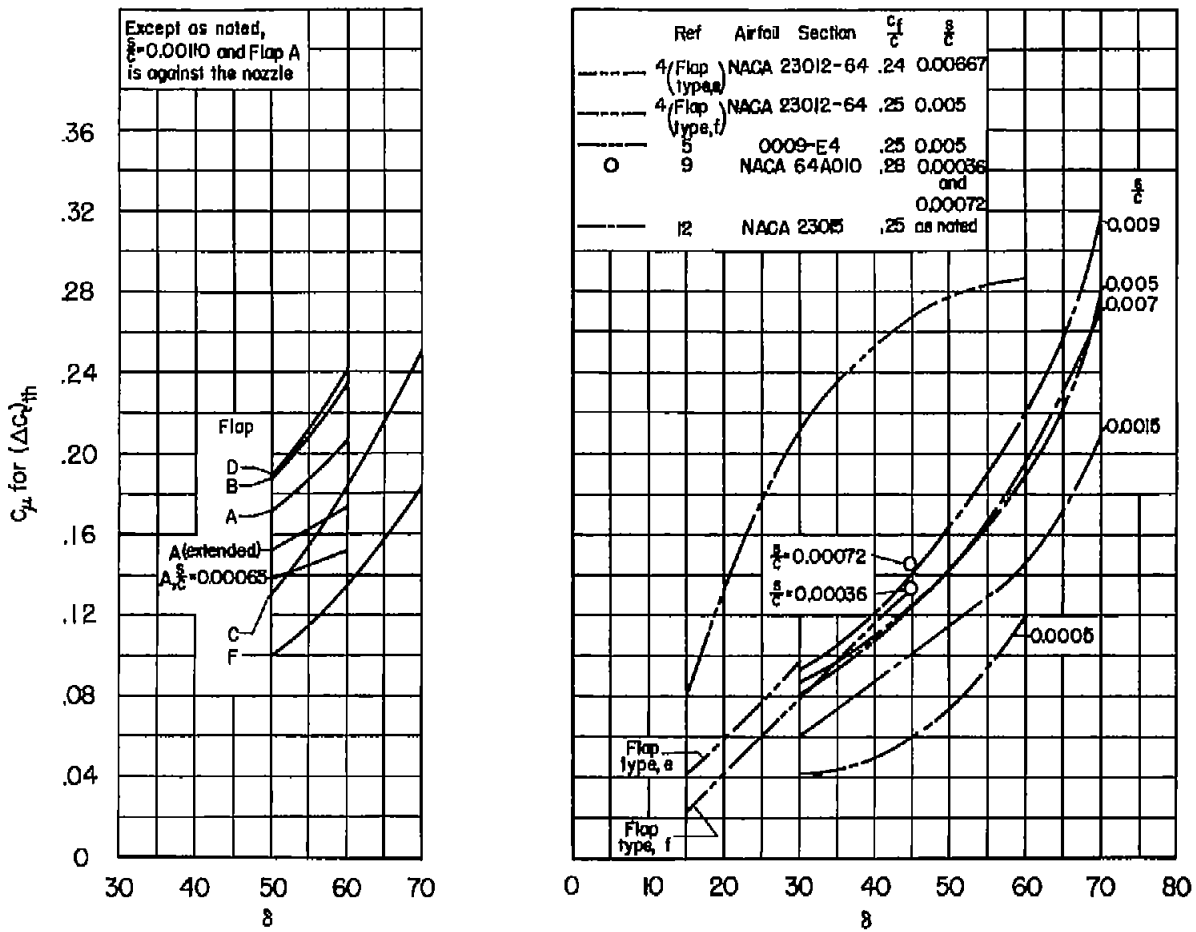

(a) Present investigation.

(b) Reference investigations.

Figure 75.- The jet-momentum coefficients required to achieve the theoretical increment of lift coefficient for the models of the present and the referenced investigations.

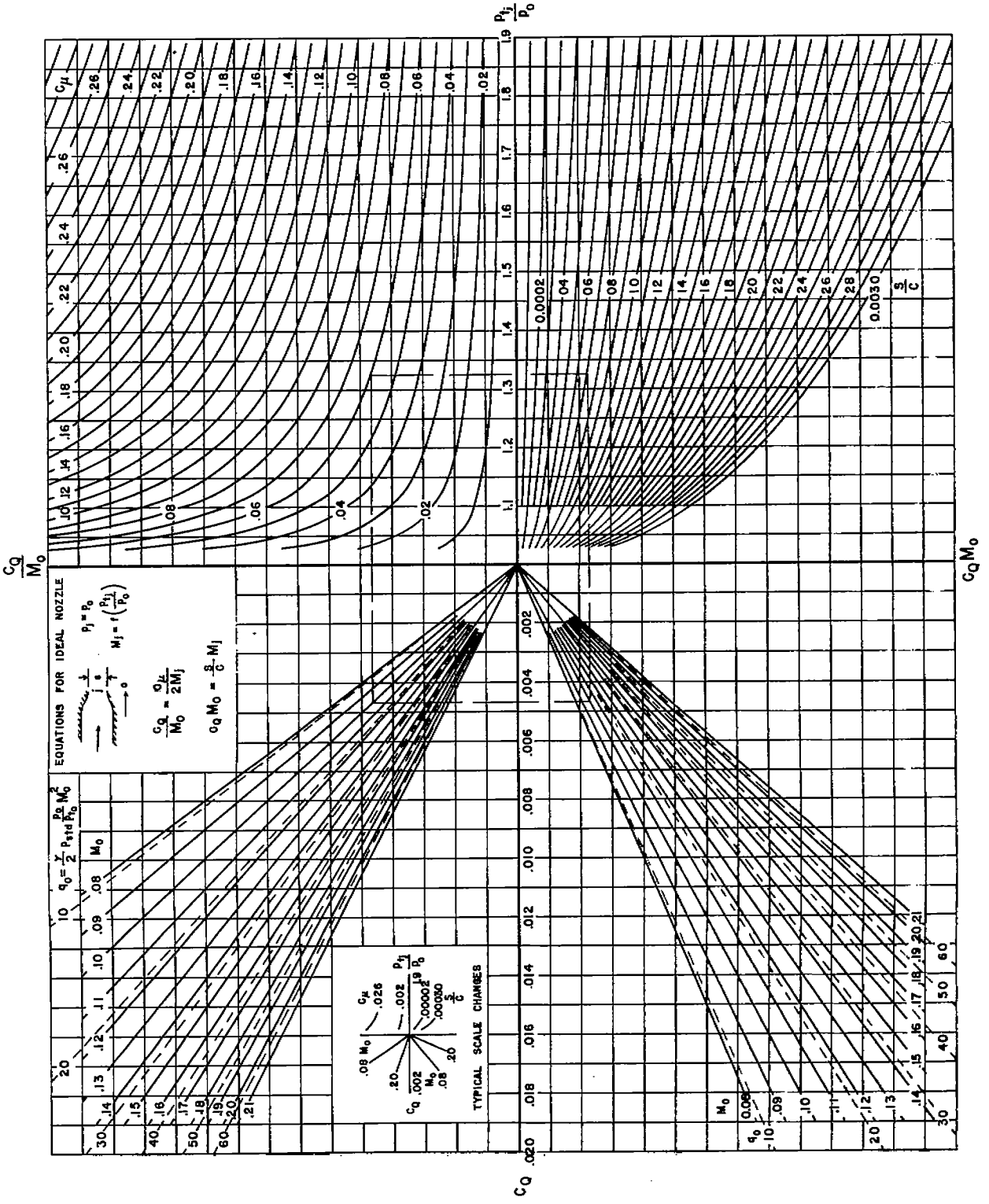

Figure 76.- Blowing-parameter relationships for subcritical pressure ratios.

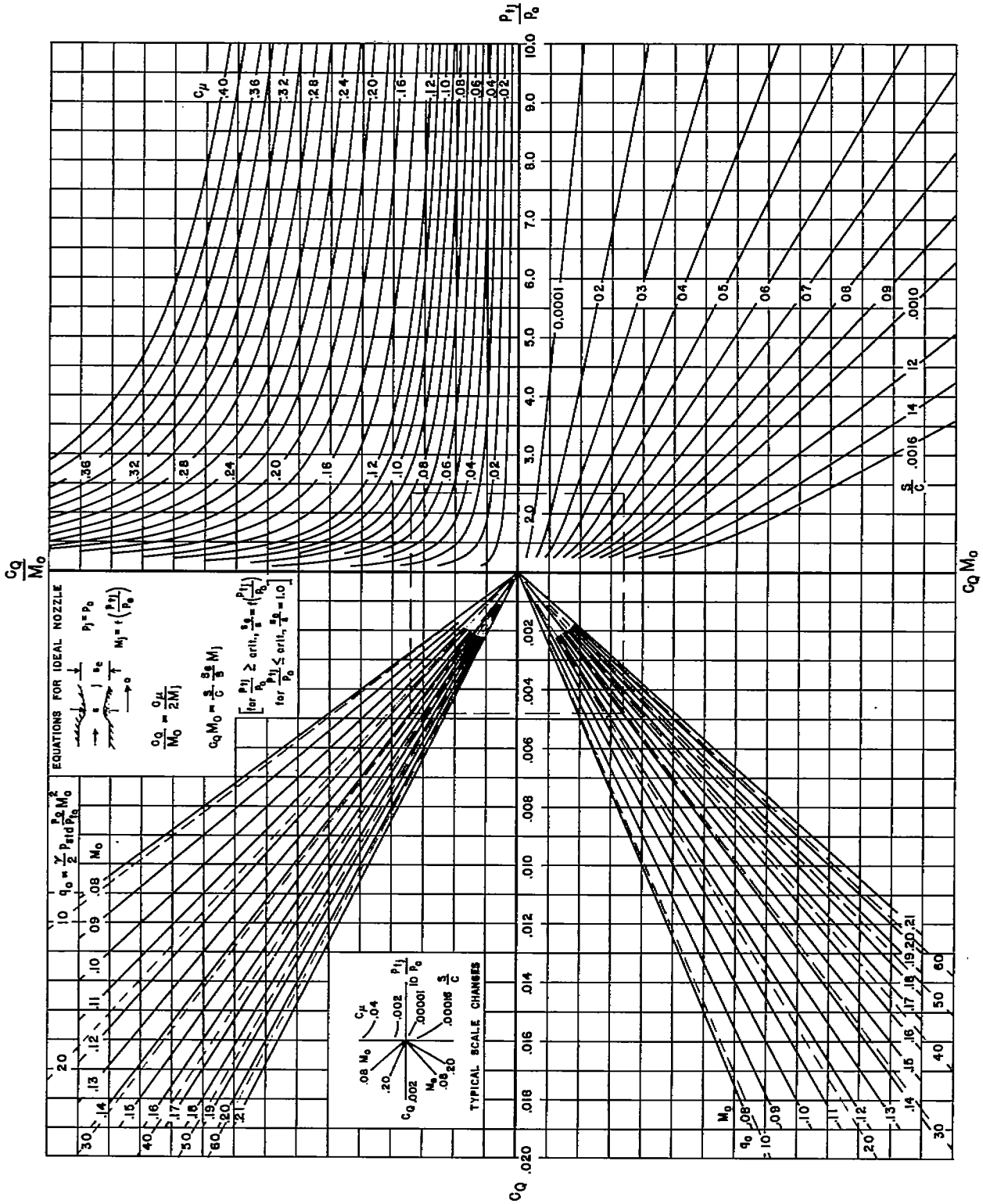

Figure 77.- Blowing-parameter relationships for pressure ratios up to 10.

[redacted]

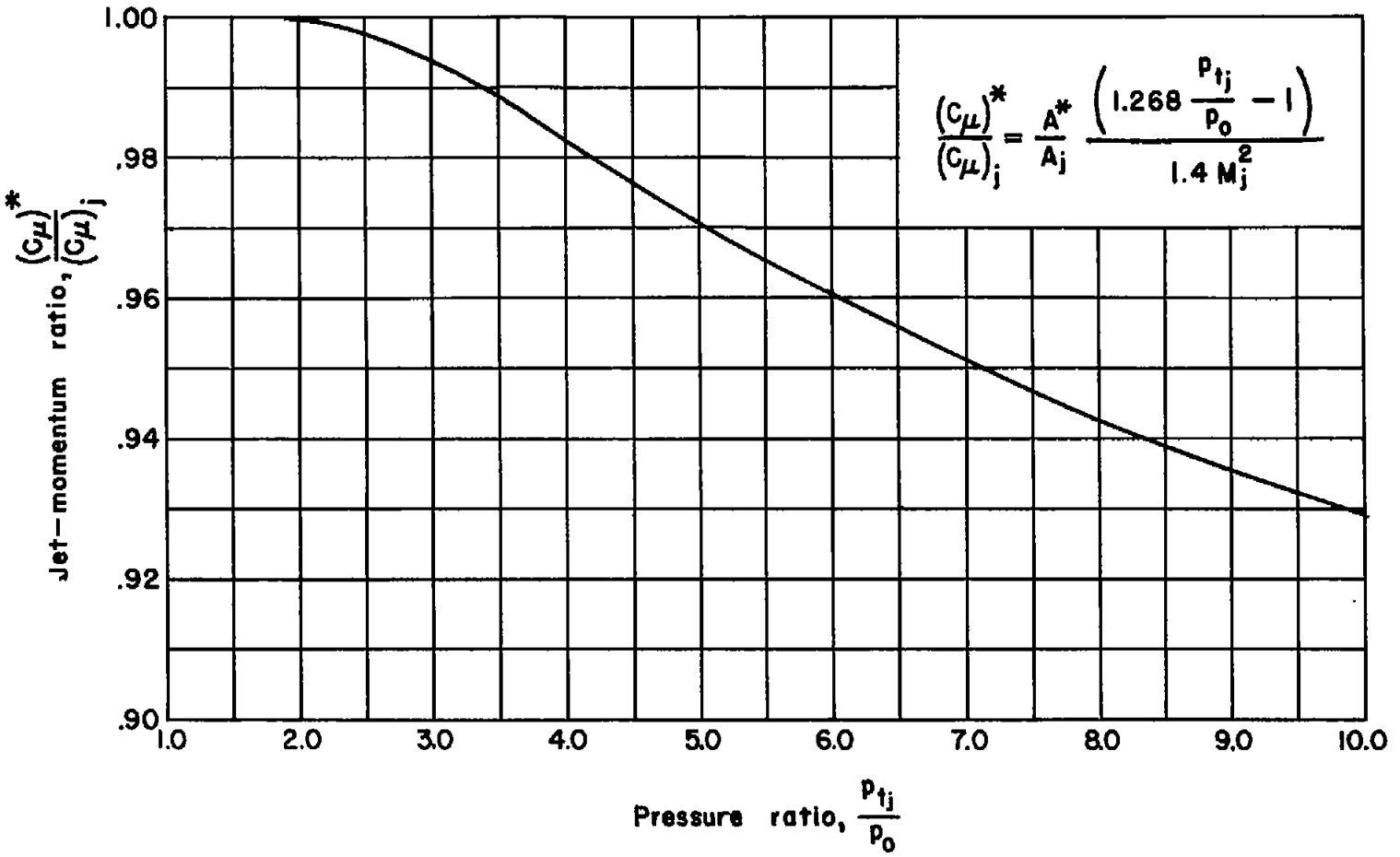

Figure 78.- The variation with the pressure ratio of the ratio of the momentum coefficient for a convergent nozzle to that for a convergent-divergent nozzle.

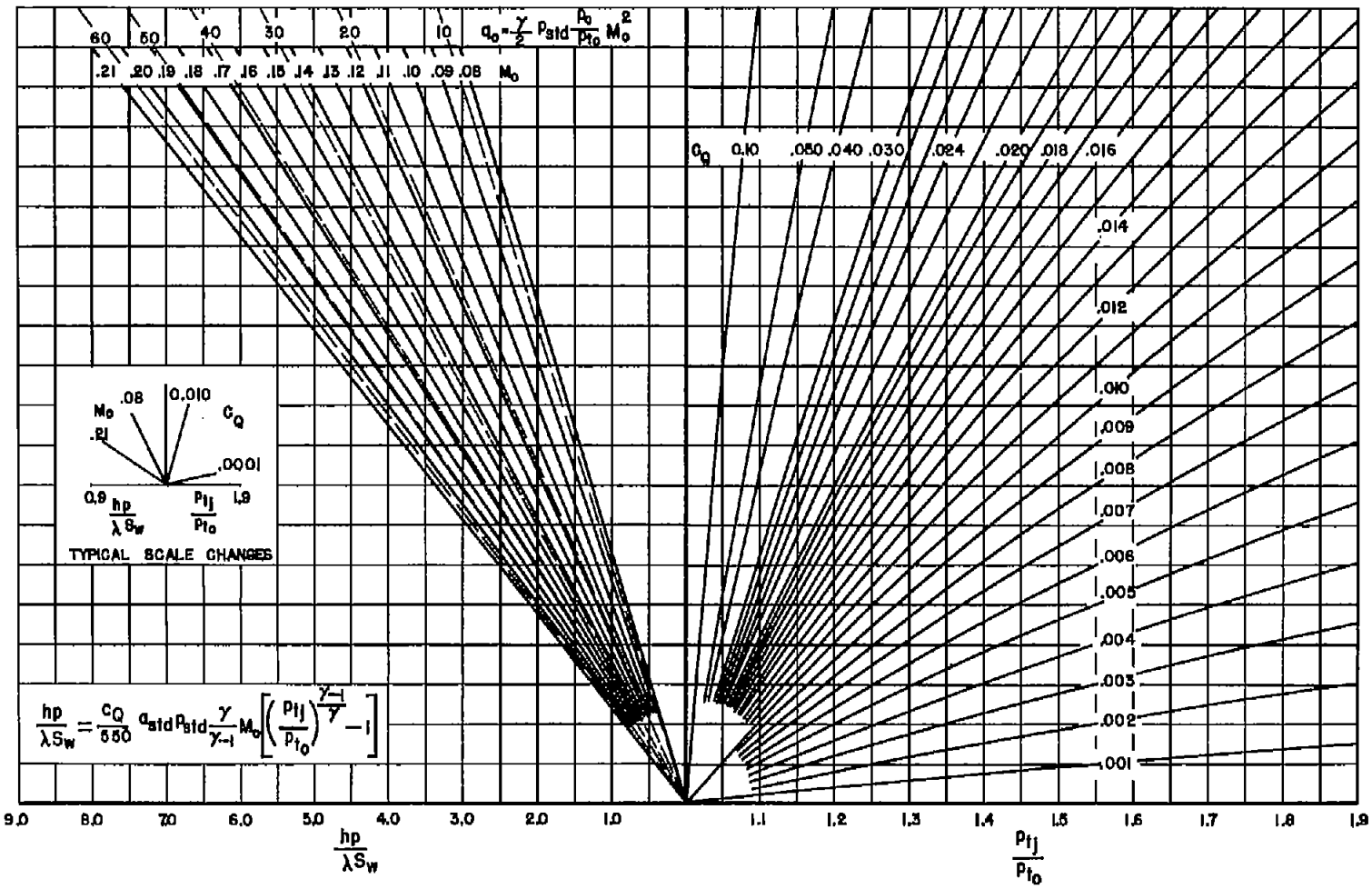

Figure 79.- Relationships among the blowing and power parameters for pressure ratios less than the critical value.

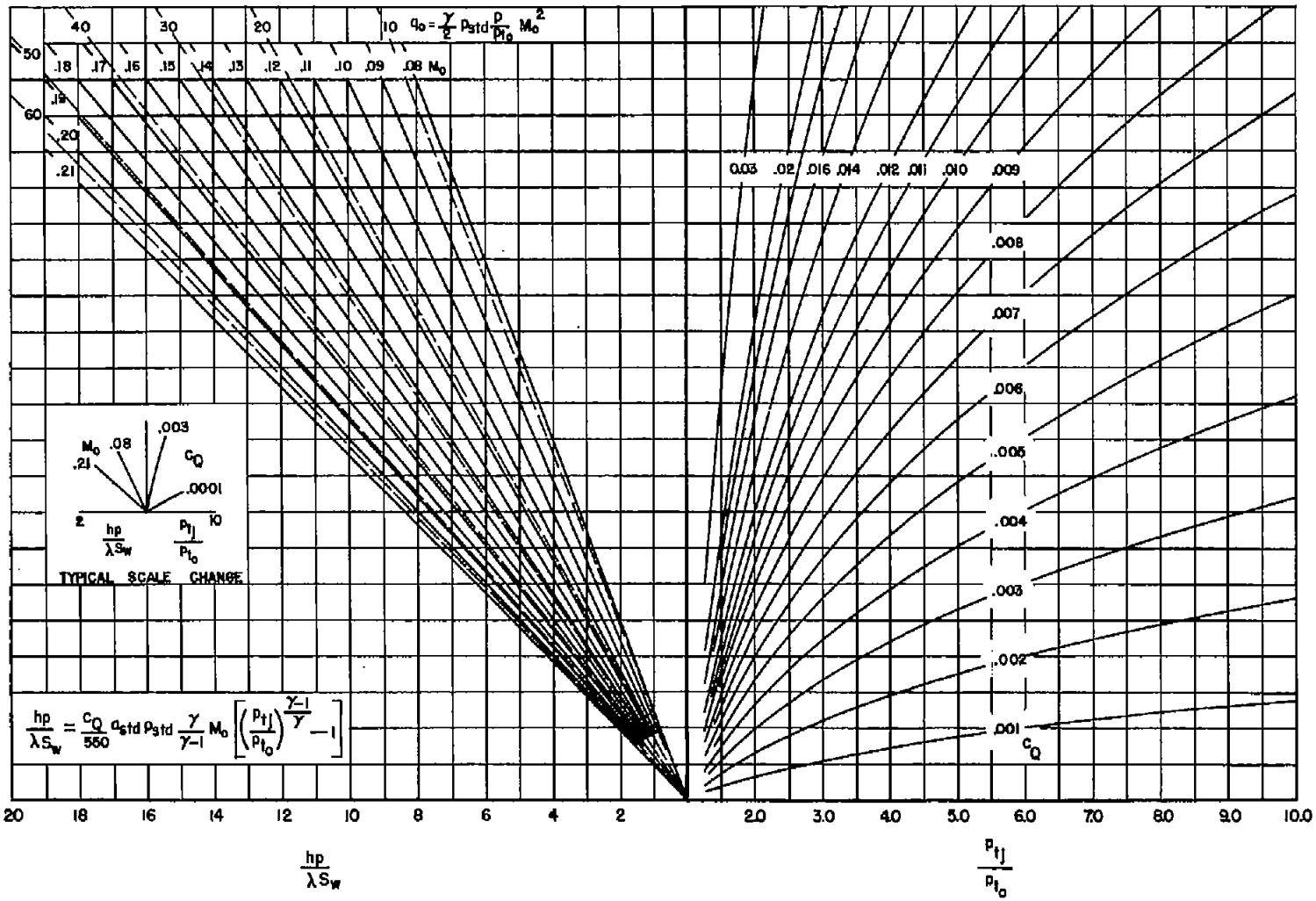

Figure 80.- Relationships among the blowing and power parameters for pressure ratios up to 10.

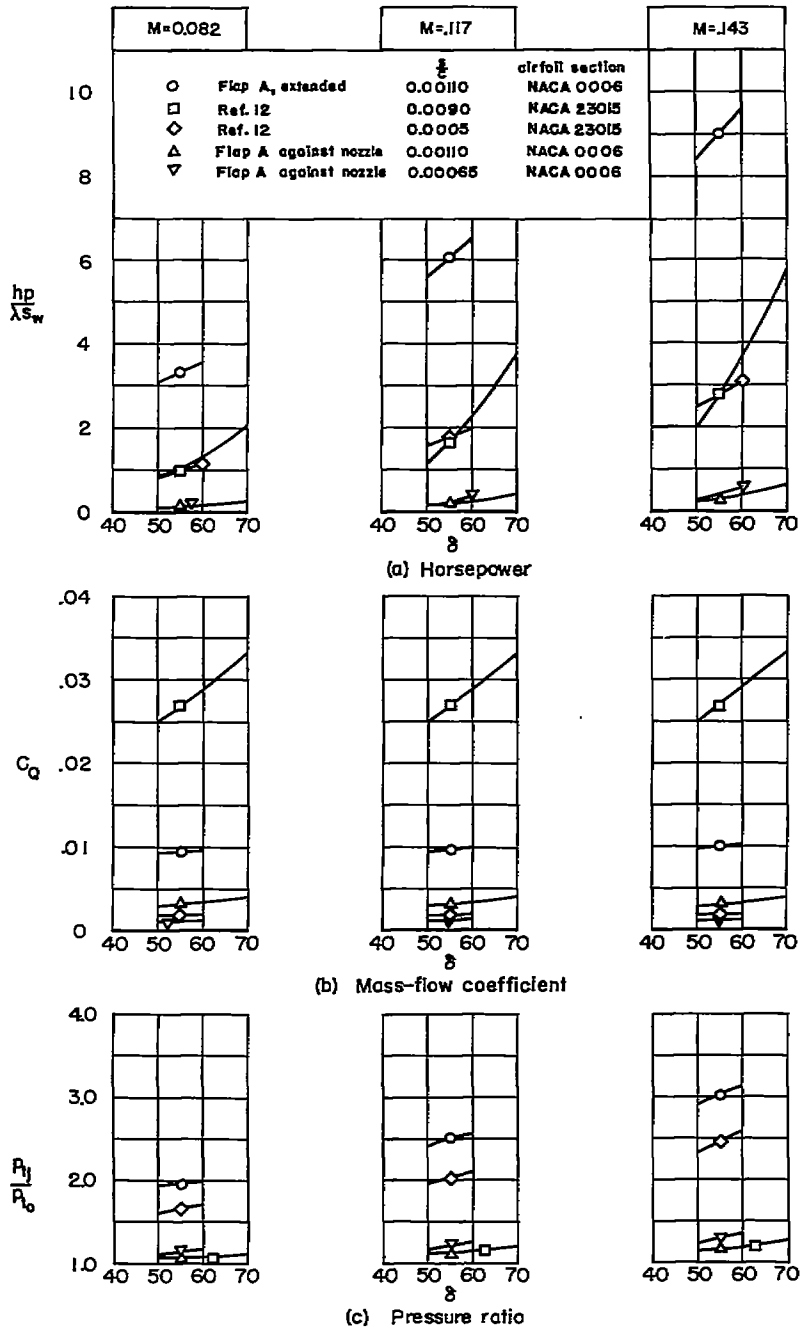

Figure 81.- Comparisons of the power, flow coefficient, and pressure ratio for the critical momentum coefficient for several blowing-flap arrangements of the present investigation and of reference 12.

[redacted]